THE STRUCTURAL INTEGRITY OF WALL CLADDING OF LARGE PANEL SYSTEMS

WASEEM U. KHALIFA, M.A.Sc.

DEPARTMENT OF CIVIL ENGINEERING
UNIVERSITY OF GLASGOW

A THESIS SUBMITTED IN CONFORMITY WITH THE
REQUIREMENTS FOR THE DEGREE OF
DOCTOR OF PHILOSOPHY
JANUARY 1995

ProQuest LLC.
789 East Eisenhower Parkway
P.O. Box 1346
Ann Arbor, MI 48106 – 1346

To,

Nina

ACKNOWLEDGEMENTS

The author wishes to acknowledge the financial support provided by the Association of Commonwealth, and at the same time is grateful to the Government of Pakistan and the University of Engineering and Technology, Lahore for providing the study leave which allowed the author to complete the degree.

The author is highly grateful and indebted to Prof. D. R. Green for his extremely valuable guidance and encouragement throughout the research, without which it would not have been possible to accomplish it. The author also wishes to thank R. W. Watson for his help and invaluable input, especially during the experimental phase of the research. The author would also like to thank Dr. Alan Agar for his contribution towards the numerical modelling.

The author is also grateful for the help received from the technical staff and would like to thank all laboratory staff as well as the secretarial staff of the Department of Civil Engineering at the University of Glasgow. Last but not least the author wishes to thank his friends and family who have been a constant source of inspiration, strength and guidance during the research.

ABSTRACT

The thesis describes the results of non-destructive tests carried out on eleven orthogonally reinforced concrete sandwich panels, for the determination of their dynamic characteristics. The objective of the present investigation was to determine through the dynamic response, the structural integrity of the sandwich panels. The main dynamic characteristic of the panels under consideration was their natural frequency. The test specimens had nominal dimensions of 175mm by 1800mm by 2400mm, consisting of two concrete leaves, which were 100mm and 50mm thick, respectively. The two leaves were separated from each other through a 25mm thick insulation layer of expanded polystyrene. The test specimens were similar to the one's used in the construction industry for the construction of large panel system dwellings erected in the late 1960s and early 1970s. The eleven specimens were different from each other in the type of constraint and connection present between the two leaves, and varied from a complete concrete connection around the perimeter to none at all. In addition to this connection around the perimeter, the two leaves were also connected to each other through a system of reinforcement ties, which varied from a minimum of one to a maximum of eight. For all test specimens, the 100mm thick concrete leaf was simply supported along the top and bottom 1800mm edge. Dynamic loads were imparted through either a sinusoidal vibrator or through the impact of a hammer blow. In addition to these dynamic loads the specimens were also subjected to an in-plane compressive load of 500kN, distributed uniformly along the 100mm thick concrete leaf.

The main objective of the research was the establishment of damage location in a panel, through changes occurring in the natural frequencies. These changes in the

natural frequencies were used to distinguish between the various structural differences in the panels. A numerical analysis was performed for all panels, through the finite element package, FLASH, to predict the natural frequencies and determine the expected mode shapes for the first six modes.

It is shown that it is possible to determine the natural frequencies of the sandwich panels under investigation, when subjected to dynamic excitation through the means of a hammer blow. It is further concluded that, it is possible to determine through changes in natural frequencies, any major structural changes occurring in the panels, without resorting to the more cumbersome experimental determination of the mode shapes. At the same time it was established that for distinguishing between minor structural changes occurring in the panels, the natural frequencies alone, are not a good enough measure, as they are too closely spaced for the successive modes and are extremely difficult to distinguish form each other.

CONTENTS

NOTATION

A, A_1, A_2	Constant
C	Constant
c	Viscous damping constant
c_c	Critical damping constant
E_c	Young's modulus of elasticity of concrete
f	Natural frequency
k	Stiffness
m	Mass
$P(t), P_0$	Exciting force
r	Frequency ratio
T	Period
t	Time
X, X_{st}	Amplitude
x	Displacement
$\dot{x}$	Velocity
$\ddot{x}$	Acceleration
α	Phase angle
δ_{st}	Static deflection
γ	Viscous damping parameter
$\lambda, \lambda_1, \lambda_2$	Frequency Parameters
ν	Poisson's ratio
$\omega, \omega_n, \omega'$	Circular natural frequency

LIST OF FIGURES

CHAPTER 1

CHAPTER 2

CHAPTER 3

CHAPTER 4

CHAPTER 5

CHAPTER 6

LIST OF TABLES

CHAPTER 1

INTRODUCTION

"Things fall apart; the centre cannot hold;

Mere anarchy is loosed upon the world"

Yeats, W. B. referred to the whole of society. We, as engineers only hold responsibility for the integrity of our infrastructure. Since May the 16th, 1968, and the catastrophic collapse of the corner flats in the Ronan Point estate, Newham, East London our procedures and judgement have been called into question for allowing the proliferation of structures built from prefabricated components. Were the quality control procedures adequate? Were the processes for the manufacture and erection sound? Questions which have still not been fully answered. On going research has identified a number of defects detrimental to the performance of the structure. One component shown to be flawed in recent times has been the concrete cladding panels of large panel system dwellings. Cladding has been an integral part of a structure for decades. Until recently its usage was limited to architectural design and aesthetic appeal, and contribution towards insulation. Nowadays, the structural contribution of cladding is being more readily recognised. Researchers have shown it's utility and importance in structural integrity through its contribution towards stiffening and bracing of the structure. Materials of all kinds, ranging from natural to artificial and man made, have been utilised for cladding purposes. The use of cladding on prefabricated systems was particularly fashionable, as it provided an eye pleasing facade in addition to serving as an efficient insulation against the vagaries of weather.

For reasons of economy and efficiency the use of industrial methods for the construction of buildings has been in vogue for about three decades now. It

received a big boost in the 1960's in Britain, when the government decided to promote these methods of construction to expand the house building industry, in order to meet the high targets of 500,000 new houses each year. The method most commonly adopted to meet this extremely high rate of growth was the use of system-built, large-panel, multi-storey buildings. In essence, it consisted of precast panels designed as floor and wall units and these were then assembled on site, with in-situ concrete joints to form the structural unit. The wall units consisted of two panels: the inner panel being the load bearing one, and the external panel, separated from the internal panel by an insulating layer, clad with a decorative finish. The two leaves (panels) of the wall unit were held together through a specified number of ties, located within the panel at the time of casting. The connection between the precast external wall and the floor unit was such that loads were transmitted through the load bearing elements only, which in this case was the internal leaf.

The reasoning behind the use of such a system was the need for mass production whilst achieving optimal use of site labour, without sacrificing standards, by fabricating high quality panel units in precasting yards. Thus, based upon the need for mass production, during the period 1966-72, many such system-built, large-panel structures were erected in Great Britain, as well as other parts of the world.

It has been only in the recent past that attention has been drawn towards the structural safety of such structures. In particular to the connection of the cladding of the external units on to the inner load bearing leaf. In 1983 and 1984 the Scottish Development Department advised all owners of high rise buildings in Scotland of possible defects in these types of structures. What necessitated such a warning was the reported failure of a few such panels. In 1979 and 1984 incidents

were reported of concrete cladding units becoming detached from multi-storey, system-built structures in Birmingham and Glasgow. Similar incidents were also reported in parts of the United States of America, such as New York and Chicago.

Once the fact was established that the cladding on such structures is a hazard, remedial measures were taken or at least considered advisable. The methods employed mainly consisted of re-bolting the outer cladding leaf to the inner load bearing leaf in a variety of ways [1, 2, 3, 6]. Little consideration was given or time spent on determining the causes of failure, or for that matter identifying the panels which might be structurally unsafe, primarily because techniques had not been developed by means of which unsafe panels could be economically and accurately identified.

1.1 CLADDING PANEL FABRICATION

As was mentioned above, a large number of system-built, large-panel, multi-storey buildings were constructed during the latter part of the 1960's. This industrial boom prompted many construction companies to move towards this form of construction. Records of construction indicate that over 160,000 dwellings have so far been constructed in Great Britain using large panel systems [2, 3]. The details of the number of multi-storey buildings of over four storeys can be found in Fig. 1.1.

The most commonly built wall panel in the pre-fabricating yards consisted of an inner leaf, which was connected to the external leaf through a system of ties. The external leaf and inner leaf were separated from each other by an insulating layer,

which was either polystyrene or cork. The inner leaf was the load bearing element in this assembly, and the structural loads were transmitted through it only. The main features of a precast sandwich panel are as detailed in Fig. 1.2 [4, 5]. Both the leaves are connected around the perimeter but for the structural connection between the two concrete leaves, goal-post ties of either delta-bronze or stainless steel were used. In certain cases ties of mild steel or phosphor bronze have also been used. The panels are cast face up. The load bearing leaf is cast first, with its required mesh of reinforcement and then the insulating layer of either polystyrene or cork is placed on top of that. Now the connecting ties are forced through the insulating layer into the still wet concrete below. Finally, the top or outer leaf is cast , with the mesh of reinforcement for the leaf being incorporated during casting. Panels of this type, that is, the sandwich panel for large panel system dwellings, especially for structures higher than four storeys, were built by many prefabricating companies, such as Bison, Reema, Wates, Jespersen, to name a few. As the basic structural and construction details of most of these panels were quite similar, the constructional details of a few types of large panel systems built by Reema is given below.

1.1.1 REEMA LARGE PANEL SYSTEM DWELLINGS

The Reema companies first housing contracts started in 1948. Three-storey flats were introduced in 1956 and multi-storey flats in 1958. A large number of Reema large panel system dwellings were built in the 1960s and early 1970s. As with most other systems, those produced by Reema were based upon large storey height precast reinforced concrete panels. The edge details of the panels and floor units forming cavities which are filled with in-situ concrete, producing a structure whose continuity is provided by reinforcement embedded in these joints. Reema produced

three basic systems, which were evolved and developed over a period of years, although with passage of time additions and variations have been made to these. The constructional details of these systems are given herein.

HOLLOW PANEL SYSTEMS

This system was used throughout the late 1940s, 1950s and early 1960s to build houses and flats up to four storeys high, although it is possible to use it for taller buildings (Fig. 1.4). The system comprises hollow panels having inner and outer leaves joined by vertical ribs. When this system was developed for multi-store dwellings (above four storeys), vertical steel reinforcement was bolted together to form a continuous load bearing structure. In later two-storey housing, it was the practice to form a solid head to the panels incorporating reinforcement as necessary and providing a tie in the columns, thus decreasing the quantity of in-situ concrete used. Initially, precast reinforced concrete beams were used to support a timber board floor, but later timber joists supported by joist hangers were used for compartment floors in flats.

The external wall panels of this system are made of a 225mm cavity construction comprising 37.5mm outer skin, 25mm inner skin and 162.5mm cavity. The panel is cast in dense concrete with right angle webs. The panels were unreinforced except for incorporation of steel lifting hooks, handling mesh, and steel reinforcement around window openings. The external finishes of the panels were mainly factory applied, such as, natural exposed aggregate using Derbyshire spar, pink limestone, grey or green Cornish granite, honey-coloured Cotswold stone, glass and china surfacing materials, stripped concrete and painted surfaces. These types of systems were mainly used for low rise buildings.

CONCLAD SYSTEMS

Reema introduced this system (sometime also known as Ribbed, Waffle or Coffered panel system) in the mid-1960s in response to the improved thermal insulation standards required by the 1965 Building Regulations. It was developed from the Hollow Panel system, and the two were used concurrently: Conclad for dwellings and Hollow Panel for public buildings. The Conclad system (Fig. 1.5, 1.6) comprises concrete external panels, strengthened by ribs on the inner face. Steel reinforcement protrudes into the cast-in-situ concrete panel (not present in the Hollow Panel system). The wall is dry lined with polystyrene-backed plasterboard, or with ordinary plasterboard that has foil-backed building paper behind it, secured with galvanised clout nails to preservative-treated softwood battens cast integral with the concrete ribs. Floors may consist of timber joists or concrete units supported by joist hangers, or hollow precast concrete floor panels.

The external wall panels consist of 175mm thick load bearing panels comprising 50mm concrete external skin with 125mm cavities and ribs. These were internally lined with 12.5mm polystyrene/9.5mm plasterboard laminate nailed to 50mm x 25mm tanalised battens cast into units. The external finishes were of either exposed aggregate or fair-faced concrete.

SANDWICH PANEL SYSTEM

This system was mainly used on buildings up to five storeys high where extra strength was required, as it is more expensive than the Conclad cladding panels but with similar thermal insulation properties. It consists of two concrete leaves connected by a regular system of ties, the intervening space being filled with expanded polystyrene (Fig. 1.7). Inner leaves of panels are of different thicknesses for load bearing or non-load bearing use. The external wall panels are normally

175mm comprising at base a panel of 75mm load bearing concrete inner skin, 25mm grade-one polystyrene, and 75mm concrete outer skin, while at the top of the panel there is a 50mm inner skin, 25mm polystyrene and 100mm outer skin.

OR

200mm concrete panel comprising a 100mm load bearing concrete inner skin, 25mm polystyrene and 75mm concrete outer skin connected with phosphor bronze ties.

OR

300mm concrete panel, comprising at base of panel a 200mm load bearing concrete inner skin, 25mm polystyrene and 75mm outer skin, while at the top of the panel, 175mm inner skin, 25mm polystyrene and 100mm outer skin.

Windows in all three cases are cast in. The external finish of the panel is mainly Quartzag with white cement. The system can be used for low, medium or high rise buildings.

CONTRAD SYSTEM

This system was introduced in 1969 to meet the demand for a system which combined the speed, standards and economy of industrialised building with the choice of traditional finishes and flexibility of planning of traditional low-rise housing. The whole system is based upon a 300mm planning grid and has a 2.6m floor-to-floor height. The Contrad system (Fig. 1.8) uses precast reinforced concrete corner units, L-shaped in plan, to form the inner leaf of low-rise crosswall houses. The external leaf of the gables is of brickwork, while prefabricated timber panel units fill in the front and rear walls.

The external panels of the system consists of the 89mm thick load bearing concrete internal skin to gable walls and separating wall ends, lined with 13mm fibreboard and skin coat plaster. Additionally a 61mm cavity and 112mm thick external skin of facing brickwork or reconstructed stone. The system is mainly used for low rise buildings.

1.2 DEFECTS IN CLADDING PANELS

In 1987 the BRE published the results of an investigation carried out on " The Structural Adequacy and Durability of Large Panel System Dwellings " [2]. The report investigated the possible causes of deterioration leading to failure of large panel system dwellings. Their findings on the precast wall panels are listed below:

1. " The precast panels themselves had generally been manufactured as specified, but in some cases the position of the reinforcement and occasionally the thickness of the 'skins' of sandwich panels were found to be incorrect. The consistency and accuracy of spacing of the reinforcement in the panels was often poor. In particular, low concrete cover to the reinforcement at edges of components and around window openings was found, which had given rise to local cracking and spalling due to the corrosion of the reinforcement as a result of the carbonation of the concrete ".

2. " In a few sandwich panels, lateral displacement of the insulating layer during panel manufacture had produced uneven thickness of concrete skins which effected adversely both the concrete cover to the panel reinforcement and the length of embedment of the ties between the skins ".

3. " The most widely reported defect in the construction of sandwich panels concerned the ties between the two skins of sandwich panels. Both the number of ties per panel and the material of manufacture were found to be at variance with the original specifications and on occasions differed from one building to another on the same site ".

As can be seen from the findings of the investigation carried out by the BRE, the single most crucial defect in the manufacture of these sandwich wall panels is the connection between the two skins, that is the load bearing leaf and the outer cladding leaf with the decorative finish, which could lead to a detachment. The investigation suggests that it is only the variance from the original structural design which has resulted in the problem. Details of a few of these faults can be found in Figs. 1.9 to 1.14.

At the same time I. A. Macleod et. al. published a report on the guidance of security of cladding on large panel concrete construction [6]. This report was prepared to provide guidance to structural engineers involved in appraisals of or remedial works to large panel concrete buildings of two or more storeys. it concentrates on the problems of cladding mainly because of the significance of this on safety. It includes a description of the panels, the defects in panels, possible testing methods and the remedial measures. The cross-section of the main sandwich panel investigated can be found in Fig. 1.15.

The most significant defects reported by I. A. Macleod et. al. were observed in ties, relating to either deterioration or positioning. Ties of four materials were identified-mild steel, phosphor bronze, manganese bronze and stainless steel. Out of these ties the manganese bronze ties were observed to have the greatest

deterioration, because of stress corrosion cracking due to the ties coming in contact with water, which acted as an electrolyte. This effect being enhanced in panels where cork based insulation was used. The positioning of ties was identified as another major defect. This related to either poor orientation, improper embedment, or poor bond.

Another defect observed and identified was the movement of the outer leaf due to inadequate structural connections between inner leaves and floors causing movement of the cladding. The deterioration of concrete, being another significant defect affecting the structural adequacy of the panels. This could be either due to carbonation of concrete, leading to corrosion of reinforcement with consequent cracking and spalling, cracking at corners, unrepaired cracks possibly during handling and erection, again leading to spalling and detachment due to water penetration, frost action etc.. Finally, exposed aggregate detachment has occurred frequently which can be attributable to weathering, inappropriate choice of type or shape of material or the workmanship when the panels were constructed.

The findings reported by Macleod et. al. were similar to the investigations carried out by the BRE and the importance of all these defects lies in the fact that they are all progressive. Some of the more commonly employed methods for investigating the cladding panels of large panel systems used were:

1. **Eddy Current Technology**: This is useful in location of ties and may also establish within limits the material of ties, as well as determining the distance from the surface. The method has its drawbacks because of interference that can be caused by foil-backed insulation board or close proximity of mesh reinforcement.

2. **Sonic Methods**: Very limited success was achieved through such techniques.
3. **Radiography**: A method that can be used quite successfully although the attendant regulations and other difficulties such as to use specialist contractors, evacuate property, locate approximate position of ties may prove onerous. It can be a most valuable tool for identifying accurately the location of ties prior to coring.
4. **Coring**: Provided that ties can be accurately located, useful information can be obtained by coring through both leaves of the panel, so that a complete section with the ties is removed. Extremely useful information such as quality of concrete, type of tie, positioning etc. can be determined. Important to secure panels prior to coring.
5. **Optical Probe**: Provided that the insulation can be removed, for example by using acetone in the case of polystyrene, the optical probe can be extremely useful in observing the interior of the panel and establishing conditions and location of ties. It might be quite important to replace the insulation as it probably plays a useful structural role.
6. **Direct Internal Observation**: Investigation of ties at window openings with the window frames removed is a useful way of establishing the location and condition of ties.
7. **Direct External Observation**: Such techniques are useful for detecting vertical and out-of-plane movements, but due to irregularities in joint widths at time of construction periodic inspections are necessary to establish any movement in a particular panel. The approach is quite useful in conjunction with other tests.
8. **Total or Partial Removal of Outer Leaf**: Used on certain occasions but subject to difficulties including disturbance to tenants, high cost and the

practical problems of removal without disruption of the structure and satisfactory reinstatement.

Macleod et. al. in their report recommend that wherever manganese bronze ties are identified the panel should be secured by additional fixings. For concrete it is recommended that suitable surface coatings may reduce the rate of carbonation and therefore increase the period before corrosion of reinforcement occurs. Alternative solutions include the complete over-cladding of the block, as this would not only eliminate water penetration problems but also remove the danger of detachment of aggregate and parts of the panel. Of course, it is necessary to ensure that the original panels were adequately tied. Secondly rendering on top of existing cladding or removal of the outer panel with subsequent replacement of an alternative.

Green [1] has also described some of the possible defects in precast large panel structures, such as poor tie orientation and lesser number of ties than specified used. The paper describes the possibility of remedial measures through the use of repinning bolts. Three possible repinning techniques have been recommended, which are; cantilever bolt, located horizontally and fixed by expansion sleeves to the inner and outer leaves, with the load transfer taking place by bending and shear in the cantilever; use of a large diameter metal dowel, located at 10 degrees to the horizontal and fixed with cementitious grout (Fig. 1.16). Load transfer to the main panel being through shear in the dowel; and the third method involved the inclined tie expansion fixing, which was achieved by inclining the axis of the bolt at 45 degrees to the plane of the panel. Tests carried out on the third type indicated towards the efficiency of the system. The work described, shows the possibility of fairly inexpensive remedial measures for the large panel systems.

Green [1] and Macleod et. al. [6] also observed the following defects in the large panel systems:

1. When manufacturing these precast large panel systems, not enough care was given to the placement of ties. Because of this a large number of panels were fabricated with ties which were poorly oriented, the details of these can be found in Fig. 1.3. This poor orientation resulted in improper connection between the two leaves of the panel and the ties were unable to sustain the cyclic load to which the panel was subjected.

2. Also, it was observed that the rapid curing methods used for the concrete, during fabrication of the panels in the manufacturing yard, resulted in poor bond between concrete and the ties. This once again contributed towards the ties not being able to sustain the applied loads.

3. Another defect that came to light was the corrosion of the ties, which contributed towards the failure of these ties. Under aggressive environmental conditions the cracking of the concrete exposed the ties to aggressive corroding agents, which led to a reduction of their strength.

4. Finally it was also observed (as in the BRE investigation) that panels contained a lesser number of ties, than specified by the original design. Most panels were designed with about twenty ties for 8.5 square meters of surface area, but a large number of panels contained a lesser number of ties.

These investigations highlighted the general structural damage that has occurred in the panels with passage of time and has also identified the variance in construction

from the original design of the wall panels. The possibility of detachment of the cladding leaf because of the inaccurate number of goal-post ties being used, was seemingly the most crucial structural damage as identified by these surveys, and the aim of this study was to look into this problem area. The practicalities of invasive testing methods applied to occupied buildings render them undesirable. Clearly an assessment of the integrity of cladding is needed through non-destructive techniques.

1.3 NON-DESTRUCTIVE TESTING

In the preceeding article a few of the non-destructive testing techniques applied for determining the defects in large panel systems have been highlighted. The present article deals with a few other possible methods that can be employed for similar purposes. The term "non-destructive testing" is used as a general name given to all test methods which permit testing or inspection of material without impairing its future usefulness. From an industrial viewpoint, the purpose of non-destructive testing is to determine whether a material or part will satisfactorily perform its intended function. The primary purpose of a non-destructive inspection is to determine the existing state or quality of a material, with a view to acceptance or rejection. By use of non-destructive testing methods and techniques it has been possible to decrease the factor of ignorance about material without decreasing the factor of safety in the finished product. The use of non-destructive testing has been and is being recognised as a means of meeting demands for better products, reduced cost and increased production.

The art and science of non-destructive testing are very old. Nearly every form of energy has been utilised in non-destructive testing. Likewise nearly every property of the materials to be inspected has been made the basis for some method and technique of non-destructive testing. These can be broadly divided into the following groups:

Visual	Acoustic
Pressure and leak	Magnetic
Penetrant	Electrical and electrostatic
Thermal	Electromagnetic induction
Radiography	Miscellaneous

The details of these various groups and the different methods of testing can be found in many standard texts such as [30, 31], in this chapter for the sake of completeness a few of the more commonly used methods are described.

1.3.1 VISUAL TESTING

Visual inspection is probably the most widely used of all the non-destructive tests. It is simple, easy to apply, quickly carried out, and usually low in cost. Because of this simplicity in use it should never be ignored and even though a specimen is to be inspected using other non-destructive testing methods it should be given a good visual examination. The basic principle used in visual non-destructive tests is to illuminate the test specimen with light, usually in the visible region. The specimen is then examined with the eye or by light sensitive devices. As in the case of all non-destructive tests, proper application and correct interpretation of the results are essential to their usefulness and success.

1.3.2 PRESSURE AND LEAK TESTING

In pressure and leak testing, defects are revealed by the flow of gas or liquid into or through the defects. The simplest and most commonly used pressure test is a hydrostatic test. In this test the pressure within the test object (hollow) is made greater than the external pressure. The hydrostatic pressure should be applied gradually and the test pressures to be used are often stipulated in codes or specifications. In addition to the hydrostatic test, the other forms of pressure and leak testing are the bubble test, and the halogen leak test.

1.3.3 LIQUID PENETRANT INSPECTION

Penetrant inspection is a non-destructive testing method that can be used for the detection of surface discontinuities or flaws which extend to the surface of the test specimen. The use of penetrants may be considered as an extension of visual inspection. Very few discontinuities are revealed by penetrants that cannot be found by experienced visual inspectors. Penetrants, however, delineate a discontinuity to a much greater extent, making the inspection much less dependant on the human element. Thus, making the method more adaptable to production testing by increasing the general reliability and speed of inspection.

1.3.4 THERMAL METHODS

The basic principle utilised in thermal tests is to apply heat to the test specimen and to measure or observe the resulting temperature distribution. Flaws alter the temperature distribution on or in the specimen. The heat may be applied by direct thermal contact with a heat source, by electrical current heating, by induction heating or by infrared heat sources. The resulting temperature distribution may be detected by use of temperature indicating substances.

1.3.5 RADIOGRAPHY

Radiography is a method of non-destructive testing which uses X-ray or gamma radiation. In order to distinguish this type of radiation from other types of radiation such as visible sound and light, X-rays and gamma rays are sometimes referred to as "penetrating radiation". Radiography is one of the oldest non-destructive tests, having been used since the early 1920s. Today it is one of the most widely used of all non-destructive tests. The basic principle being that the intensity of the penetrating radiation is modified by passage through material and by defects in the material.

1.3.6 ULTRASONICS

Ultrasonic techniques are finding increased uses and importance in the field of non-destructive testing. Striking a specimen and listening for the characteristic "ring" has been used as a means of detecting flaws. The ringing note emitted by a steel (or concrete) specimen containing a crack is dull and harsh compared with the note emitted by an identical "good" specimen. This "ringing" technique will detect only gross defects. With the development of reliable methods for generating and detecting ultrasonic waves, small defects can now be found. This is simply due to the fact that the wavelength of ultrasonic waves is approximately equal to the size of the defects to be found. The method is extremely effective for metals especially, as most metals because of their good properties readily transmit ultrasonic vibrations. If discontinuities exist, a measurable scattering or reflection will occur because of the acoustic mismatch. Vibrational waves which have a frequency above the hearing range of the normal ear are called "ultrasonic" waves. Because of their short wavelength, ultrasonic waves travel essentially in a straight line. It is this property which makes ultrasonic waves so useful for locating defects. Several different techniques have been used in ultrasonic testing such as:

pulse echo, transmission, resonance, frequency modulation, and acoustic image. A couple of these are explained herein.

PULSE ECHO: In the pulse echo technique a pulsed ultrasonic beam is sent through the couplant into the specimen. At the opposite face, the beam is reflected and the echo picked up by a transducer. The transmitting transducer can serve as the receiving transducer, or a separate transducer can be used. A discontinuity or flaw in the specimen will also send back an echo. The time intervals that elapse between the initial pulse and the arrival of the echoes are measured. In the echo pattern a flaw can be recognised by the relative position and amplitude of its echo. There may also be a number of multiple reflections displayed in the echo pattern. The resolution of this technique depends on the duration of the ultrasonic pulses. The shorter the duration of the pulse, the thinner the specimen that can be successfully tested.

RESONANCE: In the resonance technique of ultrasonic testing a tuneable variable frequency continuous wave oscillator is used to drive a transducer. The oscillator is turned through its tuning range. If the specimen has thickness resonant frequencies within the tuning range of the oscillator, the specimen will vibrate in resonance. When resonance occurs, there is an increase in the energy drawn by the transducer. This increased energy can be indicated by a suitable instrument. Thickness resonance occurs whenever the thickness of the specimen is equal to an integral number of half wavelengths of the ultrasonic wave.

1.3.7 EDDY CURRENT

Eddy current techniques can be used to inspect electrically conducting specimens for defects, irregularities in structure and variations in composition. Applications

of eddy current testing include metal sorting, detection of cracks, voids and inclusions, measurement of plate or tubing thickness. Eddy current tests are most effective for locating irregularities near the surface of the specimen. the method works on the basic principle of when a coil carrying alternating current is brought near a metal specimen, eddy currents are induced in the metal by electromagnetic induction. The magnitude of the induced eddy currents depend upon the magnitude and frequency of the alternating current; the electrical conductivity, magnetic permeability and shape of the specimen; the relative position of coil and specimen; and the presence of discontinuities or inhomogeneities in the specimen. The eddy currents induced in the metal set up a magnetic field which opposes the original magnetic field. The impedance of the exciting coil or any pickup coil in close proximity to the specimen is affected by the presence of the induced eddy currents. The path of the eddy currents is distorted by the presence of a defect or other inhomogenieties. The apparent impedance of the coil is changed by the presence of a defect. This change in impedance can be measured and used to give an indication of the defects present.

1.3.8 DYNAMIC TESTING

Dynamic testing involves the striking of a specimen and monitoring the response. The way in which a specimen is struck determines whether the fundamental, a harmonic, an over-tone or a combination of frequencies is produced. Every specimen has certain characteristic frequencies at which it can be made to vibrate. These frequencies are functions of the size, shape, mass, elastic properties, and mode of vibration produced in the specimen. Several methods of starting vibrations can be used, such as impact by a hammer blow, mehanical coupling of the specimen to a subsidiary vibrator or the electromagnetic method for magnetic materials.

More recently the application of dynamic testing of structures has been rapidly expanding to incorporate more areas, and researchers have been trying to take advantage of this method to predict damages and deterioration that may be occurring in them. The following article aims towards highlighting the works of different researchers who have successfully applied the method of dynamic testing to determine the natural frequencies and the associated mode shapes of various civil engineering structures.

1.3 REVIEW OF LITERATURE

Use of different non-destructive tests for determination of structural adequacy and defects present have been present for years. But it has been only in the recent past that use of dynamic testing is gaining importance, although this has been used for the monitoring of offshore rigs for quite sometime as shown by Kenley and Dodds [7] and Loland [8]. The dynamic testing of an offshore platform mainly consists of measuring the natural frequencies of the structure above the waterline by means of accelerometers, while subjected to a wind and wave loading. The natural frequencies of the structure are mainly dependant upon the mass, stiffness and geometry of the structure. Any deterioration in the structure, such as change in stiffness or mass is recognised through the change in natural frequency and the nature and location of damage can be identified through them as well as the associated mode shapes.

Various methods have been employed for non-destructive testing of structures and materials, with the coin tap method being one of them. Peter Cawley [9] has described the results of using a high frequency version of the coin-tap method of

non-destructive testing. The technique involves the tapping the structure with a very light striker of mass typically below 1g and monitoring the sound produced by the tap. Cawley has shown how this approach is better suited on structures fabricated from metals or un-reinforced plastics as reported in his earlier work [10, 11, 12]. The coin-tap method being one of the oldest methods of non-destructive testing and is regularly used for testing laminated structures, honeycomb constructions and bonded joints. The test requires an operator to tap each point of the structure to be inspected with a coin and to listen to the resulting sound radiated by the structure. It is found that defective regions sound "dead", and can therefore be identified. Cawley carried out tests on three 10mm thick aluminium sheets with flat-bottomed holes of different depths (Fig. 1.17). A 5.5mm diameter steel ball (mass 0.68g) was rolled down a perspex chute, which was angled at about twenty degrees to the vertical, from a height of approximately 70mm. The resulting sounds were captured by a digital oscilloscope, which was then passed through a micro computer to give a measure of the sound produced by the impact. From these investigations Cawley concluded that the results on the aluminium panels show that the high frequency version of the coin-tap test, which uses a light striker in order to excite the membrane resonances of the layer above a defect, is significantly more sensitive than the standard version, particularly for the detection of the deeper defects.

Use of non-destructive testing techniques on cladding panels, for determination of defects have been regularly applied, but very little evidence is available on the use of dynamics on such panels. Response measurements on glass cladding panels have been reported by Craig and Goodno [13] who have presented results of dynamic response tests carried out on glass cladding panels (Fig.1.18a). Tests were performed on full scale test fixtures capable of supporting a 4.9m x 2.5m section

of cladding (Fig. 1.18b). The rear of the fixture being sealed tight around six large 1.4 meters square pistons, which were driven by servo controlled hydraulic actuators to produce fluctuating pneumatic pressures of up to 1.2 kPa amplitude, and 20 Hz frequency about mean pressures up to 2.4 kPa. The cladding panel attached to the fixture consisted of a single storey section including mullions, muntins, spandrel framing, glazing materials, and four double-pane vision lights as obtained from the fabricator. For these tests the strain gauge and linear variable differential transformer (LVDT) was used for the dynamic response measurements, with the strain gauges being relatively inexpensive and simple to use being employed as the primary dynamic response transducers. With the primary objective of the dynamic response testing being to determine the basic modal characteristics the excitation was through the use of band-limited random and transient forcing functions which excited all the modes of interest concurrently. This was done through a closed-loop servo controlled hydraulic system to produce time varying pneumatic pressures across the test window with the simultaneous application of an impulse applied by hand using a large mallet. The authors demonstrated the success of the approach through the good comparisons achieved between the measured frequencies and the predicted ones. Also reported was the significance of the detection of primed modes, in which the two glass panes of the panel moved in opposite directions.

Present day developments in the use of computers for structural design and analysis have impressed upon the need for greater knowledge of material properties and the actual behaviour of structures. These can only be obtained by carrying out tests, either static or dynamic on the as-built structures. Experience has shown how much more expensive tests using static loads can be, where as applications of dynamic loads, especially transient, can be a fairly simple exercise.

It should be mentioned here though that the collection and processing of the response data is a lot more complicated and requires a great deal of skill and experience if errors are to be avoided. A lot of standard texts explaining the details of modal testing and the extraction of different modal parameters are available [35, 36, 37, 38]. The success of such an approach is mainly dependant upon the accuracy of being able to excite the specimen in a particular mode. Either steady-state forces, such as produced by sinusoidal vibrators or transient forces, such as the impact of a hammer blow, can be used for determining the modal characteristics of a specimen. The success of using transient forces for extracting the natural frequencies and modal shapes of various reinforced concrete structures, have been shown by quite a few authors.

Maguire and Severn [14] have demonstrated how hammer testing can be successfully applied to assess the dynamic properties of prototype structures. Tests were performed on three different structures:1) a 65m concrete chimney in Bristol (Fig. 1.19); 2) elevated piled tanks at Redcar (Fig. 1.20); 3) bridge beams at Basingstoke (Fig. 1.21). For case (1), the chimneys had a mass of 1,440,000 kg, and hammer tests were conducted in still conditions and ambient vibration (wind) tests were carried out on windy days. The response was measured through the use of accelerometers, and the first three cantilever type modes were observed. The second case consisted of hammer tests conducted on two elevated piled tanks at Redcar. The tanks had a mass of 860,000 kg and 5,510,000 kg respectively. Two modes of vibration were measured through the response observed from eight accelerometer locations. Tests were also carried out on four simply supported precast post-tensioned concrete bridge beams at Basingstoke. Each of the beams weighed approximately forty tons and effectively spanned 27.6m. For these beams the first three modes of vibration for the undamaged state were determined.

Maguire and Severn demonstrated that given sensitive instrumentation, hammer testing is able to determine the structural dynamic characteristics of various structures and that hammer testing can provide a quick and accurate method of assessing as built structural dynamic properties

Pavic, Williams and Waldron [15] have presented the development of a finite element model for a post-tensioned concrete floor and compared results obtained from it to results obtained from a field test. The field tests were carried out on the new Wycombe Entertainment Centre car park, located in the centre of High Wycombe, U. K.. The bay was 12.05m long by 7.3m wide with a slab thickness of 210 mm. Prestressed band beams of 665mm width and 650mm depth ran along the column lines in the longer direction (Fig. 1.22). The slabs were tested for their dynamic properties by inducing vibrations in the slab through the means of an instrumented 5.4 kg hammer, and the response was measured with an accelerometer. The tests were carried out by dividing the test bay into a 5 x 5 grid of equally spaced points. The accelerometer was attached to a single grid point on the floor and the hammer was successively moved from point to point, with the floor being impacted at each location. The analysis was performed via a spectrum analyser and the transfer function and phase together with the coherence between the two signals at each grid point was determined. The first five natural frequencies were determined in this manner, and the results obtained from the finite element model showing a fair comparison with them (Fig. 1.23). Pavic, Williams and Waldron have also demonstrated how the static and dynamic analysis of post-tensioned slabs require different assumptions. It was further observed that closely spaced modes made for extremely difficult observation from the field tests.

Brownjohn, Dumanoglu and Taylor [16] have showed how the dynamic characteristics of a 50m span pedestrian suspension footbridge (Fig. 1.24) can be experimentally determined through hammer impacts and excitation by pedestrians. They demonstrated how adequate descriptions of vibration characteristics of flexible structures can be obtained without artificial forcing. Their investigations have indicated the success of determining the various modes (such as vertical, lateral and torsional) through simple vibration methods. The testing equipment used included accelerometers located at the end points of the deck cross-beams, corresponding to nodal points in the analytical model. The exciting equipment consisted of a 13 lb. sledgehammer instrumented with a force crystal, in addition to ambient excitation from pedestrians. Signals were recorded on a four channel FM tape recorder and converted to the frequency domain by a two channel signal processor. The testing consisted of initially determining/estimating the likely natural frequencies of the bridge in vertical, torsional and lateral vibration, when under the influence of force input by the pedestrians. Once the likely natural frequencies were established, the response was measured through transient excitation provided by a hammer blow. The experimental results were compared to the analytical ones, and showed a fair comparison (Fig. 1.25), with the model under predicting by generally less then ten percent. The possible sources of error suggested by the authors mainly point towards the lower stiffness used in the analytical model because of improper restraint conditions; the contribution of the asphalt towards the stiffness not being taken into account; and the value of the Young's modulus of concrete being uncertain. The major problems encountered during testing and analysis of data included problems associated with amplifiers and cabling used with accelerometers. Modes closely spaced were difficult to identify and distinguish from each other. The major conclusions drawn were that the dynamic characteristics of relatively small bridges could be determined as long

as proper instrumentation was used, and that the comparisons with the numerical model would be viable as long as structural detail is included.

Hearn and Testa [17] have reported the non-destructive inspection of structures by modal analysis of vibration response. They studied the dependence of natural frequencies and modal damping coefficients on deterioration in structures, and have shown how the magnitude of change in natural frequencies is a function of the severity and of the location of deterioration in structures. Tests were performed to explore the effect of damage on modal parameters, on a four member welded steel frame (Fig. 1.26) which was subjected to cyclic loading, and modal parameters were monitored as progressive damage occurs by fatigue cracking, and on wire ropes under constant tension are damaged by transverse sawcuts and changes in the modal parameters are measured. The authors have demonstrated how the changes in natural frequencies provides a quantitative locator of damage for the welded frame, whereas for the wire ropes (which are insensitive to changes in natural frequencies), modal damping is used as a damage indicator. Comparisons between the experimental and the analytical results, derived from a perturbration of the equation of motion demonstrated how measurement of changes in mode shapes due to damage is not necessarily required for modal analysis inspection.

The problem of detecting a structural fault on the basis of measured dynamic characteristics can be regarded as one of pattern recognition. Measured data from the possible damaged states of a structural assembly, such as a sandwich panel, must be distinguishable from each other as well as from the undamaged system. Classical techniques have been applied to the problem of fault detection for quite some time as shown by Cawley and Adams [18], and more recently Sammam,

Biswas and Pandey [19]. In recent times, NEURAL networks have established themselves as an extremely powerful tool in identifying damage location. A number of authors have adopted this approach quite successfully and achieved fairly good comparisons with experimental results. Worden, Ball and Tomlinson [20] have shown how a neural network can be trained to report the position of a fault in a framework structure. With their work, based upon that of Kudva et. al. [21], they have demonstrated how a network trained on data from finite element simulation of the structure can successfully locate faults in the framework itself. The experimental structure used was an essentially two-dimensional cantilever latticework, mounted rigidly to a support at one end with its major axis horizontal and minor axis vertical and measuring approximately 1m x 0.25m. The lattice comprised of 19 members, arranged into four equally-sized, cross-braced square bays. Each member being made from 25.4cm x 6.4mm aluminium strip. Strain gauges were used for measuring the response and were located at the mid-spans of all members and on both sides. The strains being measured under a constant preload and three additional loads applied to each pin joint. Similar data sets were obtained by removing each of the members successively in turn. The results were then compared with results obtained from a finite element simulation of the framework established using the package LUSAS. The authors demonstrated from their results that the comparisons between measured strains and the predicted ones showed excellent agreement.

Worden and Tomlinson [22] have also shown how neural networks can be trained to locate the damage in a structure through predictions obtained from a finite element simulation, when considering features such as the first and second mode shapes of structures such as a cantilever beam and plate. The authors using dynamic test data as features, and considering mode shapes rather than

frequencies, as in their opinion they are more prone to suffer local changes in the presence of localised damage. The beam used was made of aluminium and had dimensions of 920mm x 50mm x 12.5mm, and the first five natural frequencies and mode shapes were obtained. The experimental and predicted results were again shown to be in good agreement. Similar results were achieved for the aluminium cantilevered plate having dimensions of 300mm x 200mm x 2.5mm. Although, the applications of Neural networks are still limited and not fully explored in the field of civil engineering, especially in damage location, more and more researchers are showing its usefulness as a fairly powerful tool.

A few other researchers have studied the effect of defects on the dynamic characteristics of simply supported reinforced concrete beams. Tourk [23] studied the effect of the presence and propagation of cracks in concrete, on the dynamic response. Tests were performed on nine reinforced concrete beams having dimensions of 1300mm x 50mm x 75mm. The beams were subjected to static third point loading in addition to dynamic loads applied through a magnetic vibrator at mid-span. Tourk found that natural frequencies decreased exponentially and the damping ratios increased with the increase in the static load. The experimental results did not compare well with the analytical results and this was put down to the incorrect idealisation of the analytical model. Sim [24] used the same experimental set-up but, improved the analytical model by remodelling the cracks in the finite element model. It was found that the natural frequencies decreased as the cracks increased and a better agreement between the experimental and analytical results was achieved. Hashim [25] using a similar set-up but different excitation forces tested eight singly and doubly reinforced concrete beams. His results showed that static loading affected damping and also that the natural frequencies decreased as the beams approached failure. Tan [26] examined under,

balanced and over reinforced concrete beams. The test set-ups were similar to the ones used by Tourk, Sim and Hashim, but instead of applying steady state vibration, impact tests were carried out. The results indicated good relationship between the experimental and predicted values. Priosulistyo [27] investigated the dynamic response of reinforced concrete beams as they were loaded to failure (Fig. 1.27). the beams investigated had built-in defects of cracks and partially unbonded reinforcement. The test specimens were subjected to static and steady state vibration loads. Priosulistyo concluded that the defects present in the reinforced concrete beams could be identified from the changes in the dynamic characteristics if proper digital signal was used.

Signal processing plays a significant and important part in correctly determining the dynamic parameters. It includes the problems of digitising data, Fourier transformation and filter designs. These subjects are covered extensively in many standard texts [28, 29, 30, 31] and shall not be discussed here.

1.5 SCOPE OF PRESENT INVESTIGATION

The present research was aimed towards the development of non-destructive experimental techniques which would enable the engineers to determine the structural integrity of a particular panel and at the same time allow them to locate and detect the type of structural damage present in the panel. To achieve this aim, it was decided to use the dynamic properties of the panels, as it was perceived that the changes occurring in the natural frequencies, depending upon the structural variances, would give an indication of the extent of damage present. The research was aimed towards initially developing a numerical model based upon a typical, undamaged panel and obtaining the results of its dynamic characteristics, such as

the natural frequencies and the associated modal shapes. These properties were then to be compared to similar results obtained for panels having different extent of damage and varying number of goal-post ties and the pattern recognition established. Once these variations in the natural frequencies and the modal shapes had been identified, they were to be used as the basis of the experimental models and varified through experimental procedures.

As the primary objective of the research was the development of a workable experimental model which could be applied with efficiency and economy to in-situ panels, full-scale experimental models were opted for. The complications associated with the dynamic testing of panels of this size and stiffness were given due consideration. Recent developments in the field of dynamic testing of reinforced concrete structures certainly leads us to recognize the relative attractiveness, in ease of application and success in determining the dynamic characteristics of these structures through simple non-destructive tests, which can be used to predict with a fair degree of certainty the damage present in them .

The thesis describes the results of the present investigation, carried out on the dynamic characteristics of precast wall panels and, the success of the approach towards the development of a relatively simple procedure for determining damage location in such panels. The panels investigated were similar to the sandwich panel system described earlier (article 1.1). It is divided into two basic parts: numerical and experimental.

Chapter 2 gives an insight into the basics of dynamic analysis and discusses the various approaches for determining the dynamical response of a structure with a

single degree of freedom. It also gives details of the properties and the numerical analysis of the wall cladding panels under investigation.

Chapter 3 contains the results of the numerical analysis. The models were analysed for their natural frequencies for the first six modal shapes through the finite element program FLASH [34]. The numerical models were analysed for these dynamic characteristics for different material properties, with the variable being mass, Young's modulus of elasticity and Poisson's ratio. The results of the analyses are presented in tabular and graphical form.

Chapter 4 gives details of the experimental program and the test specimens in addition to explaining briefly modal testing techniques. Finally, the experimental results as well as the comparison between them and the numerical models and the conclusions drawn are presented in chapters 5 to 7.

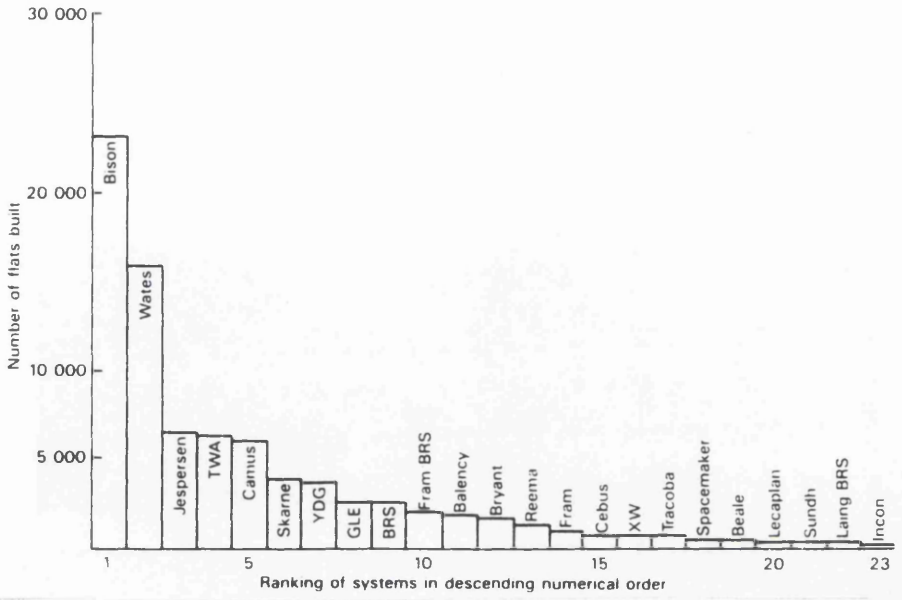

Fig. 1.1: Number of flats in multi-storey buildings constructed from different large panel systems.

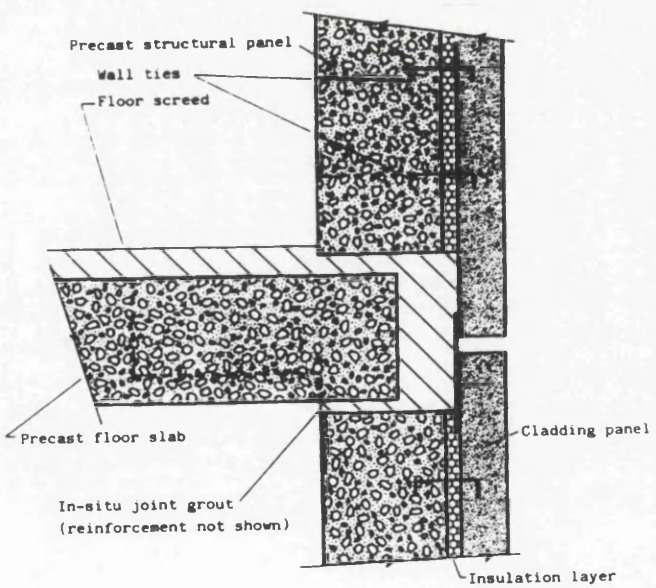

Fig. 1.2: Cross-section of external wall panel.

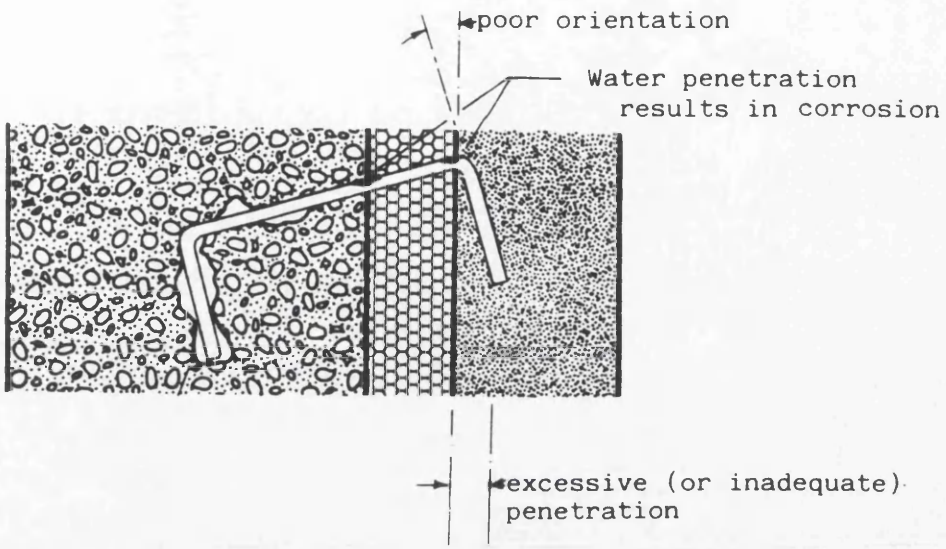

Fig. 1.3: Possible causes of failure of ties.

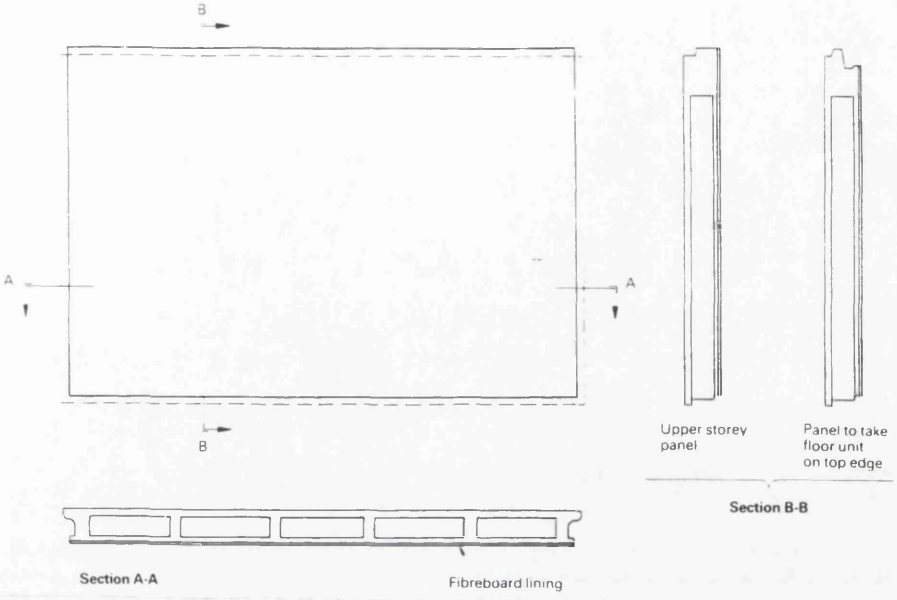

(a) External wall unit.

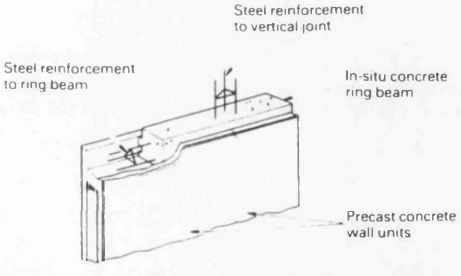

(b) Construction of in-situ concrete ring beam.

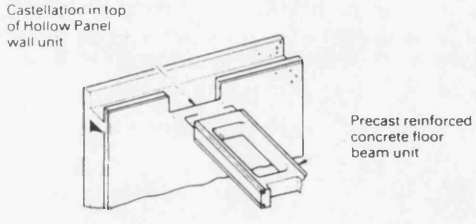

c) Construction of joint between floor unit and wall unit.

Fig. 1.4: Details of the Hollow Panel System.

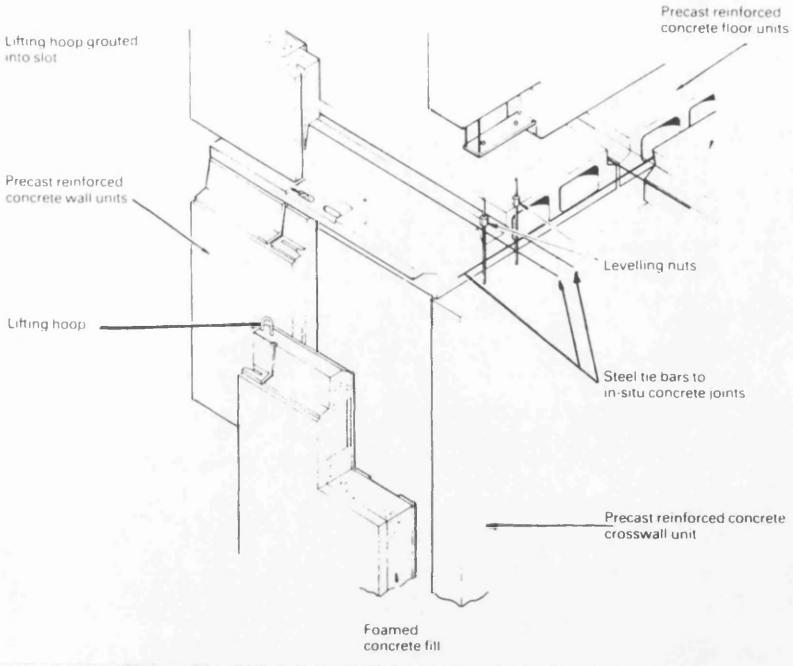

(a) Constructional details of the system.

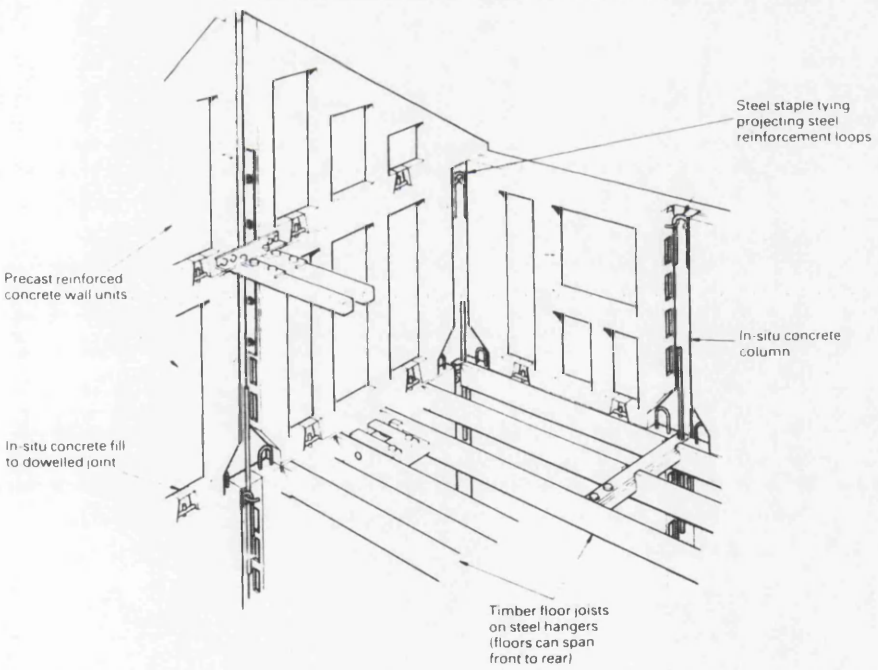

(b) Constructional joints in the system.

Fig. 1.5: Details of the Conclad system.

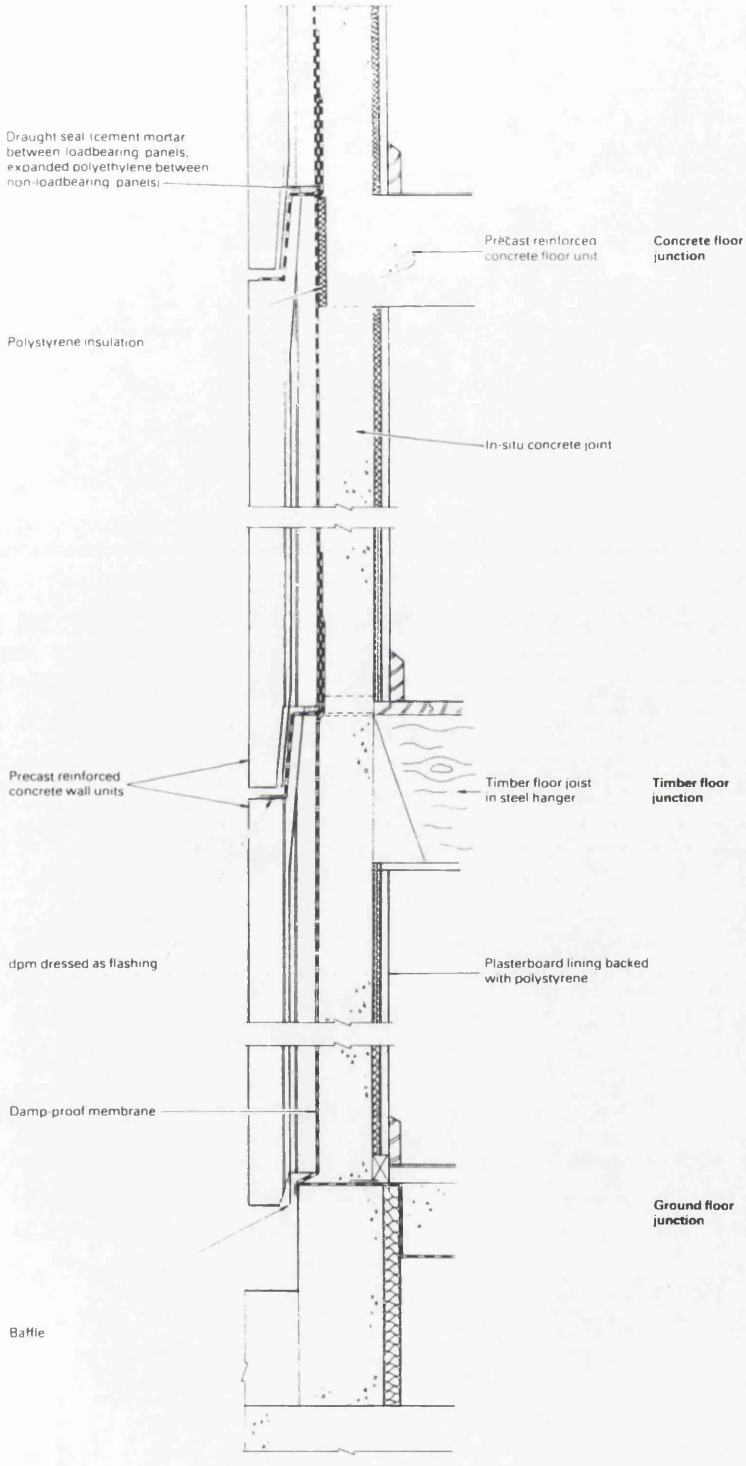

Fig. 1.6: Details of constructional joints used in the Conclad system.

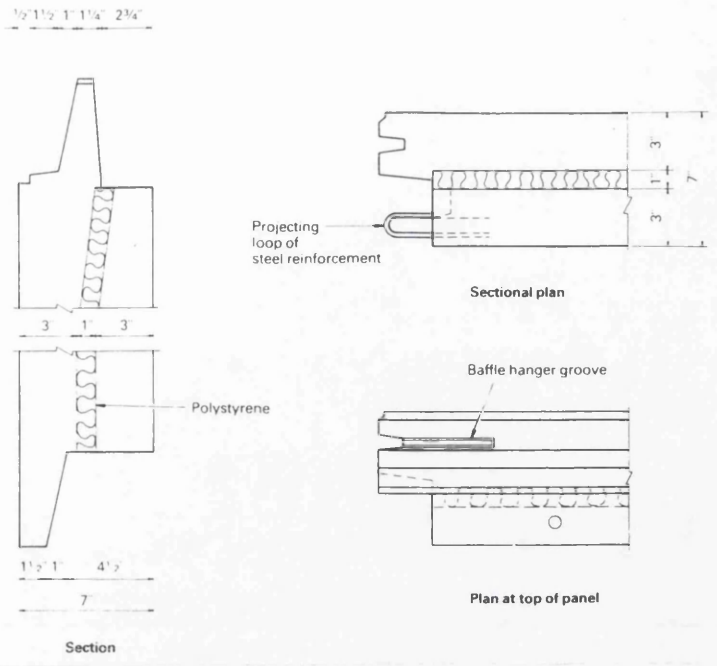

(a) External Sandwich panel wall unit.

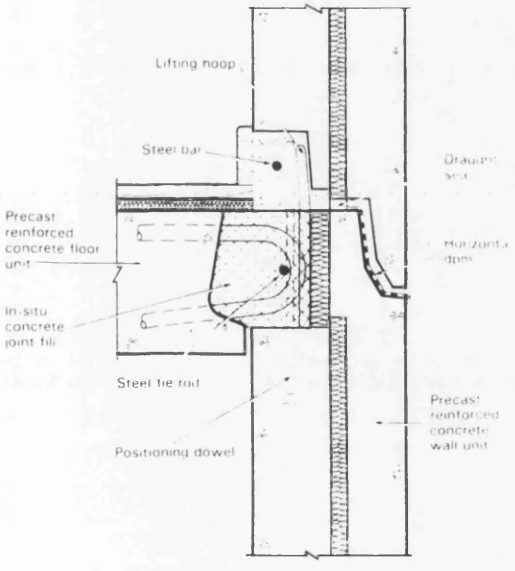

(b) Constructional joints used for the Sandwich panel.

Fig. 1.7: Details of the Sandwich panel of the Conclad system.

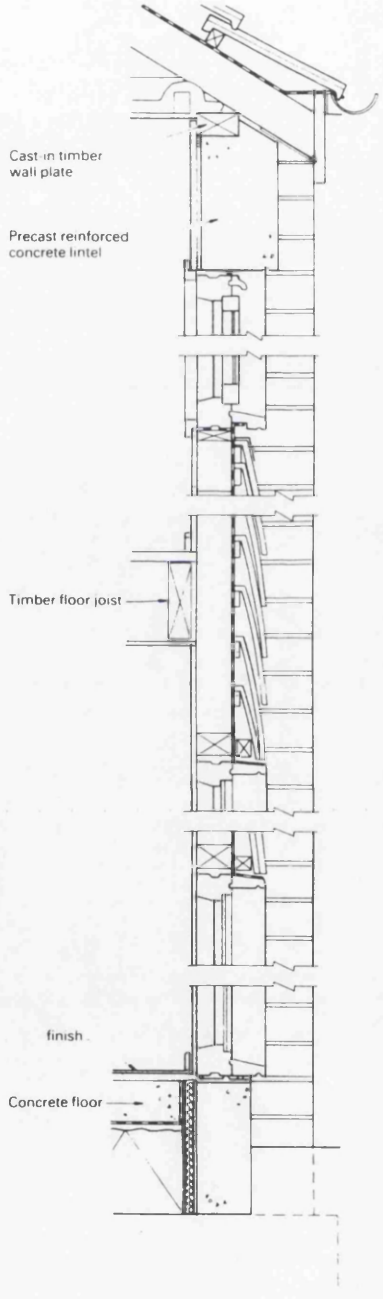

Fig. 1.8: Constructional details of the Contrad system.

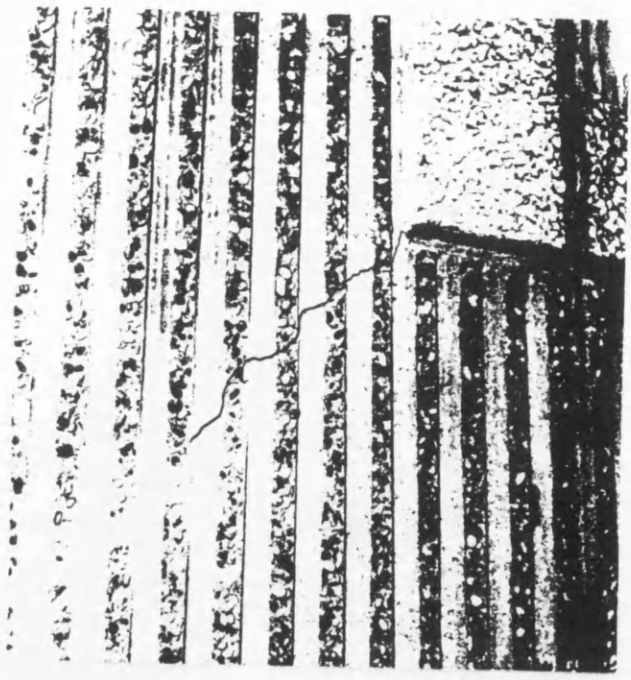

Fig. 1.9: Diagonal cracking originating from corner of window opening.

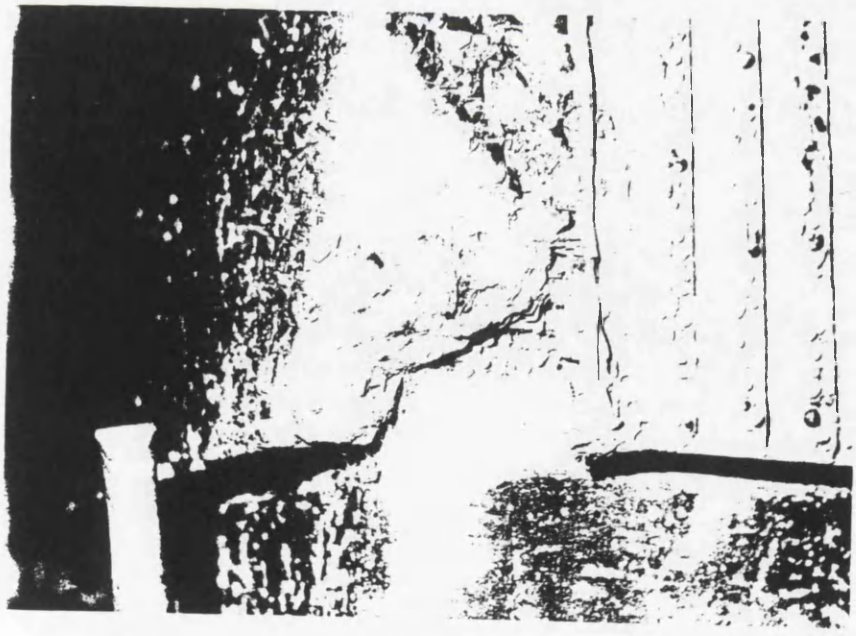

Fig. 1.10: Failure of factory repair to panel (Bison).

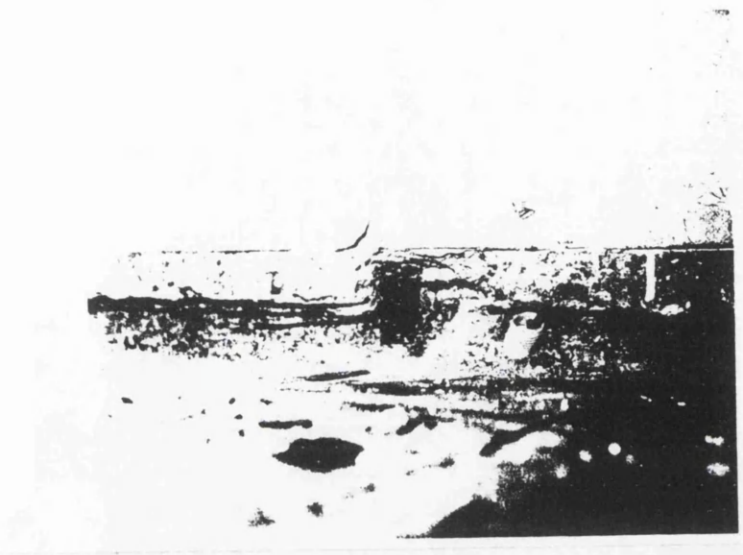

Fig. 1.11: Missing dry pack; support provided by levelling bolts.

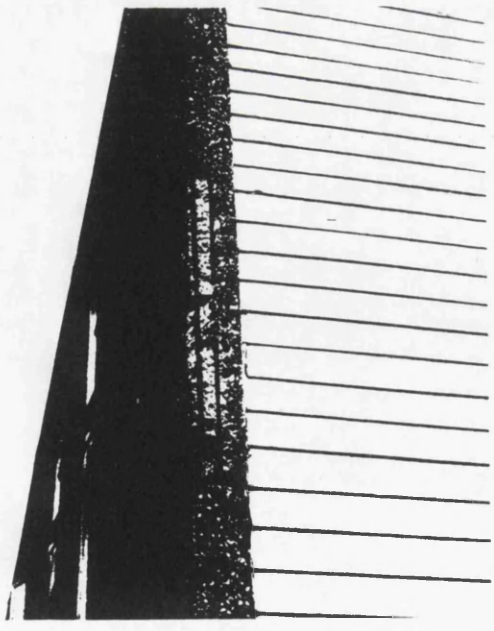

Fig. 1.12: Spalling of concrete associated with reinforcement corrosion.

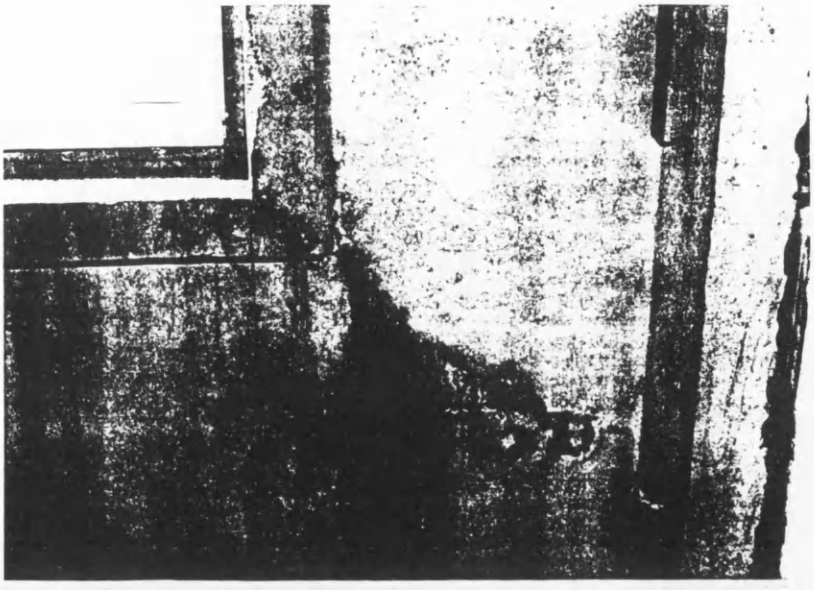

Fig. 1.13: Rain penetration through cracking at window opening.

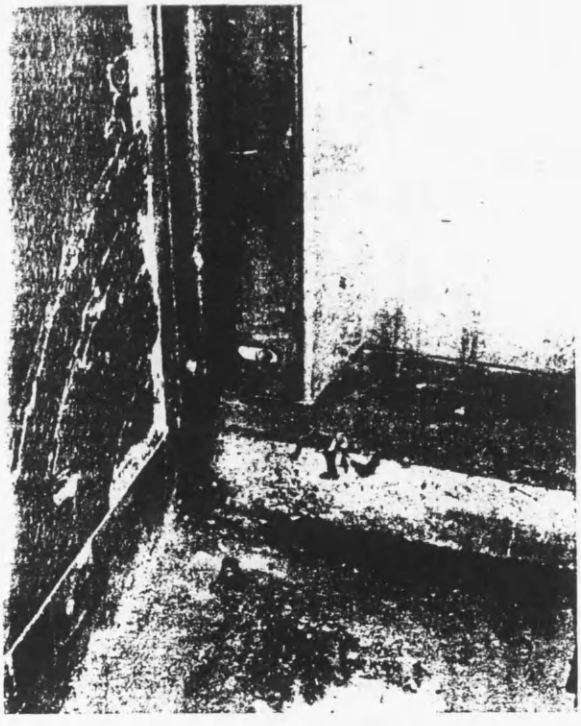

Fig. 1.14: Omission of bolts from connection plates.

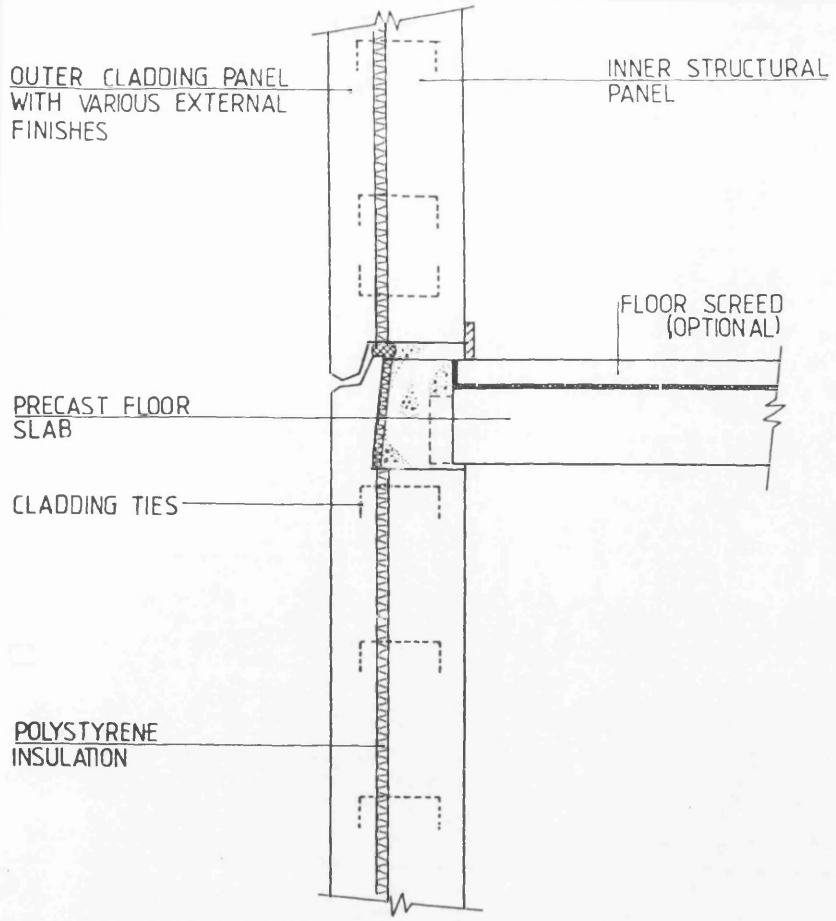

Fig. 1.15: Typical cross-section through cladding panels.

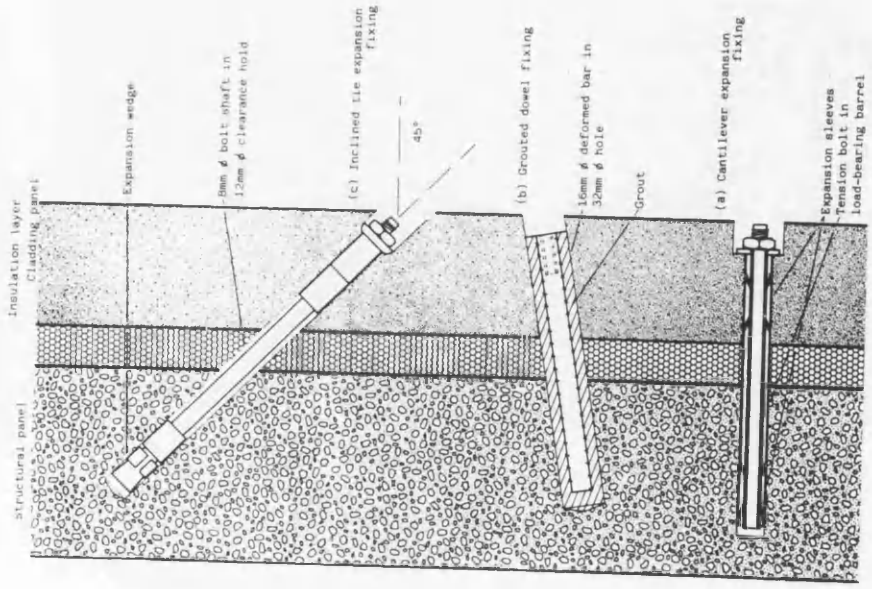

Fig. 1.16: Various repinning approaches.

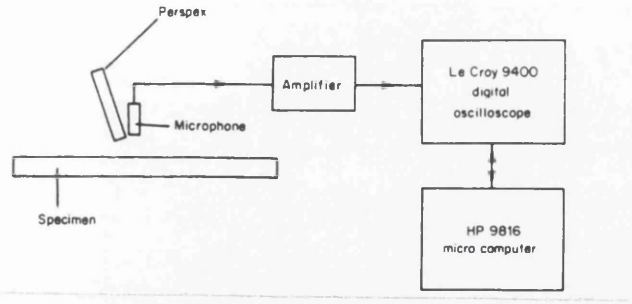

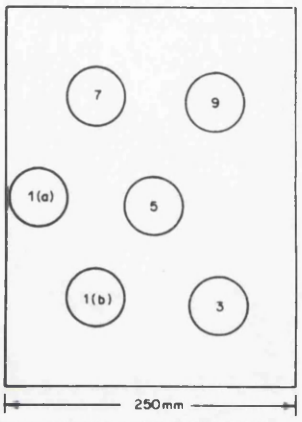

(a) Schematic diagram of test set-up. **(b) Aluminium plate investigated.**

Fig. 1.17: Coin-tap investigations of Cawley.

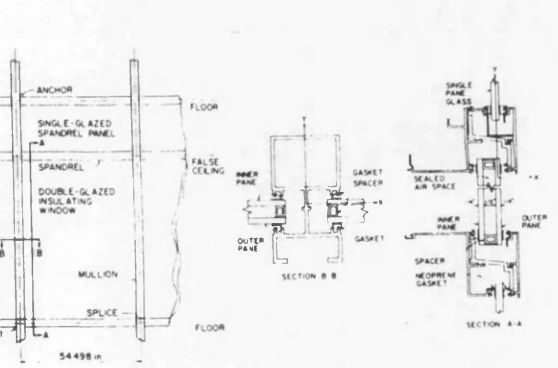

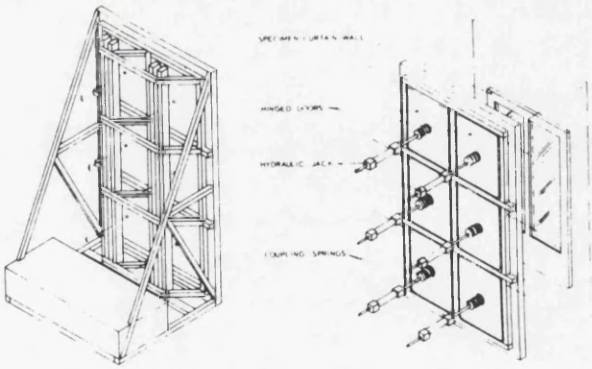

(a) Cladding system **(b) Laboratory test fixture.**

Fig. 1.18: Glass cladding panels investigated by Craig and Goodno.

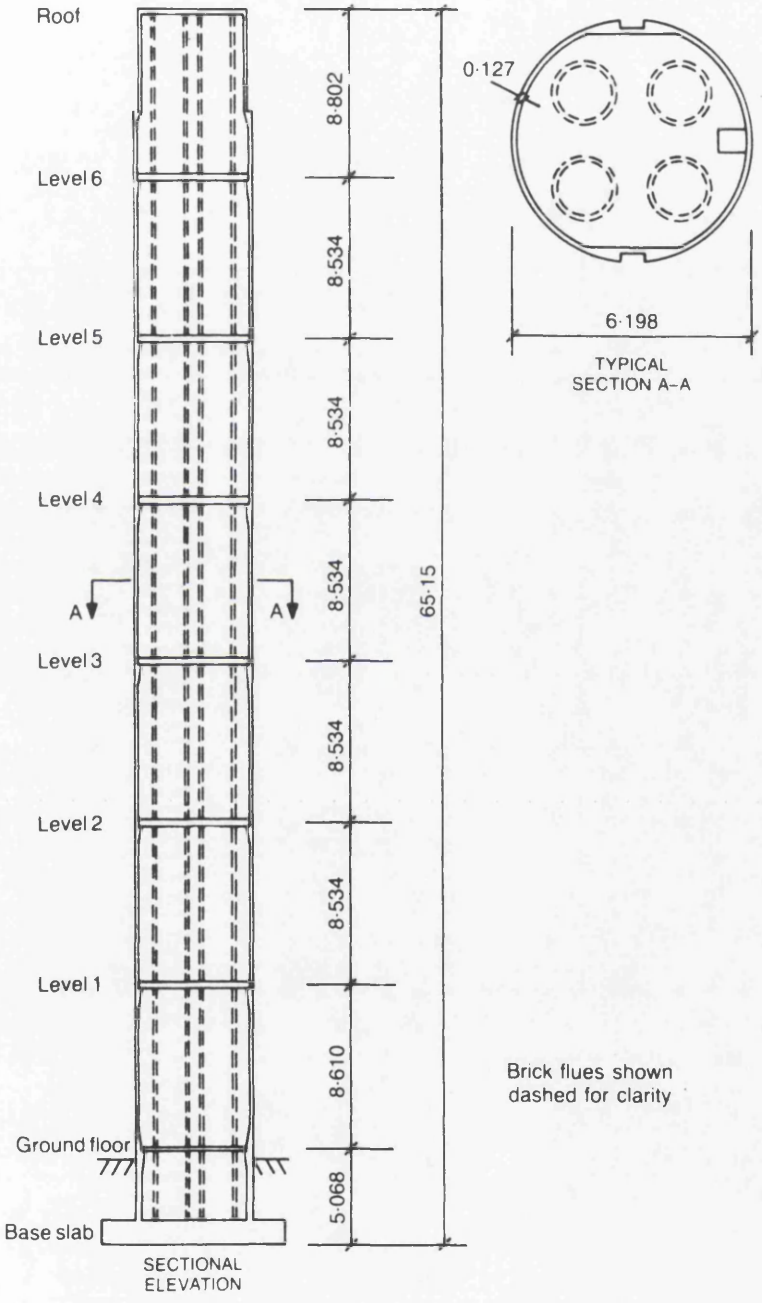

Fig. 1.19: Bristol Royal Infirmary chimney (dimensions in m).

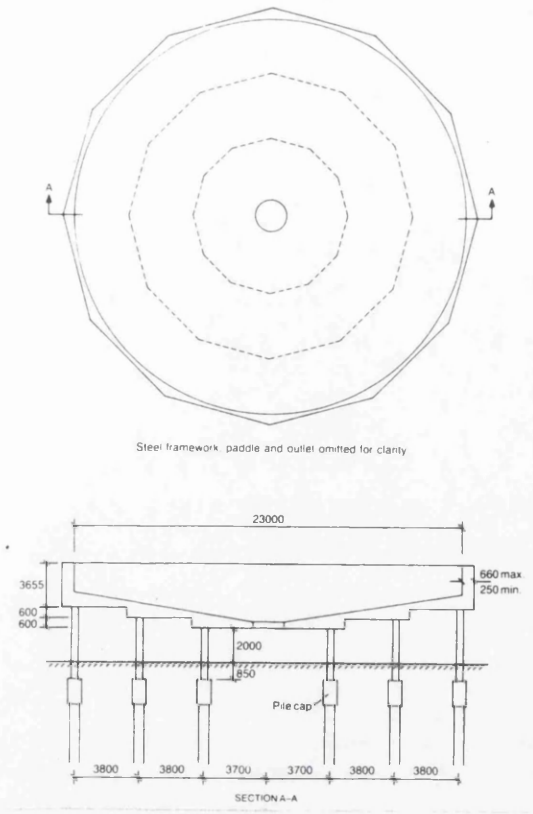

(a) Pellet plant thickener tank.

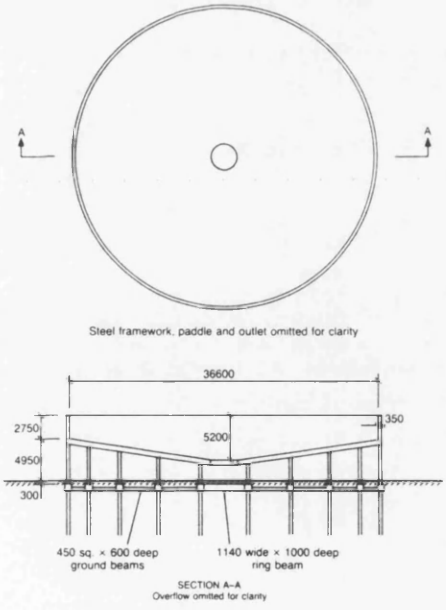

(b) Blast furnace thickener tank.

Fig. 1.20: Elevated piled tanks at Redcar (dimensions in mm).

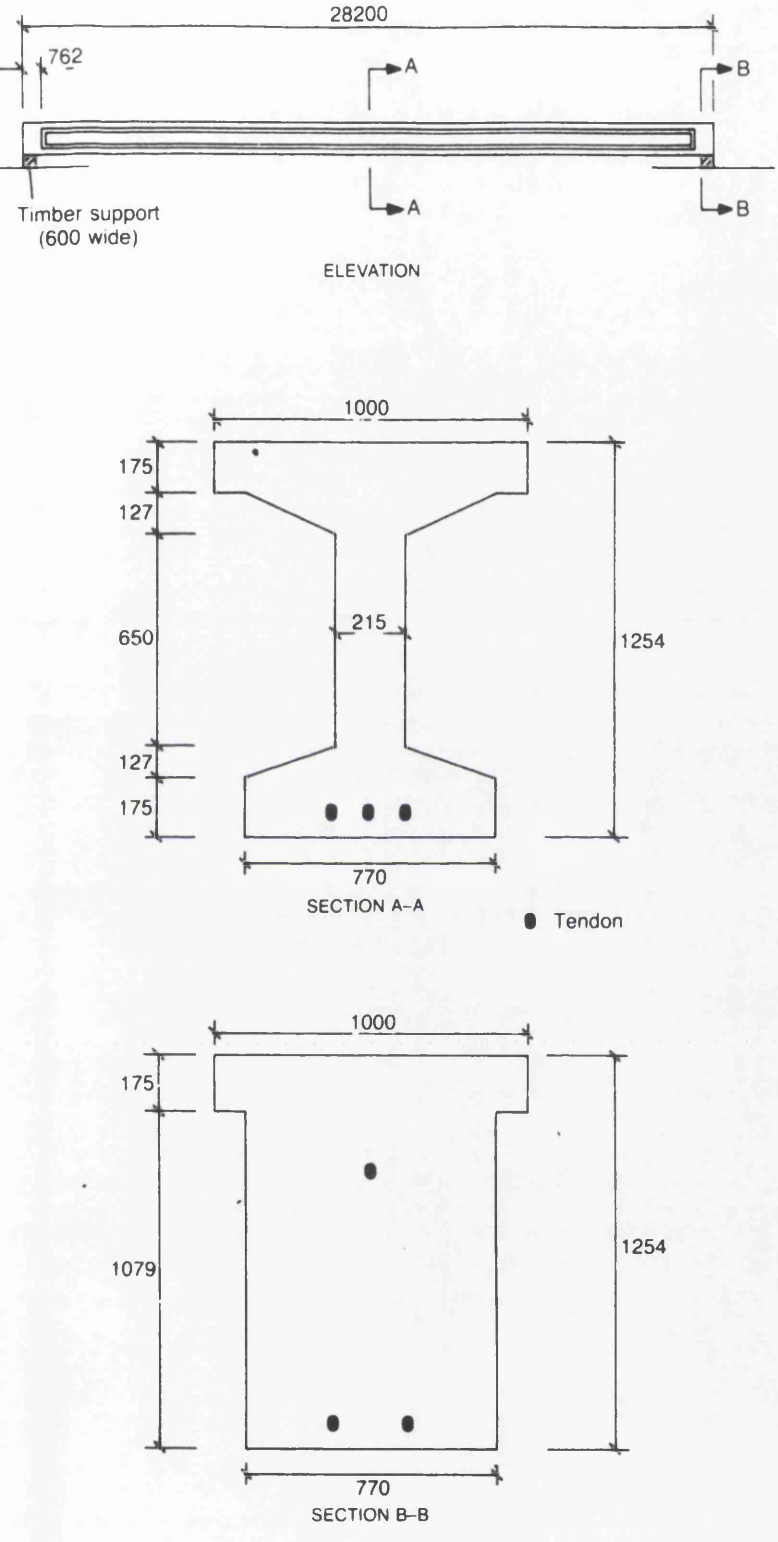

Fig. 1.21: Basingstoke beams (dimensions in mm).

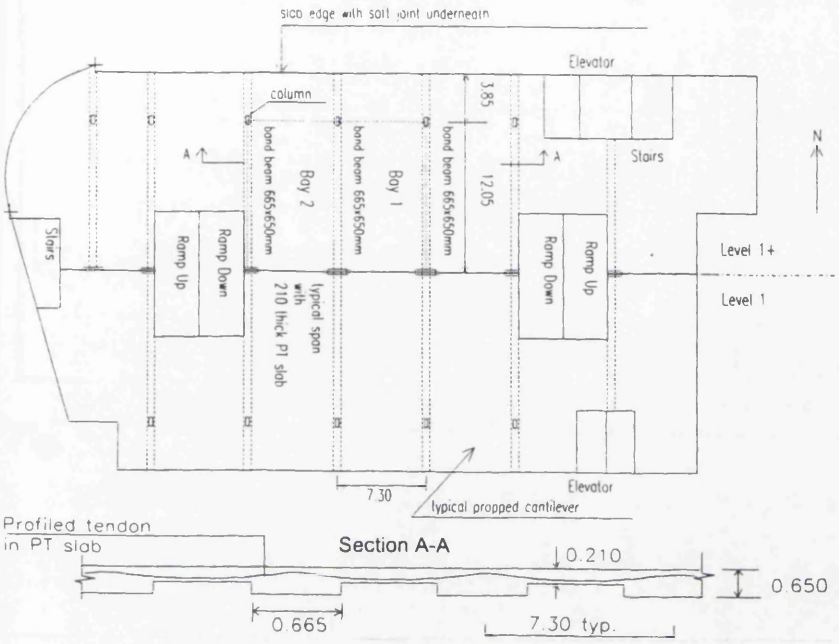

(a) Plan of the post-tensioned test slab.

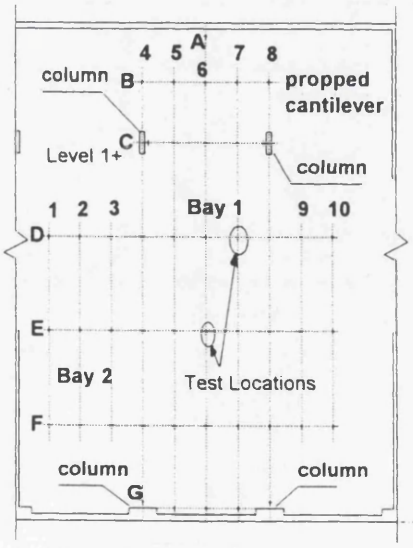

(b) Test grid layout.

Fig. 1.22: Details of the test slab and the test grid layout.

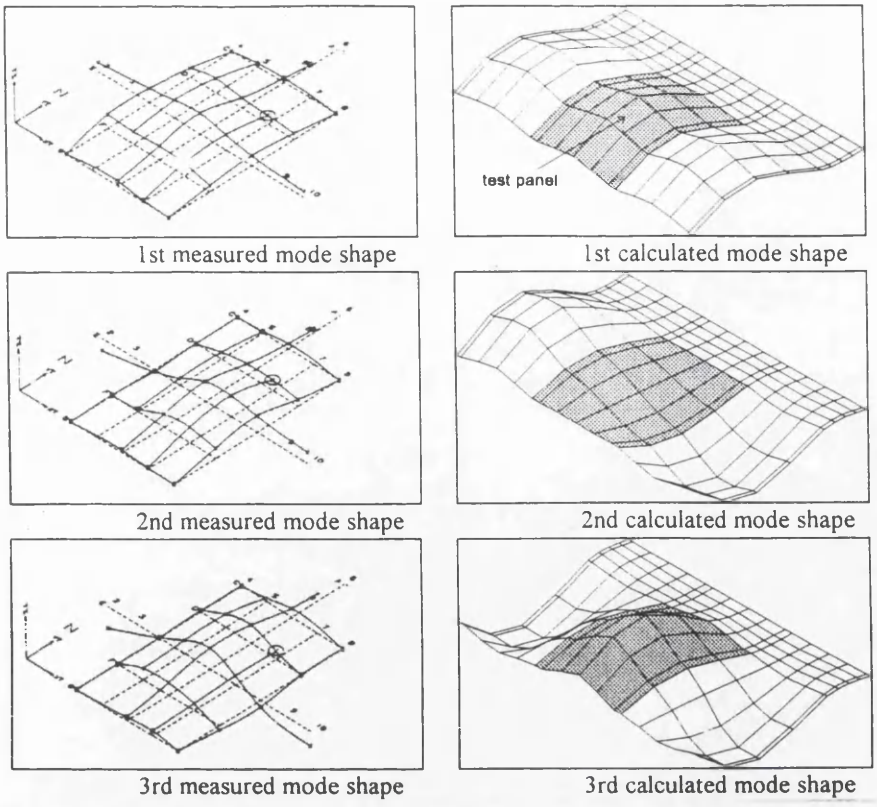

Fig. 1.23: The first three measured and calculated mode shapes.

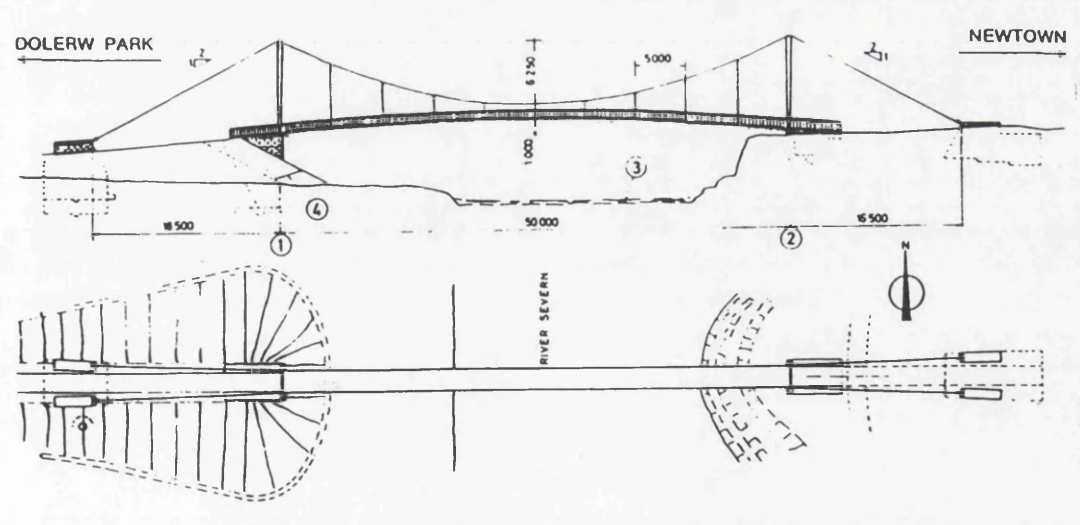

Fig. 1.24: Elevation and plan of the Dolerw bridge.

mode identifier	nodes	type/symmetry	f_{th}/Hz	f_{exp}/Hz	damping (%)
V1	1	V-A	0.885	1.053	2.68
V2	0	V-S	1.226	1.227	0.50
V3	2	V-S	1.874	2.127	0.84
V4	3	V-A	3.094	3.330	0.27
V5	4	V-S	4.759	4.910	0.28
V6	5	V-A	8.780	6.850	0.29
L1	0	L-S	2.220	1.690	1.00
L2	1	L-A	-	6.980	0.70
T1	0	T-S	3.239	3.560	0.84
T2	1	T-A	3.865	4.780	0.50
T3	2	T-S	5.409	7.340	-

Fig. 1.25: Comparison of measured and theoretical modes.

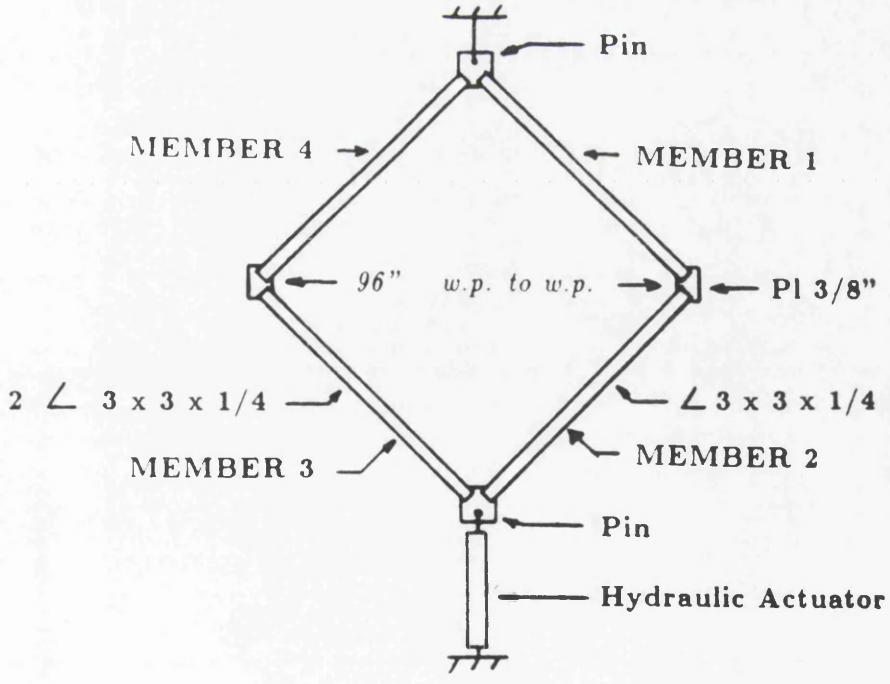

Fig. 1.26: Welded steel frame investigated by Hearn and Testa.

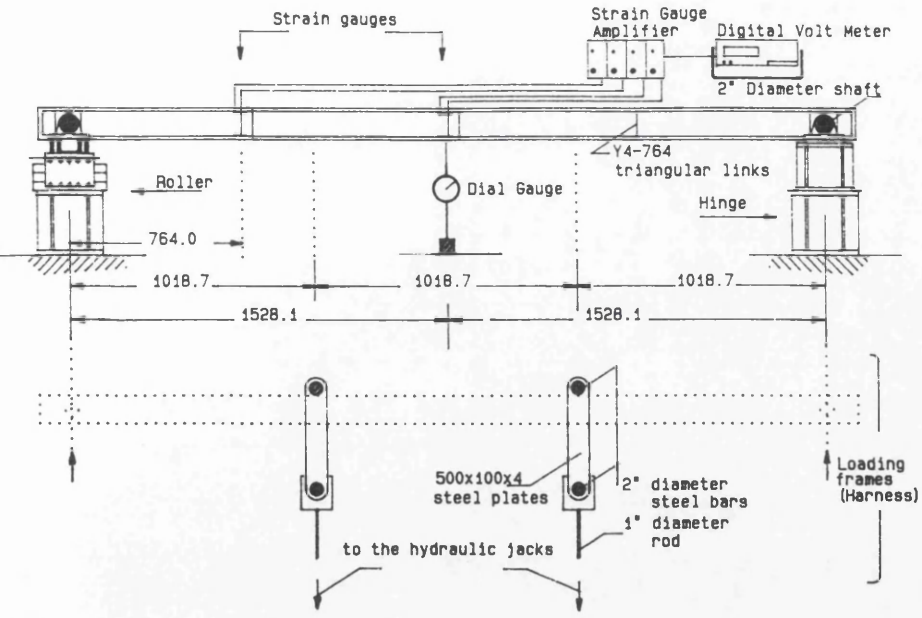

Fig. 1.27: Experimental set-up for flexural loading.

CHAPTER 2

NUMERICAL ANALYSIS

2.1 INTRODUCTION

Although the dynamic response of a practical structure will be complex, it is necessary to begin a study of the dynamical behaviour of structures by considering the fundamental vibrations of simple systems. The complexity of a dynamical system is dependant upon the number of degrees of freedom possessed by the system. This number is equal to the number of independent co-ordinates required to specify completely the displacement of the system, such as a rigid body constrained to move in the XY-plane would possess three degrees of freedom. The displacement of an elastic body has to be specified at each point by using a continuous equation, and has an infinite number of degrees of freedom. In a dynamical problem the number of modes of vibration is equal to the number of degrees of freedom, thus the simplest structure would have only one degree of freedom and hence one mode of vibration. To understand the mechanics of dynamics, a single degree of freedom structure is explained below.

Fig. 2.1 shows the usual representation of a system with one degree of freedom. It consists of a mass 'm' constrained to move in the X-direction by friction less guides and restrained by the spring of stiffness 'k'. It is further assumed that the mass of the spring is negligible compared with 'm'. In such a system the displacement is specified completely by 'x', the displacement of the mass, and the system has therefore one degree of freedom.

There are several types of excitations to which structures may be subjected. In Fig. 2.1 a force $P(t)$ is applied to the mass; this force is a function of time. There are, generally speaking, three main types of this exciting force:

(i) Harmonic forces, such as $P(t)= P_o \sin\omega t$ or $P(t)= c\omega^2 \sin\omega t$. A force which is periodic but not harmonic can be expressed as a sum of harmonic terms, using fourier series, and for a linear system the total response can be obtained by superposing the individual responses from each harmonic component of the force.

(ii) Transient or aperiodic forces: usually these are forces which are applied suddenly or for a short period of time. Simple examples illustrating the two are shown in Fig. 2.2.

(iii) Random forces: the force $P(t)$ cannot be specified as a known function of time, but can be described only in statistical terms. Forces due to gusts of wind forms an example of this type of excitation.

2.2 GENERAL EQUATION OF MOTION

The general equation of motion for any structure is derived by considering the forces acting on the mass 'm' of Fig. 2.1 at any time 't'. If the displacement of the mass, 'x', is measured from the position of static equilibrium, then the equation of motion is

$$m\ddot{x} + c\dot{x} + kx = P(t) \qquad [2.1]$$

where,

c is the damping coefficient,

k is the spring constant,

$\ddot{x}=d^2x/dt^2$ and $\dot{x} = dx / dt$

The above equation relates to a single degree-of-freedom system subjected to a disturbing force. If no disturbing force is applied to the system, but the mass is subjected to an initial displacement or velocity, free vibrations will occur, which will gradually die out due to the damping present in the system, and the equation of vibration will be given as

$$m\ddot{x} + c\dot{x} + kx = 0 \qquad [2.2]$$

which has the solution of the form

$$x = A\exp(\lambda t) \qquad [2.3]$$

provided that

$$m\lambda^2 + c\lambda + k = 0 \qquad [2.4]$$

that is

$$\lambda = -\frac{c}{2m} \pm \left[\left(\frac{c}{2m}\right)^2 - \frac{k}{m}\right]^{1/2} \qquad [2.5]$$

If $(c/2m)^2>k/m$, the two roots of equation [2.5] are real, and the complete solution of the equation [2.2] is given by

$$x = A_1\exp(\lambda_1 t) + A_2\exp(\lambda_2 t) \qquad [2.6]$$

and with λ_1 and λ_2 real and negative it represents a gradual creeping back of the mass 'm', towards the equilibrium position. For this to occur the damping must be considerably greater than that existing in practice. On the other hand, if $(c/2m)^2<(k/m)$, the roots of the equation [2.5] are complex and the solution of the equation [2.2] can be written as

$$x = \exp\left(-\frac{c}{2m}t\right)(A_1 \sin\omega' t + A_2 \cos\omega' t) \qquad [2.7]$$

where,

$$\omega' = \left[\frac{k}{m} - \left(\frac{c}{2m}\right)^2\right]^{1/2} \qquad [2.8]$$

the constants A_1 and A_2 being determined from the initial conditions, usually the values of x and $\dot{x}$ at $t = 0$. Two cases that should be considered are those with undamped vibrations and damped vibrations.

Free undamped vibrations $(c = 0)$

For this case the solution of equation [2.2] takes the form

$$x = A_1 \sin\omega_n t + A_2 \cos\omega_n t \qquad [2.9]$$

where

$$\omega_n^{\ 2} = k/m$$

The above equation can also be expressed as

$$x = A\sin(\omega_n t + \alpha) \qquad [2.10]$$

where

$$A = (A_1^2 + A_2^2)^{1/2} \quad \text{and} \quad \tan\alpha = A_2/A_1$$

The above equation is plotted out in Fig. 2.3, and from the equation and the figure

$$\omega_n T = 2\pi \quad \text{and} \quad f = 1/T$$

where, ω_n is the circular natural frequency of the system, with ω_n being measured in radians per second if the natural frequency f is in hertz and α is the phase angle.

Free damped vibration

The damping ratio is defined as $\gamma = c/c_c$, i.e. the ratio of the actual damping constant to the critical damping value, where critical damping value is the value of the damping coefficient at the changeover from the "creeping" motion to the damped vibration and

$$c_c = 2m\omega_n$$

Thus, the solution of equation [2.6] for this case can be written as

$$x = A\exp(-\gamma\omega_n t)\sin(\omega' t + \alpha) \qquad [2.11]$$

which is presented in Fig. 2.4. In practice $\omega' \approx \omega_n$ and γ is small (<0.2). In structures the value of γ depends on the material and on the type of connections at the joints (looseness increases the damping). For practical values of damping the

frequency of the damped vibrations is approximately equal to the natural frequency of free vibrations of the system.

2.3 RESPONSE TO HARMONIC EXCITATION

The response of the systems with one degree-of-freedom (Fig. 2.1) to a harmonic applied force is now considered, i. e., $P(t)= P_0 \cos\omega t$ in Fig. 2.1, P_0 is a constant and $\omega/2\pi$ is the frequency of the applied force. Then from equation [2.1] the relevant equation of motion will be

$$m\ddot{x} + c\dot{x} + kx = P_0 \cos\omega t \qquad [2.12]$$

The complete solution of the above equation consists of the complimentary function and particular integral, and can be expressed as

$$x = \exp(-\gamma\omega_n t)(A_1 \sin\omega^1 t + A_2 \cos\omega' t) \\ \ldots\ldots + \frac{P_0 \cos(\omega t - \alpha)}{[(k - m\omega^2)^2 + c^2\omega^2]^{1/2}} \qquad [2.13]$$

As for previous cases, the constants A_1 and A_2 are determined from the initial conditions. Physically, the complete response is the sum of the starting transient (the complementary function), which decreases exponentially with time, and the steady-state response (the particular integral). If the vibrations during the first few cycles are of interest, the above equation has to be investigated, but in most problems only the response after the starting transient has died away is required. The steady state response is given by the equation

$$x = \frac{P_0 \cos(\omega t - \alpha)}{[(k - m\omega^2)^2 + c^2\omega^2]^{1/2}} \qquad [2.14]$$

with

$$\tan\alpha = \frac{c\omega}{k - m\omega^2} \qquad [2.15]$$

Now, if X is the amplitude of the steady forced vibration, i. e., $x = X\cos(\omega t - \alpha)$, and $X_{st} = P_0/k$, the displacement for a static force P_0, then, replacing $c_c = 2k/\omega_n$, $\gamma = c/c_c$ and $r = \omega/\omega_n$,

$$\frac{X}{X_{st}} = \frac{1}{[(1-r^2)^2+(2\gamma r)^2]^{1/2}} \qquad [2.16]$$

and

$$\tan\alpha = \frac{2\gamma r}{1-r^2} \qquad [2.17]$$

In the above equation the angle α is the phase angle by which the response lags behind the applied force. The ratio X/X_{st} is known as the (dynamic) magnification factor or gain. The above equations express the magnification factor and the phase angle in terms of the frequency ratio r and the damping factor γ, and are interpreted graphically in Figs. 2.5 and 2.6. These figures illustrate the phenomenon of "resonance"- that when the frequency of the applied force equals the natural frequency, the amplitude of forced vibration is large for practical values of damping.

2.4 ENERGY EXPRESSIONS

For any vibrating system, energy, equal to the work done by the applied force, is supplied to the system. Energy is dissipated by the damping mechanism and is

stored as kinetic energy and potential energy. Thus from the principle of conservation of energy,

(work done by the applied force) - (energy dissipated by damping)

= increase in kinetic energy and potential energy

For free undamped vibrations, there is no applied force and no energy is dissipated by damping, thus the sum of the kinetic energy and potential energy is a constant.

$$\frac{1}{2}m\dot{x}^2 + \frac{1}{2}k(x+\delta_{st})^2 - mg(x+\delta_{st}) = C \qquad [2.18]$$

rearranging and noting that $k\delta_{st} = mg$,

$$\frac{1}{2}m\dot{x}^2 + \frac{1}{2}kx^2 = C \qquad [2.19]$$

If $x = A\omega_n \cos(\omega_n t + \alpha)$, and noting that the total energy is a constant, only if the coefficients of the terms in $\sin^2(\omega_n t + \alpha)$ and $\cos^2(\omega_n t + \alpha)$ are equal,

$$\frac{1}{2}mA^2\omega_n^2 = \frac{1}{2}kA^2, \quad \text{or} \quad \omega_n^2 = k/m \qquad [2.20]$$

Similarly, applying the energy principle to one complete cycle of steady state forced vibrations, the work done by the applied force, $P_0 \cos\omega t$, is $P_0 \cos\omega t dx$. The limits of integration corresponding to one complete cycle, are $t = 0$, and $t = 2\pi/\omega$. Thus, the work done by the applied force per cycle

$$\begin{aligned} &= -\omega P_0 X \int_0^{2\pi\omega} \cos\omega t \sin(\omega t - \alpha) dt \\ &= \pi P_0 X \sin\alpha \end{aligned} \qquad [2.21]$$

And the energy dissipated per cycle

$$\int c\dot{x}dx = \int_0^{2\pi/\omega} c\dot{x}^2 dt = \pi c X^2 \omega \qquad [2.22]$$

Making use of equations [2.14] and [2.15] it can be seen that equations [2.21] and [2.22] are similar.

2.5 DETAILS OF NUMERICAL MODELS ANALYZED

The numerical analysis through the use of FLASH was carried out on eleven different numerical models, divided in three different batches depending upon the type of constraint conditions present between the two leaves of the sandwich panel. The criterion for selecting the various models was mainly dependant upon the actual wall panels used in pre-fabricated construction. All panels were analysed for their dynamic properties, such as the natural frequencies and their associated modal shapes.

Before going any further in the description of the models analysed, it is important to describe the finite element program used to carry out the dynamic analysis. The computer program FLASH (Finite eLement Analysis of SHells) calculates by the finite element method, homogeneous, linear-elastic: shells and plates in addition to folded-plate structures, slabs, space-frames, plane-frames and grillages, under static and dynamic loading, for first-order or second-order theory. Flash operates with flat triangular and quadrilateral elements as well as with straight prismatic beam elements. It allows for the analysis of four different types, which differ from

one another in their static behaviour in a structural sense and is reflected in the kind of elements and number of degrees of freedom as shown in Figures 2.7 to 2.9. The input scheme for the program is included at the end in Appendix A, in addition to a typical input data file for the dynamic analysis of a sandwich panel, analysed as a plate structure.

Considering the structural members under investigation, reinforced concrete sandwich panels, it is possible to treat them as either plate bending elements or shell elements. Carrying out the analysis for the model as a shell rather than a plate, would result in an excessive amount of computer time, although the use of shell elements does allow the flexibility of incorporating in-plane loads, which is not possible with the use of plate bending elements. The analysis carried out for the wall panels produced the natural frequencies of the panels and the associated mode shapes for the first six modes. The results were then used for modelling the test parameters. The wall panels were investigated for various possible boundary conditions and the different constraint conditions existing between the two plates of the sandwich panel. The details of these different models are explained in detail in the proceeding article.

2.6 NUMERICAL MODELS

The geometry and the structural and material properties of the models analysed were based upon the actual pre-fabricated panels used in construction. The basic panel investigated for its dynamic properties was a reinforced concrete sandwich panel having nominal dimensions of 1800mm width and 2400mm height. The two elements of the sandwich panel were taken to be 50mm and 100mm thick

respectively. The sandwich panels were analysed for various boundary support conditions and the constraints present between the two elements.

As already mentioned in the previous chapter, the basic panel under consideration, in its original condition, has the two elements connected around the periphery over a certain width in addition to being connected within the section at specified locations. In the precast panels under investigation, these connections are through the use of "goal post" ties, made out of delta or phosphor bronze, as already explained in the first chapter. The number of these connecting ties used per wall panel is specified by the designer, and depends upon the size of the panel. The program FLASH allows for the displacements and/or the rotations of one joint to be constrained together with that of another. This facility was used for modelling the connections between the two leaves of the sandwich panel.

As has been discussed previously, in reality most of the panels in use rarely conform to the original specified design. Certain differences are present, either at the time of manufacture, which mainly relates to the use of an incorrect number of ties (generally fewer than required), or the panel undergoes some structural changes during its service life. The changes could occur under the influence of the applied loading or the aggressive environmental conditions to which the panels are likely to be subjected. These could produce peripheral cracking of the panels or affect the structural ties within the section, thus reducing the load transfer capability. The eleven wall panels analysed had 'built-in' variations in them based upon the possible defects and structural changes l ikely to occur in them. The structural details of the various panels analysed are given below.

MODEL GK-1: The reinforced concrete sandwich panel was treated as a plate bending element, with the two "leaves" being treated as separate plate bending elements, having three degrees of freedom associated with each node. Both skins were modelled independently as plates having overall geometric dimensions of 1800mm width and 2400mm height, and were a 100mm and 50mm thick respectively. Both plates were discretized into a 200mm finite element mesh as shown in Fig. 2.10. For analysis of the two plates for their dynamic characteristics, the plates were modelled in the X-Y co-ordinate system and were placed side-by-side as indicated in Fig. 2.10. For modelling the connection between the two plates, the property of the program allowing the flexibility to constrain joints together was used. This particular model had joints constrained over a 200mm width around the perimeter on all four sides and this was the only structural connection present between the two plates. The support conditions for the model consisted of simply supporting the 100mm thick plate along the two 1800mm edges. Each of the models were analysed for their dynamic characteristics for varying material properties to carry out a parameteric study and observe the affect of E_c,ω and ν on these characteristics.

MODEL GK-2: This model was similar to GK-1 in structural and geometric properties. It was again treated as a plate element and the two plates had the same discretization as the first one in addition to having the same boundary support conditions. the difference in the two models was in the structural connection between the two plates. Unlike GK-1 this model in addition to having a connection between the two plates around the perimeter over a width of 200mm was also connected together at two central locations. The details of the model are presented in Fig. 2.11.

MODEL GK-3: Once again the model being similar to the first two models. The difference again being only between the structural connection present between the two plates. In addition to the connection around the perimeter, this model, the last in the first batch of three models, had four more joints constrained. The details of these are provided in Fig. 2.12.

MODEL GK-4: The second batch of numerical models were quite similar to the three models analysed in the first batch, as far as the geometric properties of the panels were concerned. The similarities ended here. In this batch the models were modelled to simulate a crack along one of the edges as well as reducing the structural constraints present between the two plates. This was done to study the effect of reduction in stiffness of the panel on the natural frequencies and the modal shapes of the basic panel under investigation. The first model of this batch had a mesh discretization of 200mm for most of the plate section, except for around the perimeter, where it was reduced to 50mm. This was done to allow the introduction of a structural constraint over a width of only 50mm around three edges of the perimeter thus, simulating a crack along one edge in addition to reducing the overall stiffness. The details of this mesh discretization can be found in Fig. 2.13. Model GK-4 had only this structural constraint present between the two plates .

MODEL GK-5: The second model in this batch had quite similar structural and geometric properties as to the previous model. The difference for this model was, that like GK-2 this one also had an additional constraint in the centre to provide a stiffer structural connection between the two plates. Details of the model can be found in Fig. 2.14.

MODEL GK-6: Similar to GK-4 and GK-5 in overall geometric properties and the structural constraints around the perimeter, but with additional constraints introduced within the section, which were similar to GK-3. The details of the finite element mesh and the joint constraints are presented in Fig. 2.15.

MODEL GK-88, 87, 86, 85, 84: The five models analysed in the third batch had the same overall geometric dimensions of the first two batches. Unlike those numerical models, which had some form of structural connection around the perimeter, the ones in this batch were only structurally connected at certain discrete points. The first two batches were designed to study the effect of decreasing structural stiffness of the models, on the dynamic characteristics of the sandwich panels under investigation. Continuing on the same principle, the numerical models in this batch were designed to have an even lower stiffness. This was achieved by eliminating the connection between the two concrete leaves around the perimeter. The first numerical model in this batch, GK-88, had eight point connections between the two leaves, the details of which can be seen from Fig. 2.16. The remaining models were all similar to this one, the only difference being in the number of point constraints present between the two leaves, which were reduced by one for each successive numerical model. The details of these are presented in Figs. 2.17-2.20. The two concrete leaves were treated as plate bending elements and each plate consisted of 72 joints (Figs. 2.16-2.20). All models were simply supported along the top and bottom 1800mm edges of the 100mm thick plate. Each of the models was analysed for their dynamic characteristics for varying material properties and the effect of E_c,ω and ν on these characteristics was studied.

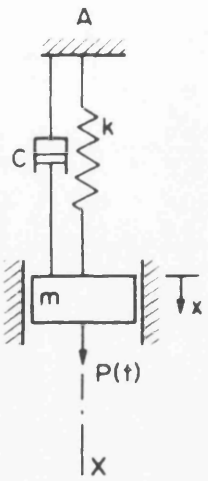

Fig. 2.1: Single-degree-of-freedom system.

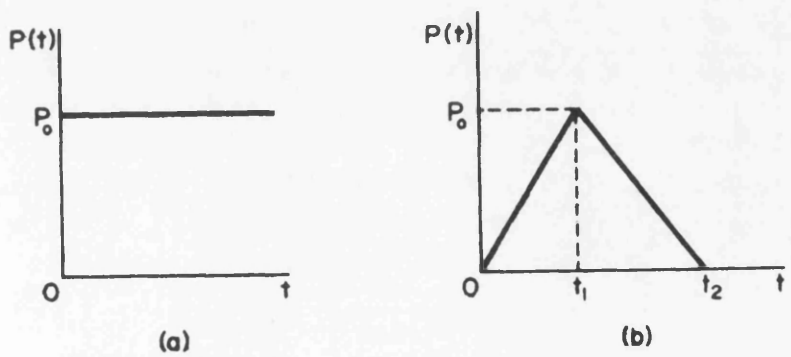

Fig. 2.2: Two examples of transient force excitation.

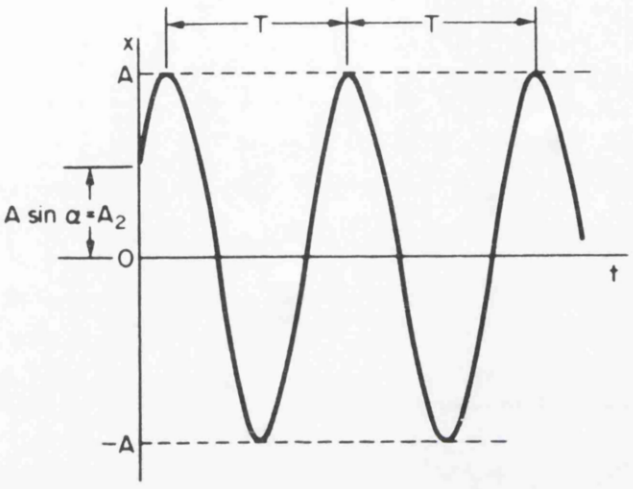

Fig. 2.3: Free undamped vibrations.

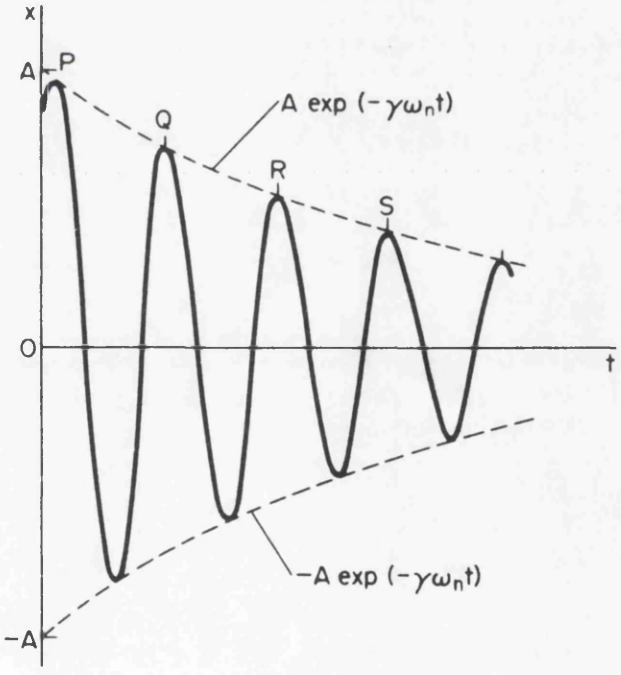

Fig. 2.4: Free damped vibration.

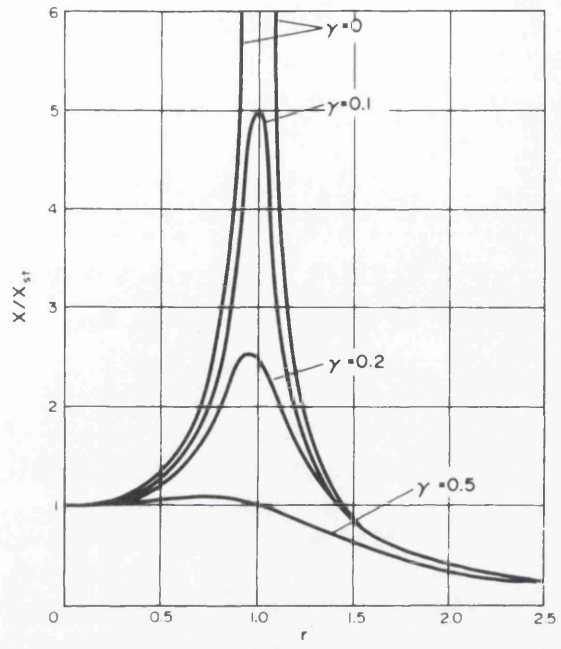

Fig. 2.5: Response to forced vibration.

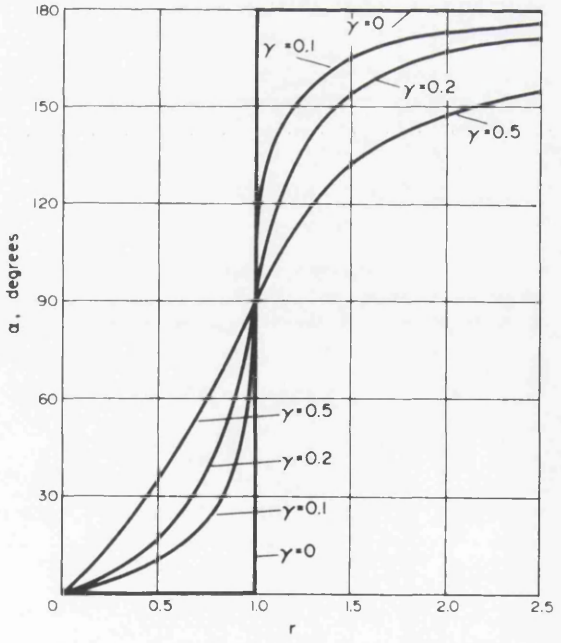

Fig. 2.6: Variation of phase lag with frequency.

In-plane structures and axisymmetric solids

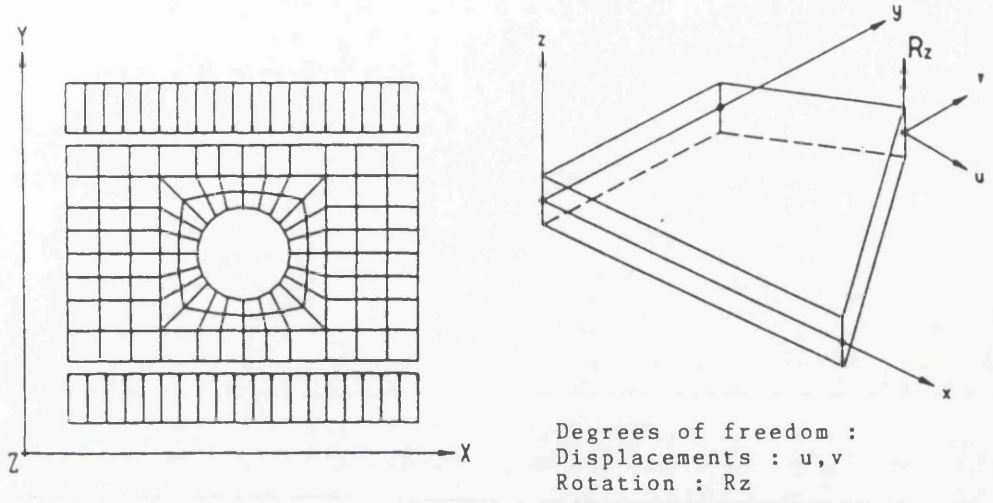

Degrees of freedom :
Displacements : u,v
Rotation : Rz

Fig. 2.7: Global co-ordinates and inplane degrees of freedom.

Plate structures

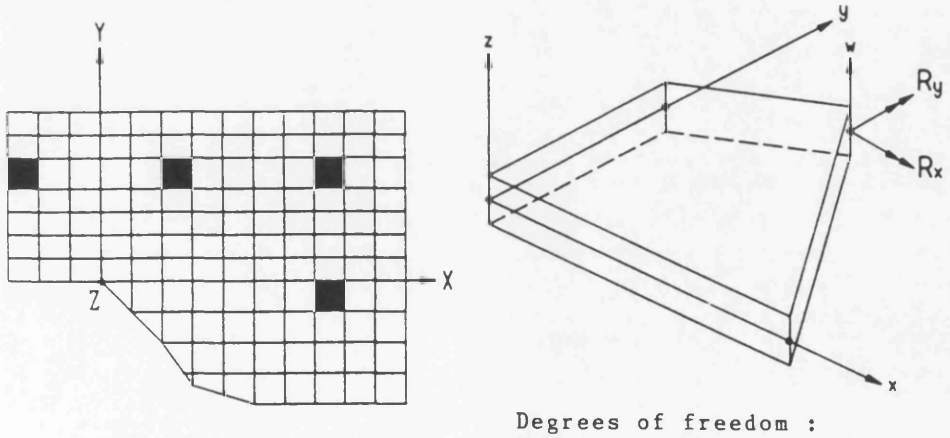

Degrees of freedom :
Displacement : w
Rotations : Rx,Ry

Fig. 2.8: Global co-ordinates and plate degrees of freedom.

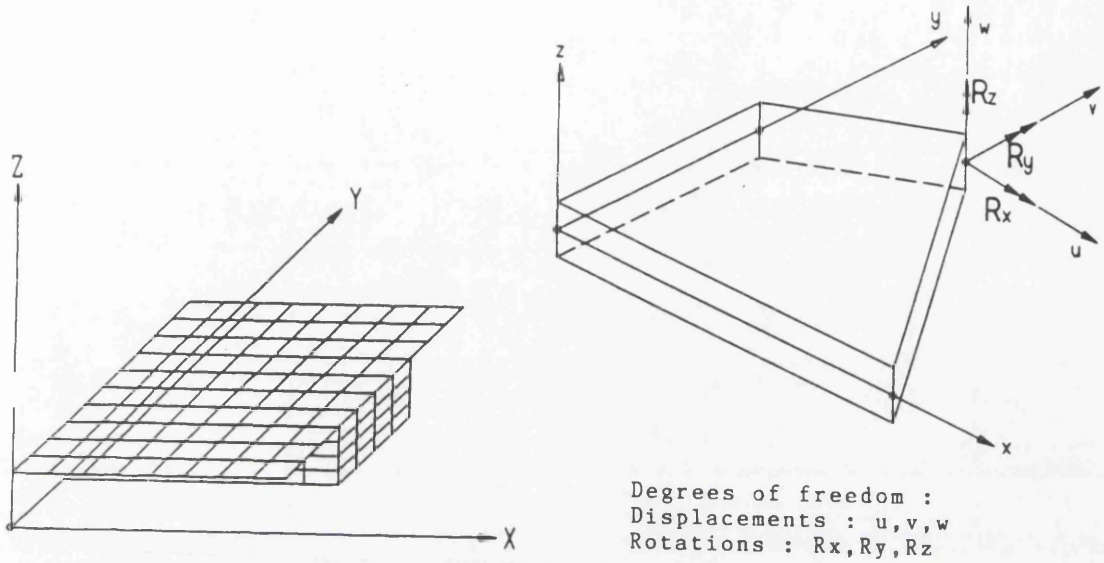

Fig. 2.9: Global co-ordinates and shell degrees of freedom.

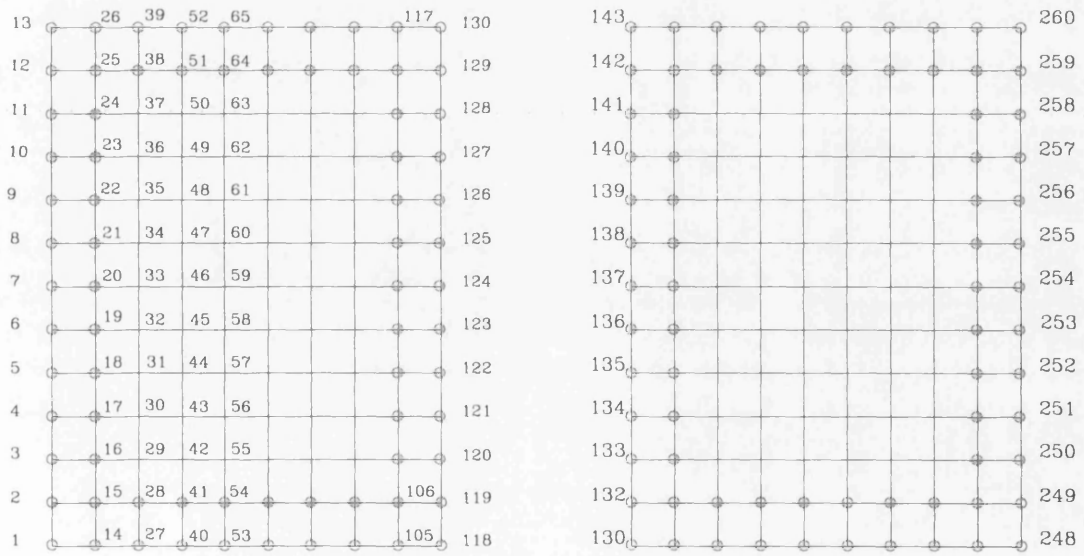

Fig. 2.10: Details of the mesh discretization of numerical model GK-1.

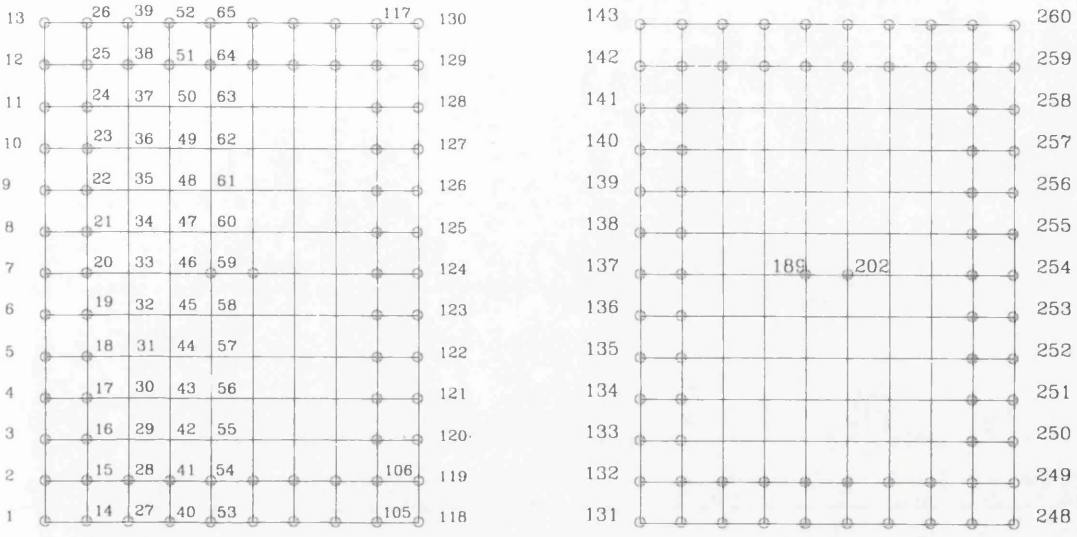

Fig. 2.11: Details of the mesh discretization of numerical model GK-2.

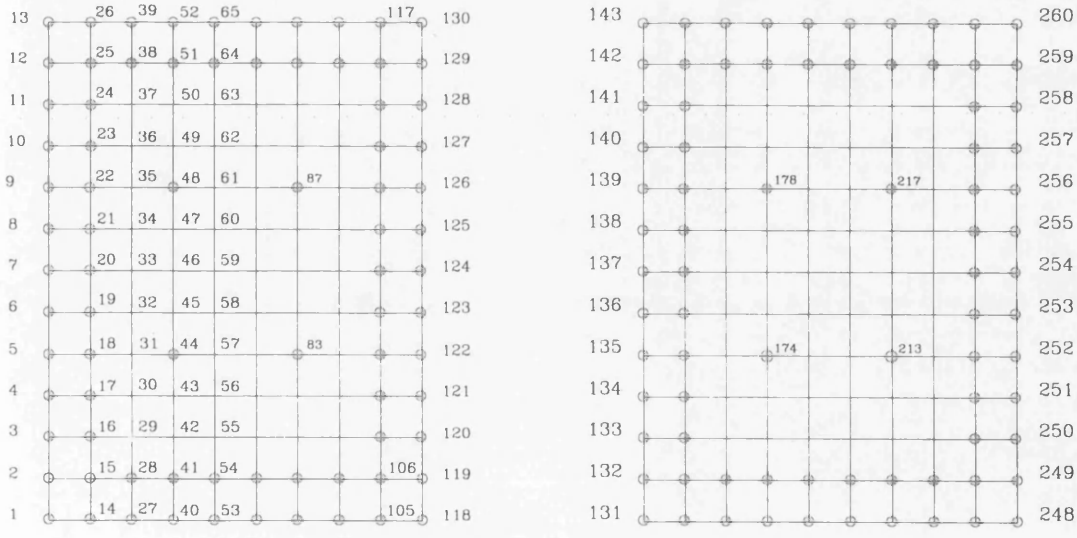

Fig. 2.12: Details of the mesh discretization of numerical model GK-3.

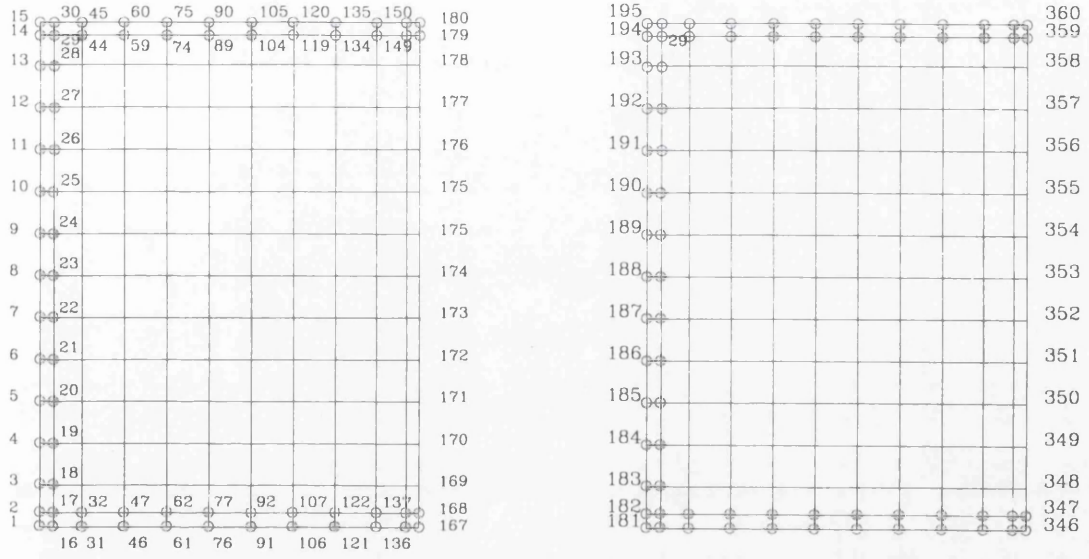

Fig. 2.13: Details of the mesh discretization of numerical model GK-4.

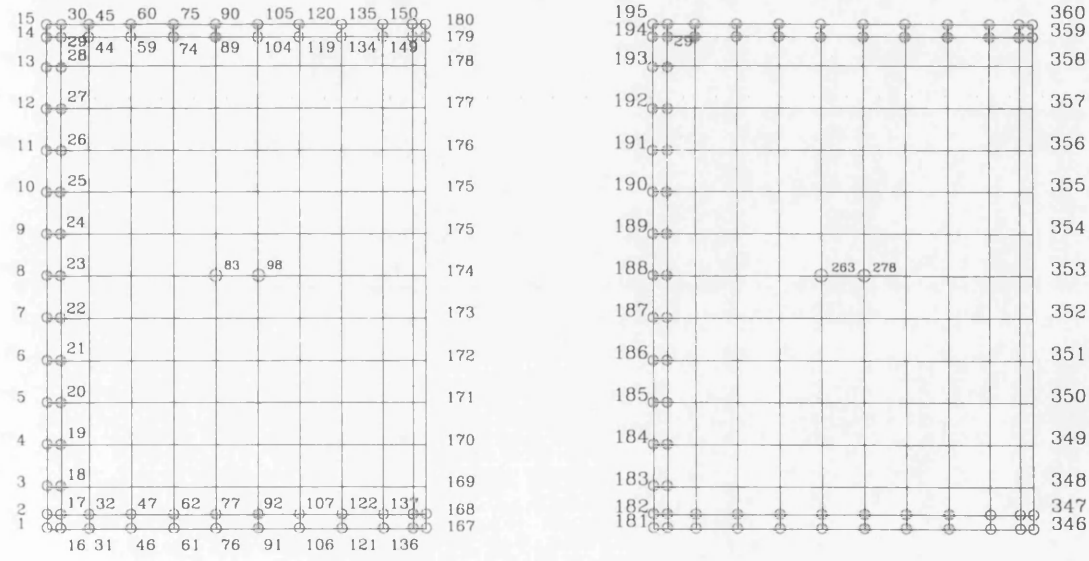

Fig. 2.14: Details of the mesh discretization of numerical model GK-5.

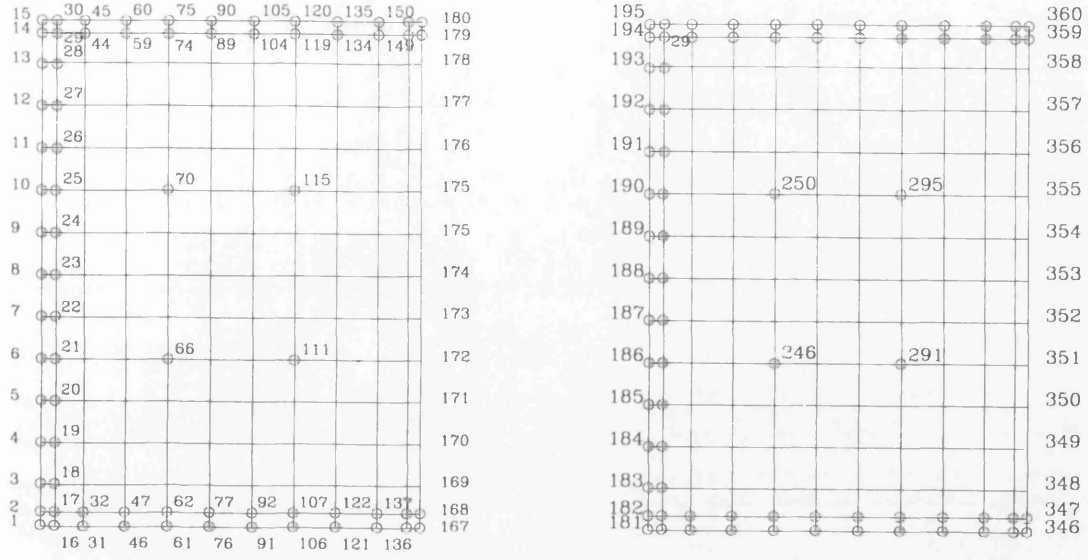

Fig. 2.15: Details of the mesh discretization of numerical model GK-6.

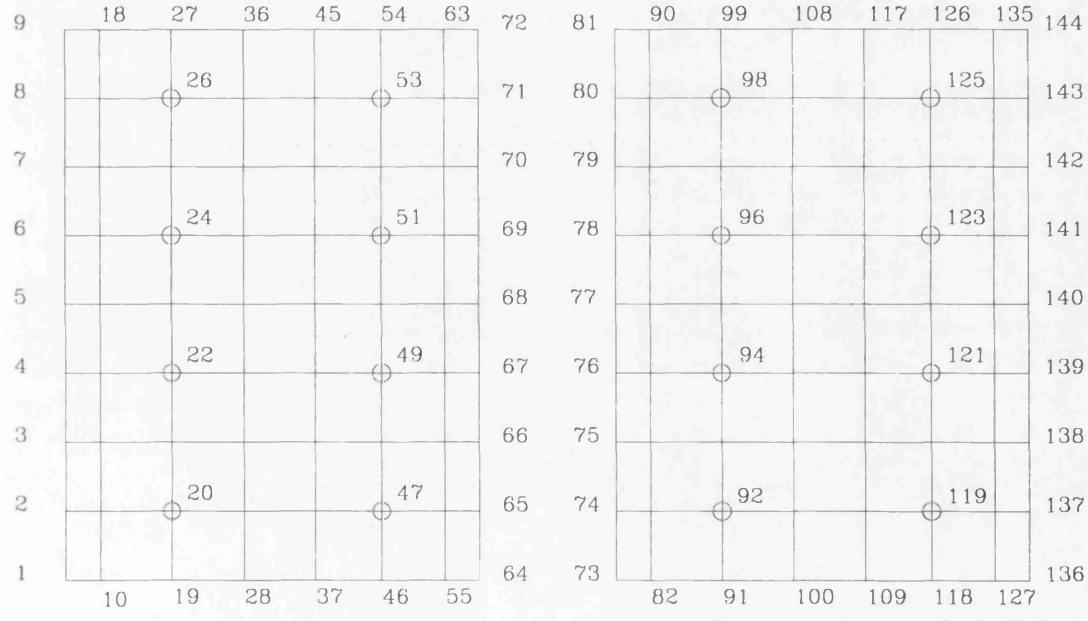

Fig. 2.16: Details of the mesh discretization of numerical model GK-88.

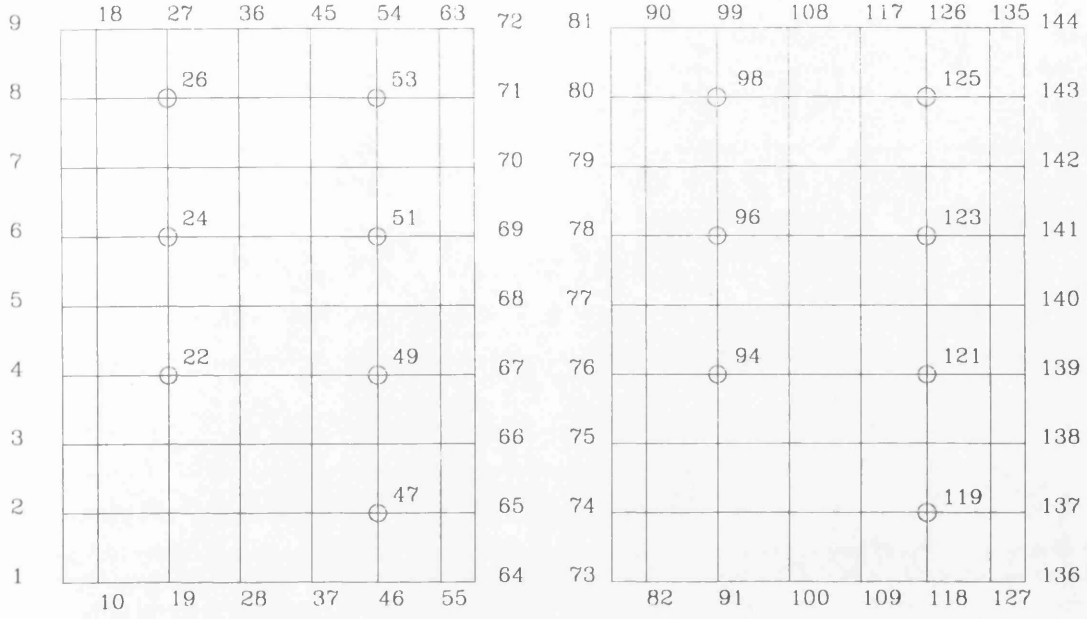

Fig. 2.17: Details of the mesh discretization of numerical model GK-87.

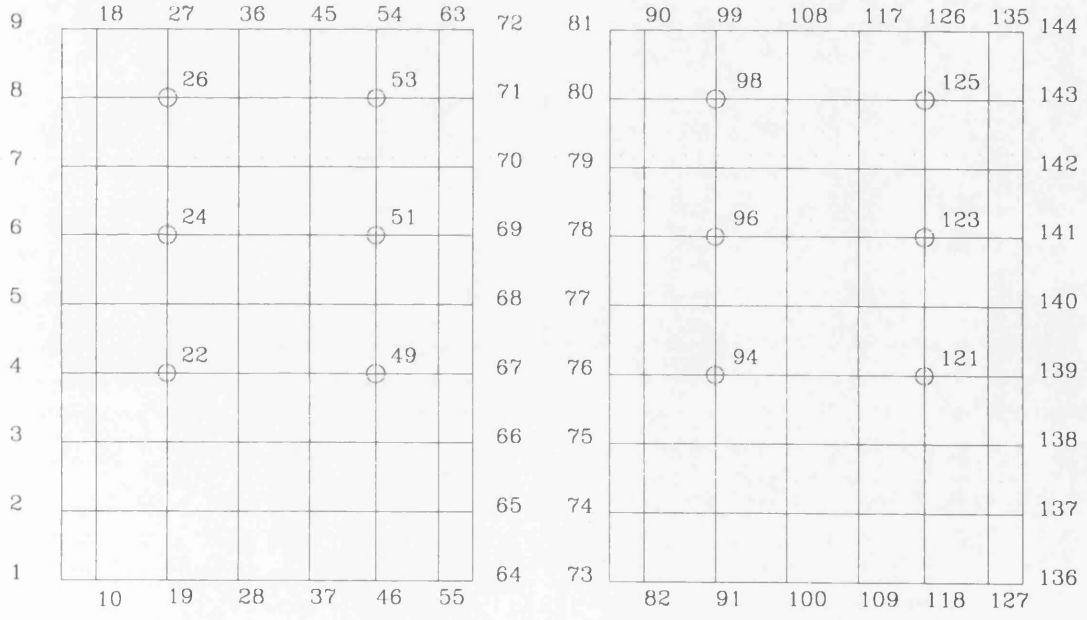

Fig. 2.18: Details of the mesh discretization of numerical model GK-86.

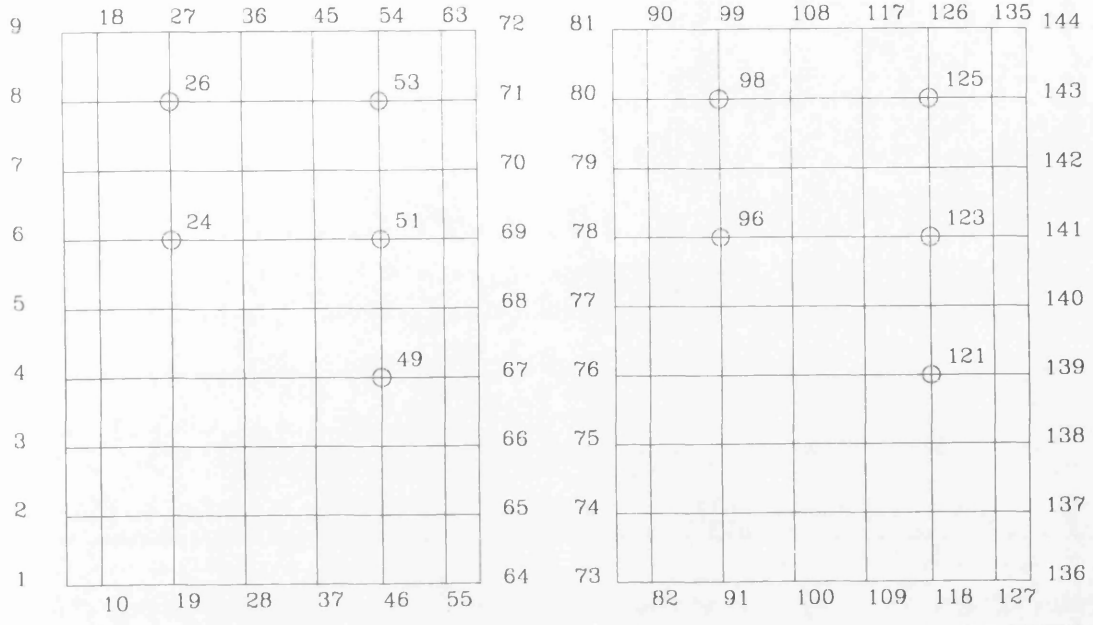

Fig. 2.19: Details of the mesh discretization of numerical model GK-85.

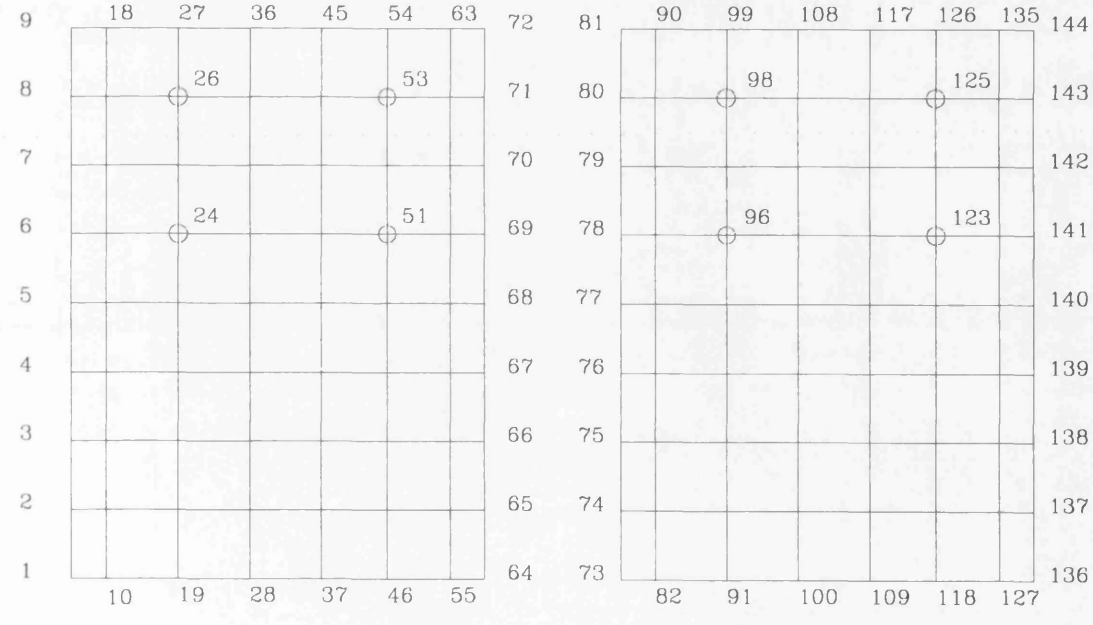

Fig. 2.20: Details of the mesh discretization of numerical model GK-84.

CHAPTER 3

RESULTS AND DISCUSSION OF THE NUMERICAL ANALYSIS

3.1 INTODUCTION

This chapter deals with the results of the numerical analysis performed on the models described in the previous chapter. The numerical models were analysed for their dynamic characteristics, with emphasis being placed mainly on the natural frequencies and their related modal shapes. All the models were analysed for the first six modal shapes, as the natural frequencies for this range would presumably be low enough to be measured relatively easily when performing the experimental work. The material properties used for obtaining these natural frequencies and the associated modal shapes were similar to the ones which were to be used later in the experimental program. In addition, a parameteric study of the numerical models was also carried out. For this analysis the material properties, such as, the Modulus of Elasticity and the mass were varied over a certain range and the effect of these variations on the natural frequencies was studied.

In the present chapter a detailed analysis of the results is presented in graphical and tabular form and conclusions are drawn on the feasibility of using this approach experimentally to determine the structural integrity of the precast sandwich wall panels.

3.2 NUMERICAL MODELS GK-1, 2, 3

The details of the dynamic characteristics of the basic model for this first batch are presented in Table 3.1. The relationship between the natural frequencies for the six

modes of the three numerical models are presented in Fig. 3.1. The corresponding modal shapes for the first six natural frequencies are also presented in Figs. 3.25-3.42. As can be observed from Table 3.1, there is effectively no difference in the first three natural frequencies of the models GK-1, 2, 3 in spite of the additional constraints present in the numerical models GK-2, 3. These are also portrayed in the modal shapes and it can be seen that the first two modal shapes are identical apart from the magnitude of displacement (Figs. 3.25,26,31,32,37,38). The third modal shape for GK-3 is slightly different, which is to be expected, because of the placement of four additional constraints present in this model. As we move on to the higher modes, the differences between the natural frequencies become more noticeable (especially for the sixth mode) and this can be seen from the related modal shapes as well (Figs. 3.30,36,42). The higher modal shapes though, becoming more complicated, hence making it a lot more difficult to detect them experimentally.

The results for these models quite clearly indicate that the dynamic characteristics, especially the natural frequencies, are dominated by the stiffness of the connection between the two skins of the sandwich panel, around the perimeter. The additional constraints provided by introducing the extra connections between the two skins of the panel have an insignificant effect on the natural frequencies, although the modal shapes do exhibit a change for the higher modes which is to be expected. It could be inferred from these results that although it is possible to detect, through experimental observations, the natural frequencies of the basic panel of this batch, it is likely to be extremely difficult to detect any minor structural changes occurring in the panel (such as the introduction of additional constraints and the resulting increased stiffness), because of the over-riding stiffness of the connection around the perimeter. On similar grounds, it would again be difficult to distinguish

the three panels from each other, through experimental observations based upon the modal shapes. The first three modal shapes being effectively identical, and for the higher modes, the modal shapes being too complicated to be detected through experimental techniques.

The results of the parameteric study performed on this batch of numerical models are presented in Tables 3.2-3.4 and Figs. 3.3-3.8. The models were analysed for different values of the Modulus of Elasticity and mass, while the Poison's ratio and the boundary conditions were kept constant. The results are indicative of the trends that would be expected for the variables chosen, although it is observed that the natural frequencies for modes 4 and 5 are effectively the same for the different values of the variables considered.

3.3 NUMERICAL MODELS GK-4, 5, 6

The details of the natural frequencies for the first six modes for the three numerical models in this batch are presented in Table 3.1. The corresponding modal shapes are given in Figs. 3.43-3.60. As can be seen from Table 3.1, the natural frequencies for the six modes analysed for this batch are somewhat lower than the corresponding one's for those of the previous batch. This slight decrease is to be expected, because of the lower stiffness of the numerical model, which had a stiff connection around only three edges along the perimeter over a 50mm width, as compared to one of 200mm width along all four edges for models GK-1, 2, 3. The results further indicate that although the natural frequencies for the first mode are similar, the remaining modes do show a greater difference, as compared to the first

batch. Observing the modal shapes (Figs. 3.43-3.69) it can be seen that apart from the first mode, which is identical for all three models, the remaining modes are fairly distinct, although demonstrating complicated characteristics as we move on to the higher modes. These results are indicative of the fact that with the stiffness of the connection reduced around the perimeter, the effect of the additional constraints provided is enhanced. As with the first batch, the natural frequencies although are numerically different, but these are not significant enough to be easily detected through experimental observations. The results of the natural frequencies for the six modes are presented in Fig. 3.1.

The results of the parameteric study for this batch of models are presented in Tables 3.5-3.7 and Figs. 3.9-3.14. These models were again analysed for variables similar to the first three numerical models and were simply supported as before. As for the set of models, the results are quite predictable and it can be seen that the natural frequencies for modes 4 and 5 for GK-4 are fairly closely spaced and do not show any discernible influence of either the variation of the modulus of elasticity or the mass.

3.4 NUMERICAL MODELS GK-88, 87, 86, 85, 84

This batch of numerical models was quite different from the first two batches, in the fact that they had no connection present between the two skins of the panel around the perimeter. The only connections present were the varying number of point constraints between the two concrete leaves, as explained in detail in the previous chapter. The details of the numerical analysis for these five models are presented in Table 3.1 and Fig. 3.2. As can be observed from these values there is

a greater percentage difference between the natural frequencies for the different models, although in this case as we get to the higher modes, the changes in the natural frequencies are much smaller, especially for models GK-86, 85, 84 where, for mode 4, 5 and 6, the difference is almost negligible. It can also be observed that the natural frequencies for this batch are in general much lower than those for the earlier batches. This clearly indicates that the connection between the two skins of the sandwich panel, and as a consequence the reduced stiffness, has a much more significant affect on the natural frequencies, while the stiff connection provided through the use of point constraints does not produce anywhere near the same stiffness. At the same time, the reduction of these constraints from eight to four has a greater effect on the natural frequencies. It must again be stated that although the percentage difference in these numerical values is reasonable, the change in magnitude is not all that discernible to be able to detect from experimental observations the structural changes that would be occurring in a panel through the loss of a few constraints.

The modal shapes for the first six natural frequencies for the five numerical models are presented in Figs. 3.61-3.90. The modal shapes are once again as expected as the constraints are successively removed, with the higher modes again being quite complicated. As can be observed from these figures the third modal shape for GK-88, the fourth for GK-87 and the fifth for GK-86, 85, 84 are seemingly identical, but closer observation of the modal shapes will highlight distinct differences in the shapes as well as magnitude of deformation. Differences in the behaviour of the 100mm thick skin are detectable but for the 50mm thick skin the deformations seem quite similar. This once again reinforces the fact that it could be quite difficult to detect the differences between the sandwich panels through experimental observations.

The results of the parameteric study are presented in Tables 3.8-3.12 and Figs. 3.15-3.24. It can be observed from these values that once again as for the previous batches the fourth and the fifth mode for most models do not show much of a difference between the natural frequencies for corresponding values of either the modulus of elasticity or the mass.

3.5 CONCLUSIONS

The three batches of numerical models were designed to study what effect the major and minor structural changes occurring in the panel would have, on the natural frequencies for the different modes and the related modal shapes. The structural changes introduced in the different models were chosen, giving due consideration to the actual defects and inconsistencies that could be encountered in practice.

The results of the numerical analysis indicate that any major structural change occurring in the panel, such as the separation of the two skins along any number of edges, can be detected through the changes in the natural frequencies as well as the deformations of the panels for the different modes. As can be observed from the natural frequencies of the three batches of numerical models (Table 3.1, Figs. 3.2, 3.3), the variation between them is large enough, to lead to the conclusion that any significant structural change can be readily detected through the numerical change in the frequency value for the different modes, At the same time, the results indicate that within the three batches, the minor changes occurring do not show up clearly in the changes affected in the dynamic characteristics. Looking at the

modal shapes for the various numerical models (Figs. 3.25-3.90), similar conclusions can be drawn. The modal shapes show a significant change as we compare the three batches, and as to be expected, the separation of the two skins around the perimeter have a significant effect on the deformation of the panels.

Consequently, the main conclusion that can be drawn from the results of the numerical analysis, suggests that it should be possible to detect any major structural changes occurring in the panels, through the change in the dynamic characteristics, from experimental observations. However, it would be difficult to pick up the changes in the natural frequencies for minor structural changes as these are effectively indiscernible.

MODEL NO.	MATERIAL PROPERTIES			NATURAL FREQUENCIES *Hz*					
	$E_c(kN/m^2)$	$Mass(Kg/m^3)$	ν	MODE 1	MODE 2	MODE 3	MODE 4	MODE 5	MODE 6
GK-1	$3.0x10^7$	2400	0.17	0.765	1.645	3.024	3.360	4.202	4.832
GK-2	$3.0x10^7$	2400	0.17	0.765	1.645	3.024	4.202	4.338	5.586
GK-3	$3.0x10^7$	2400	0.17	0.765	1.646	3.071	4.215	4.361	6.418
GK-4	$3.0x10^7$	2400	0.17	0.745	1.332	1.798	2.719	2.818	3.608
GK-5	$3.0x10^7$	2400	0.17	0.762	1.552	2.274	2.719	3.608	4.269
GK-6	$3.0x10^7$	2400	0.17	0.765	1.608	2.724	3.023	3.931	4.545
GK-88	$3.0x10^7$	2400	0.17	0.761	1.539	1.775	2.443	2.991	3.011
GK-87	$3.0x10^7$	2400	0.17	0.742	1.066	1.643	1.776	2.463	2.997
GK86	$3.0x10^7$	2400	0.17	0.644	0.902	1.171	1.776	1.776	2.482
GK-85	$3.0x10^7$	2400	0.17	0.459	0.815	1.004	1.742	1.776	2.467
GK-84	$3.0x10^7$	2400	0.17	0.301	0.715	0.829	1.736	1.767	2.201

TABLE 3.1: RESULTS OF THE NUMERICAL ANALYSIS PERFORMED ON MODELS GK-1 to GK-84.

MODEL NO.	MATERIAL PROPERTIES			NATURAL FREQUENCIES *Hz*					
	$E_c(kN/m^2)$	$Mass(Kg/m^3)$	ν	MODE 1	MODE 2	MODE 3	MODE 4	MODE 5	MODE 6
GK-1	$1.5x10^7$	2400	0.17	0.541	1.163	2.138	2.376	2.971	3.417
GK-1	$2.0x10^7$	2400	0.17	0.624	1.343	2.469	2.743	3.431	3.946
GK-1	$2.5x10^7$	2400	0.17	0.698	1.501	2.761	3.067	3.836	4.411
*GK-1	$3.0x10^7$	2400	0.17	0.765	1.645	3.024	3.360	4.202	4.832
GK-1	$3.5x10^7$	2400	0.17	0.826	1.777	3.266	3.629	4.539	5.219
GK-1	$3.0x10^7$	2000	0.17	0.838	1.902	3.313	3.680	4.603	5.293
GK-1	$3.0x10^7$	2200	0.17	0.799	1.718	3.158	3.509	4.389	5.047
GK-1	$3.0x10^7$	2400	0.17	0.765	1.645	3.024	3.360	4.202	4.832
GK-1	$3.0x10^7$	2600	0.17	0.735	1.580	2.905	3.228	4.037	4.643
GK-1	$3.0x10^7$	2800	0.17	0.708	1.523	2.800	3.110	3.890	4.474

TABLE 3.2: RESULTS OF THE NUMERICAL ANALYSIS PERFORMED ON MODEL GK-1.
(* corresponds to the frequency values for the exhibited modal shapes)

MODEL NO.	MATERIAL PROPERTIES			NATURAL FREQUENCIES *Hz*					
	$E_c(kN/m^2)$	$Mass(Kg/m^3)$	ν	MODE 1	MODE 2	MODE 3	MODE 4	MODE 5	MODE 6
GK-2	$1.5x10^7$	2400	0.17	0.542	1.163	2.138	2.971	3.067	3.950
GK-2	$2.0x10^7$	2400	0.17	0.626	1.343	2.469	3.431	3.542	4.561
GK-2	$2.5x10^7$	2400	0.17	0.699	1.502	2.761	3.836	3.960	5.100
*GK-2	$3.0x10^7$	2400	0.17	0.765	1.645	3.024	4.202	4.338	5.586
GK-2	$3.5x10^7$	2400	0.17	0.828	1.777	3.266	4.539	4.685	6.034
GK-2	$3.0x10^7$	2000	0.17	0.839	1.802	3.313	4.603	4.752	6.120
GK-2	$3.0x10^7$	2200	0.17	0.800	1.718	3.158	4.389	4.531	5.835
GK-2	$3.0x10^7$	2400	0.17	0.765	1.645	3.024	4.202	4.338	5.586
GK-2	$3.0x10^7$	2600	0.17	0.736	1.581	2.905	4.037	4.168	5.367
GK-2	$3.0x10^7$	2800	0.17	0.709	1.523	2.800	3.890	4.016	5.172

TABLE 3.3: RESULTS OF THE NUMERICAL ANALYSIS PERFORMED ON MODEL GK-2
(* corresponds to the frequency values for the exhibited modal shapes)

MODEL NO.	MATERIAL PROPERTIES			NATURAL FREQUENCIES *Hz*					
	$E_c(kN/m^2)$	$Mass(Kg/m^3)$	ν	MODE 1	MODE 2	MODE 3	MODE 4	MODE 5	MODE 6
GK-3	$1.5x10^7$	2400	0.17	0.542	1.164	2.171	2.980	3.083	4.538
GK-3	$2.0x10^7$	2400	0.17	0.626	1.344	2.508	3.441	3.561	5.240
GK-3	$2.5x10^7$	2400	0.17	0.700	1.502	2.804	3.847	3.981	5.859
*GK-3	$3.0x10^7$	2400	0.17	0.765	1.646	3.071	4.215	4.361	6.418
GK-3	$3.5x10^7$	2400	0.17	0.828	1.778	3.317	4.552	4.710	6.932
GK-3	$3.0x10^7$	2000	0.17	0.840	1.803	3.364	4.617	4.777	7.031
GK-3	$3.0x10^7$	2200	0.17	0.801	1.719	3.208	4.402	4.555	6.703
GK-3	$3.0x10^7$	2400	0.17	0.765	1.646	3.071	4.215	4.361	6.418
GK-3	$3.0x10^7$	2600	0.17	0.736	1.581	2.951	4.190	4.190	6.166
GK-3	$3.0x10^7$	2800	0.17	0.710	1.524	2.843	3.902	4.037	5.941

TABLE 3.4: RESULTS OF THE NUMERICAL ANALYSIS PERFORMED ON MODEL GK-3.
(* corresponds to the frequency values for the exhibited modal shapes)

MODEL NO.	MATERIAL PROPERTIES			NATURAL FREQUENCIES *Hz*					
	$E_c(kN/m^2)$	$Mass(Kg/m^3)$	ν	MODE 1	MODE 2	MODE 3	MODE 4	MODE 5	MODE 6
GK-4	$1.5x10^7$	2400	0.17	0.527	0.942	1.271	1.923	1.993	2.552
GK-4	$2.0x10^7$	2400	0.17	0.609	1.088	1.468	2.220	2.301	2.946
GK-4	$2.5x10^7$	2400	0.17	0.680	1.217	1.641	2.482	2.572	3.294
*GK-4	$3.0x10^7$	2400	0.17	0.745	1.332	1.798	2.719	2.818	3.608
GK-4	$3.5x10^7$	2400	0.17	0.805	1.439	1.942	2.937	3.044	3.898
GK-4	$3.0x10^7$	2000	0.17	0.817	1.460	1.970	2.979	3.087	3.953
GK-4	$3.0x10^7$	2200	0.17	0.779	1.392	1.878	2.840	2.944	3.769
GK-4	$3.0x10^7$	2400	0.17	0.745	1.332	1.798	2.719	2.818	3.608
GK-4	$3.0x10^7$	2600	0.17	0.716	1.280	1.727	2.612	2.708	3.467
GK-4	$3.0x10^7$	2800	0.17	0.690	1.234	1.665	2.517	2.609	3.341

TABLE 3.5: RESULTS OF THE NUMERICAL ANALYSIS PERFORMED ON MODEL GK-4.
(* corresponds to the frequency values for the exhibited modal shapes)

MODEL NO.	MATERIAL PROPERTIES			NATURAL FREQUENCIES *Hz*					
	$E_c(kN/m^2)$	$Mass(Kg/m^3)$	ν	MODE 1	MODE 2	MODE 3	MODE 4	MODE 5	MODE 6
GK-5	$1.5x10^7$	2400	0.17	0.539	1.097	1.608	1.923	2.552	3.018
GK-5	$2.0x10^7$	2400	0.17	0.623	1.267	1.857	2.220	2.946	3.485
GK-5	$2.5x10^7$	2400	0.17	0.696	1.417	2.076	2.482	3.294	3.897
*GK-5	$3.0x10^7$	2400	0.17	0.762	1.552	2.274	2.719	3.608	4.269
GK-5	$3.5x10^7$	2400	0.17	0.824	1.676	2.457	2.937	3.898	4.611
GK-5	$3.0x10^7$	2000	0.17	0.835	1.700	2.591	2.979	3.953	4.676
GK-5	$3.0x10^7$	2200	0.17	0.796	1.621	2.375	2.840	3.769	4.458
GK-5	$3.0x10^7$	2400	0.17	0.762	1.552	2.274	2.719	3.608	4.269
GK-5	$3.0x10^7$	2600	0.17	0.733	1.491	2.185	2.612	3.467	4.101
GK-5	$3.0x10^7$	2800	0.17	0.706	1.437	2.106	2.517	3.341	3.952

TABLE 3.6: RESULTS OF THE NUMERICAL ANALYSIS PERFORMED ON MODEL GK-5.
(* corresponds to the frequency values for the exhibited modal shapes)

MODEL NO.	MATERIAL PROPERTIES			NATURAL FREQUENCIES *Hz*					
	$E_c(kN/m^2)$	$Mass(Kg/m^3)$	ν	MODE 1	MODE 2	MODE 3	MODE 4	MODE 5	MODE 6
GK-6	$1.5x10^7$	2400	0.17	0.541	1.137	1.926	2.138	2.779	3.214
GK-6	$2.0x10^7$	2400	0.17	0.625	1.313	2.224	2.468	3.209	3.711
GK-6	$2.5x10^7$	2400	0.17	0.699	1.467	2.486	2.760	3.588	4.149
*GK-6	$3.0x10^7$	2400	0.17	0.765	1.608	2.724	3.023	3.931	4.545
GK-6	$3.5x10^7$	2400	0.17	0.827	1.736	2.942	3.265	4.245	4.909
GK-6	$3.0x10^7$	2000	0.17	0.838	1.761	2.984	3.312	4.306	4.979
GK-6	$3.0x10^7$	2200	0.17	0.799	1.679	2.845	3.157	4.105	4.747
GK-6	$3.0x10^7$	2400	0.17	0.765	1.608	2.724	3.023	3.931	4.545
GK-6	$3.0x10^7$	2600	0.17	0.735	1.544	2.617	2.904	3.776	4.366
GK-6	$3.0x10^7$	2800	0.17	0.709	1.488	2.522	2.799	3.639	4.208

TABLE 3.7: RESULTS OF THE NUMERICAL ANALYSIS PERFORMED ON MODEL GK-6.
(* corresponds to the frequency values for the exhibited modal shapes)

MODEL NO.	MATERIAL PROPERTIES			NATURAL FREQUENCIES *Hz*					
	$E_c(kN/m^2)$	$Mass(Kg/m^3)$	ν	MODE 1	MODE 2	MODE 3	MODE 4	MODE 5	MODE 6
GK-88	$1.5x10^7$	2400	0.17	0.538	1.088	1.255	1.728	2.115	2.129
GK-88	$2.0x10^7$	2400	0.17	0.621	1.256	1.449	1.995	2.442	2.458
GK-88	$2.5x10^7$	2400	0.17	0.694	1.405	1.621	2.230	2.730	2.748
*GK-88	$3.0x10^7$	2400	0.17	0.761	1.539	1.775	2.443	2.991	3.011
GK-88	$3.5x10^7$	2400	0.17	0.882	1.662	1.917	2.639	3.230	3.252
GK-88	$3.0x10^7$	2000	0.17	0.833	1.686	1.945	2.676	3.276	3.298
GK-88	$3.0x10^7$	2200	0.17	0.794	1.607	1.854	2.552	3.124	3.114
GK-88	$3.0x10^7$	2400	0.17	0.761	1.539	1.775	2.443	2.991	3.011
GK-88	$3.0x10^7$	2600	0.17	0.731	1.478	1.705	2.347	2.873	2.892
GK-88	$3.0x10^7$	2800	0.17	0.704	1.425	1.643	2.262	2.769	2.787

TABLE 3.8: RESULTS OF THE NUMERICAL ANALYSIS PERFORMED ON MODEL GK-88.
(* corresponds to the frequency values for the exhibited modal shapes)

MODEL NO.	MATERIAL PROPERTIES			NATURAL FREQUENCIES *Hz*					
	$E_c(kN/m^2)$	$Mass(Kg/m^3)$	ν	MODE 1	MODE 2	MODE 3	MODE 4	MODE 5	MODE 6
GK-87	$1.5x10^7$	2400	0.17	0.525	0.754	1.161	1.256	1.741	2.119
GK-87	$2.0x10^7$	2400	0.17	0.606	0.871	1.341	1.450	2.011	2.446
GK-87	$2.5x10^7$	2400	0.17	0.677	0.973	1.499	1.621	2.248	2.735
*GK-87	$3.0x10^7$	2400	0.17	0.742	1.066	1.643	1.776	2.463	2.997
GK-87	$3.5x10^7$	2400	0.17	0.801	1.152	1.774	1.918	2.660	3.236
GK-87	$3.0x10^7$	2000	0.17	0.813	1.168	1.799	1.946	2.698	3.282
GK-87	$3.0x10^7$	2200	0.17	0.775	1.114	1.716	1.855	2.572	3.129
GK-87	$3.0x10^7$	2400	0.17	0.742	1.066	1.643	1.776	2.463	2.997
GK-87	$3.0x10^7$	2600	0.17	0.713	1.024	1.578	1.707	2.366	2.879
GK-87	$3.0x10^7$	2800	0.17	0.687	0.987	1.521	1.644	2.280	2.744

TABLE 3.9: RESULTS OF THE NUMERICAL ANALYSIS PERFORMED ON MODEL GK-87.
(* corresponds to the frequency values for the exhibited modal shapes)

MODEL NO.	MATERIAL PROPERTIES			NATURAL FREQUENCIES *Hz*					
	$E_c(kN/m^2)$	$Mass(Kg/m^3)$	ν	MODE 1	MODE 2	MODE 3	MODE 4	MODE 5	MODE 6
GK-86	$1.5x10^7$	2400	0.17	0.456	0.638	0.828	1.255	1.256	1.755
GK-86	$2.0x10^7$	2400	0.17	0.526	0.737	0.956	1.449	1.450	2.2027
GK-86	$2.5x10^7$	2400	0.17	0.588	0.824	1.069	1.620	1.621	2.266
*GK-86	$3.0x10^7$	2400	0.17	0.644	0.902	1.171	1.776	1.776	2.482
GK-86	$3.5x10^7$	2400	0.17	0.696	0.975	1.265	1.917	1.919	2.681
GK-86	$3.0x10^7$	2000	0.17	0.706	0.988	1.283	1.945	1.946	2.719
GK-86	$3.0x10^7$	2200	0.17	0.673	0.942	1.223	1.854	1.855	2.592
GK-86	$3.0x10^7$	2400	0.17	0.644	0.902	1.171	1.776	1.776	2.482
GK-86	$3.0x10^7$	2600	0.17	0.619	0.867	1.125	1.705	1.855	2.385
GK-86	$3.0x10^7$	2800	0.17	0.596	0.835	1.084	1.643	1.644	2.298

TABLE 3.10: RESULTS OF THE NUMERICAL ANALYSIS PERFORMED ON MODEL GK-86
(* corresponds to the frequency values for the exhibited modal shapes)

MODEL NO.	MATERIAL PROPERTIES			NATURAL FREQUENCIES *Hz*					
	$E_c(kN/m^2)$	$Mass(Kg/m^3)$	ν	MODE 1	MODE 2	MODE 3	MODE 4	MODE 5	MODE 6
GK-85	$1.5x10^7$	2400	0.17	0.324	0.576	0.710	1.232	1.256	1.745
GK-85	$2.0x10^7$	2400	0.17	0.375	0.665	0.820	1.422	1.450	2.014
GK-85	$2.5x10^7$	2400	0.17	0.419	0.744	0.917	1.590	1.621	2.252
*GK-85	$3.0x10^7$	2400	0.17	0.459	0.815	1.004	1.742	1.776	2.467
GK-85	$3.5x10^7$	2400	0.17	0.496	0.880	1.085	1.881	1.918	2.665
GK-85	$3.0x10^7$	2000	0.17	0.503	0.892	1.100	1.908	1.945	2.703
GK-85	$3.0x10^7$	2200	0.17	0.479	0.851	1.049	1.819	1.855	2.577
GK-85	$3.0x10^7$	2400	0.17	0.459	0.815	1.004	1.742	1.776	2.467
GK-85	$3.0x10^7$	2600	0.17	0.441	0.783	0.965	1.673	1.706	2.370
GK-85	$3.0x10^7$	2800	0.17	0.425	0.754	0.930	1.613	1.644	2.284

TABLE 3.11: RESULTS OF THE NUMERICAL ANALYSIS PERFORMED ON MODEL GK-85.
(* corresponds to the frequency values for the exhibited modal shapes)

MODEL NO.	MATERIAL PROPERTIES			NATURAL FREQUENCIES *Hz*					
	$E_c(kN/m^2)$	$Mass(Kg/m^3)$	ν	MODE 1	MODE 2	MODE 3	MODE 4	MODE 5	MODE 6
GK-84	$1.5x10^7$	2400	0.17	0.205	0.513	0.586	1.227	1.249	1.556
GK-84	$2.0x10^7$	2400	0.17	0.236	0.592	0.677	1.417	1.443	1.797
GK-84	$2.5x10^7$	2400	0.17	0.264	0.662	0.757	1.584	1.613	2.009
*GK-84	$3.0x10^7$	2400	0.17	0.301	0.725	0.829	1.736	1.767	2.201
GK-84	$3.5x10^7$	2400	0.17	0.313	0.784	0.895	1.875	1.909	2.377
GK-84	$3.0x10^7$	2000	0.17	0.317	0.795	0.908	1.901	1.936	2.410
GK-84	$3.0x10^7$	2200	0.17	0.302	0.758	0.866	1.813	1.845	2.298
GK-84	$3.0x10^7$	2400	0.17	0.301	0.725	0.829	1.736	1.767	2.201
GK-84	$3.0x10^7$	2600	0.17	0.278	0.697	0.796	1.668	1.698	2.114
GK-84	$3.0x10^7$	2800	0.17	0.268	0.672	0.767	1.607	1.636	2.037

TABLE 3.12: RESULTS OF THE NUMERICAL ANALYSIS PERFORMED ON MODEL GK-84.
(* corresponds to the frequency values for the exhibited modal shapes)

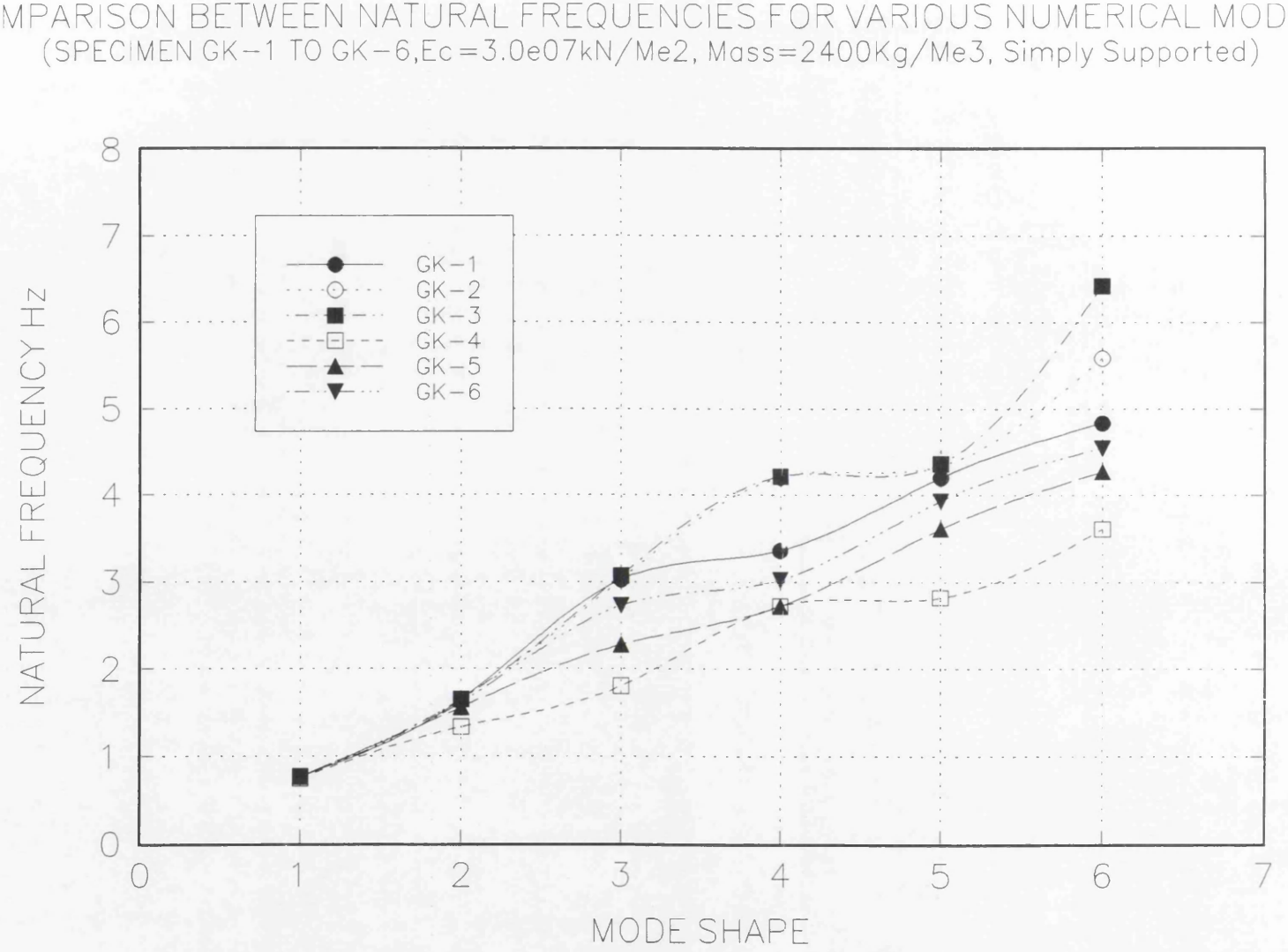

Fig. 3.1 :Natural frequencies for numerical models GK-1 to GK-6.

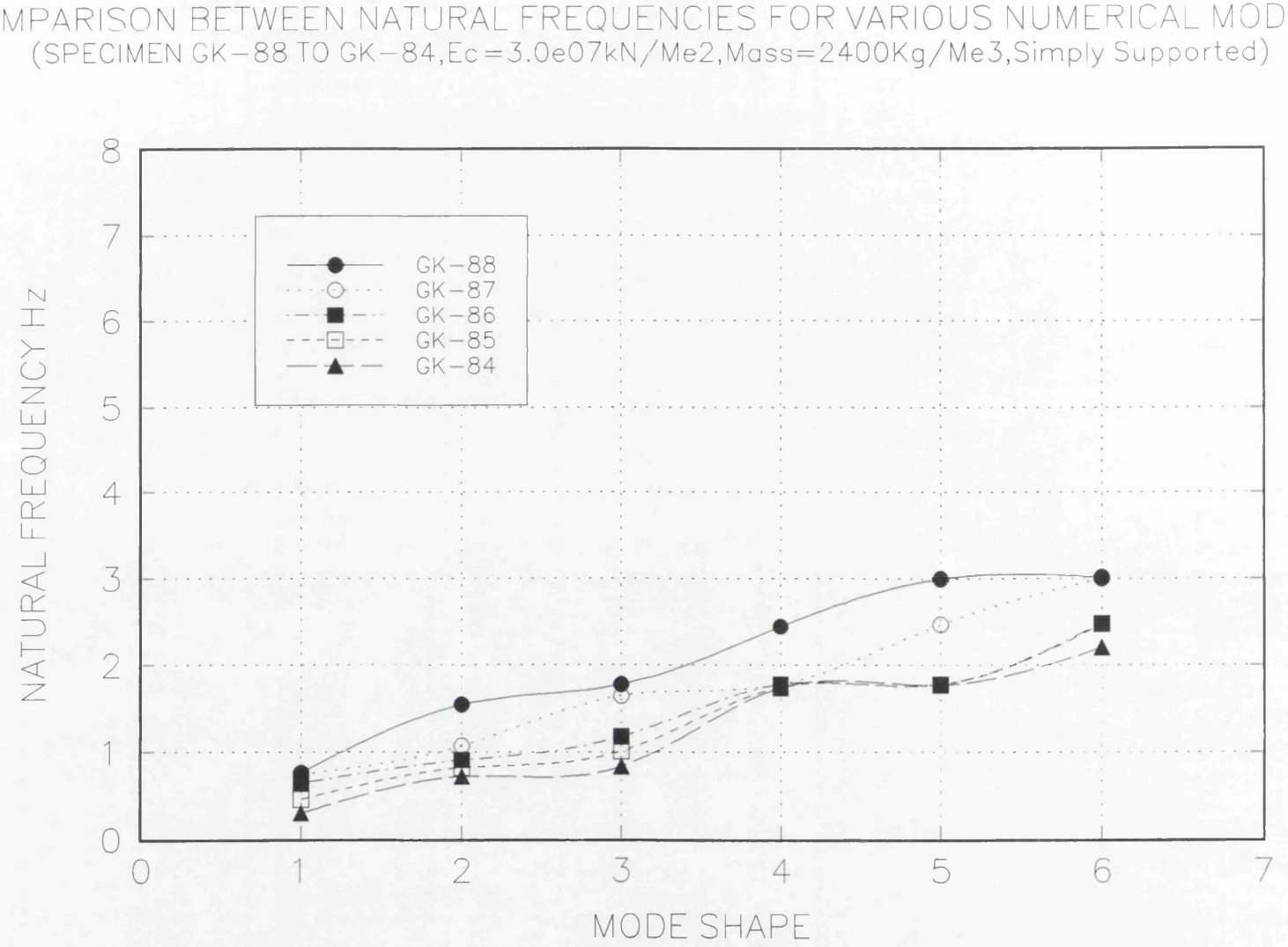

Fig. 3.2:Natural frequencies for numerical models GK-88, 87, 86, 85 ,84.

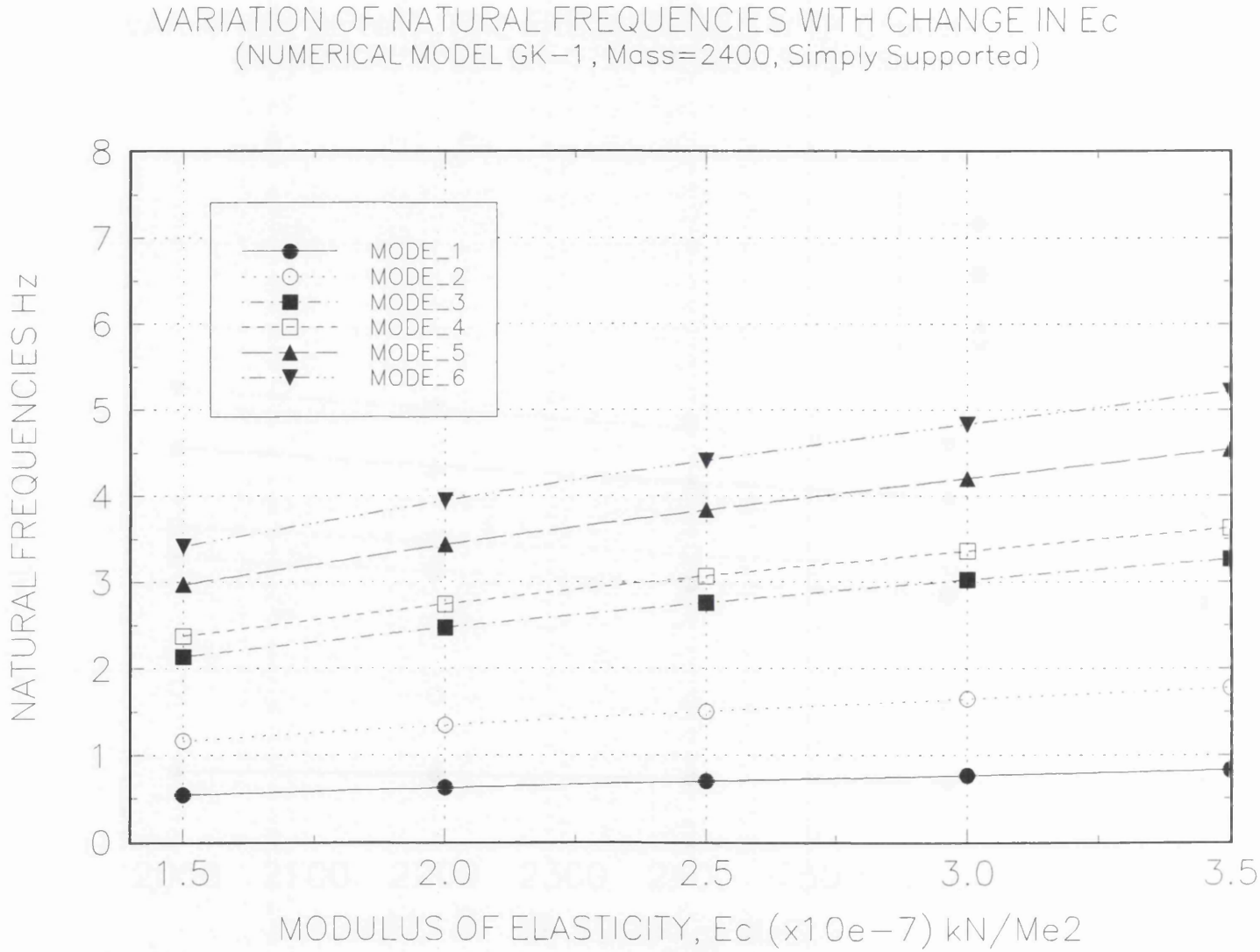

Fig. 3.3:Variation in natural frequencies with change in Ec for GK-1.

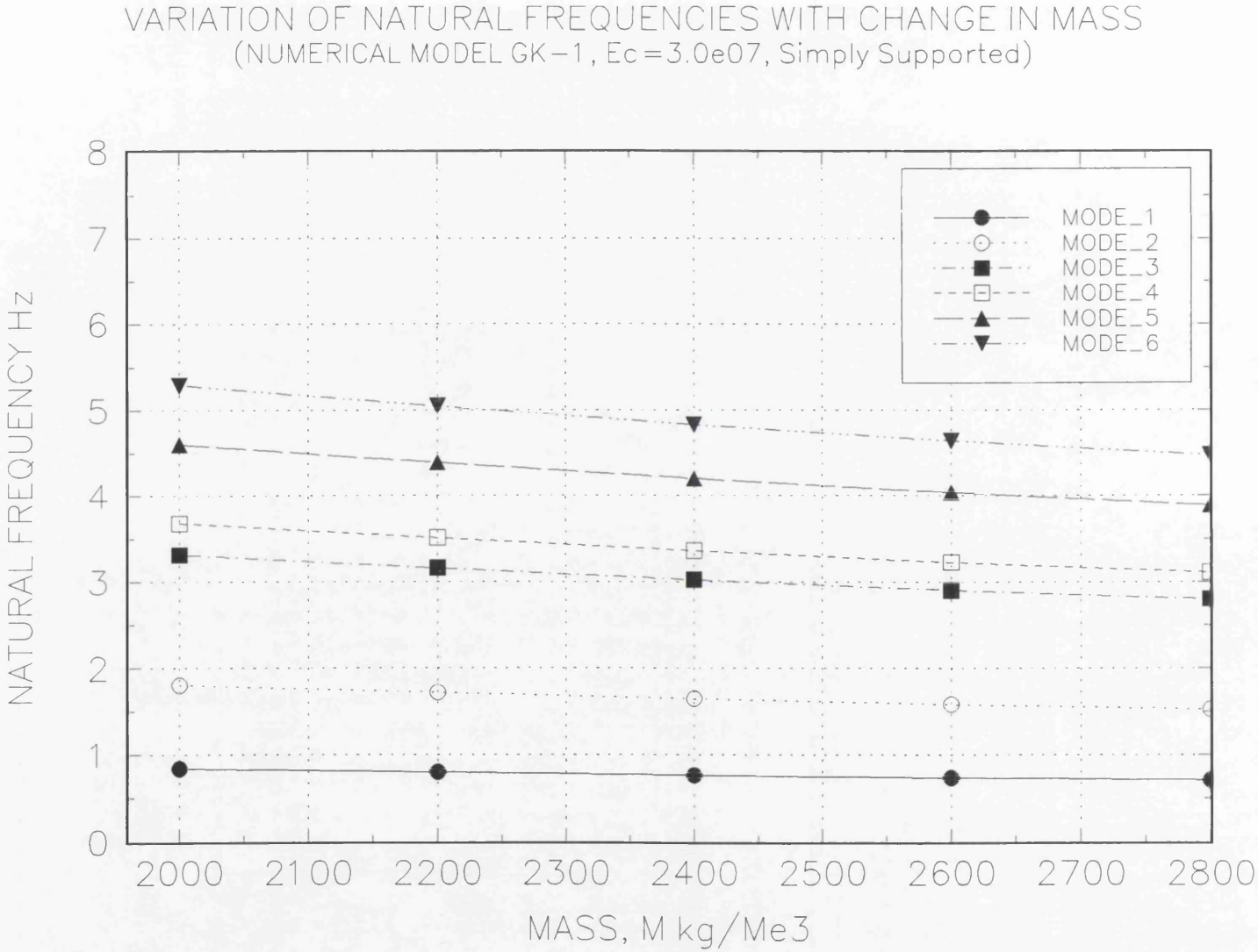

Fig. 3.4:Variation in natural frequencies with change in mass for GK−1.

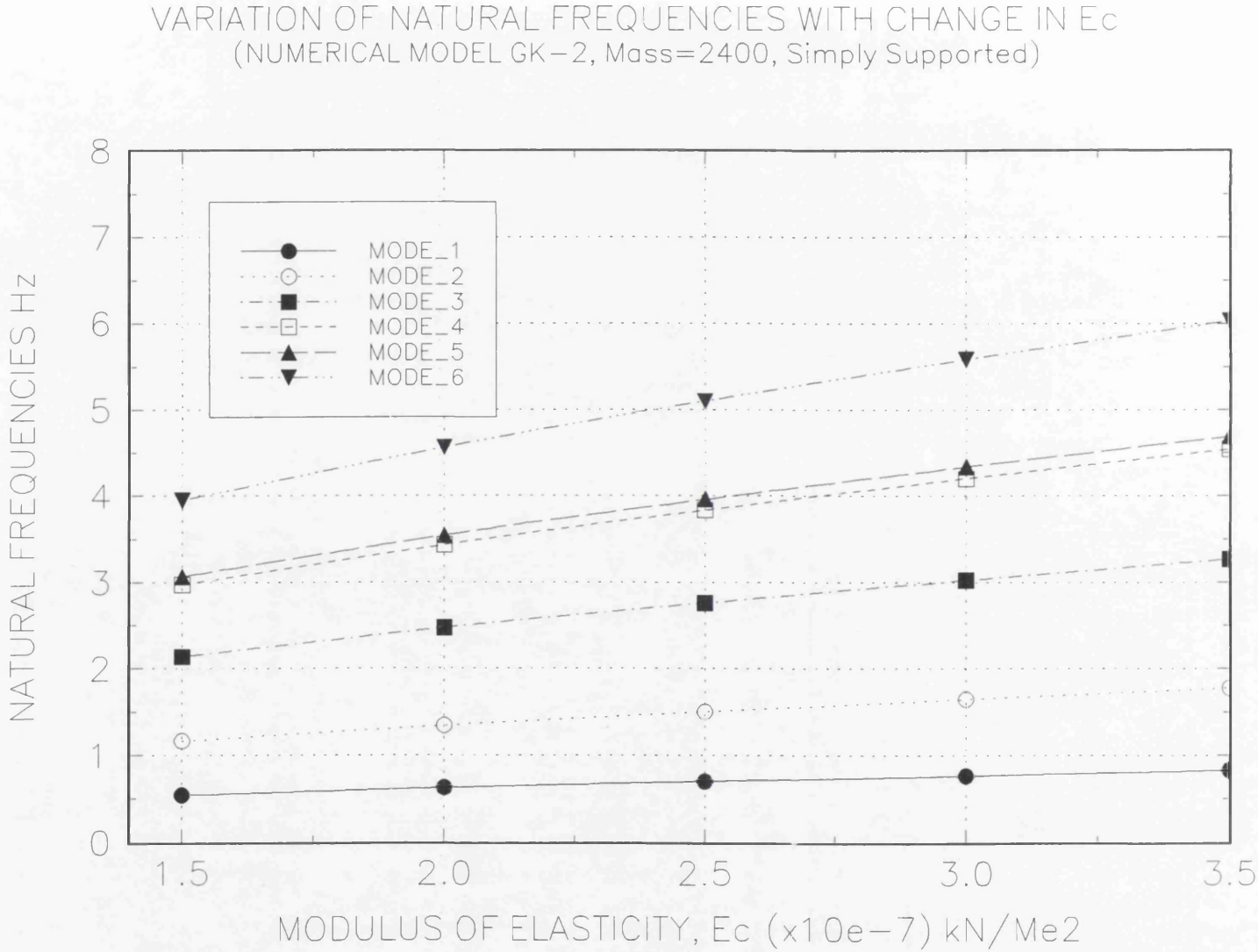

Fig. 3.5:Variation in natural frequencies with change in Ec for GK-2.

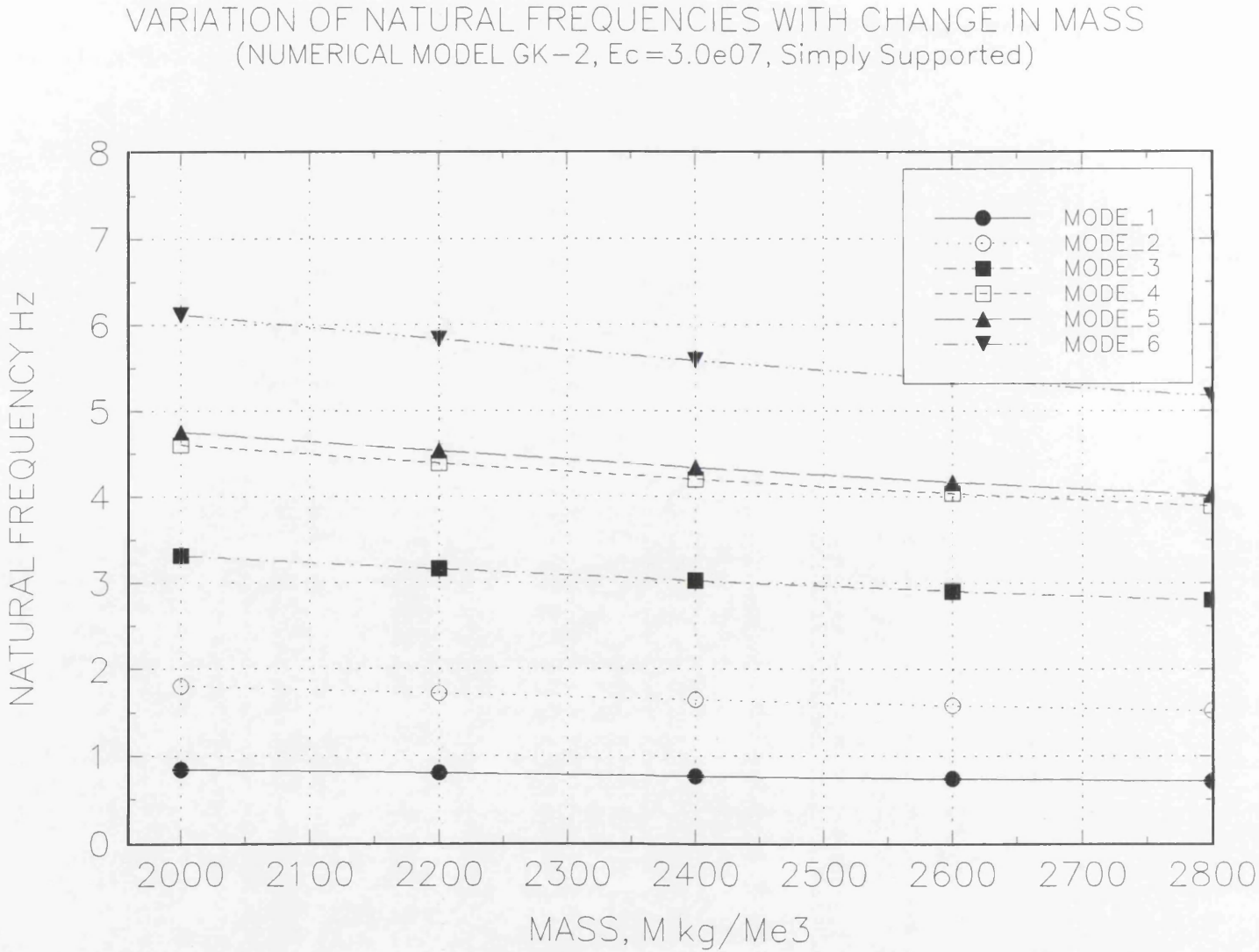

Fig. 3.6:Variation in natural frequencies with change in mass for GK−2.

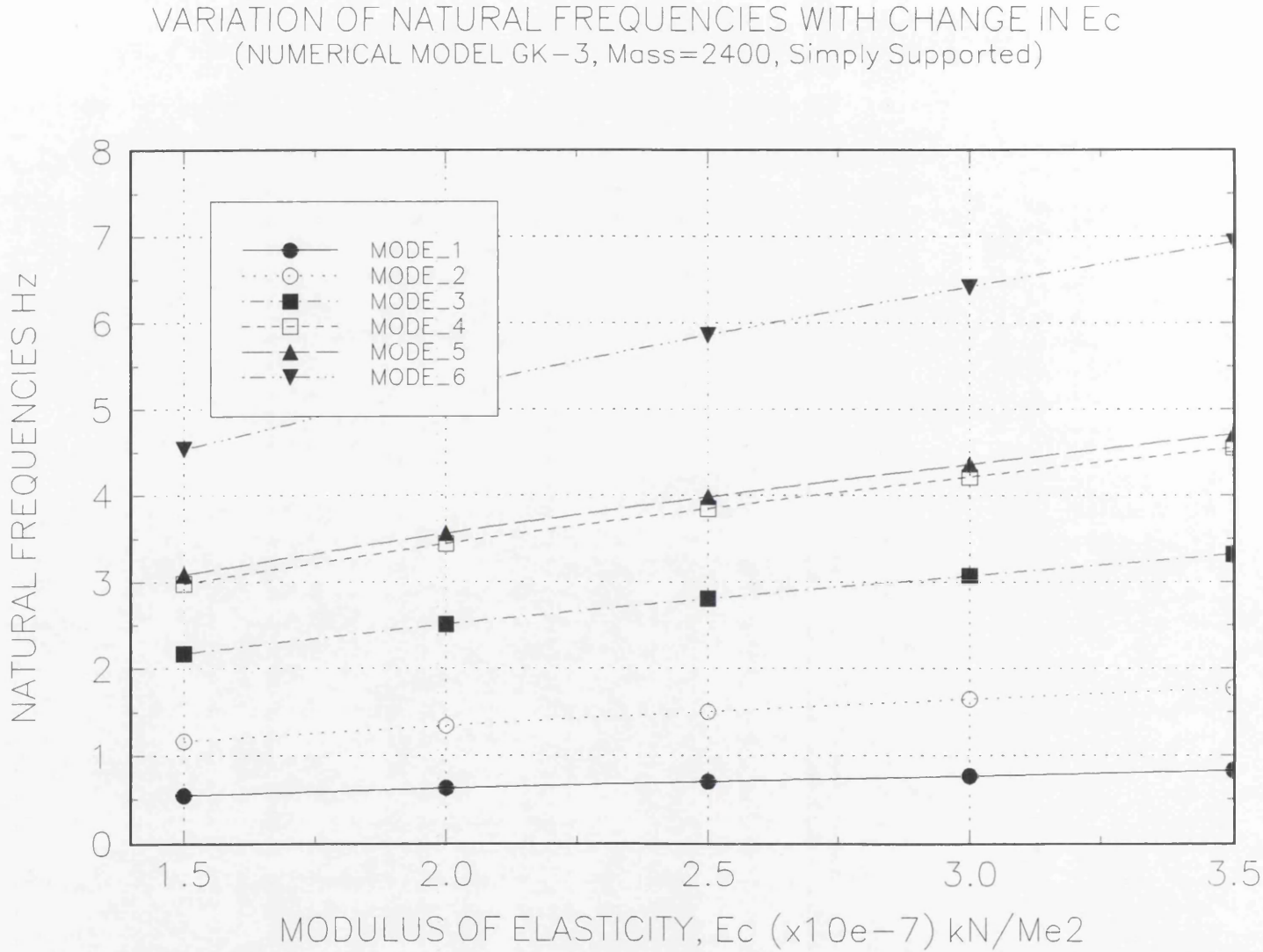

Fig. 3.7:Variation in natural frequencies with change in Ec for GK-3.

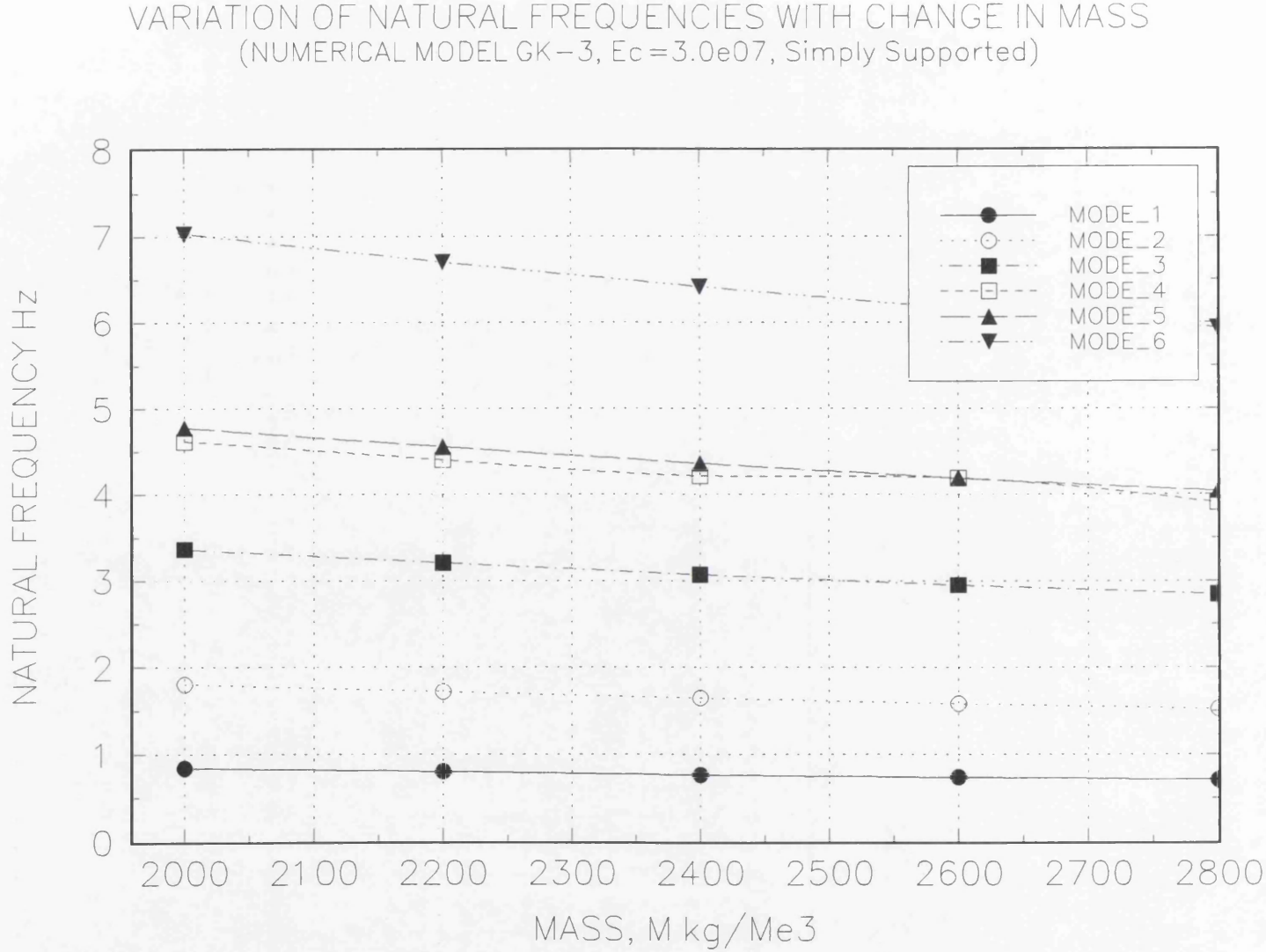

Fig. 3.8:Variation in natural frequencies with change in mass for GK-3.

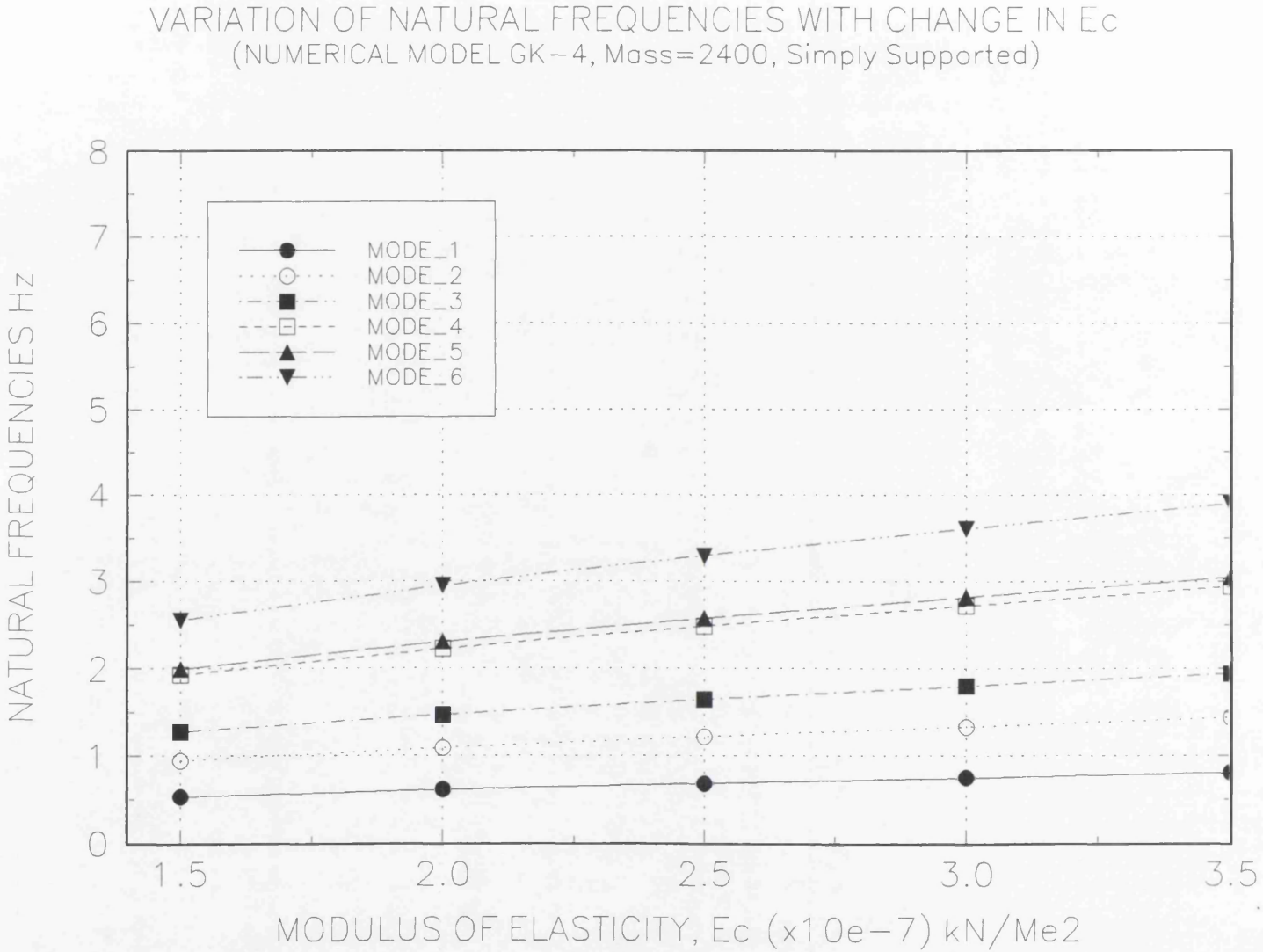

Fig. 3.9:Variation in natural frequencies with change in Ec for GK-4.

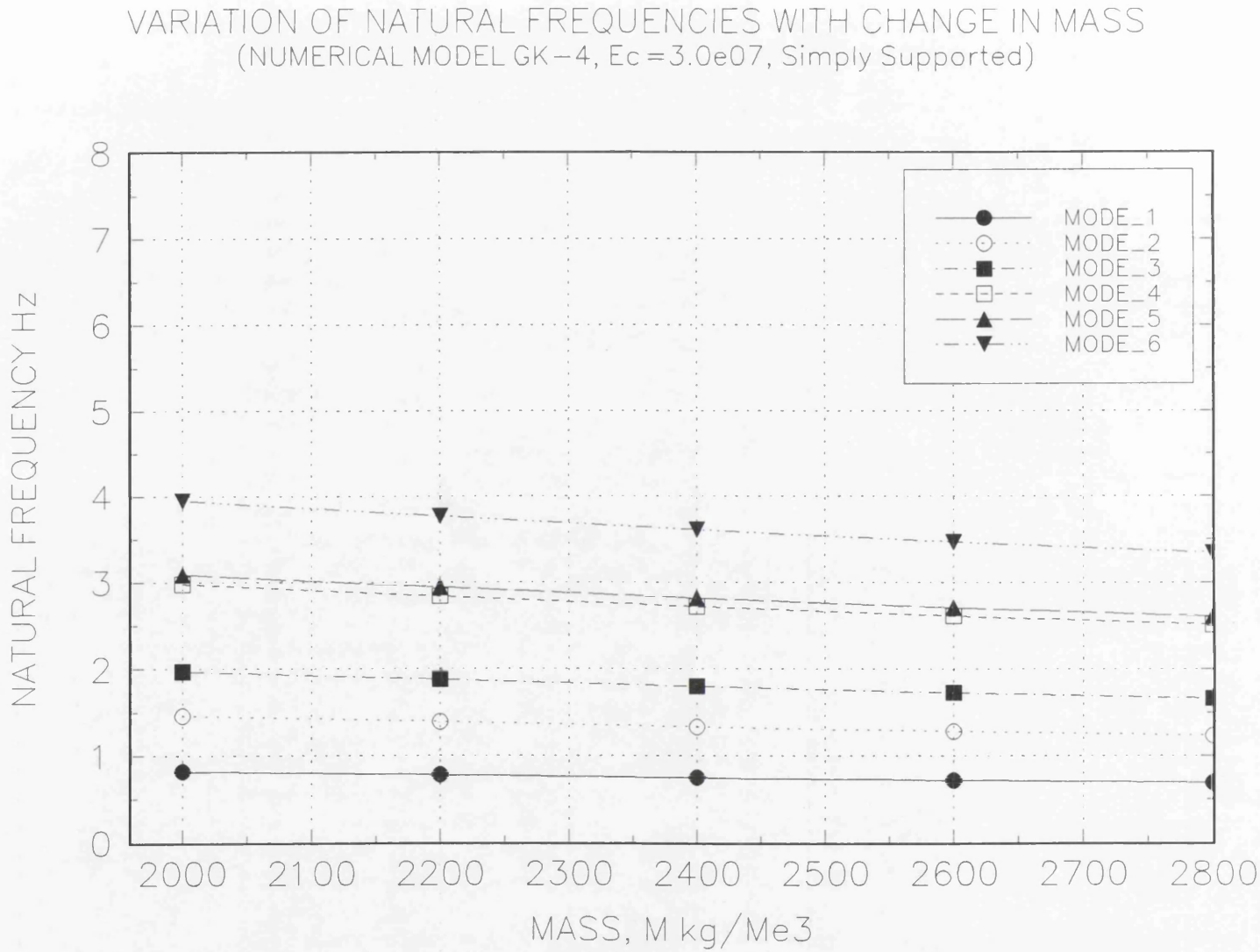

Fig. 3.10:Variation in natural frequencies with change in mass for GK−4.

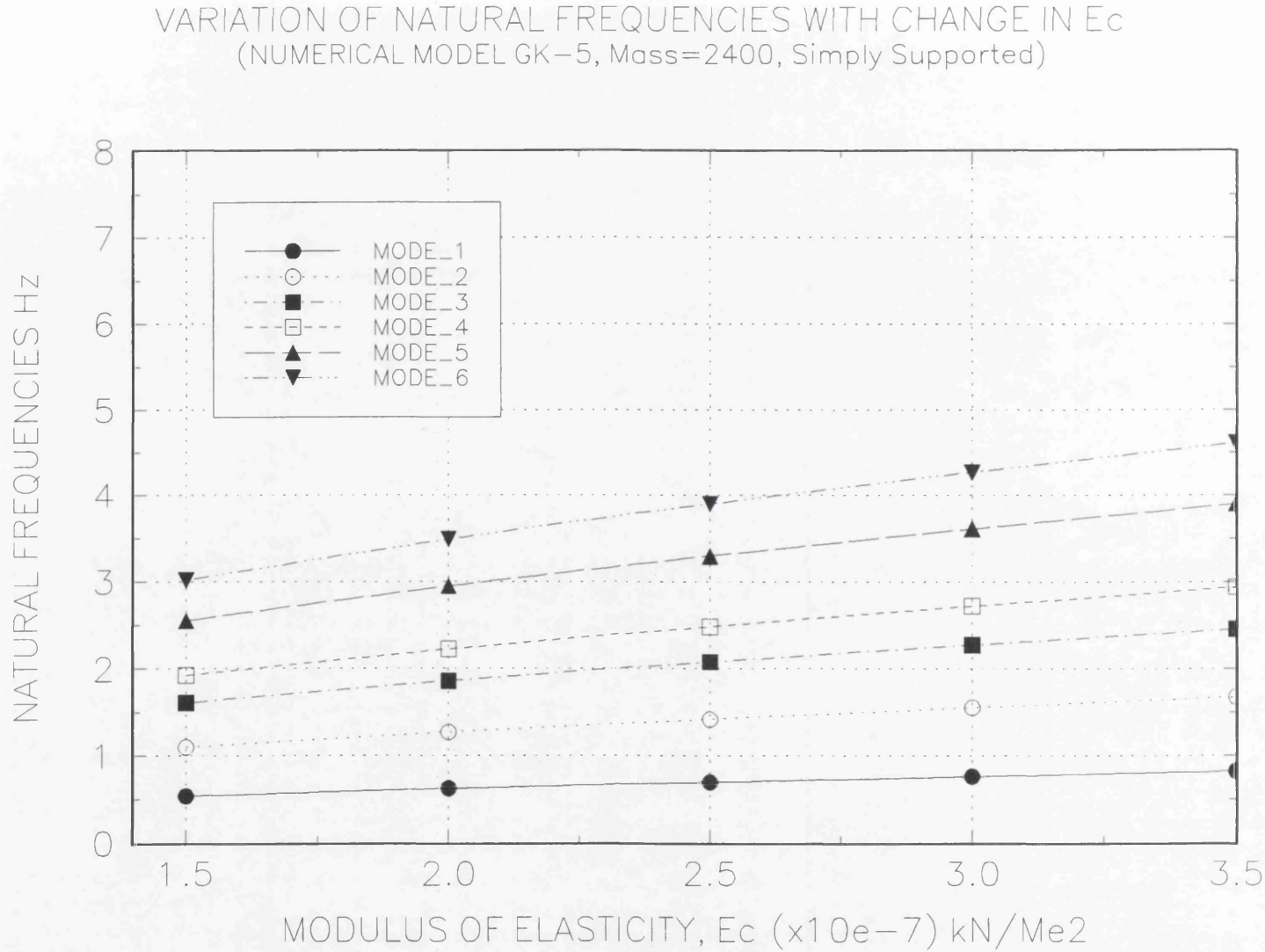

Fig. 3.11 :Variation in natural frequencies with change in Ec for GK-5.

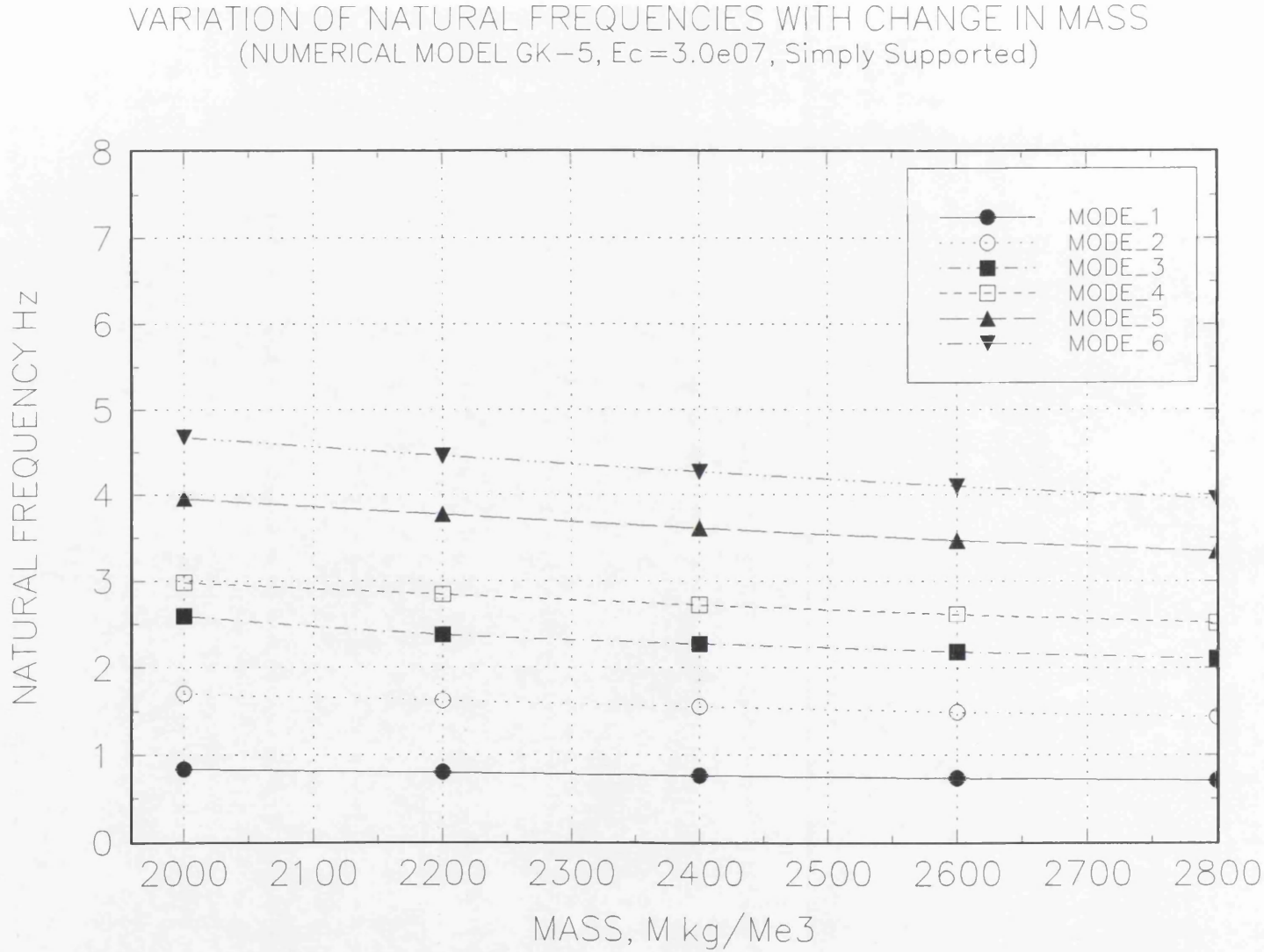

Fig. 3.12:Variation in natural frequencies with change in mass for GK−5.

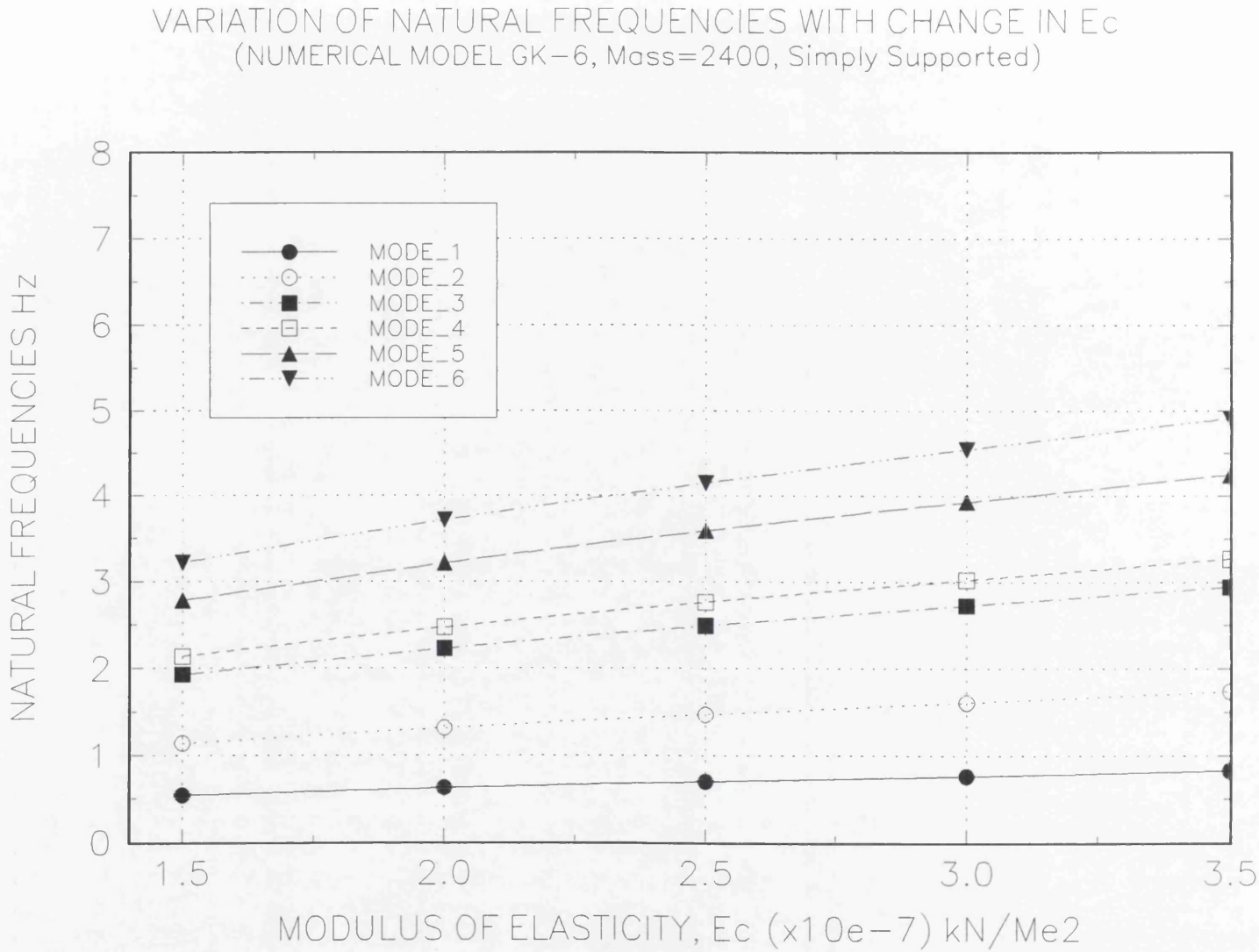

Fig. 3.13:Variations in natural frequencies with change in Ec for GK-6.

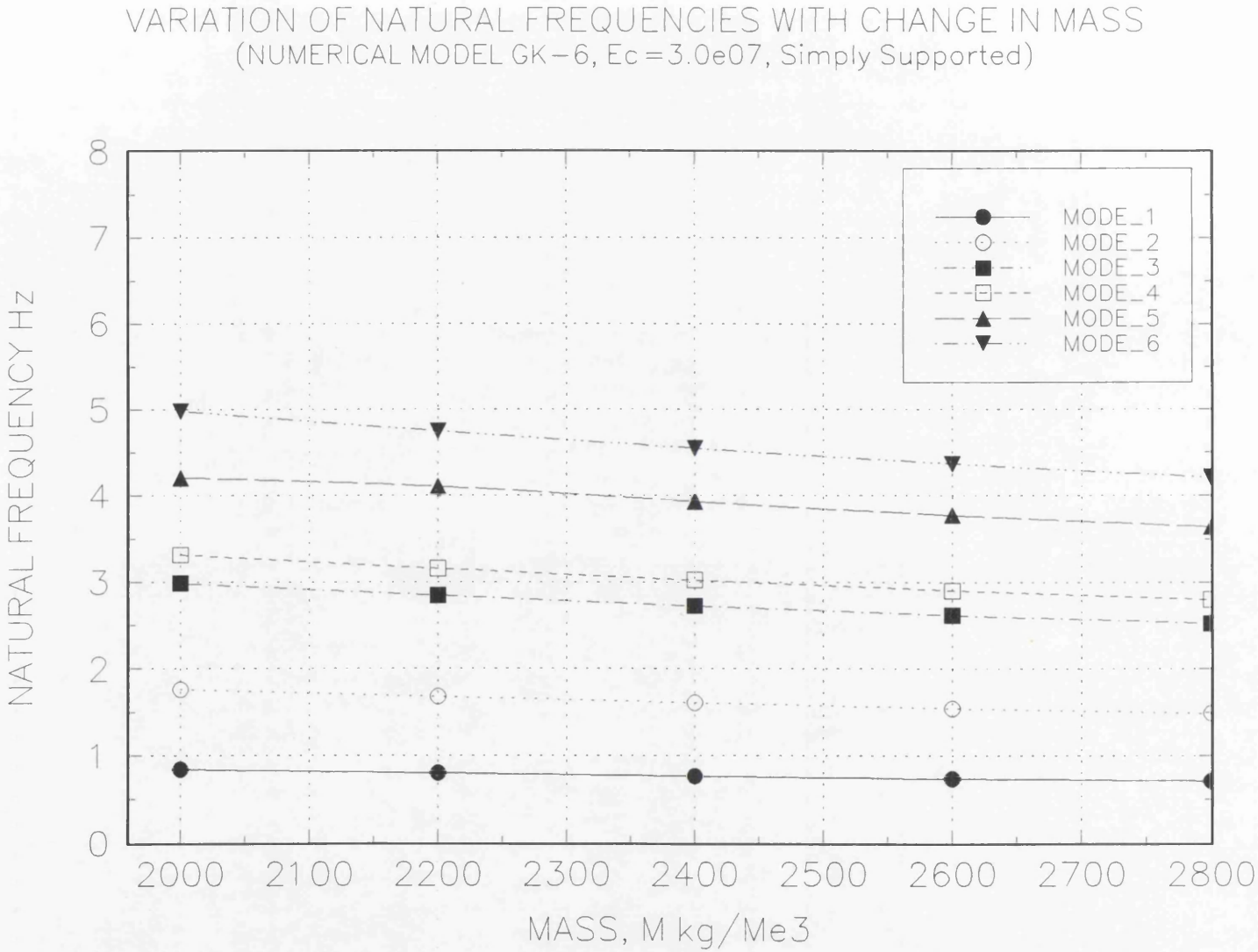

Fig. 3.14:Variation in natural frequencies with change in mass for GK−6.

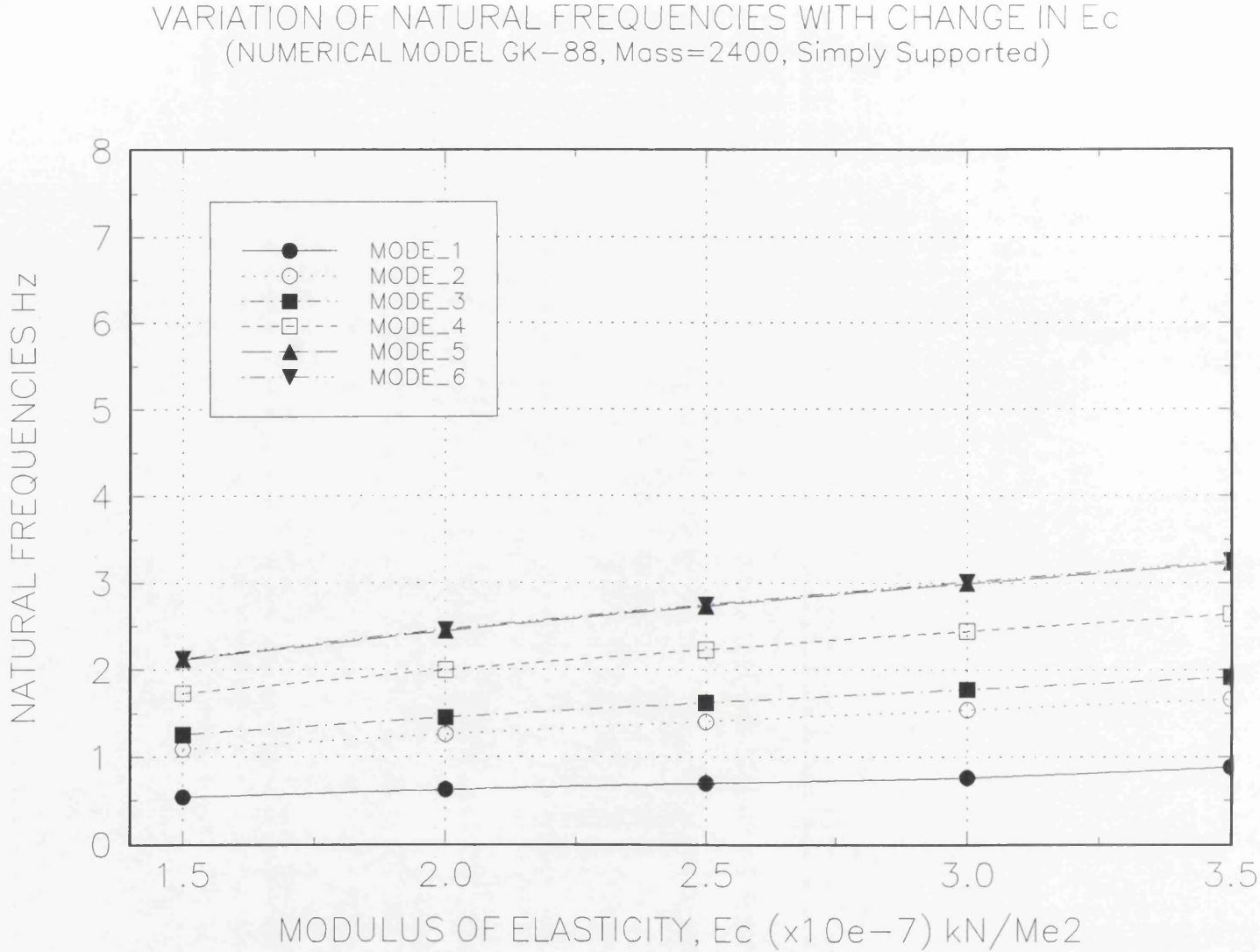

Fig. 3.15:Variations in natural frequencies with change in Ec for GK−88.

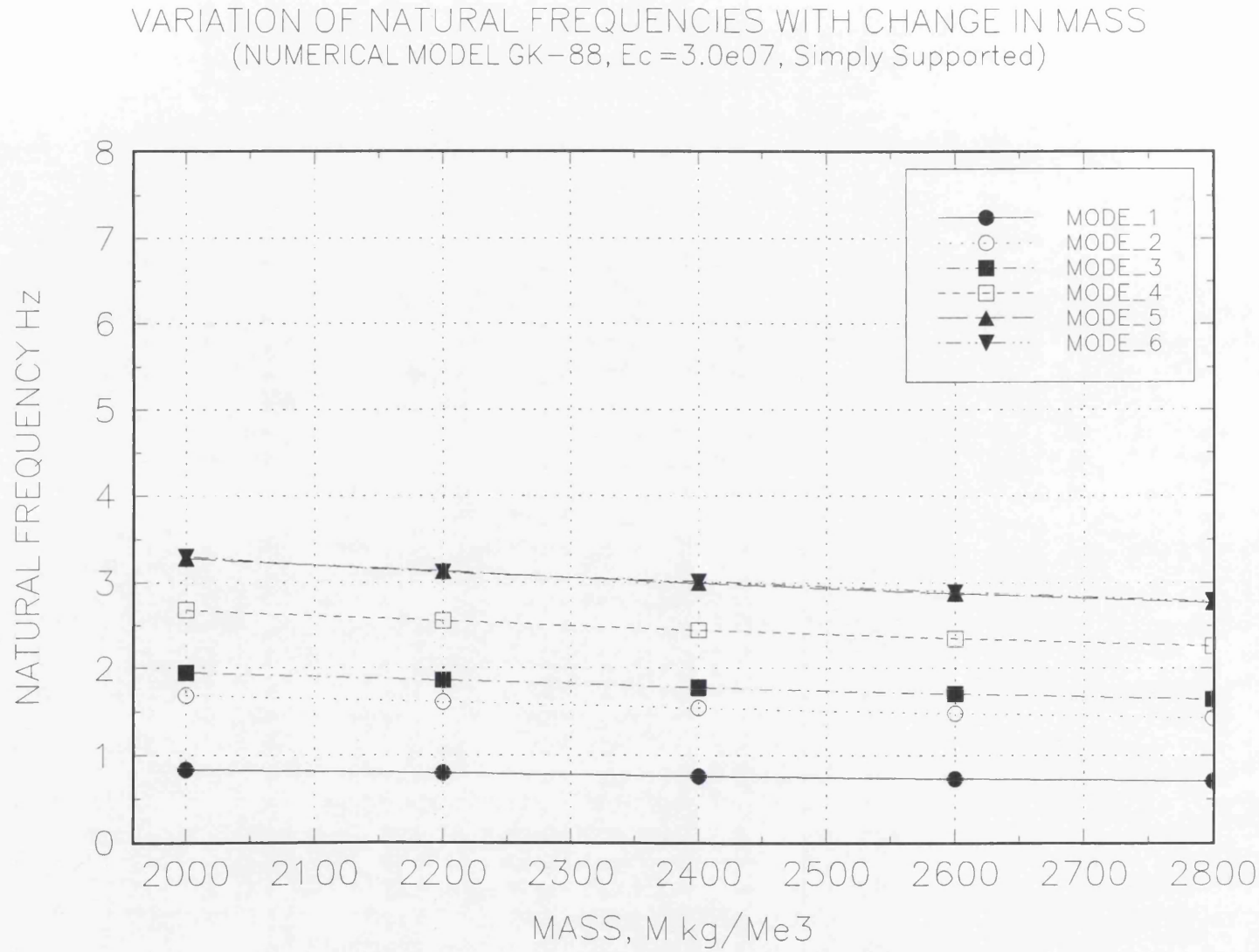

Fig. 3.16:Variation in natural frequencies with change in mass for GK−88.

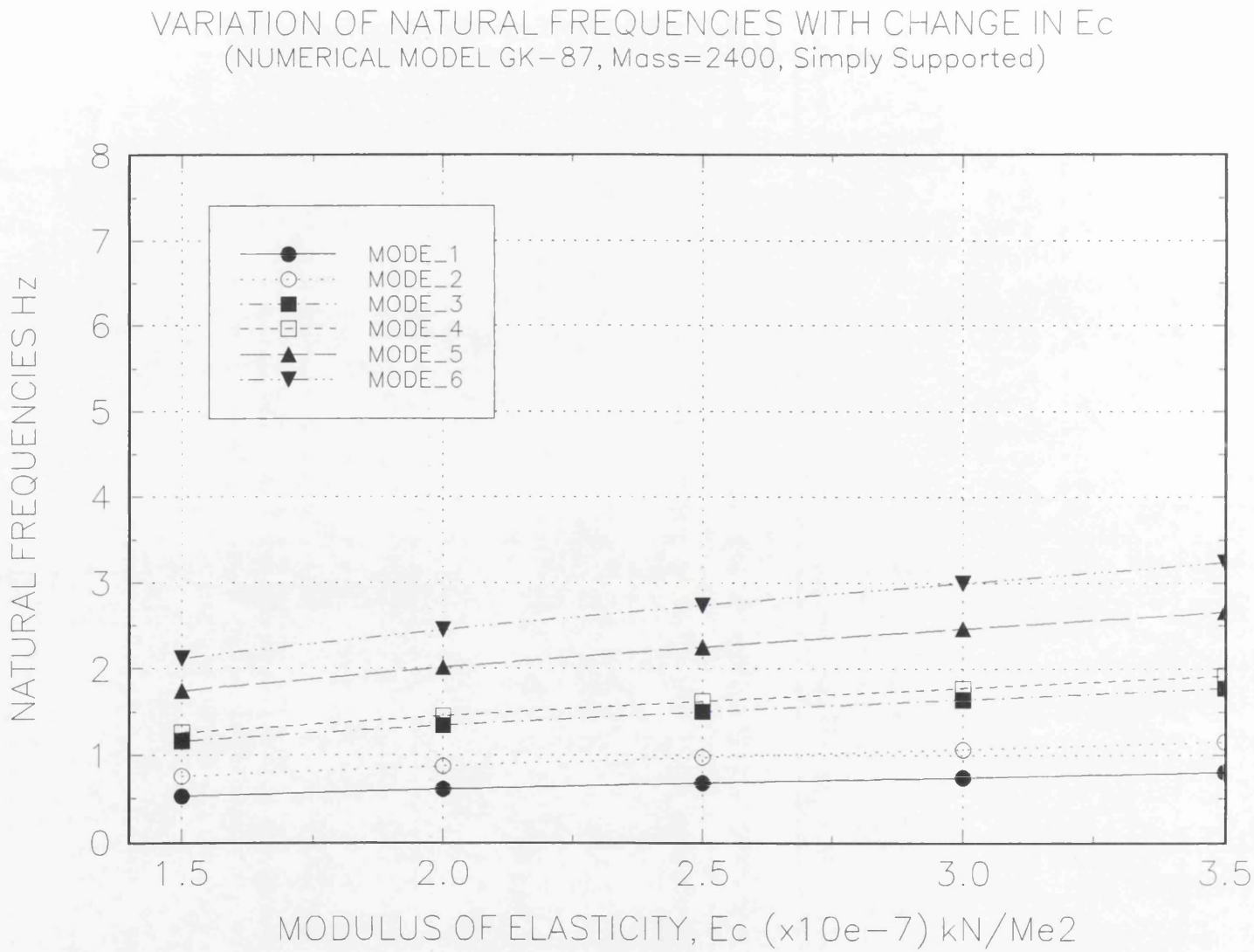

Fig. 3.17:Variations in natural frequencies with change in Ec for GK-87.

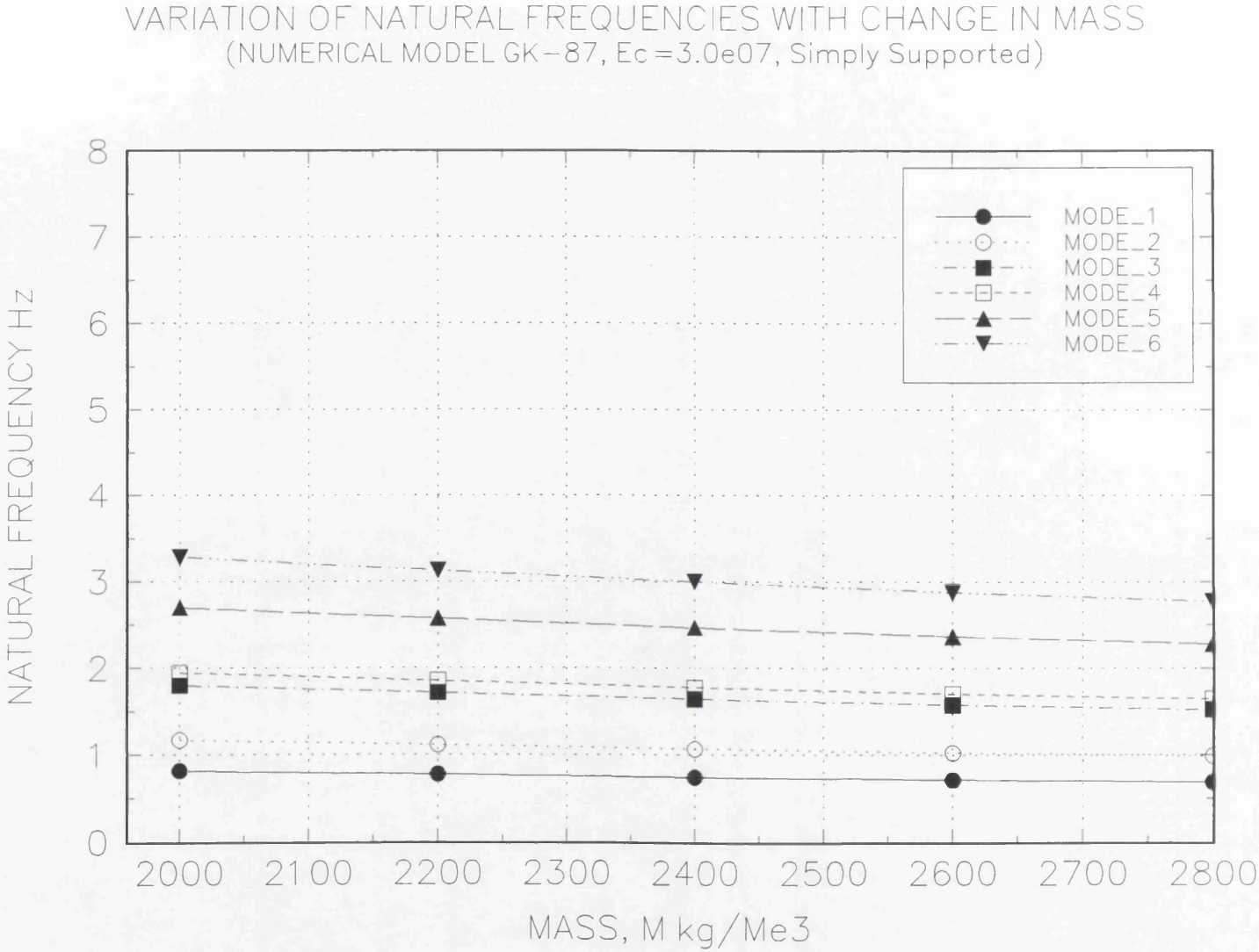

Fig. 3.18:Variation in natural frequencies with change in mass for GK−87.

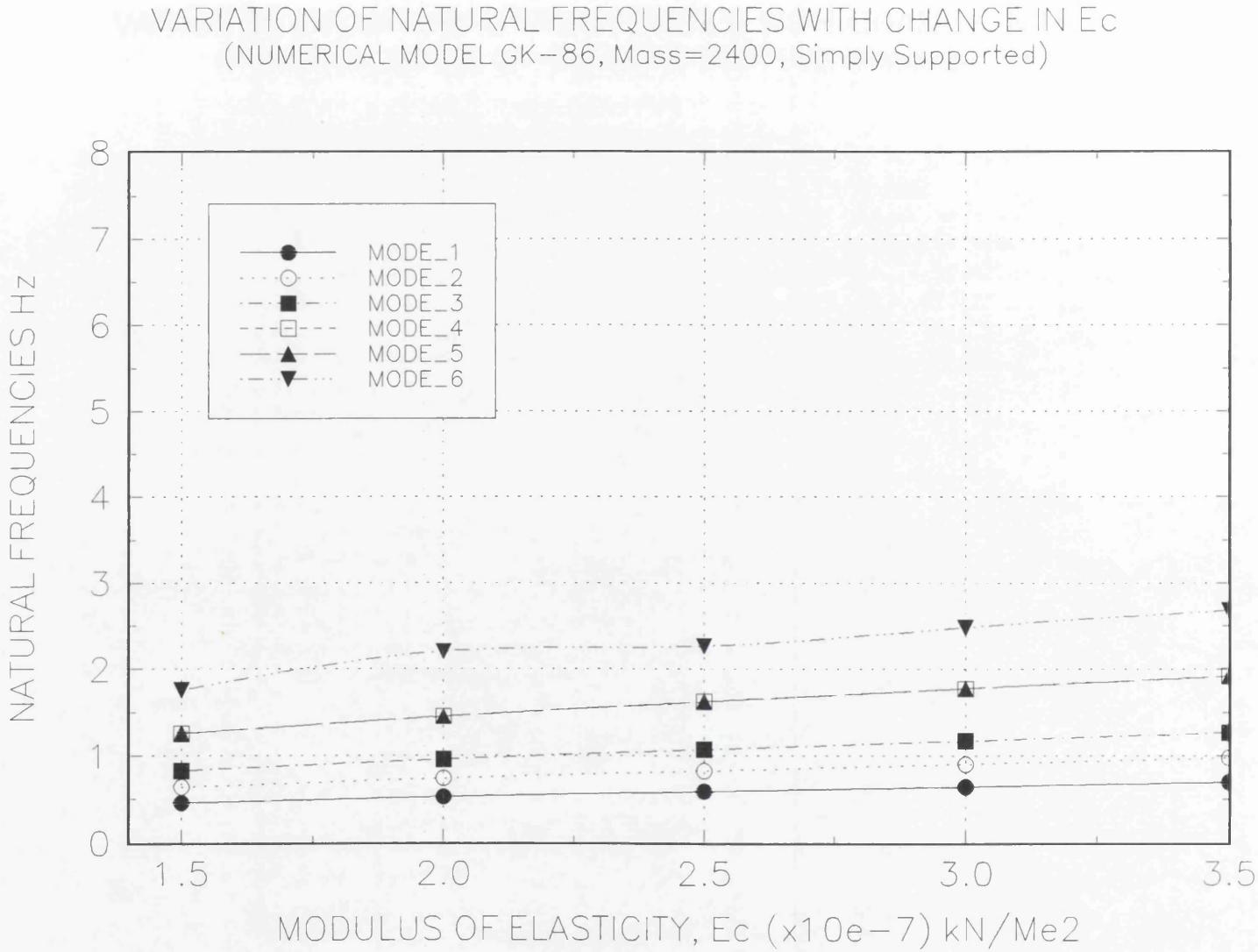

Fig. 3.19:Variation in natural frequencies with change in Ec for GK-86.

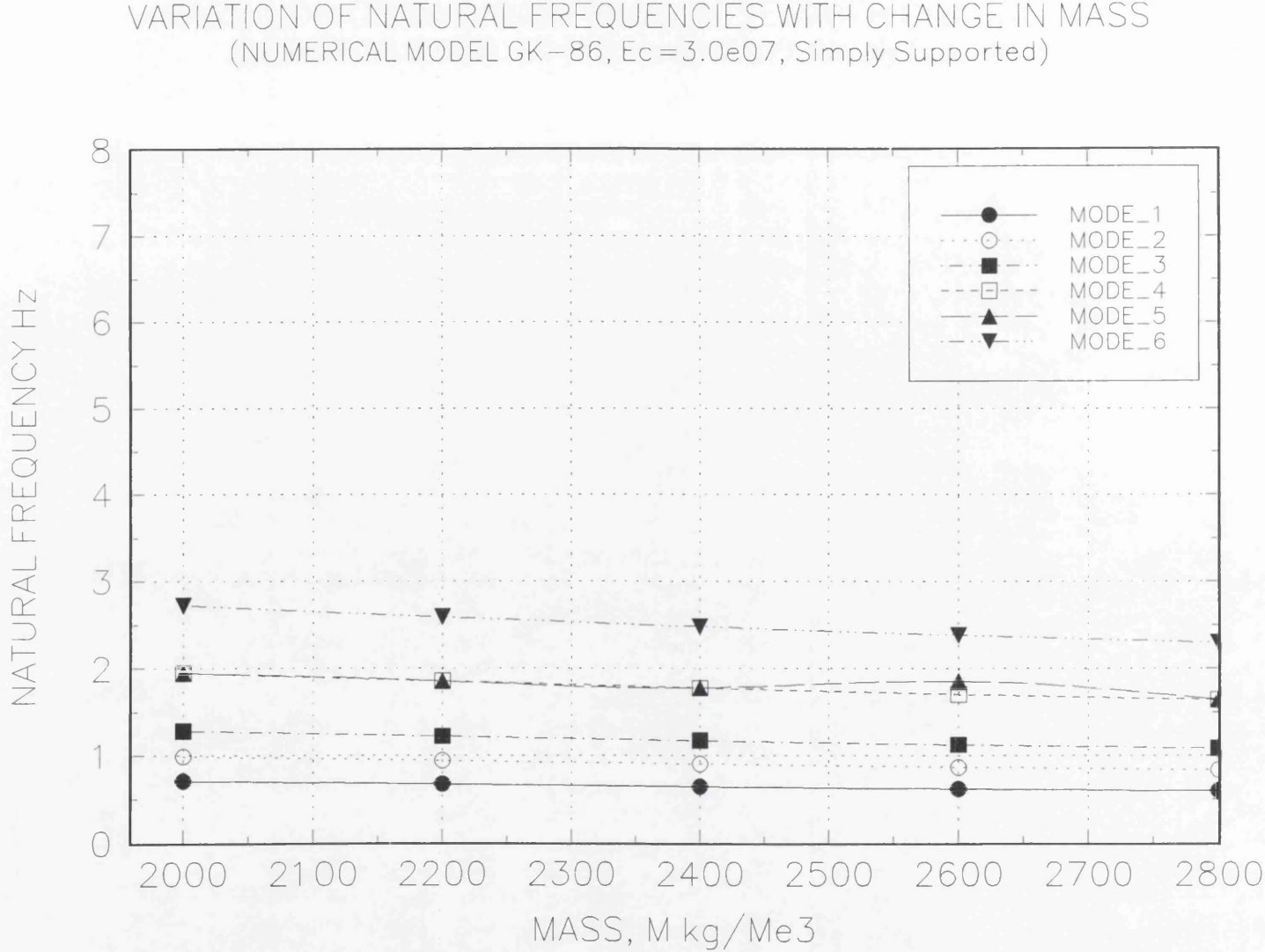

Fig. 3.20:Variation in natural frequencies with change in mass for GK-86.

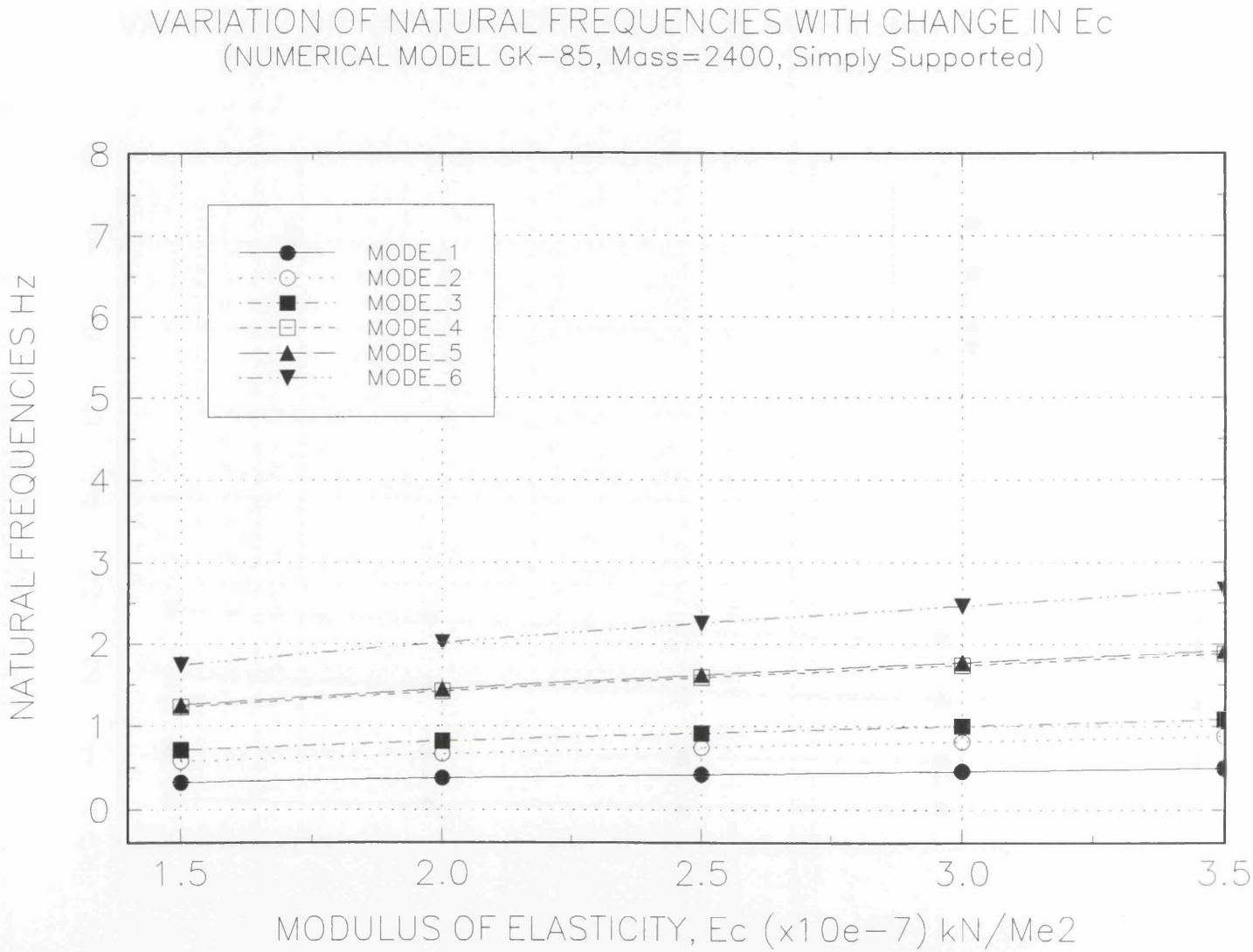

Fig. 3.21 :Variation in natural frequencies with change in Ec for GK-85.

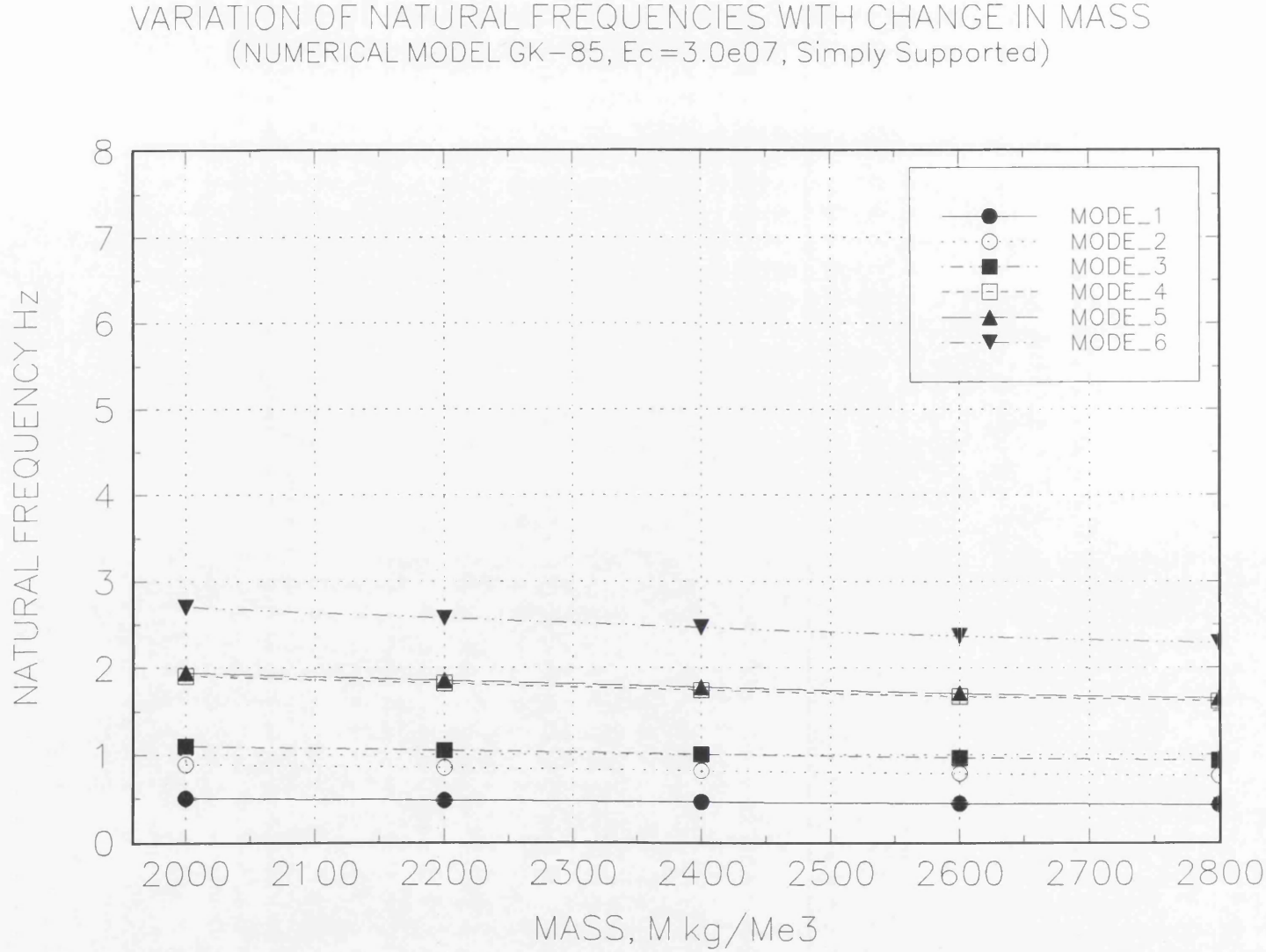

Fig. 3.22:Variation in natural frequencies with change in mass for GK−85.

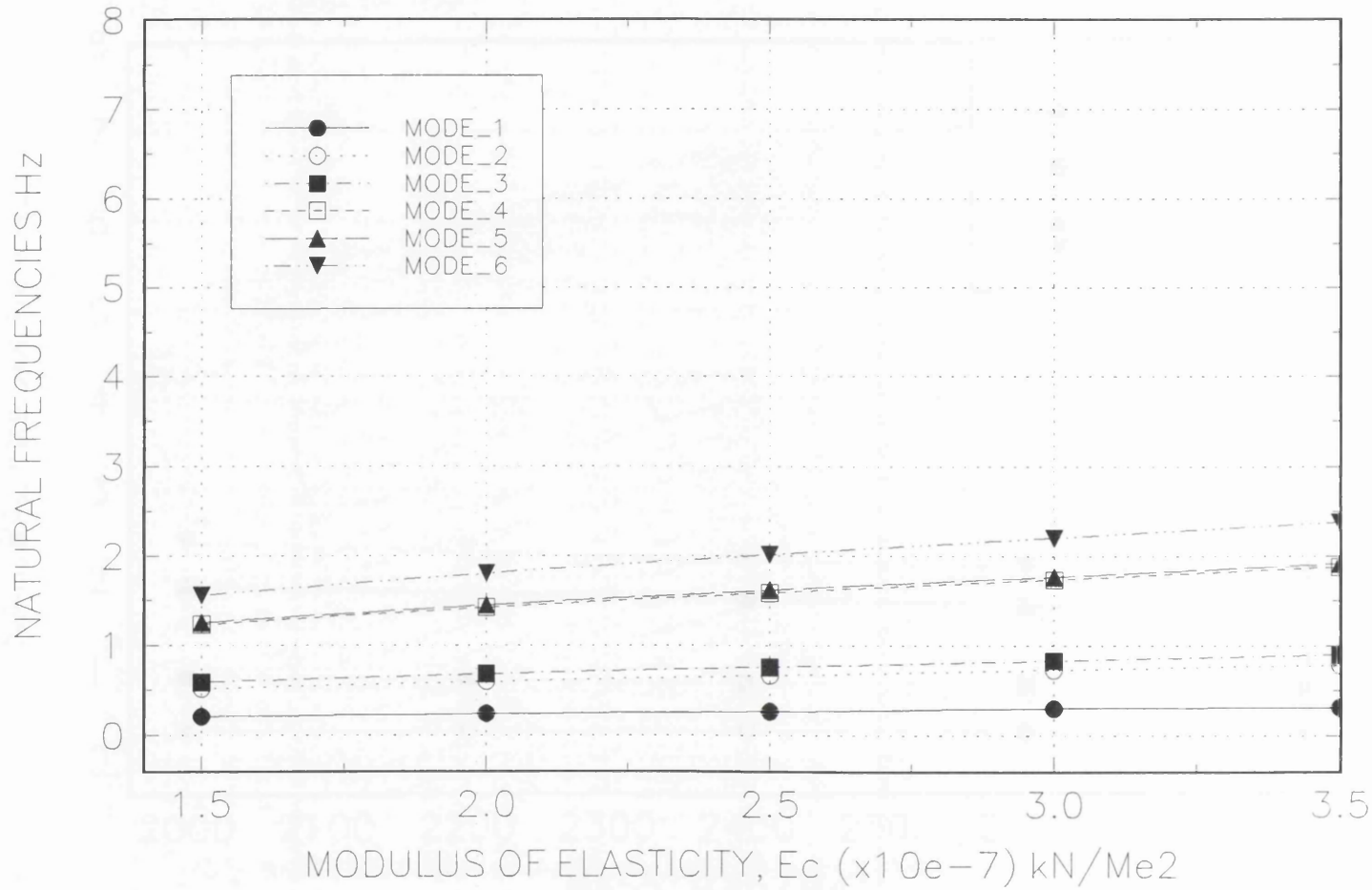

Fig. 3.23:Variation in natural frequencies with change in Ec for GK-84.

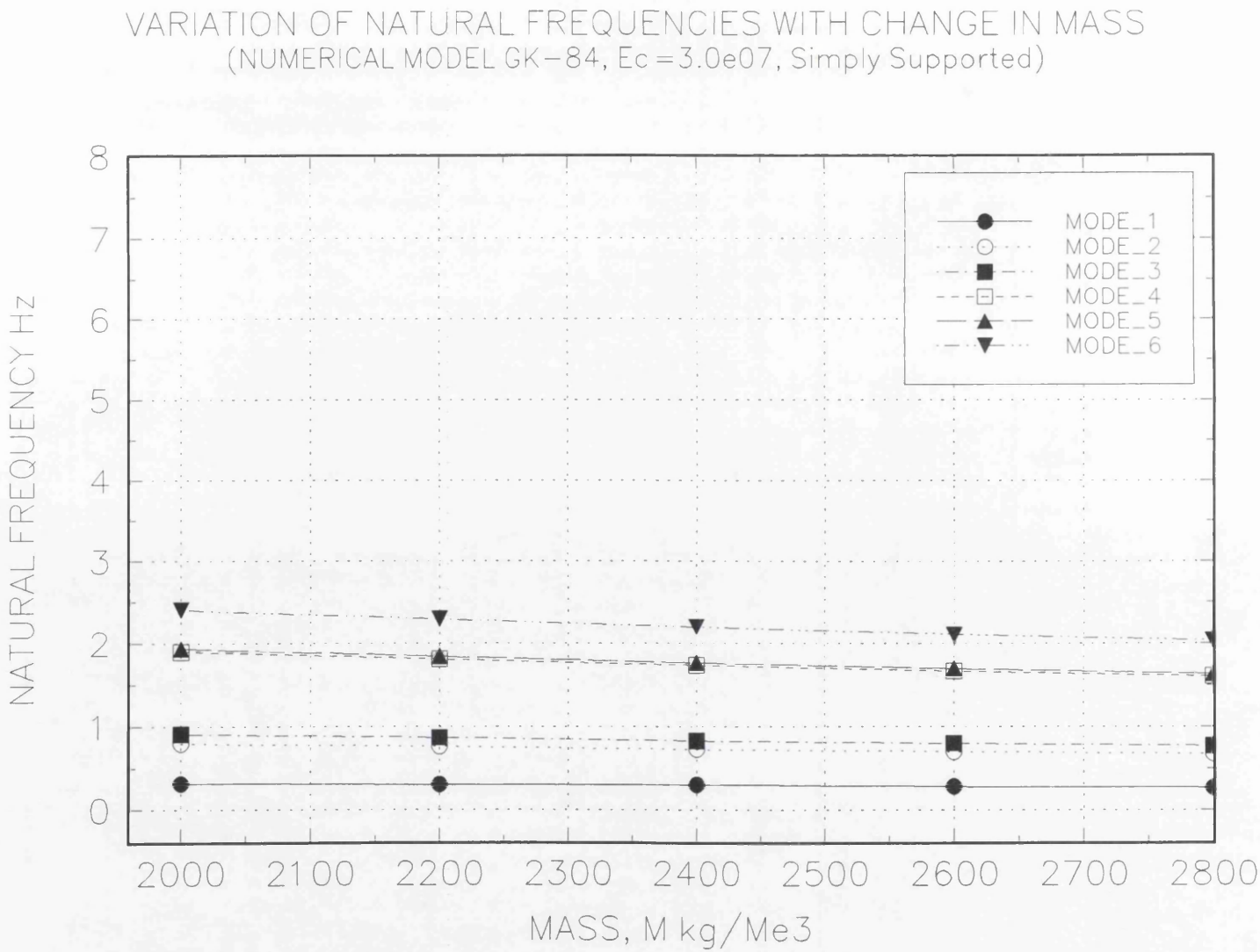

Fig. 3.24:Variation in natural frequencies with change in mass for GK−84.

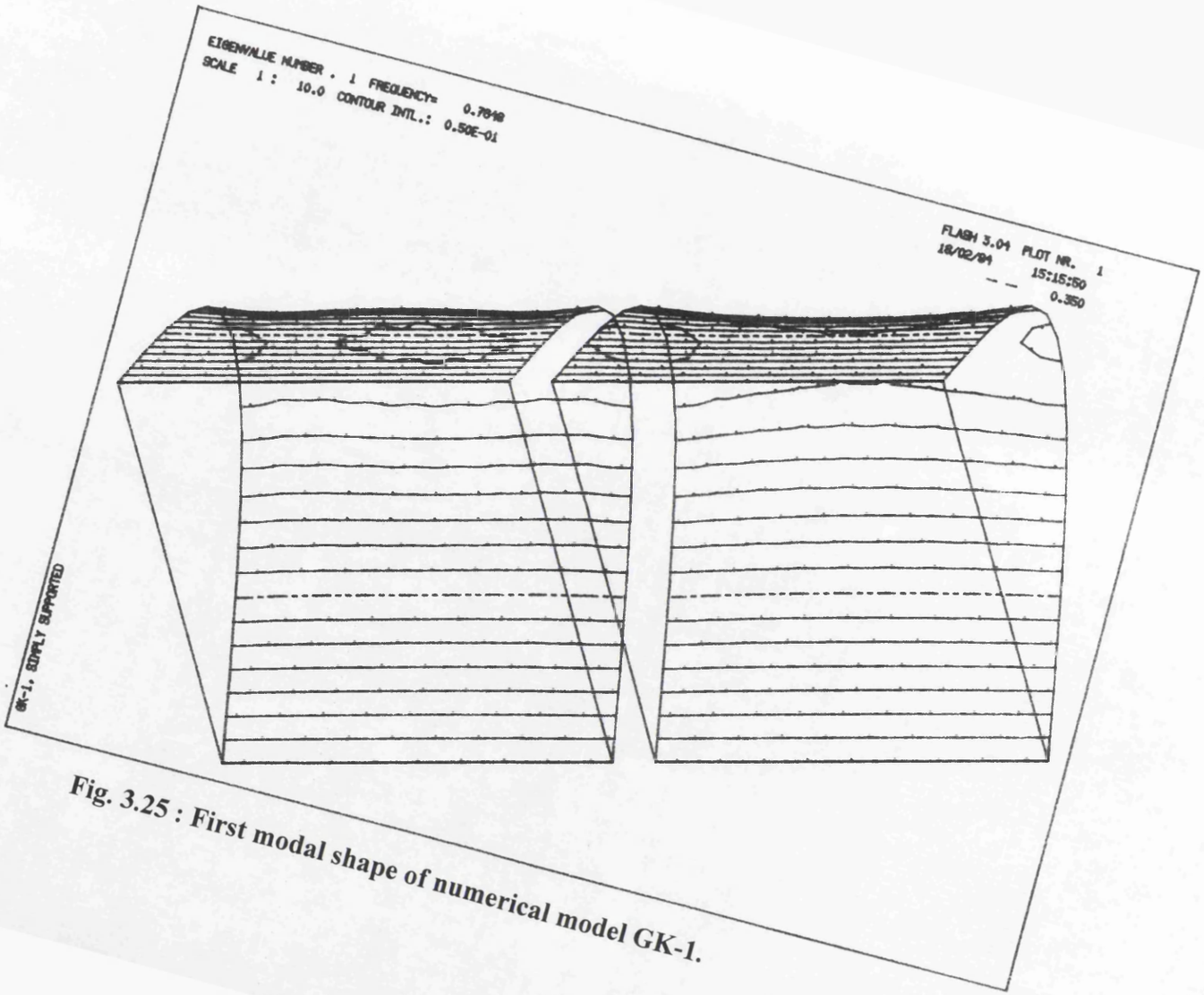

Fig. 3.25 : First modal shape of numerical model GK-1.

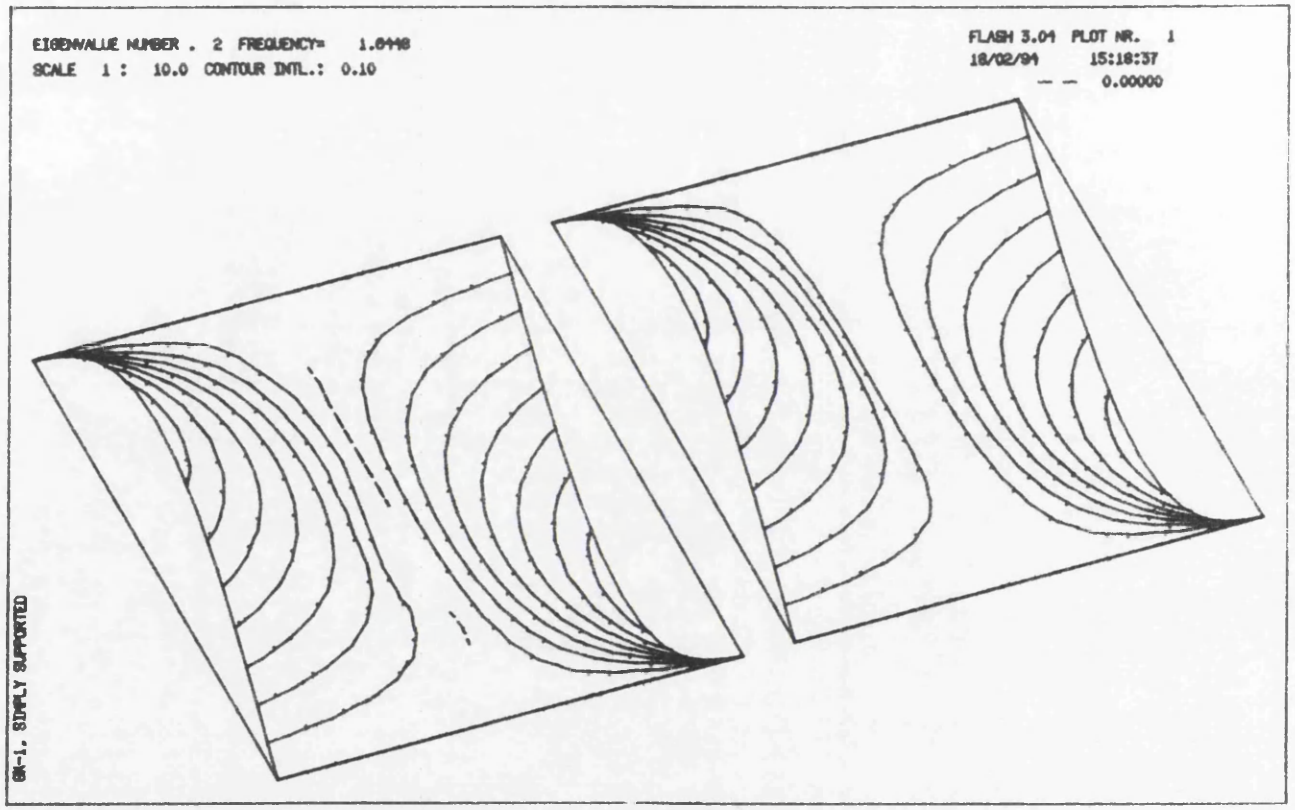

Fig. 3.26 : Second modal shape of numerical model GK-1.

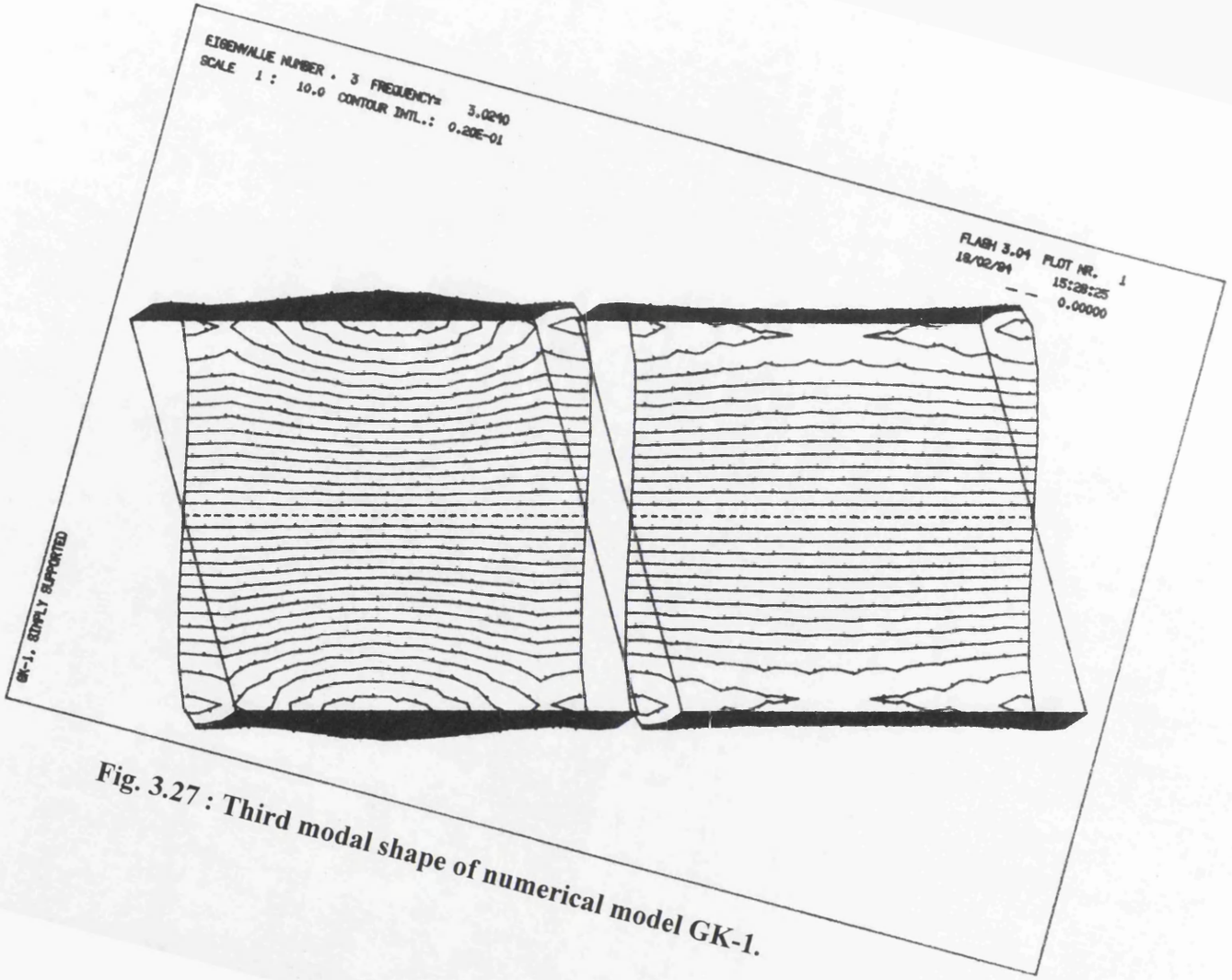

Fig. 3.27 : Third modal shape of numerical model GK-1.

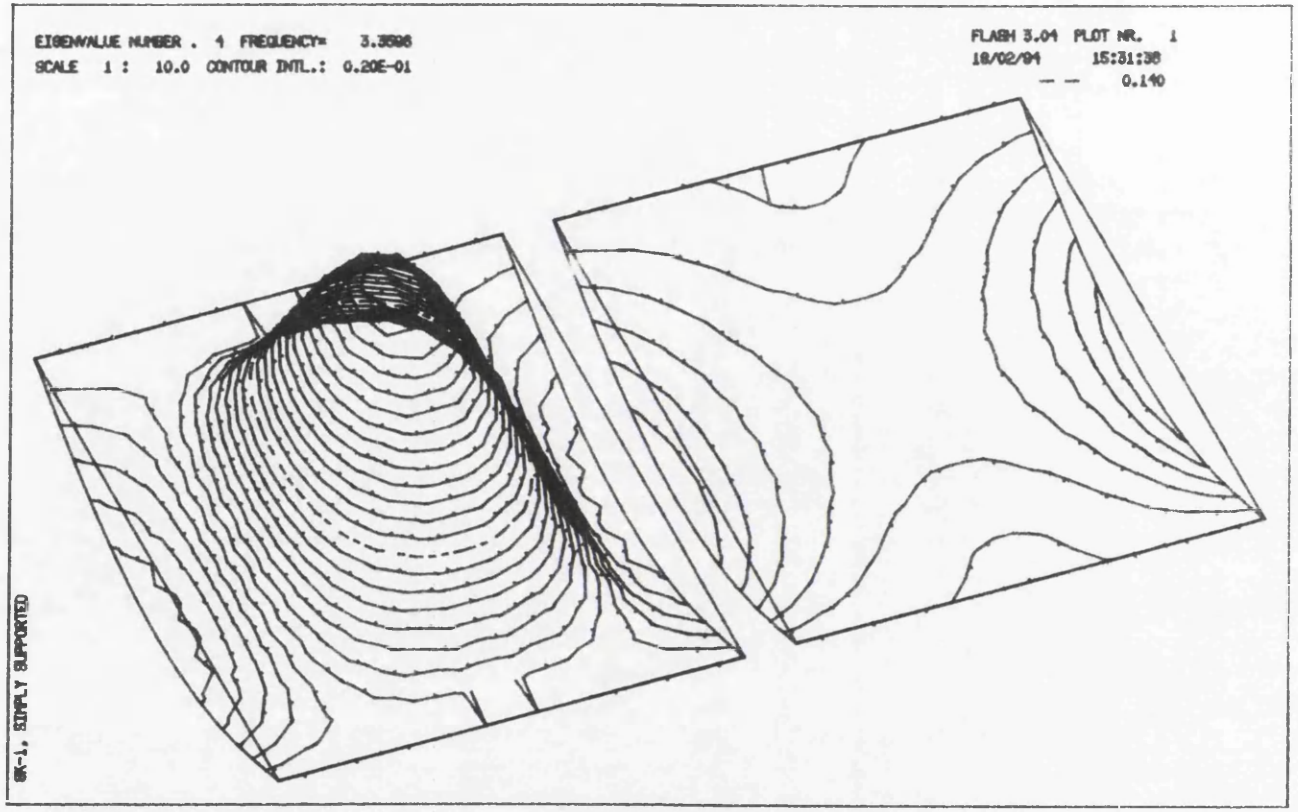

Fig. 3.28: Fourth modal shape of numerical model GK-1.

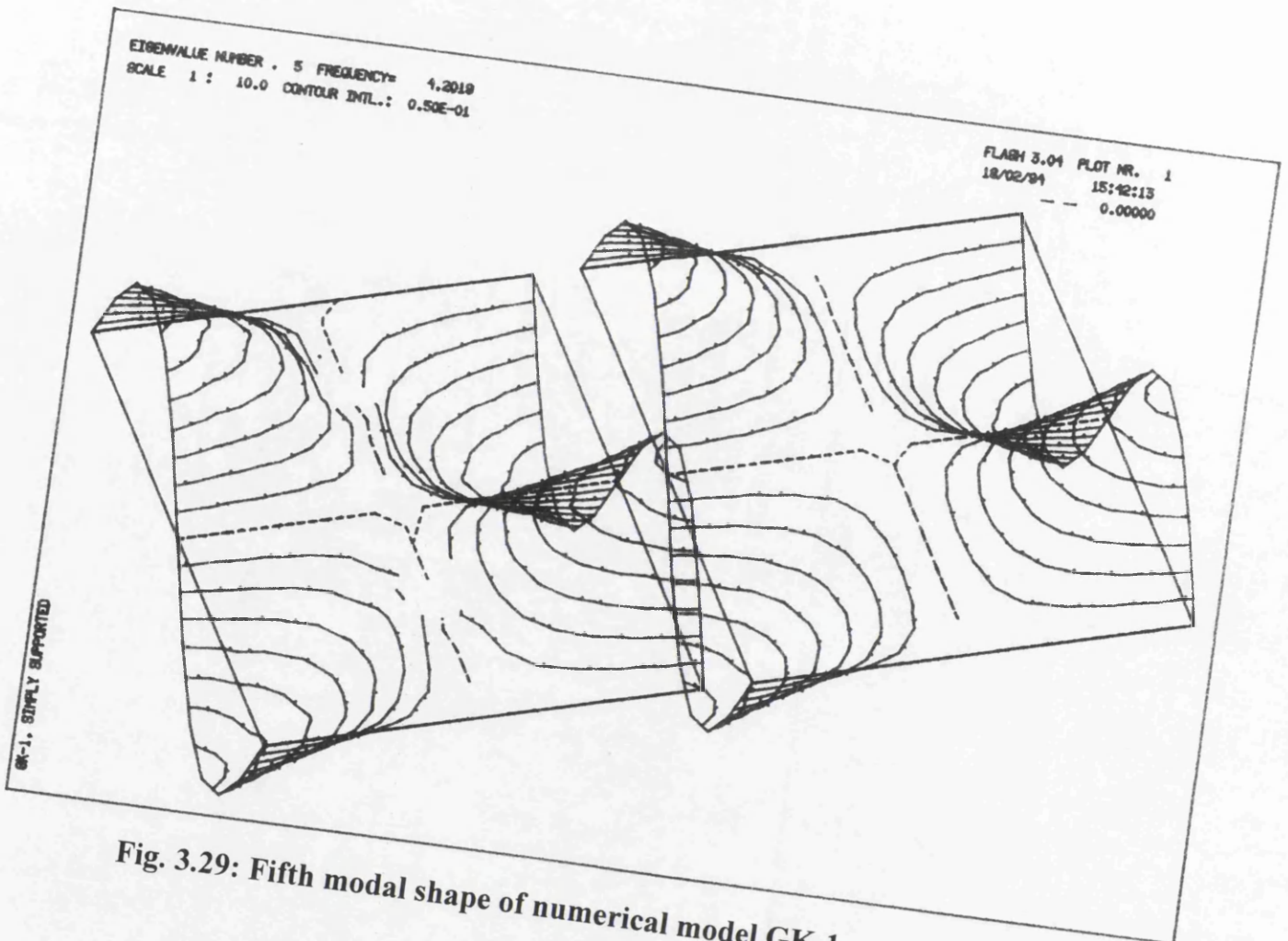

Fig. 3.29: Fifth modal shape of numerical model GK-1.

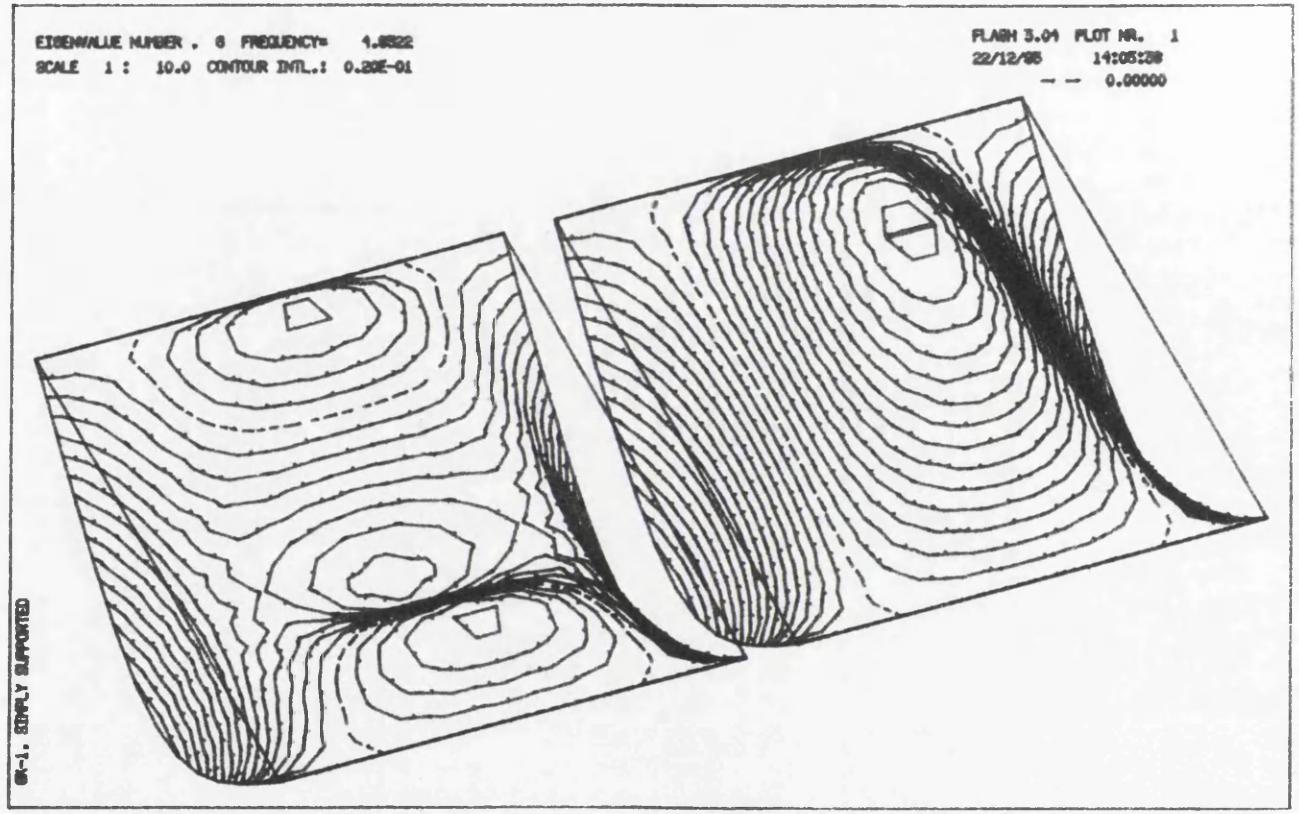

Fig. 3.30: Sixth modal shape of numerical model GK-1.

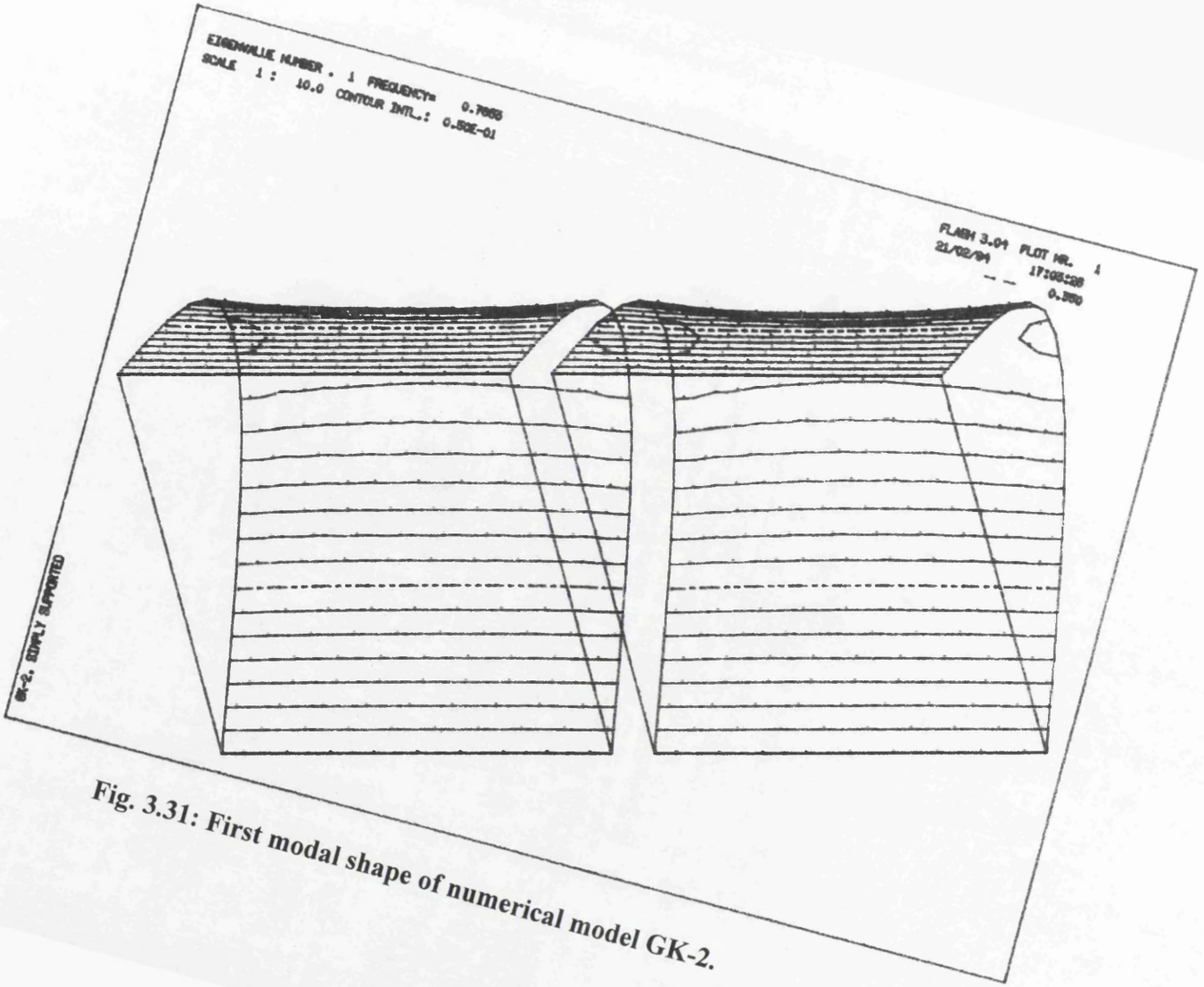

Fig. 3.31: First modal shape of numerical model GK-2.

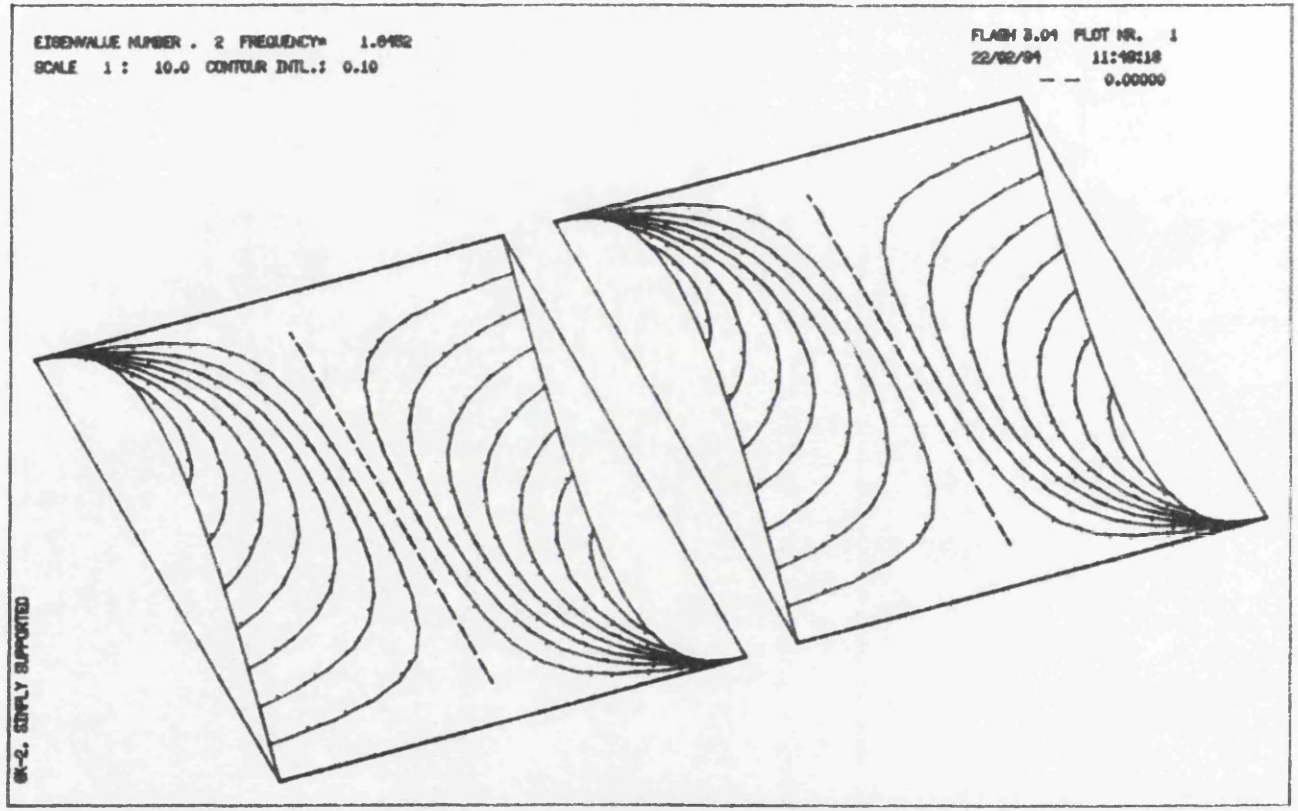

Fig. 3.32: Second modal shape of numerical model GK-2.

Fig. 3.33: Third modal shape of numerical model GK-2.

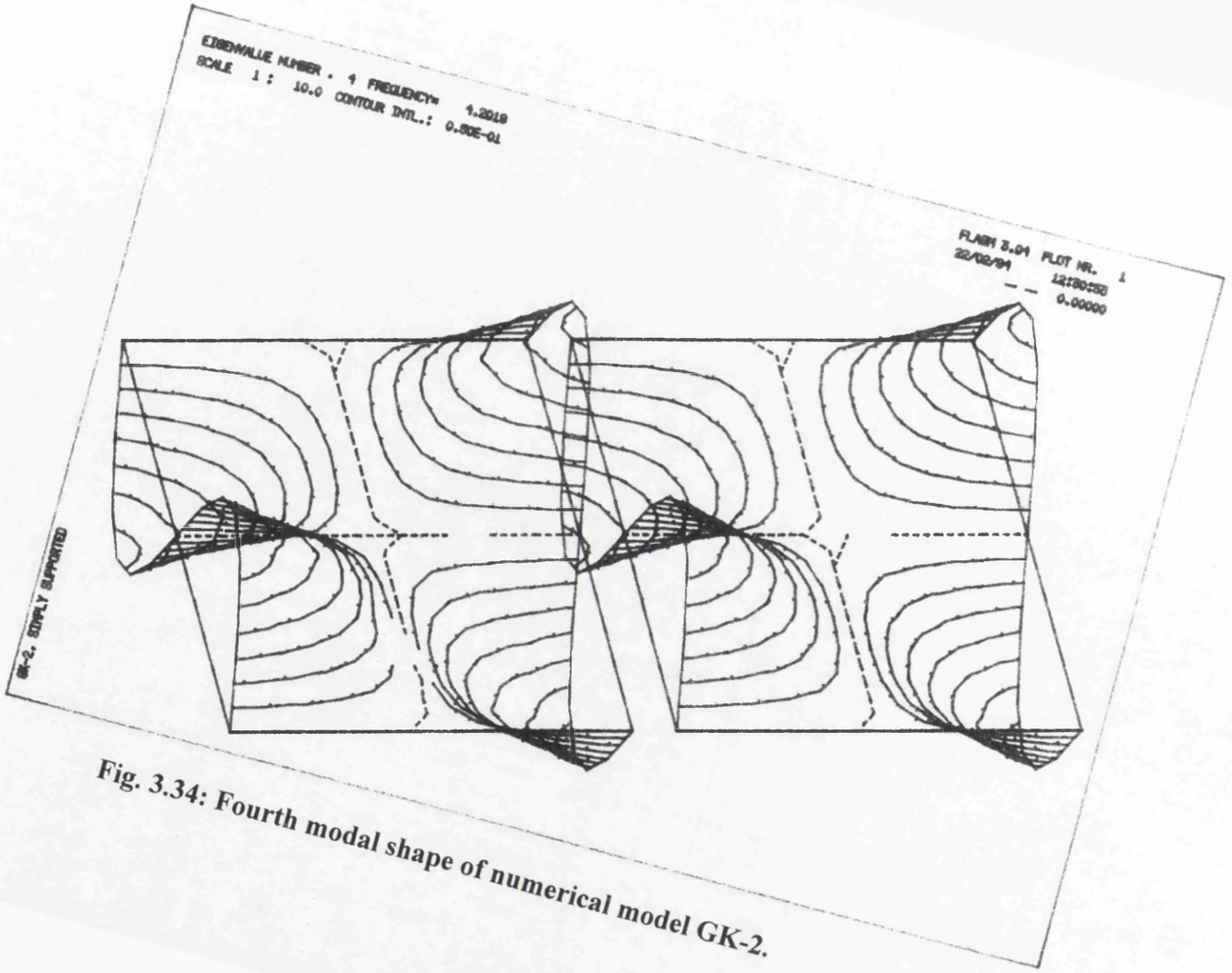

Fig. 3.34: Fourth modal shape of numerical model GK-2.

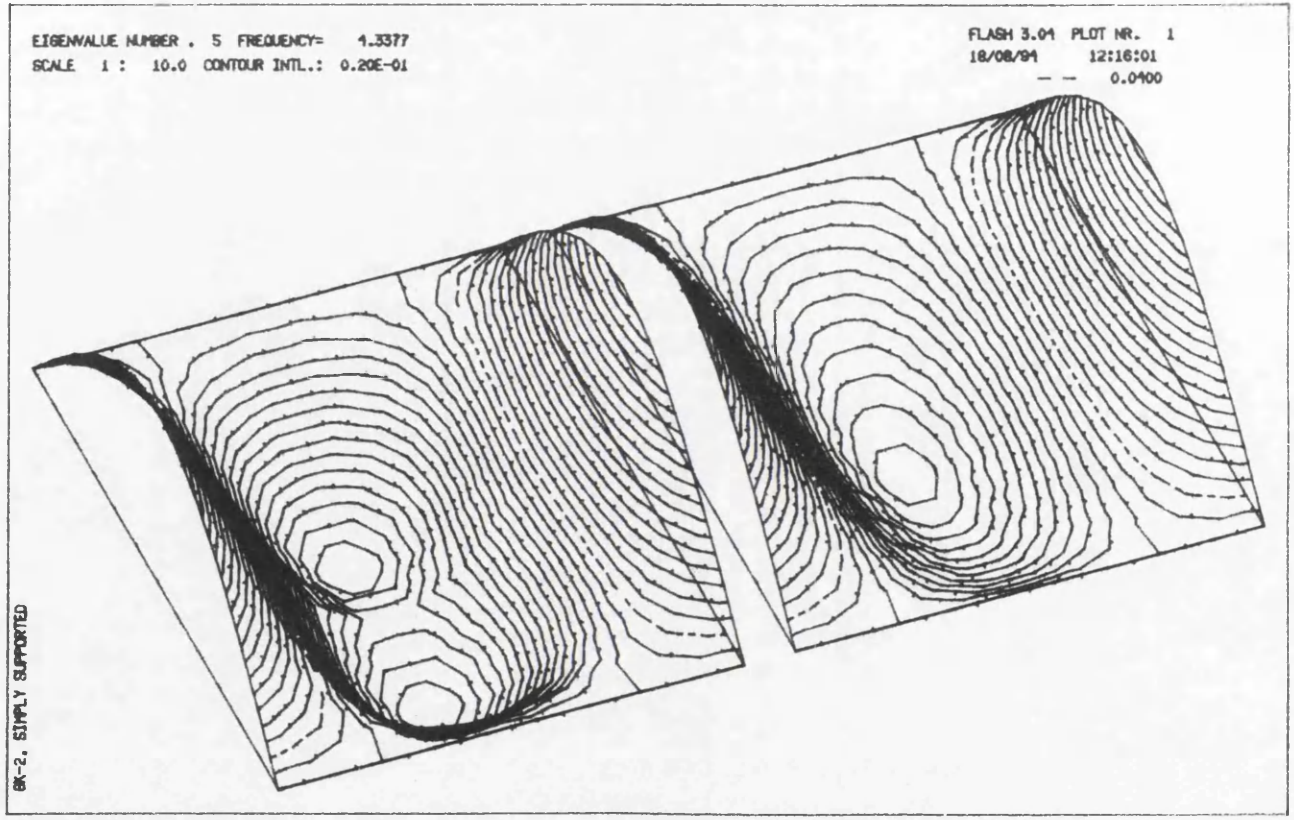

Fig. 3.35: Fifth modal shape of numerical model GK-2.

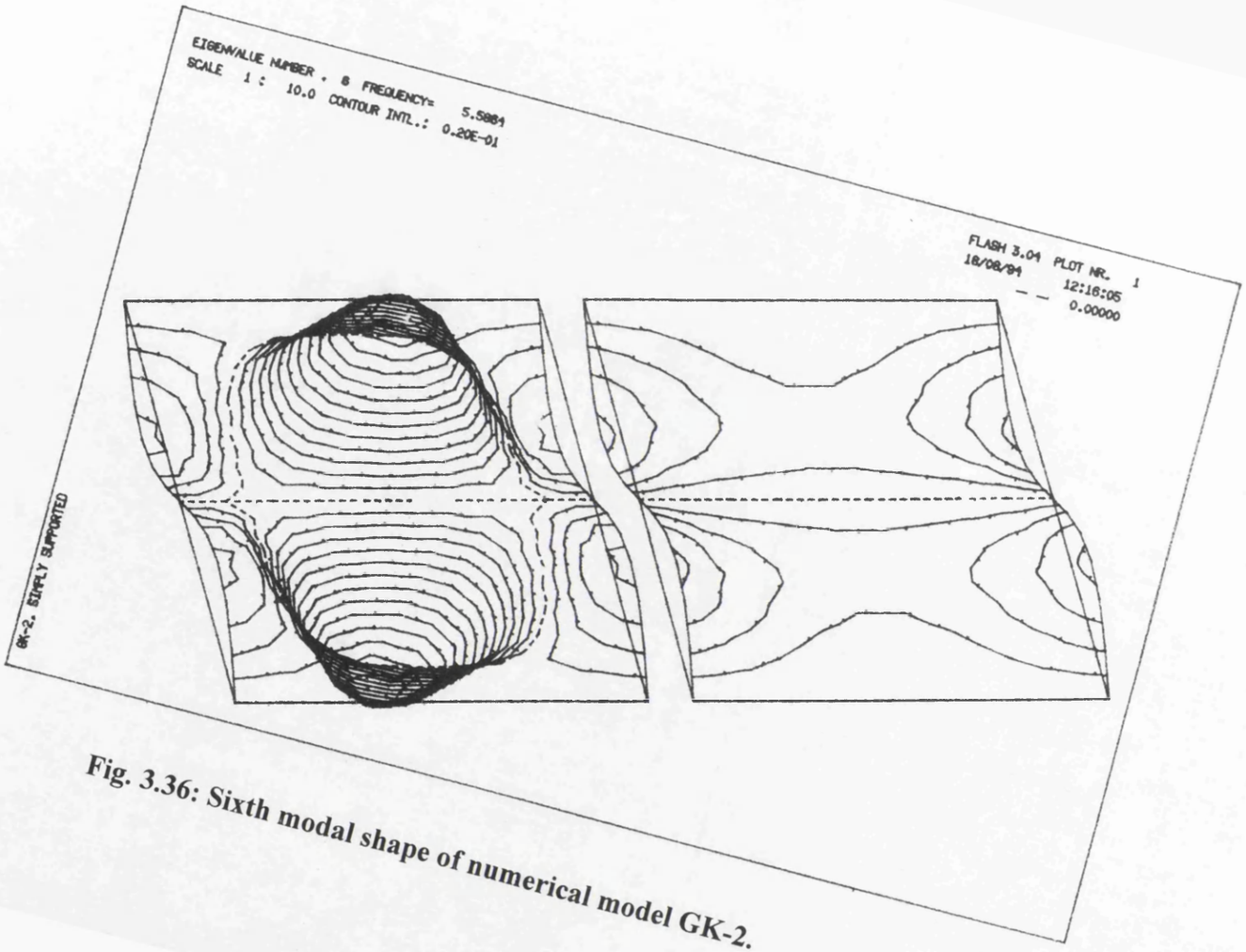

Fig. 3.36: Sixth modal shape of numerical model GK-2.

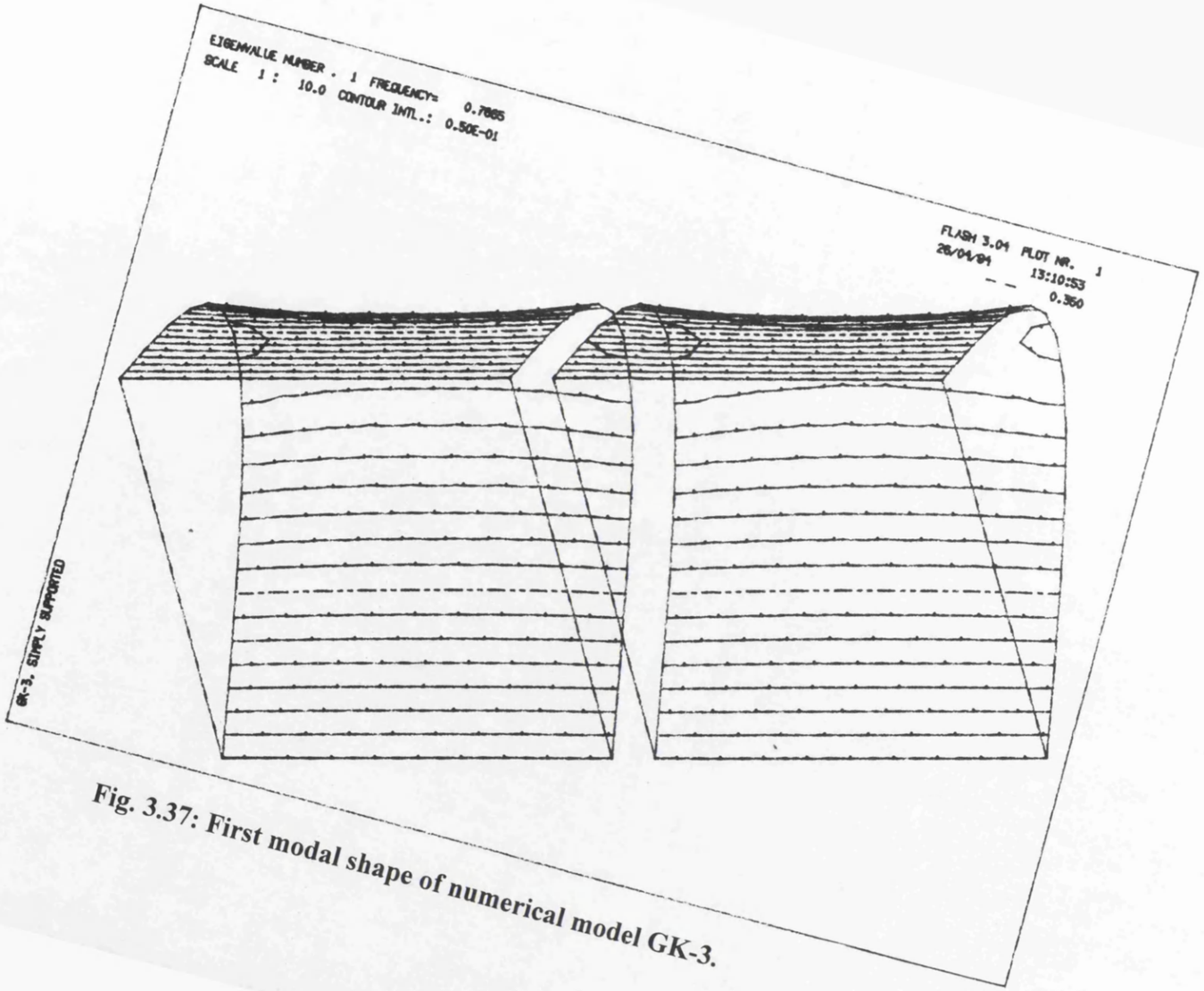

Fig. 3.37: First modal shape of numerical model GK-3.

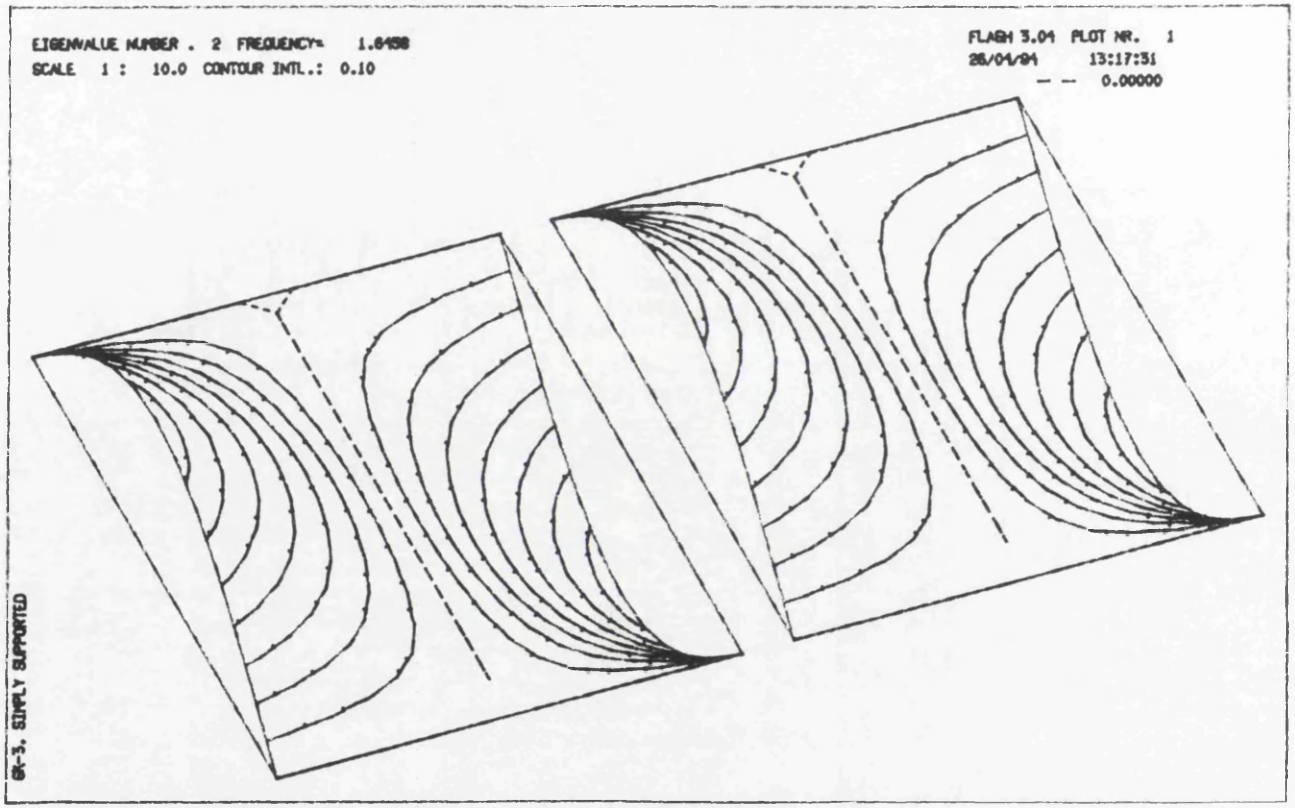

Fig. 3.38: Second modal shape of numerical model GK-3.

Fig. 3.39: Third modal shape of numerical model GK-3.

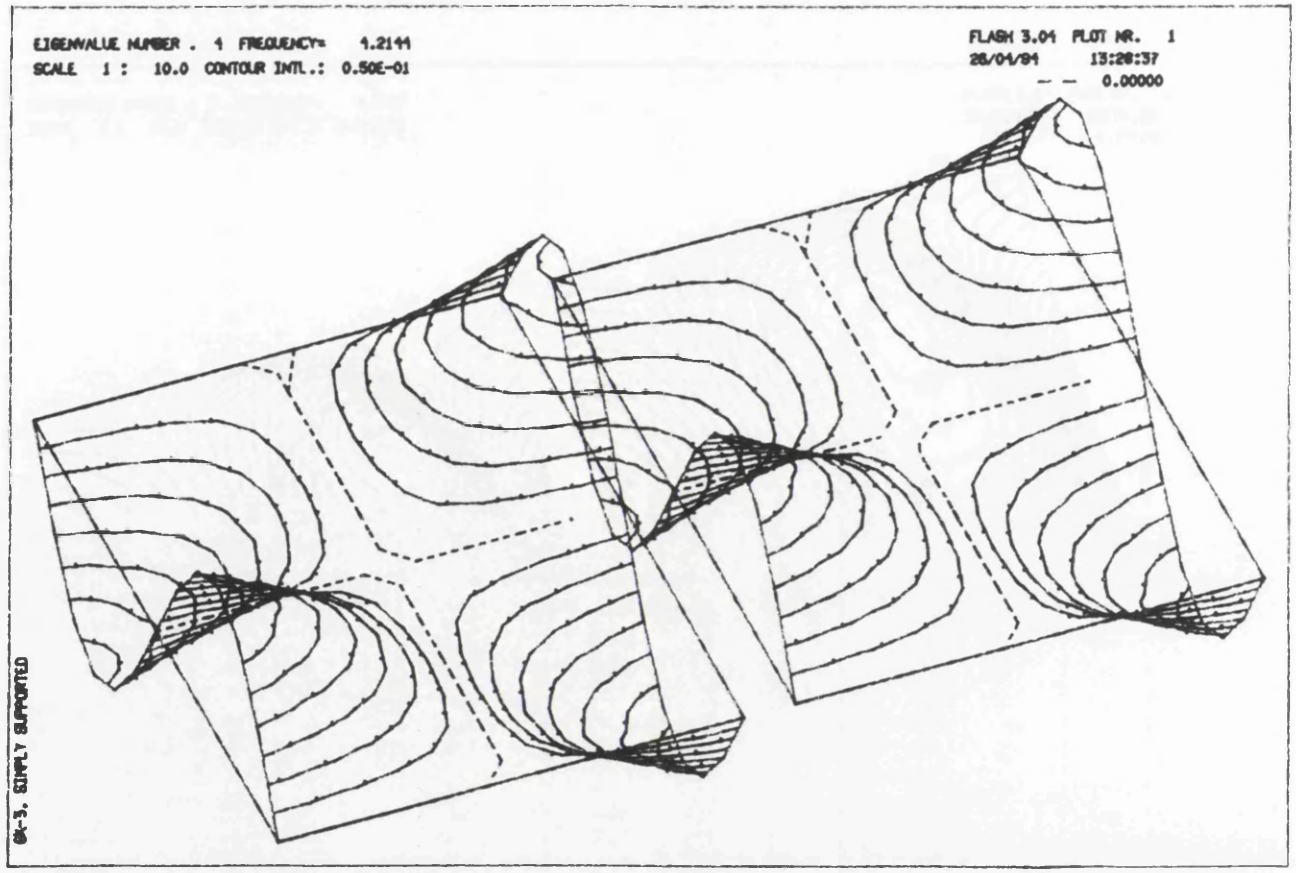

Fig. 3.40: Fourth modal shape of numerical model GK-3.

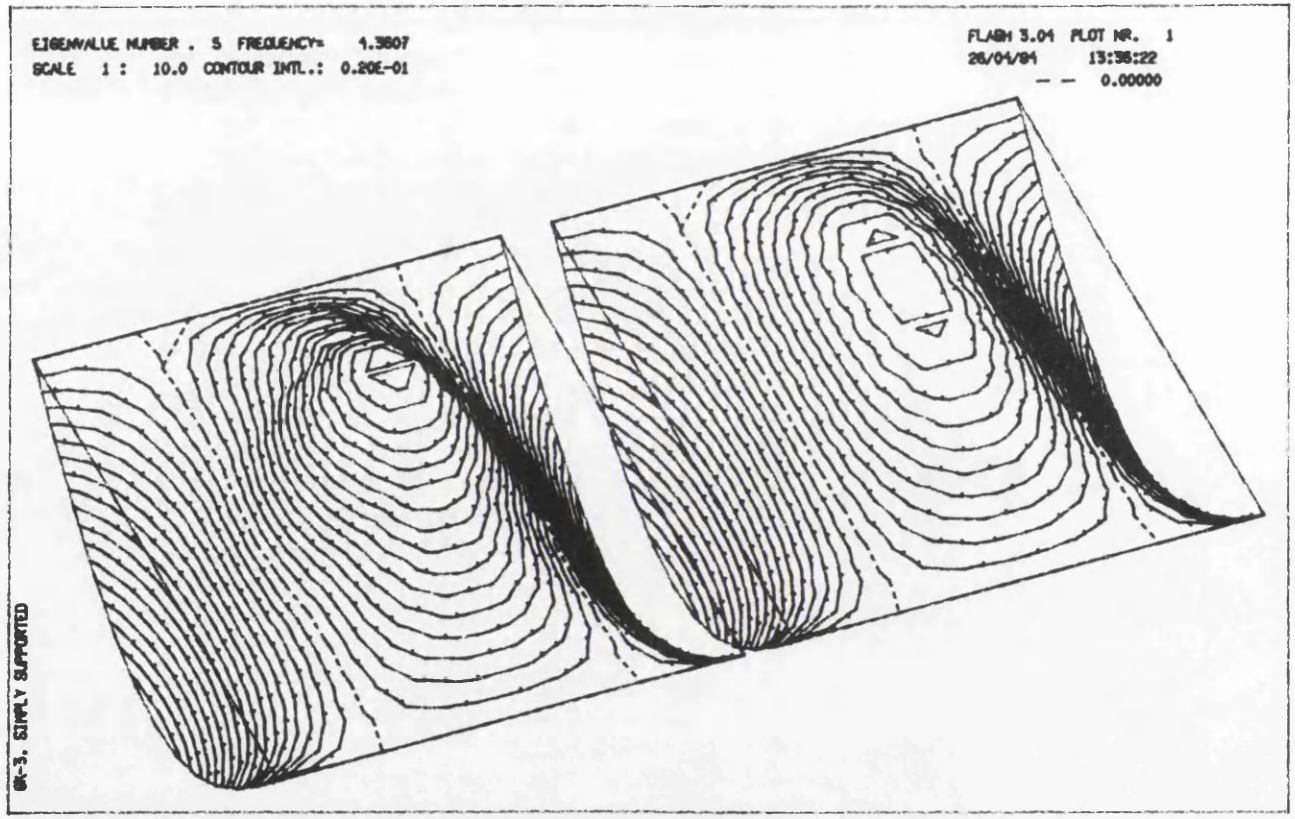

Fig. 3.41: Fifth modal shape of numerical model GK-3.

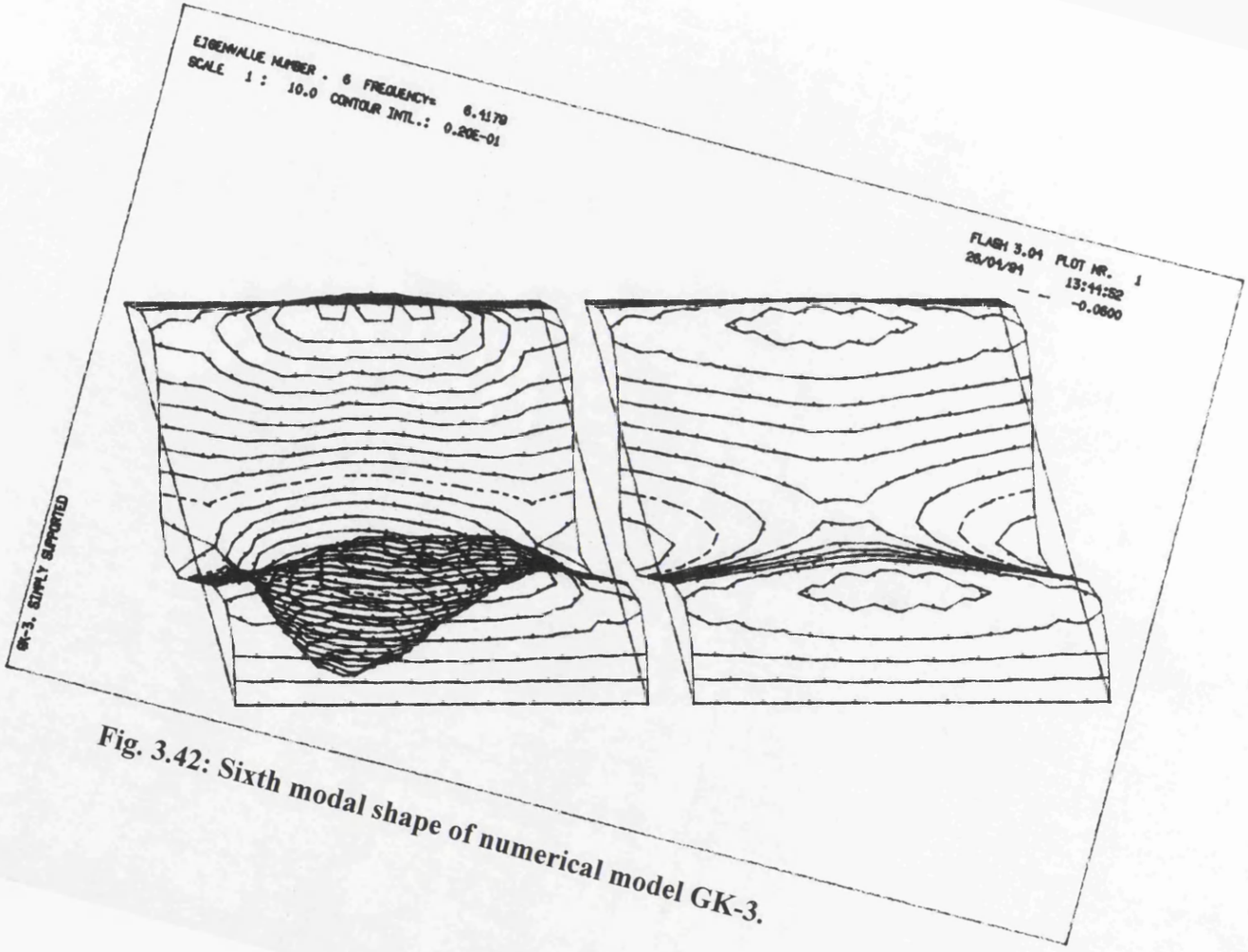

Fig. 3.42: Sixth modal shape of numerical model GK-3.

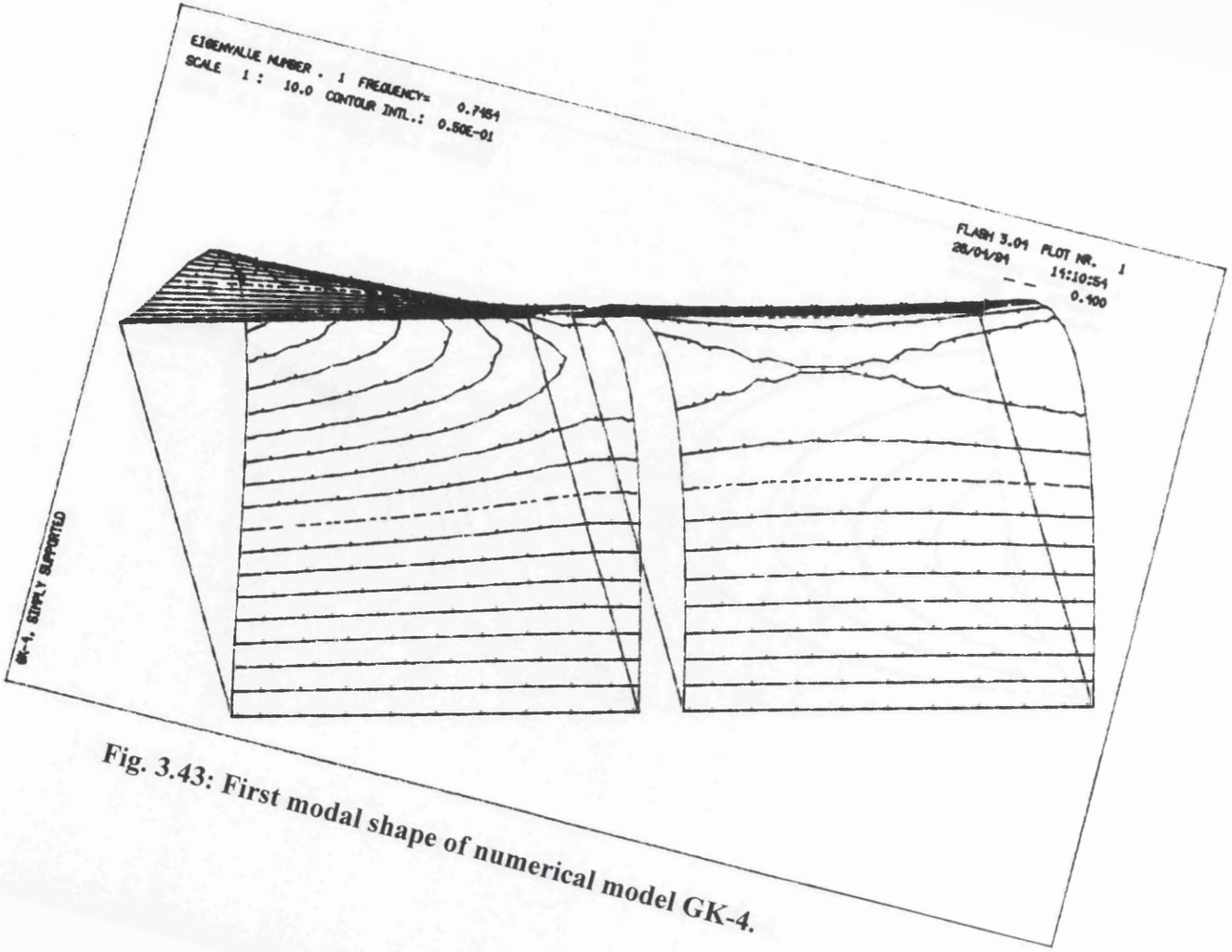

Fig. 3.43: First modal shape of numerical model GK-4.

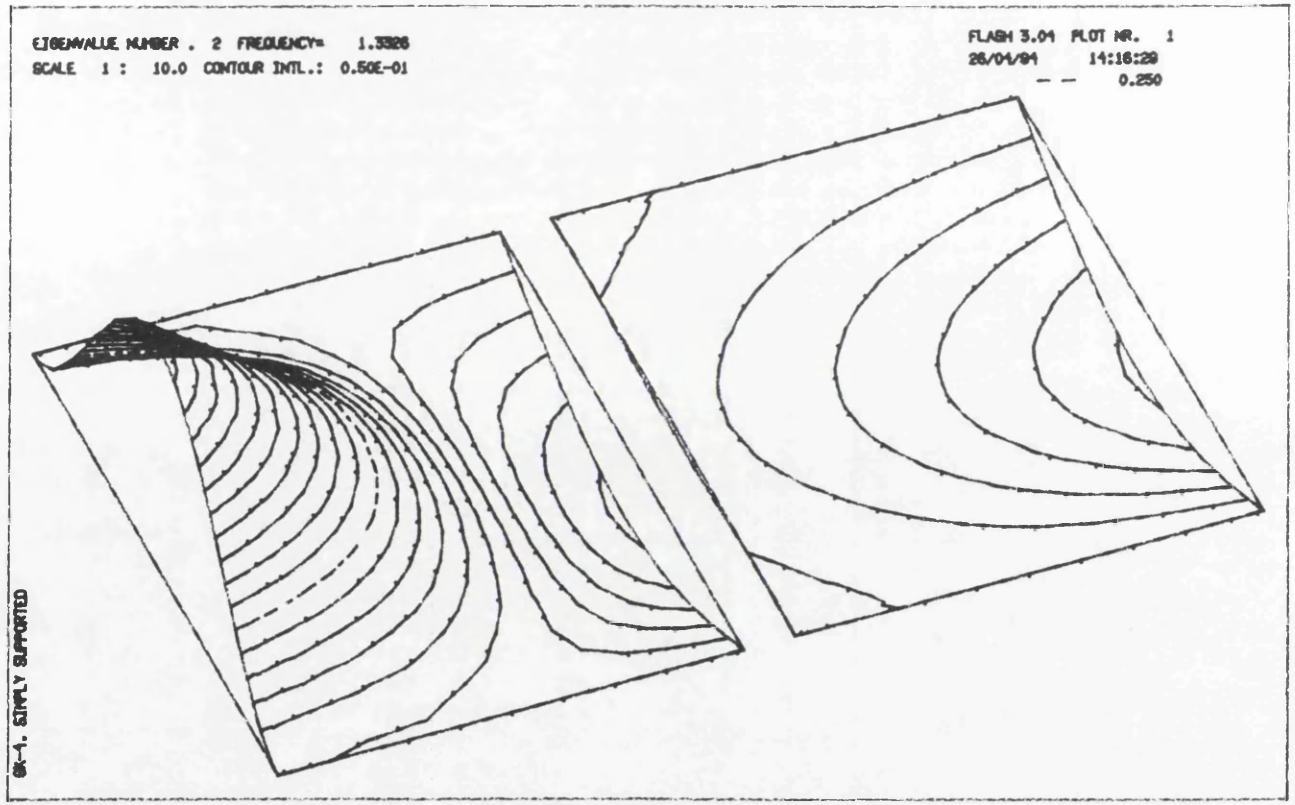

Fig. 3.44: Second modal shape of numerical model GK-4.

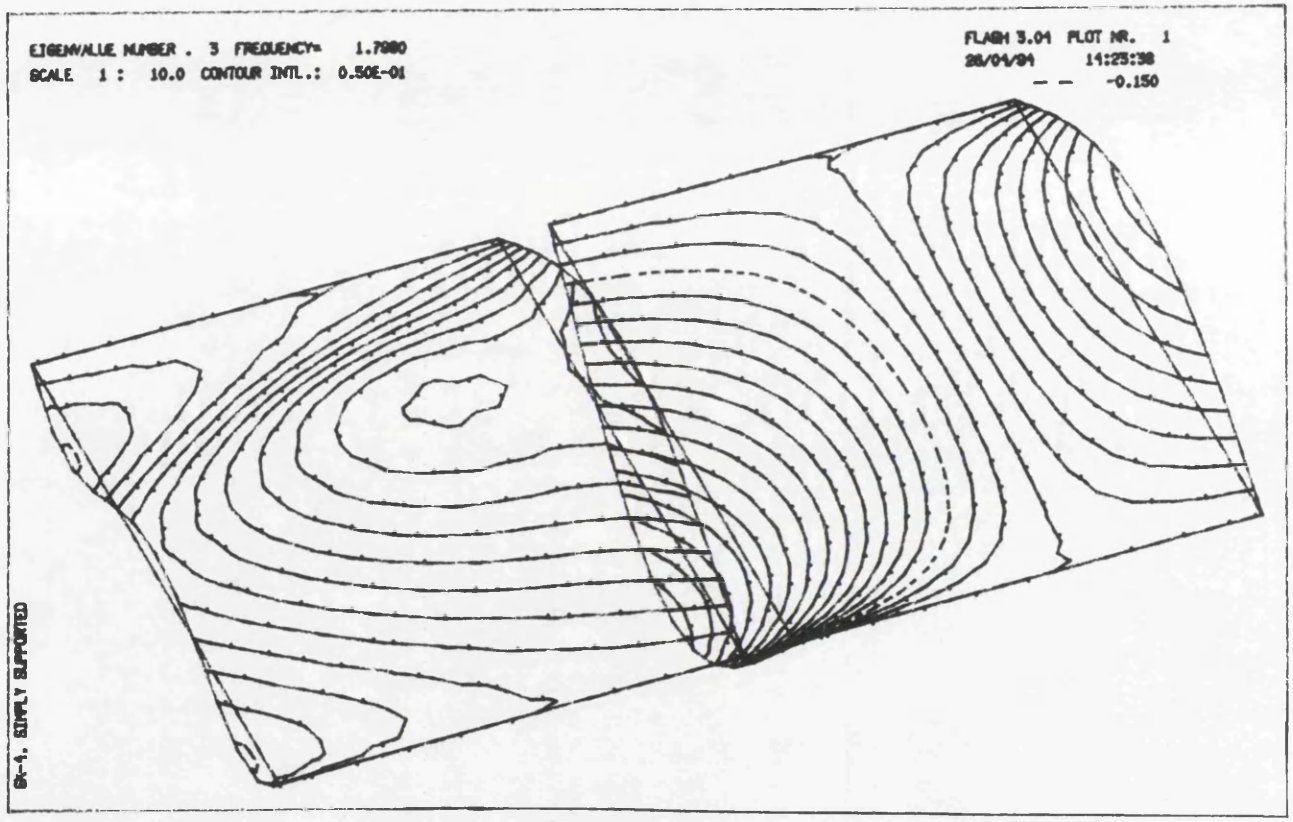

Fig. 3.45: Third modal shape of numerical model GK-4.

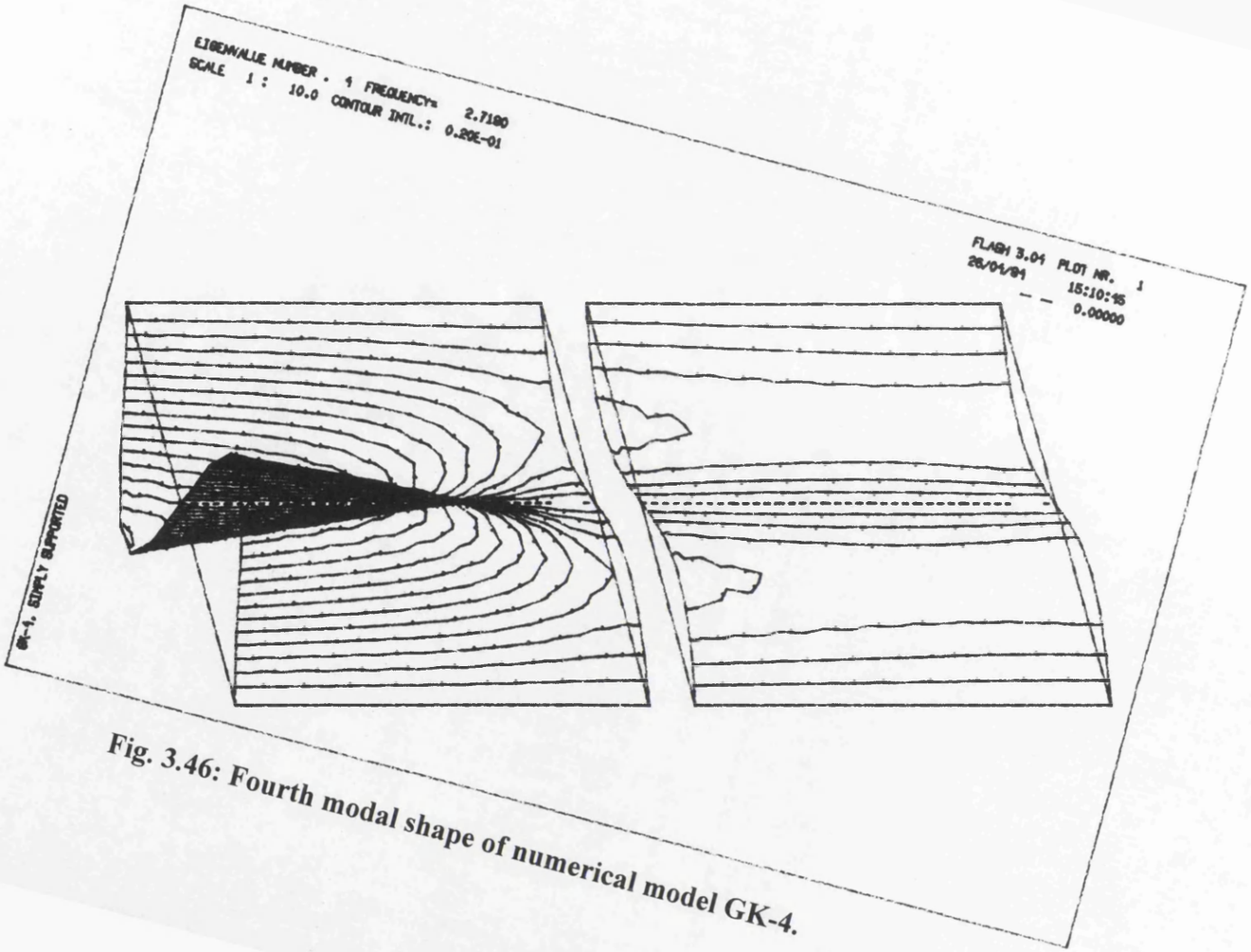

Fig. 3.46: Fourth modal shape of numerical model GK-4.

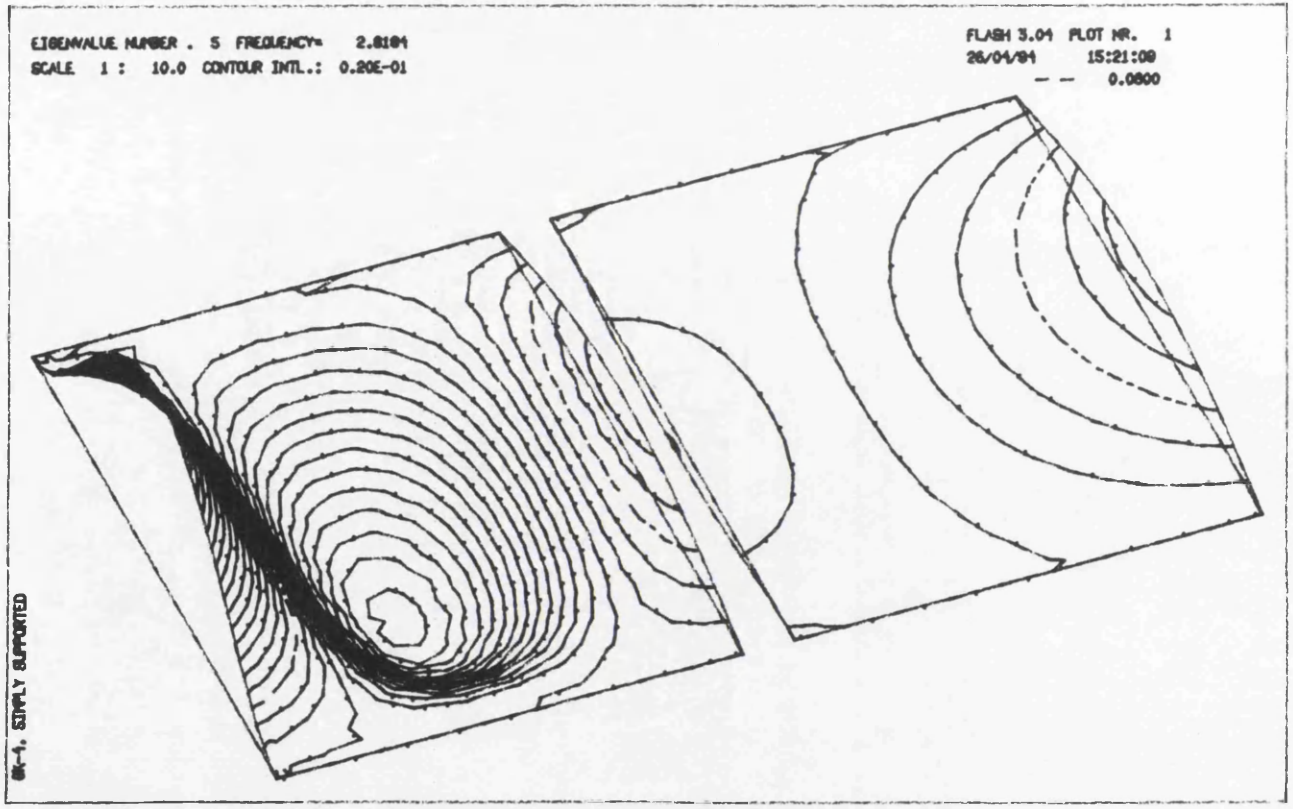

Fig. 3.47: Fifth modal shape of numerical model GK-4.

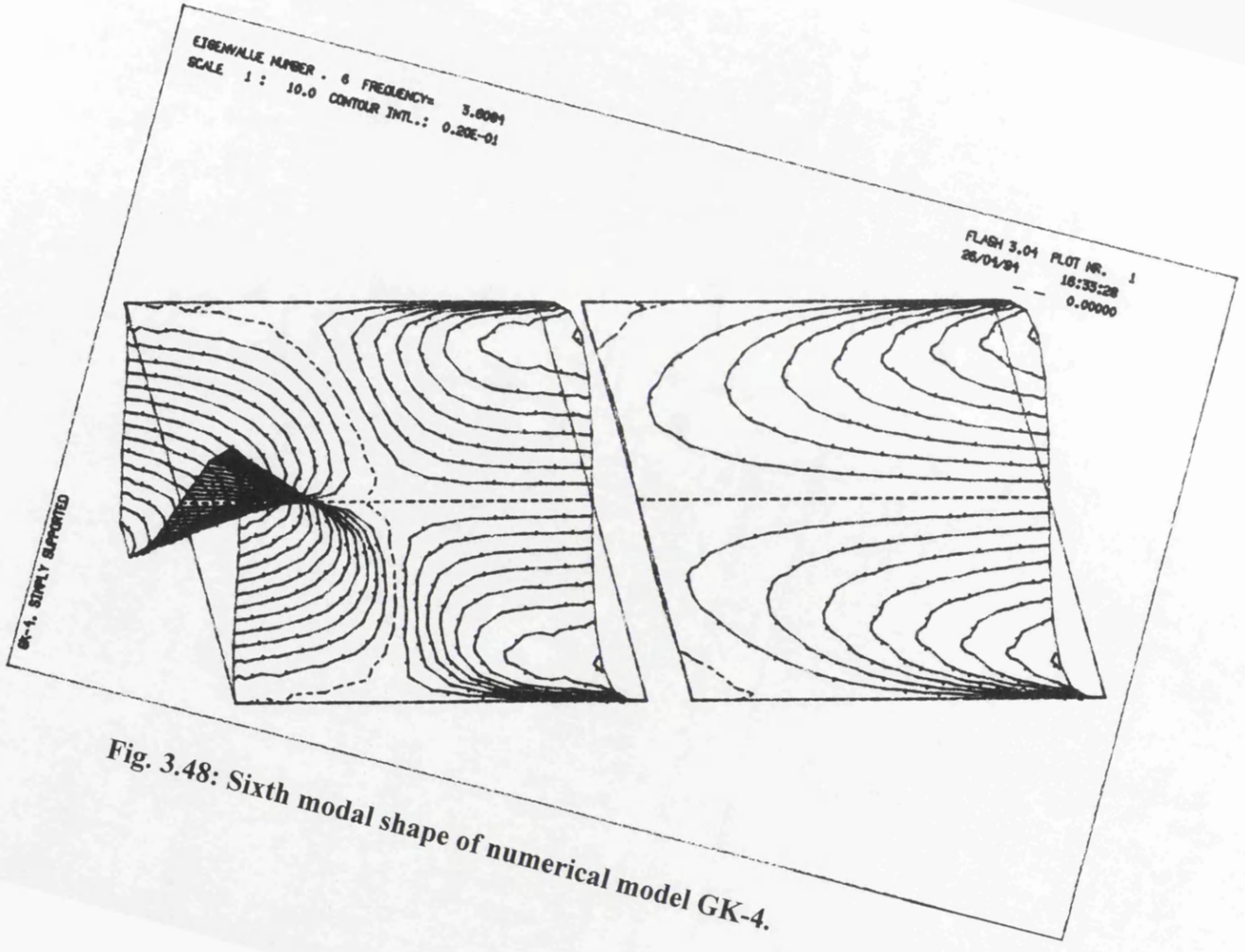

Fig. 3.48: Sixth modal shape of numerical model GK-4.

Fig. 3.49: First modal shape of numerical model GK-5.

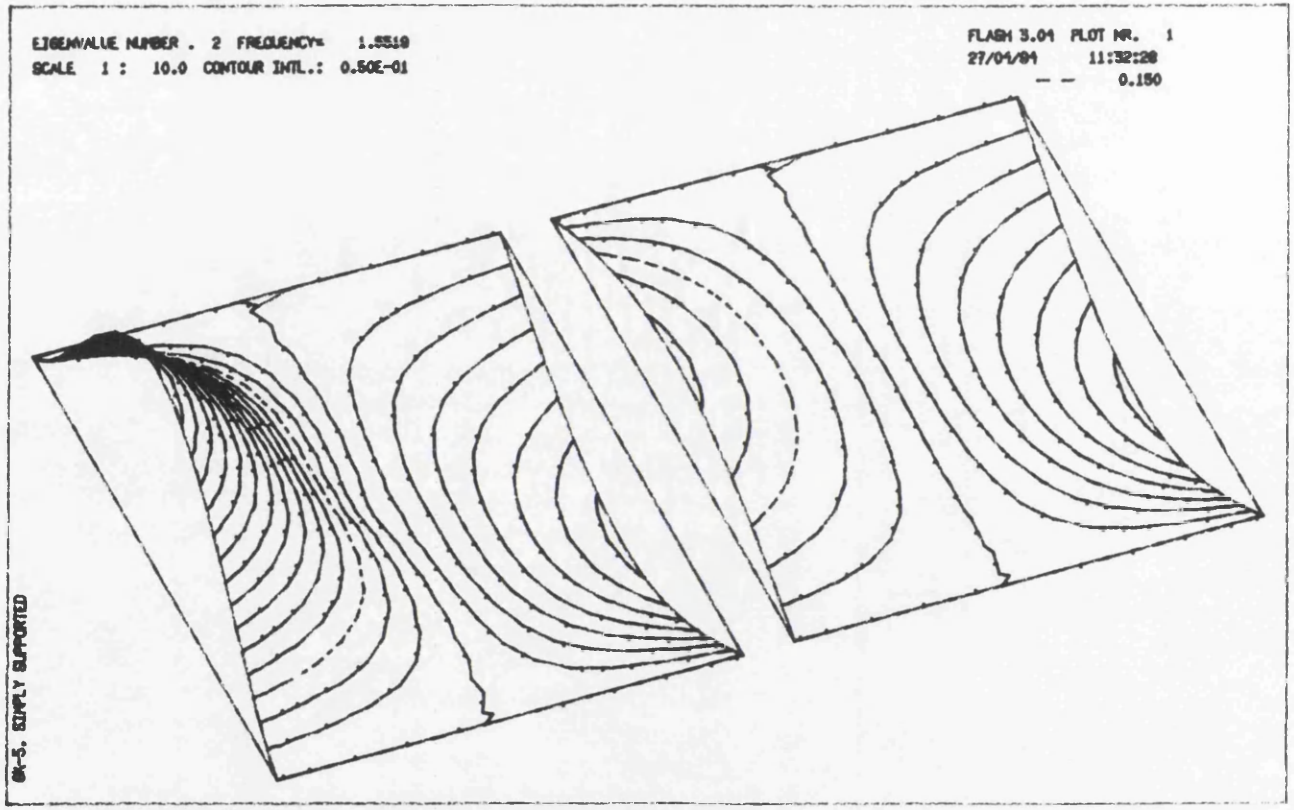

Fig. 3.50: Second modal shape of numerical model GK-5.

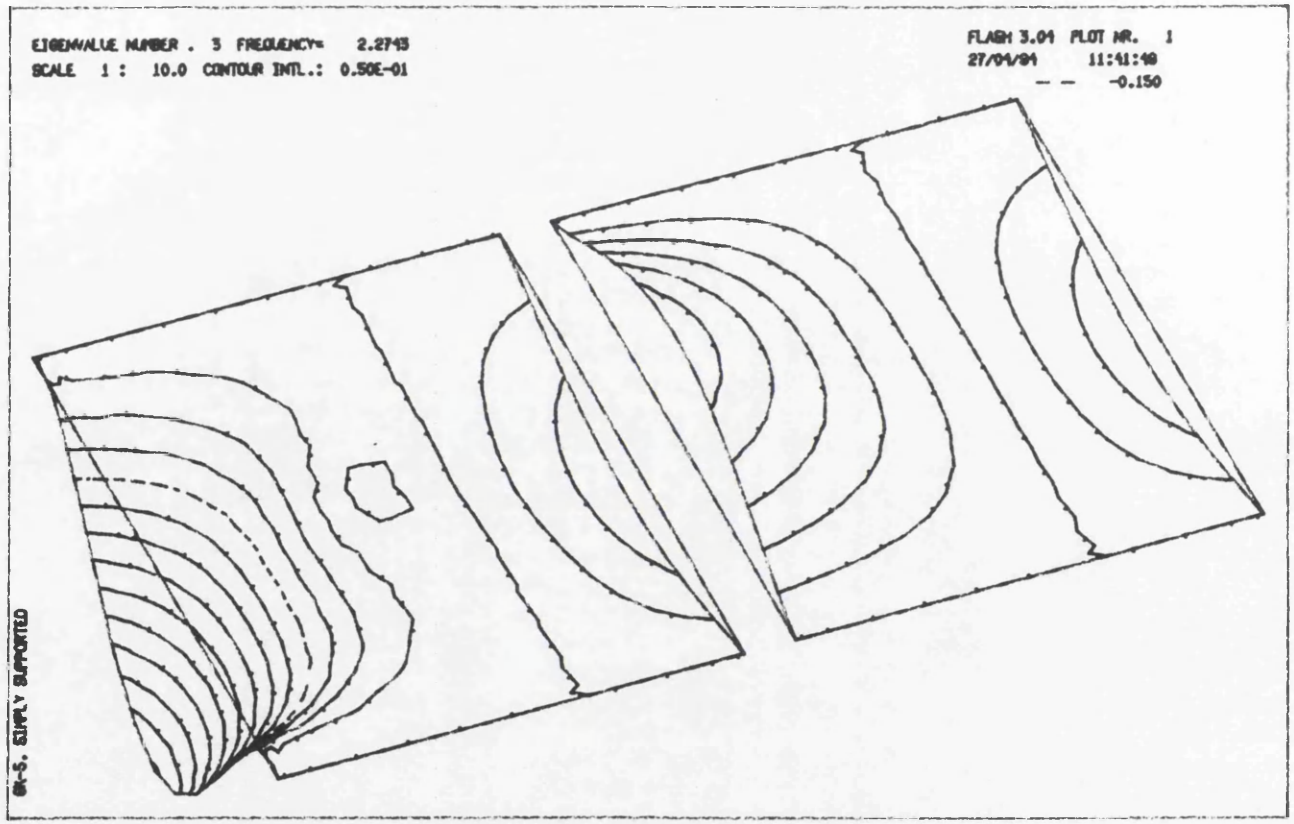

Fig. 3.51: Third modal shape of numerical model GK-5.

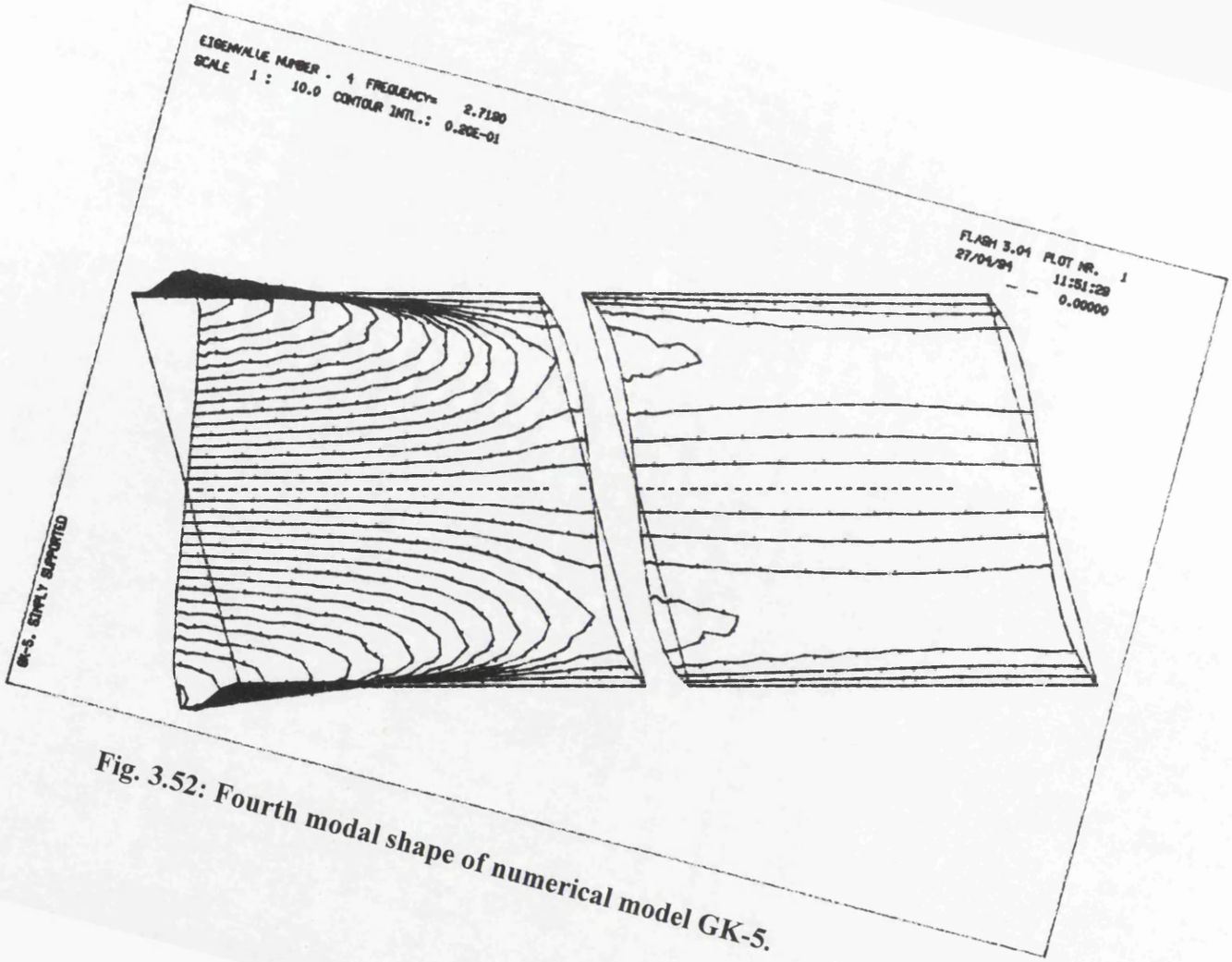

Fig. 3.52: Fourth modal shape of numerical model GK-5.

Fig. 3.53: Fifth modal shape of numerical model GK-5.

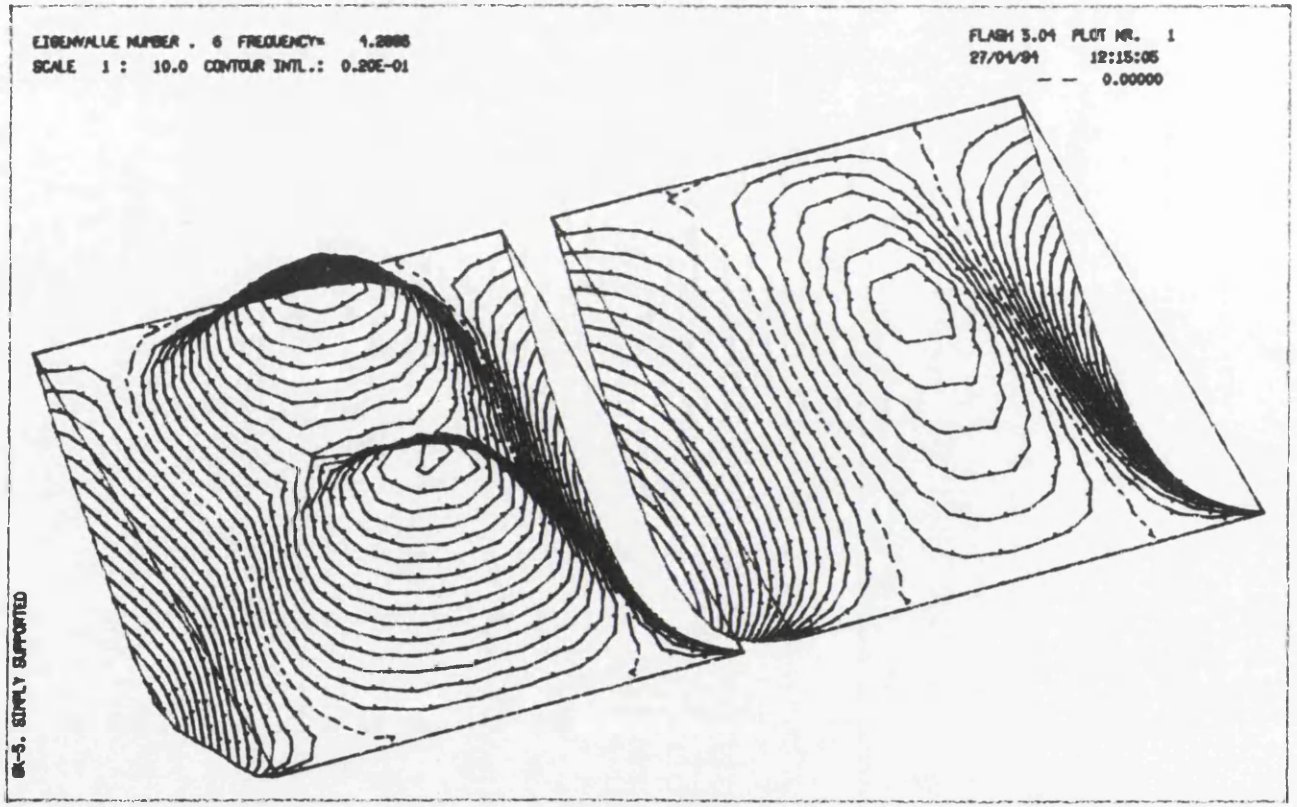

Fig. 3.54: Sixth modal shape of numerical model GK-5.

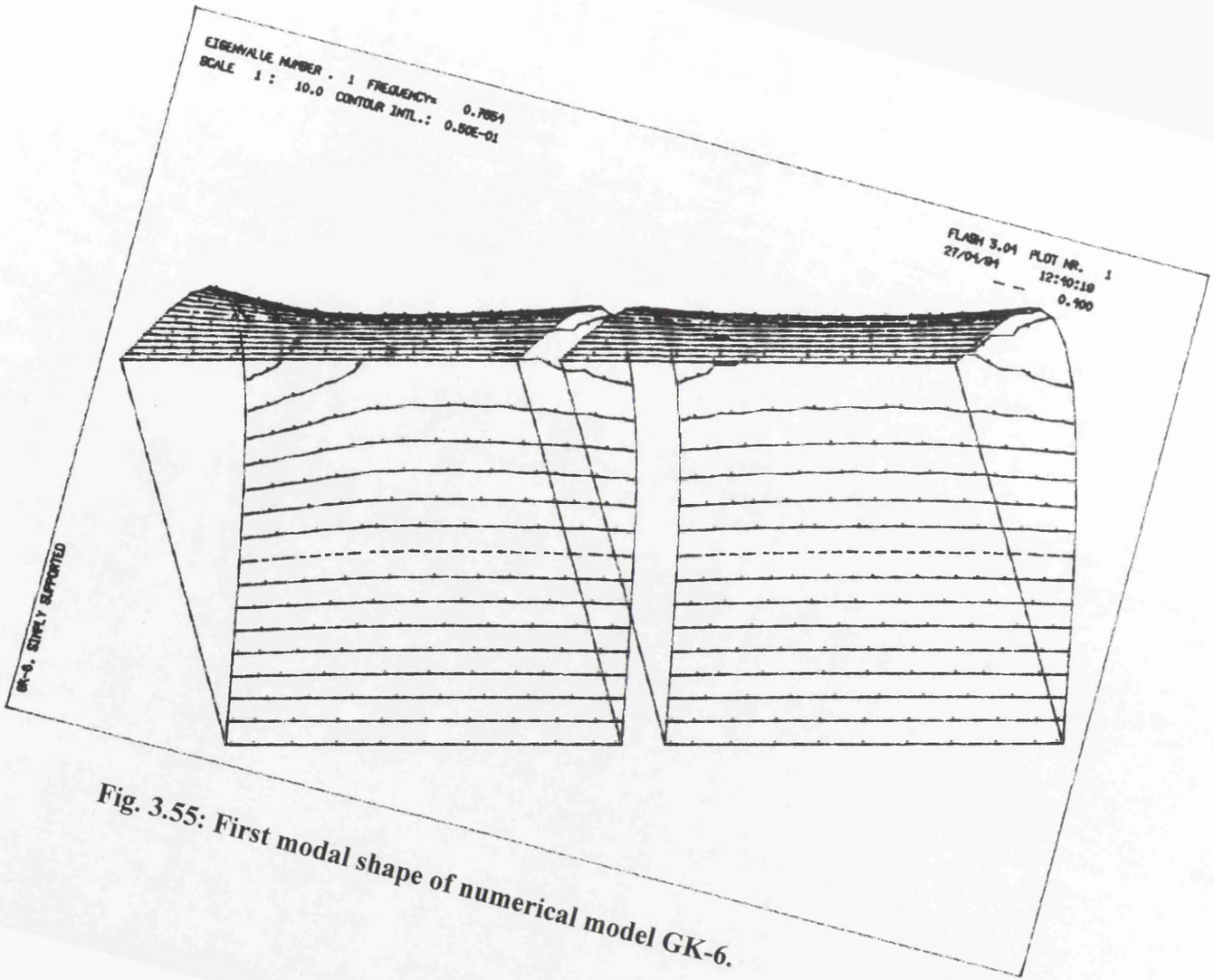

Fig. 3.55: First modal shape of numerical model GK-6.

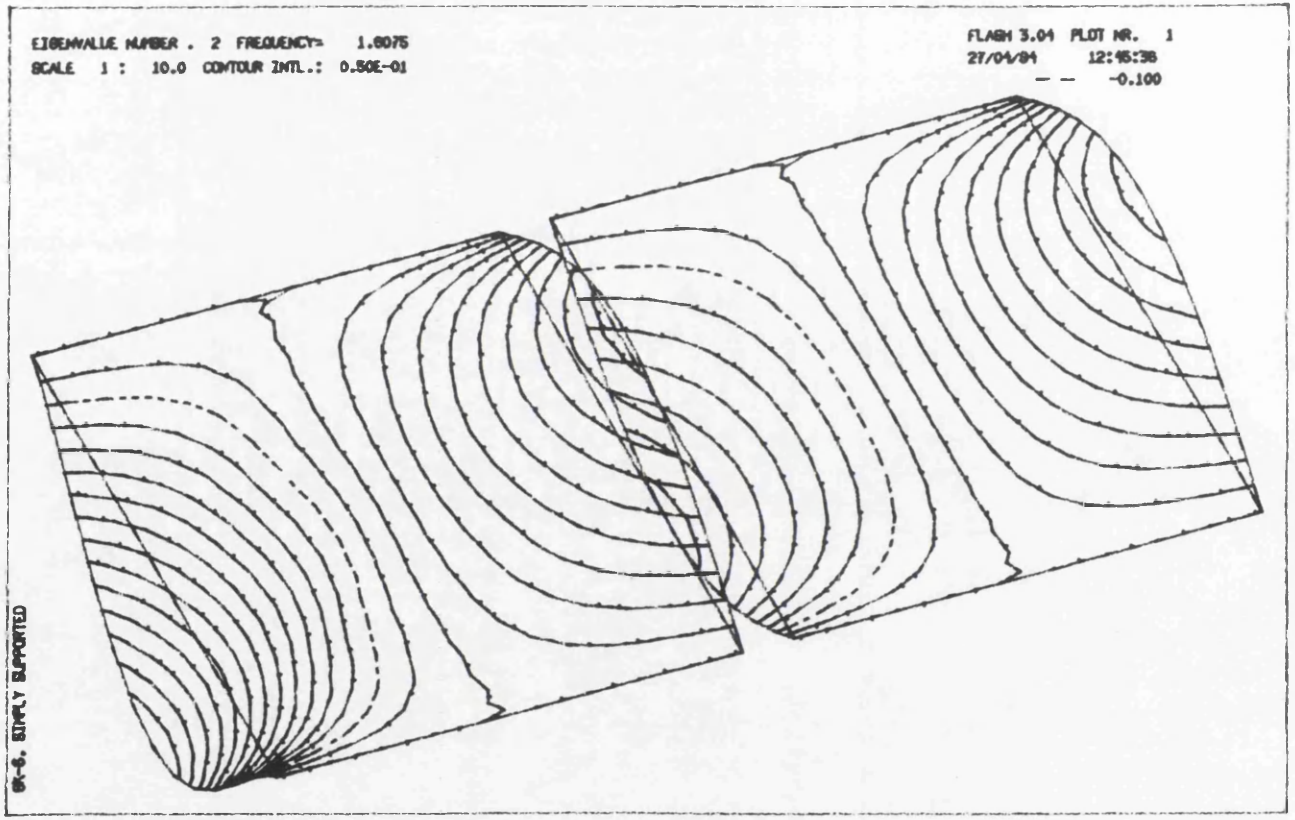

Fig. 3.56: Second modal shape of numerical model GK-6.

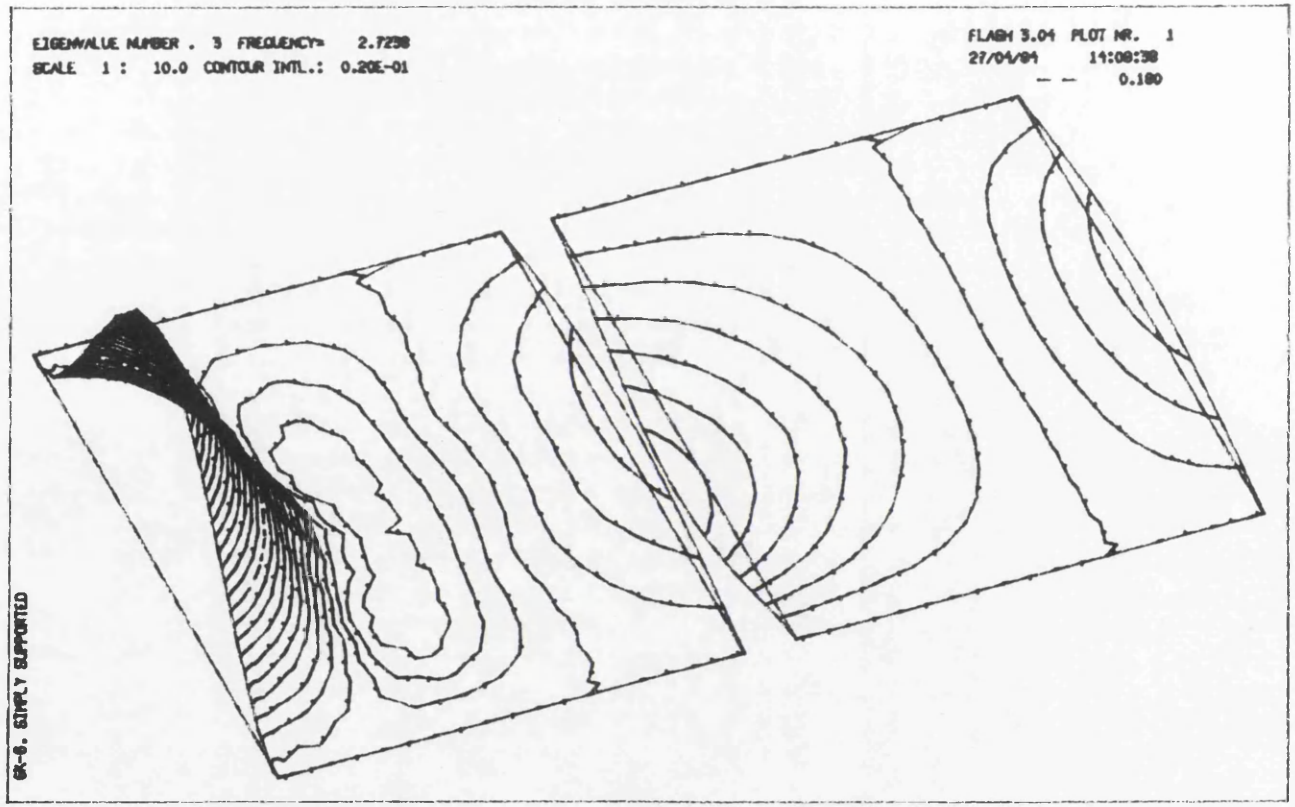

Fig. 3.57: Third modal shape of numerical model GK-6.

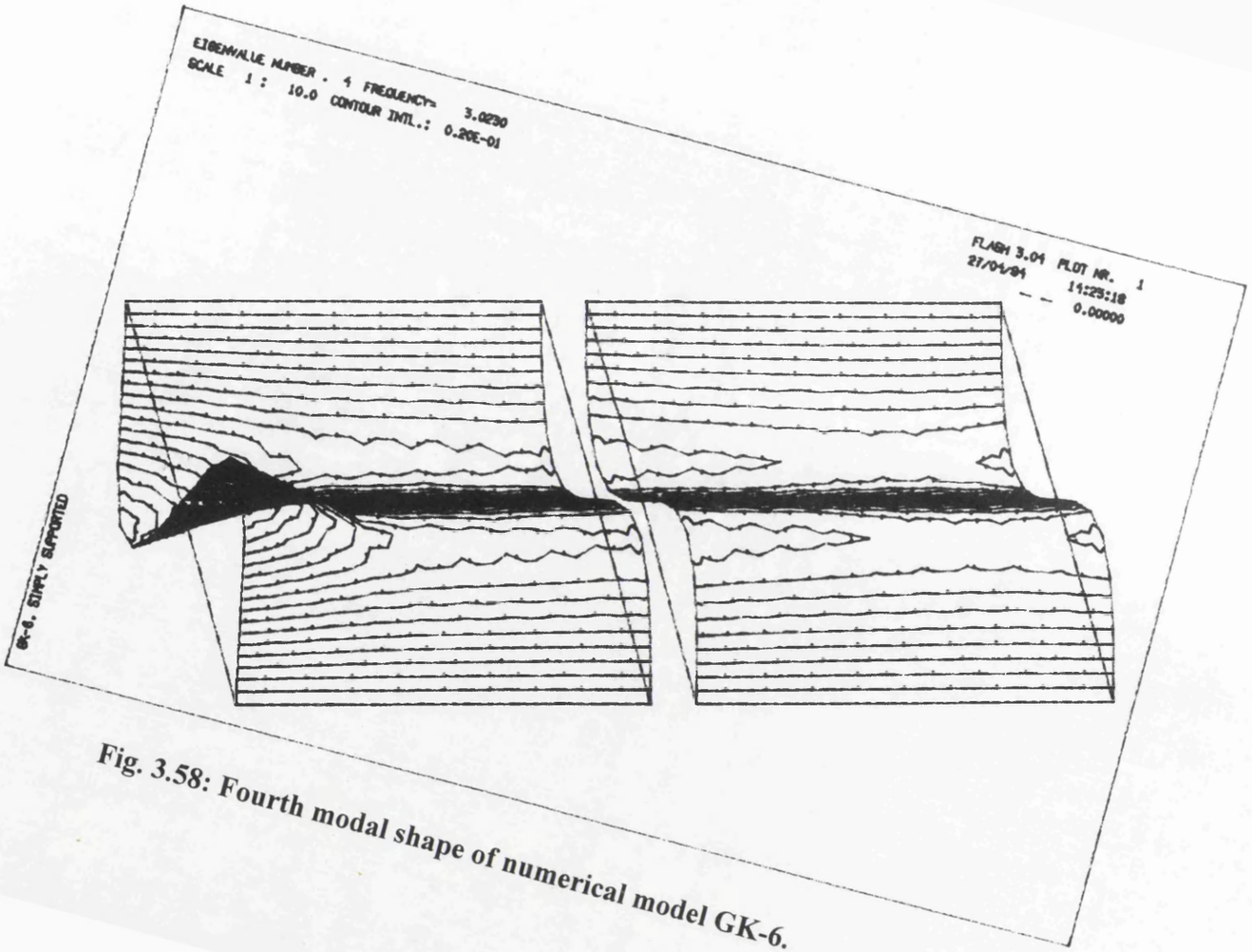

Fig. 3.58: Fourth modal shape of numerical model GK-6.

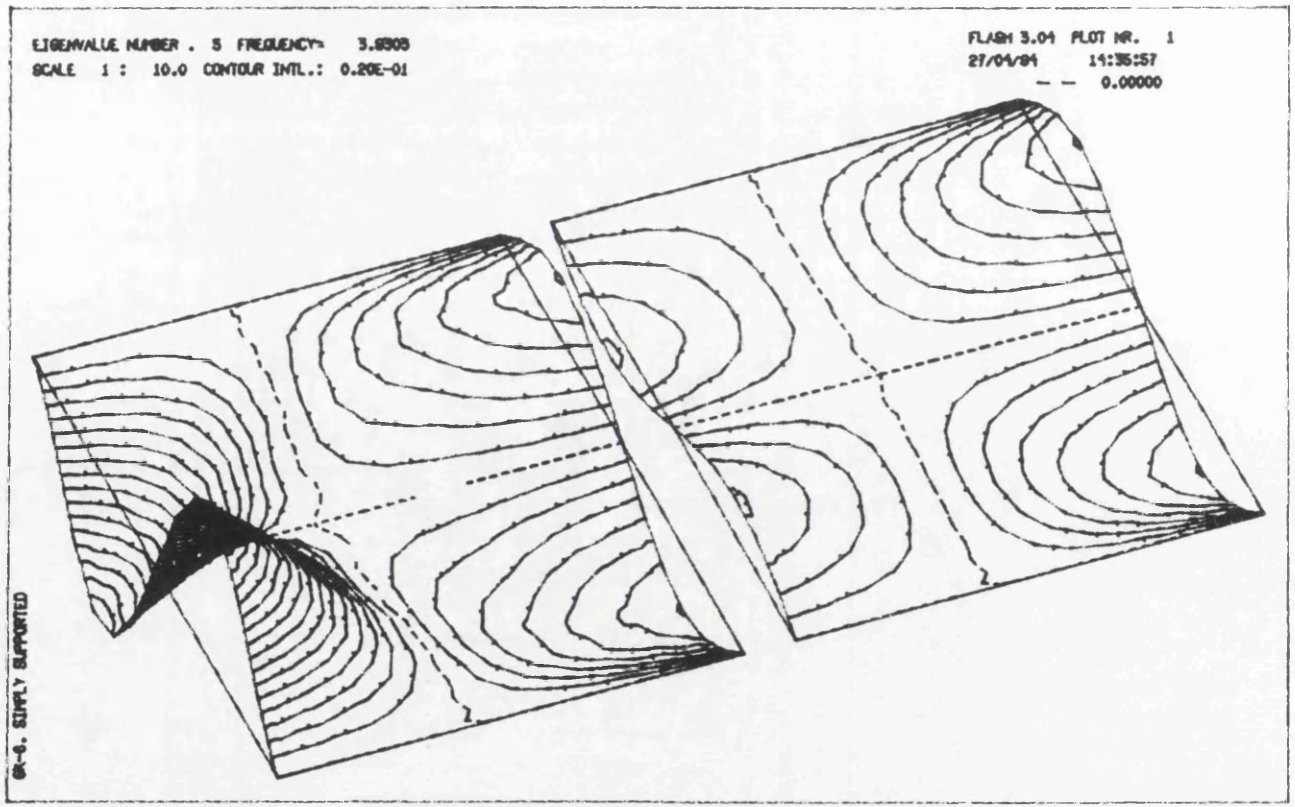

Fig. 3.59: Fifth modal shape of numerical model GK-6.

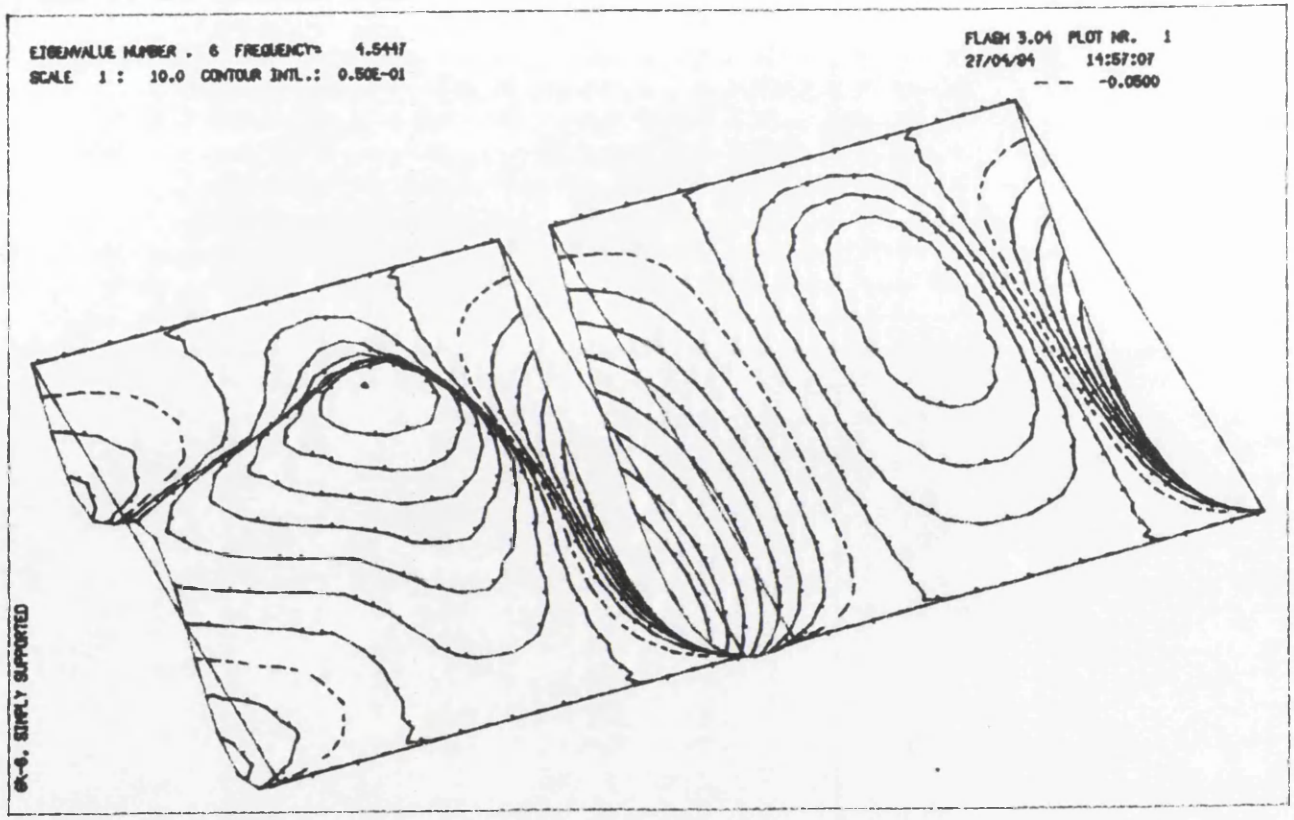

Fig. 3.60: Sixth modal shape of numerical model GK-6.

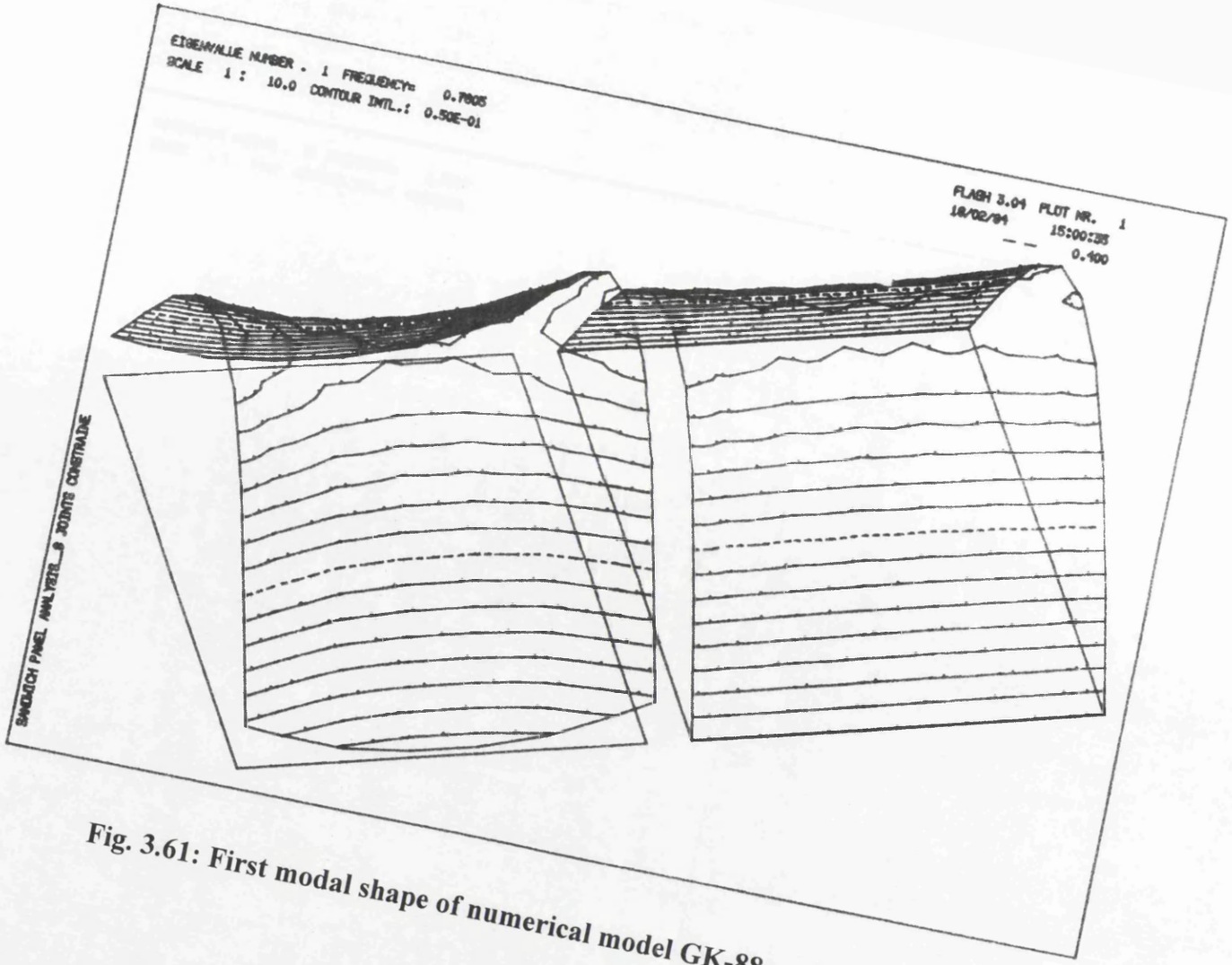

Fig. 3.61: First modal shape of numerical model GK-88.

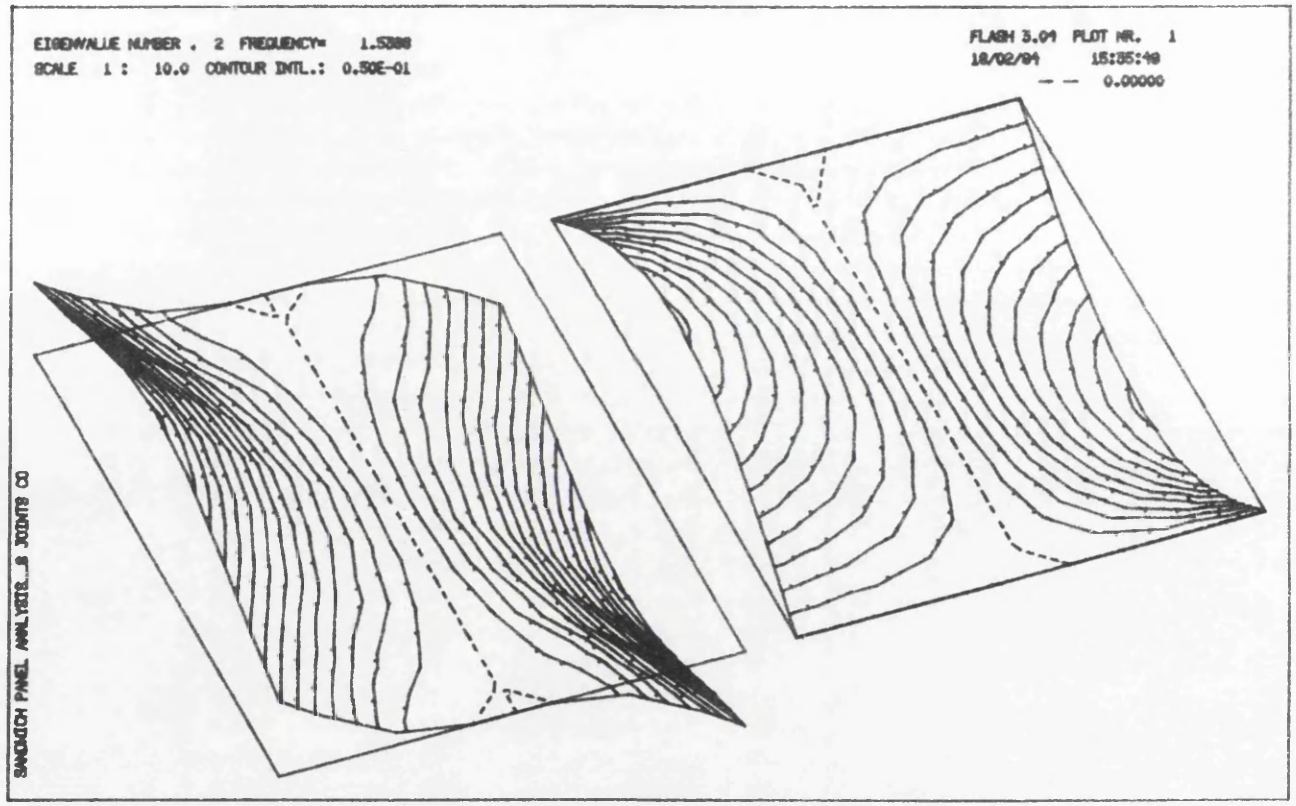

Fig. 3.62: Second modal shape of numerical model GK-88.

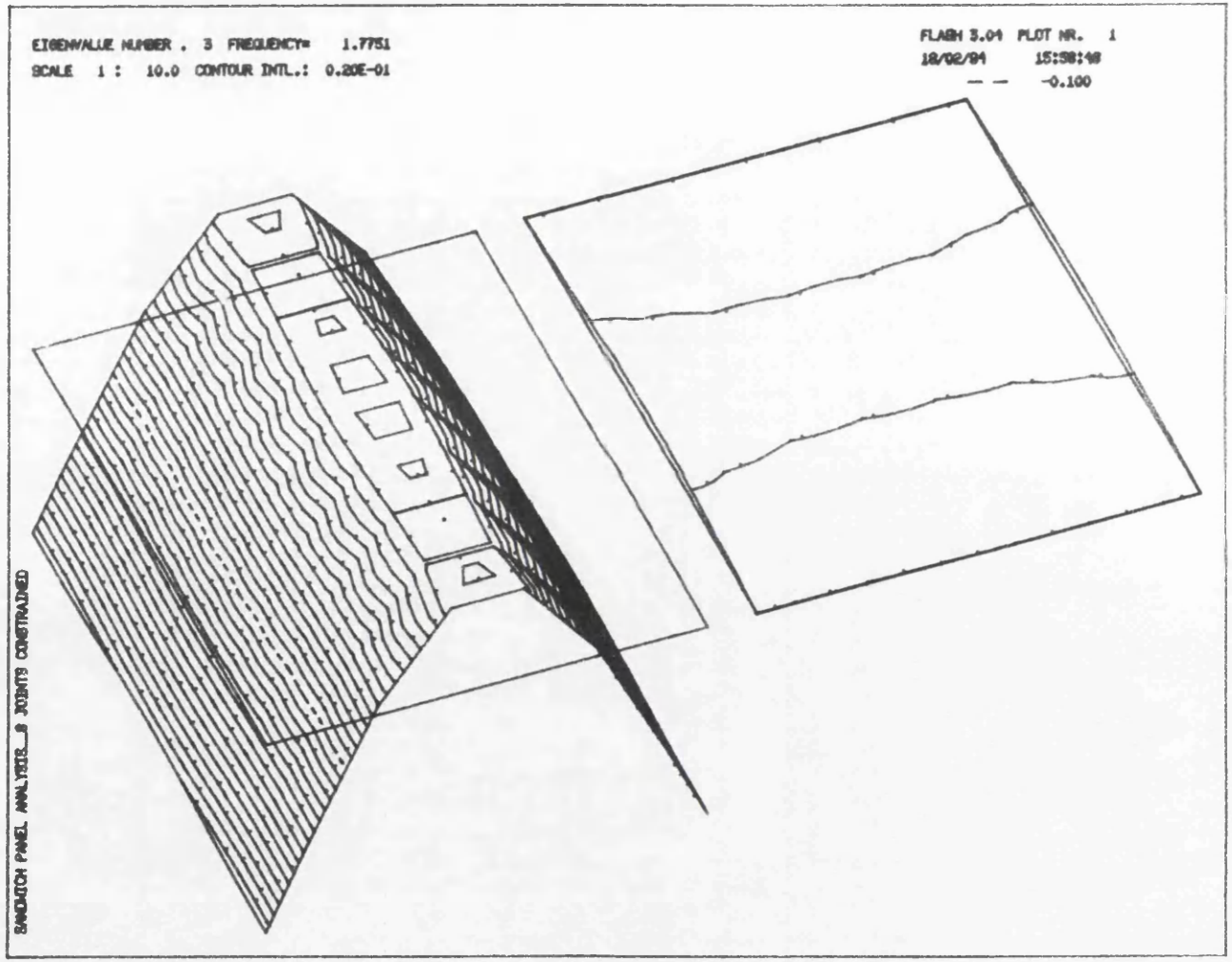

Fig. 3.63: Third modal shape of numerical model GK-88.

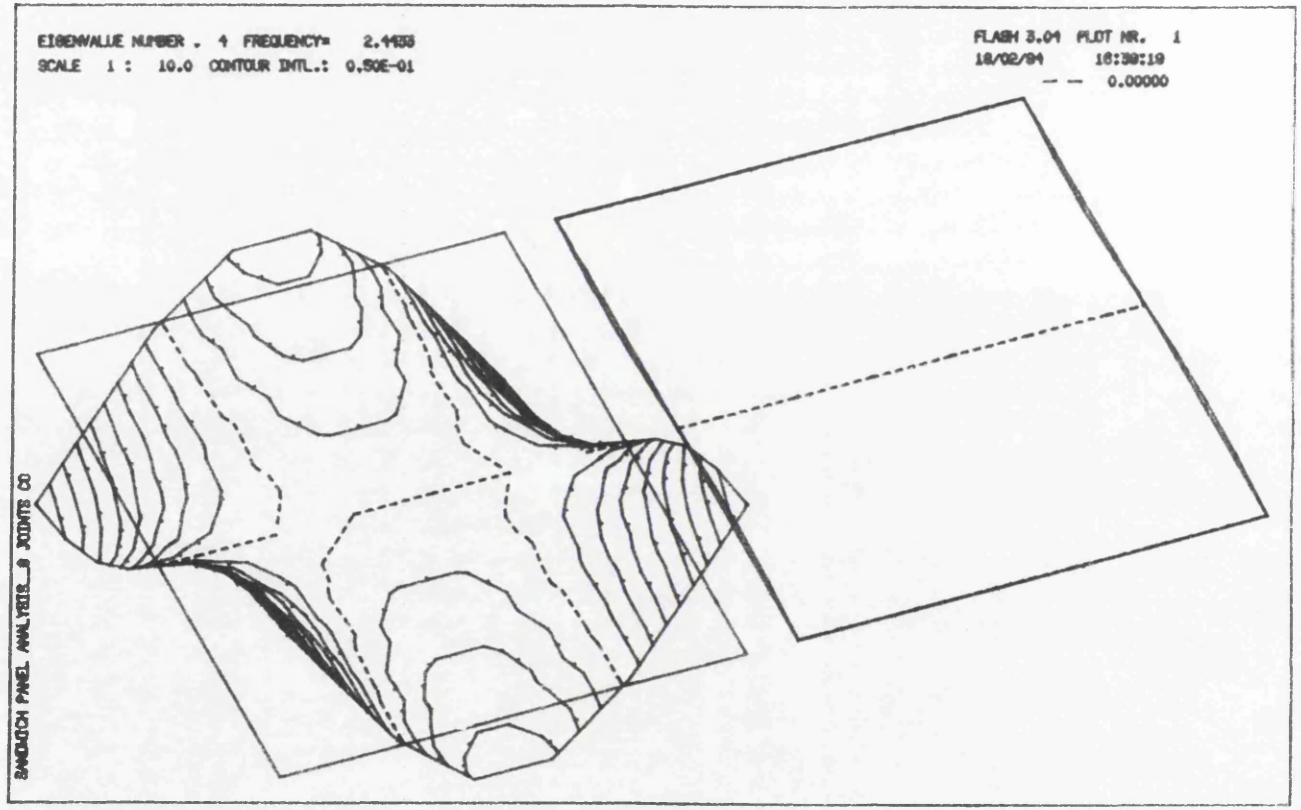

Fig. 3.64: Fourth modal shape of numerical model GK-88.

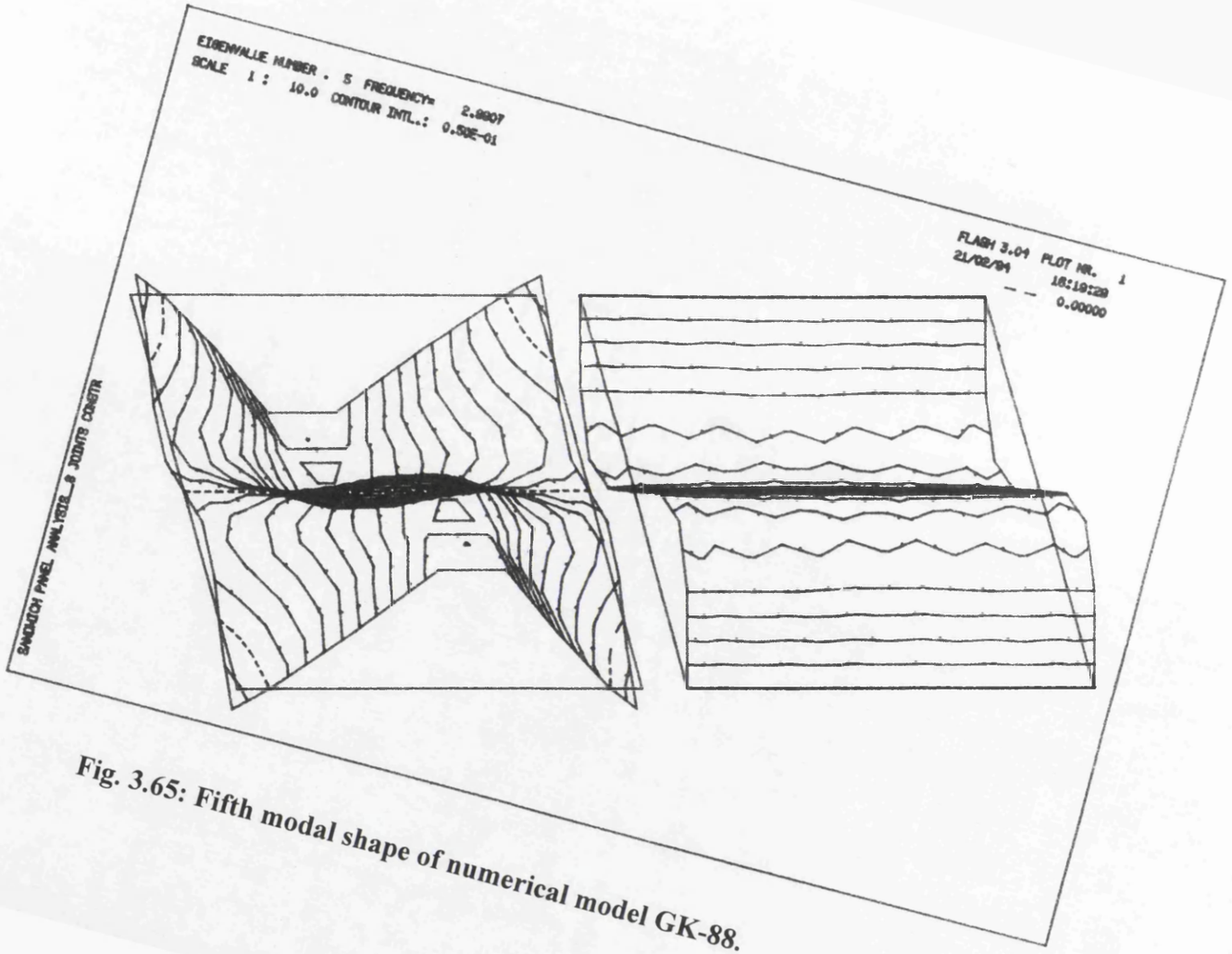

Fig. 3.65: Fifth modal shape of numerical model GK-88.

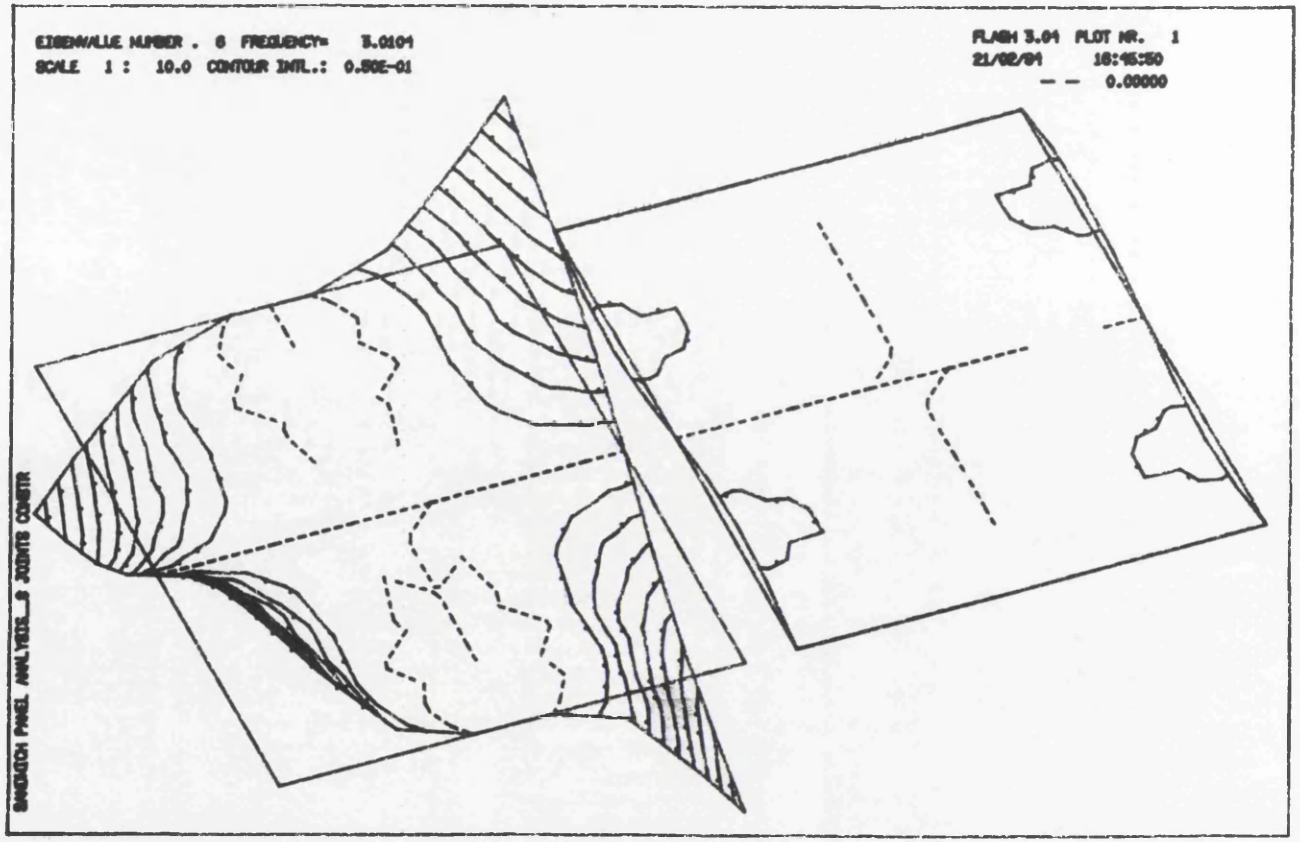

Fig. 3.66: Sixth modal shape of numerical model GK-88.

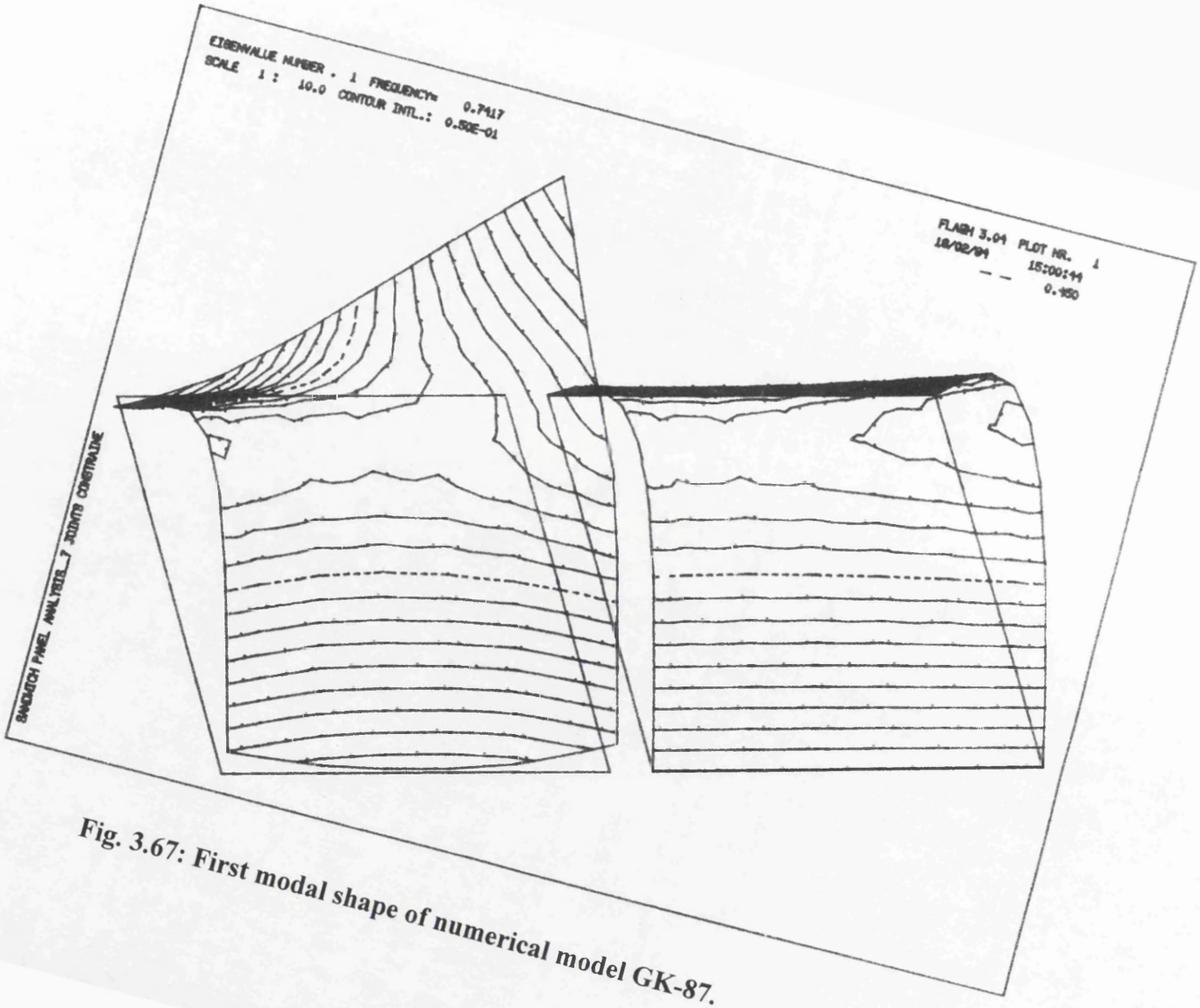

Fig. 3.67: First modal shape of numerical model GK-87.

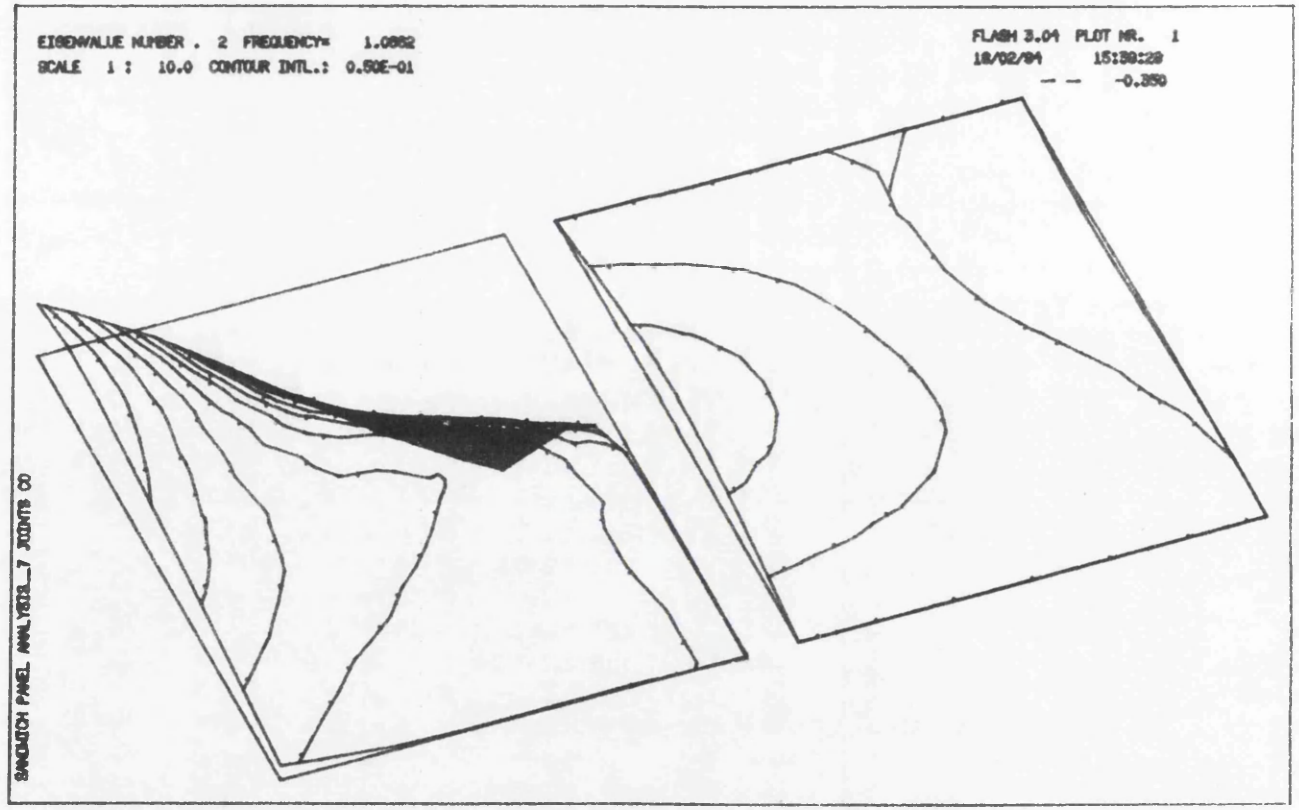

Fig. 3.68: Second modal shape of numerical model GK-87.

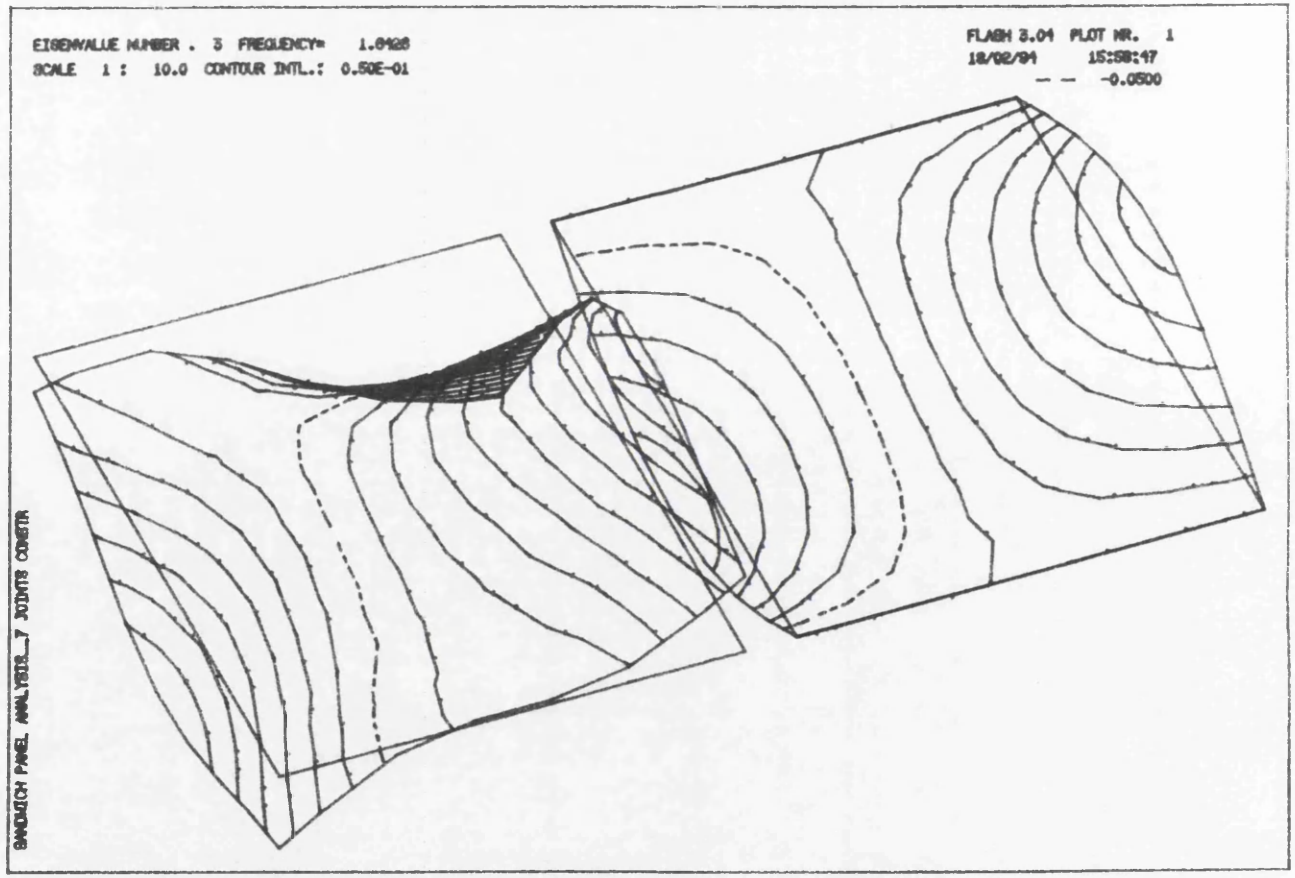

Fig. 3.69: Third modal shape of numerical model GK-87.

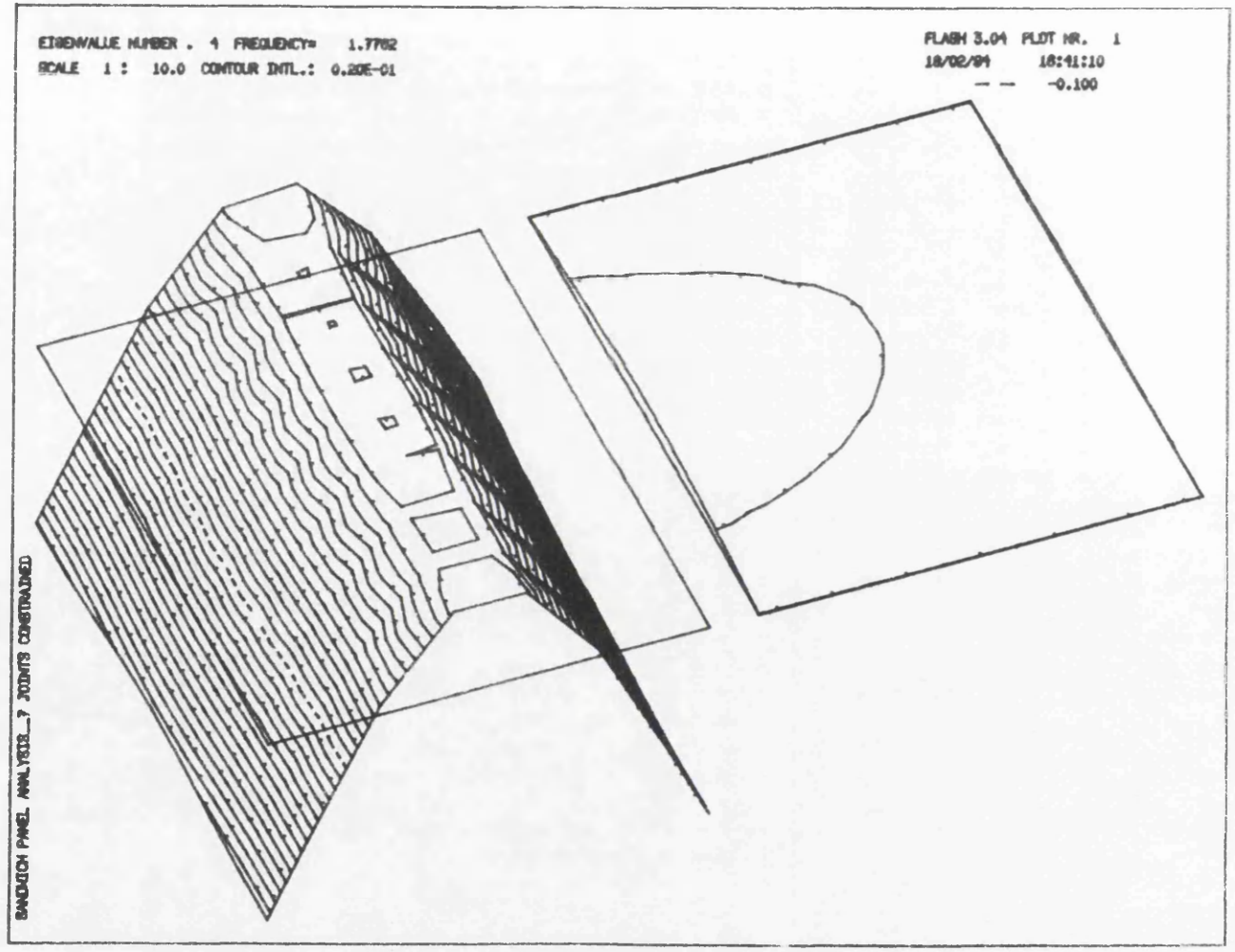

Fig. 3.70: Fourth modal shape of numerical model GK-87.

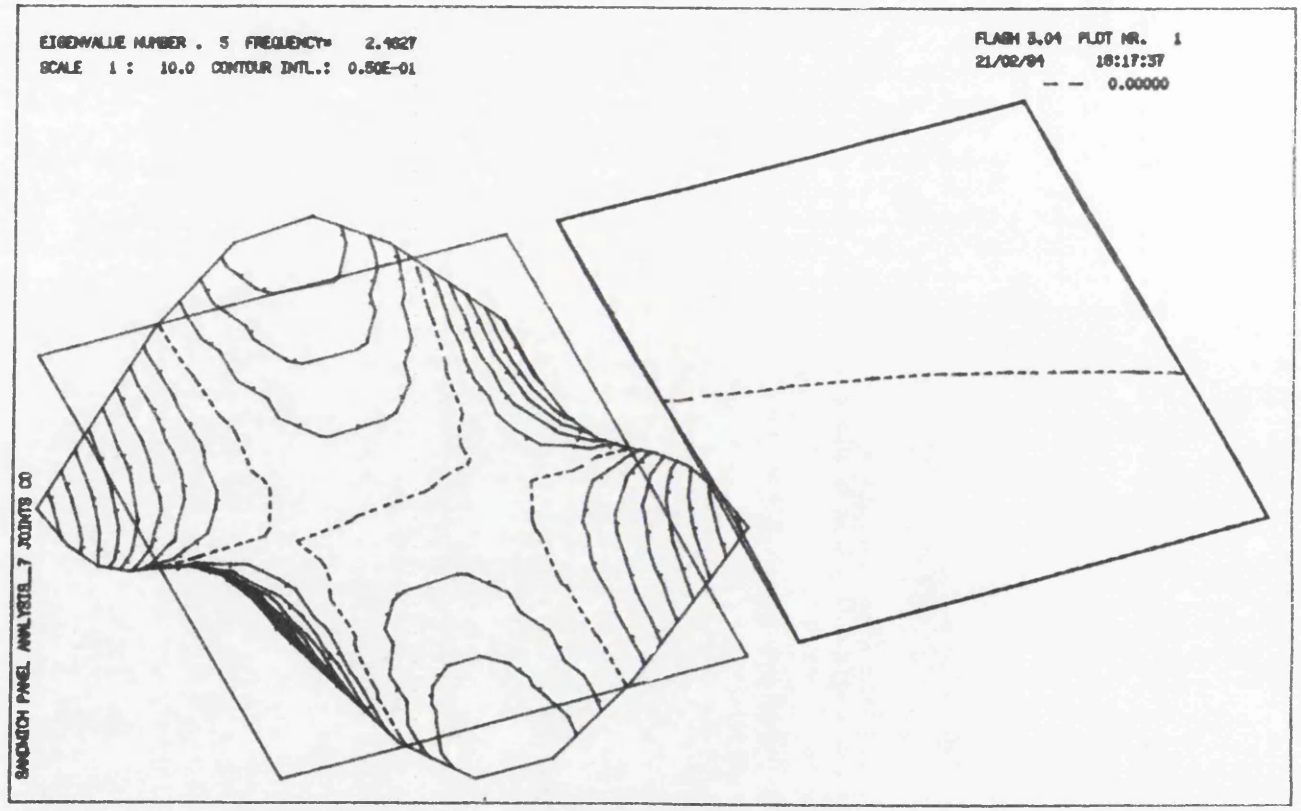

Fig. 3.71: Fifth modal shape of numerical model GK-87.

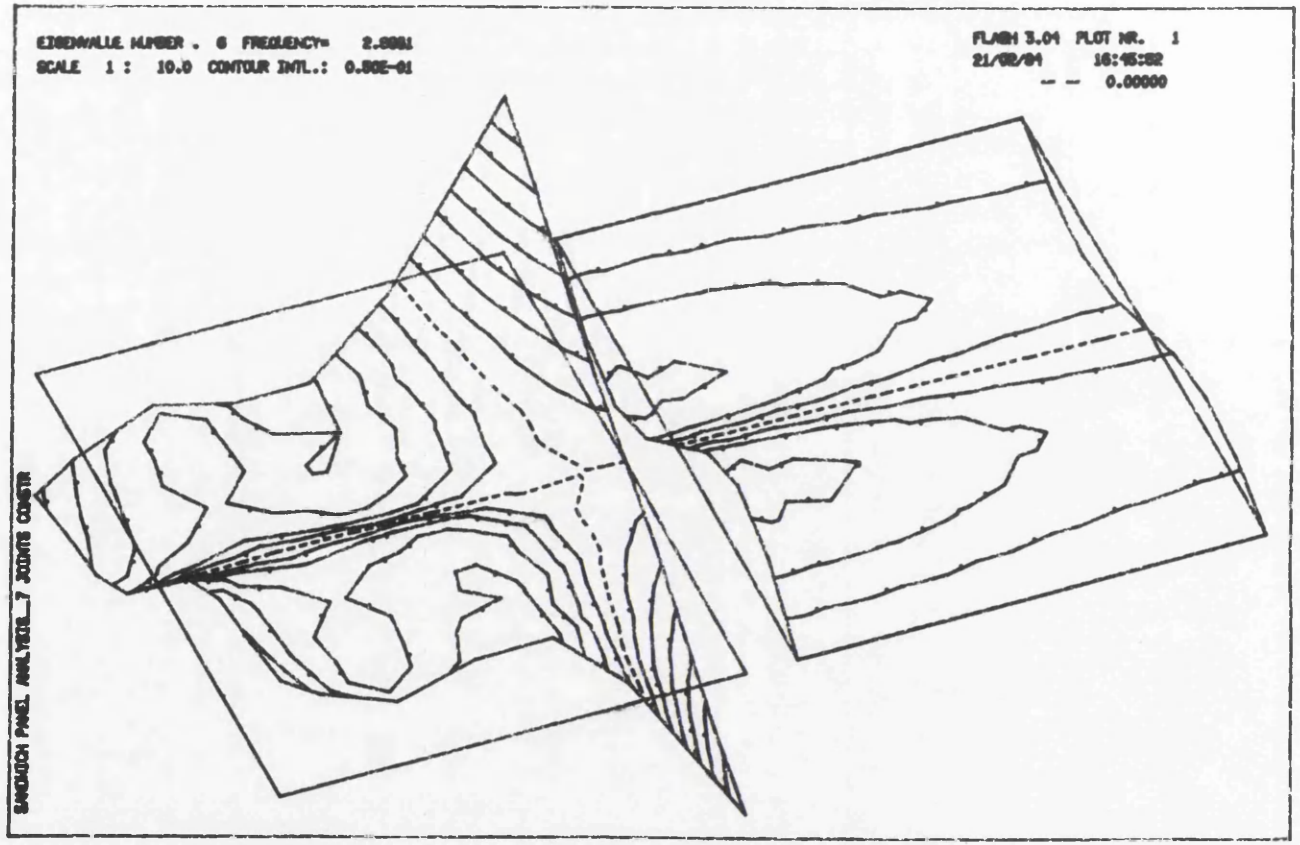

Fig. 3.72: Sixth modal shape of numerical model GK-87.

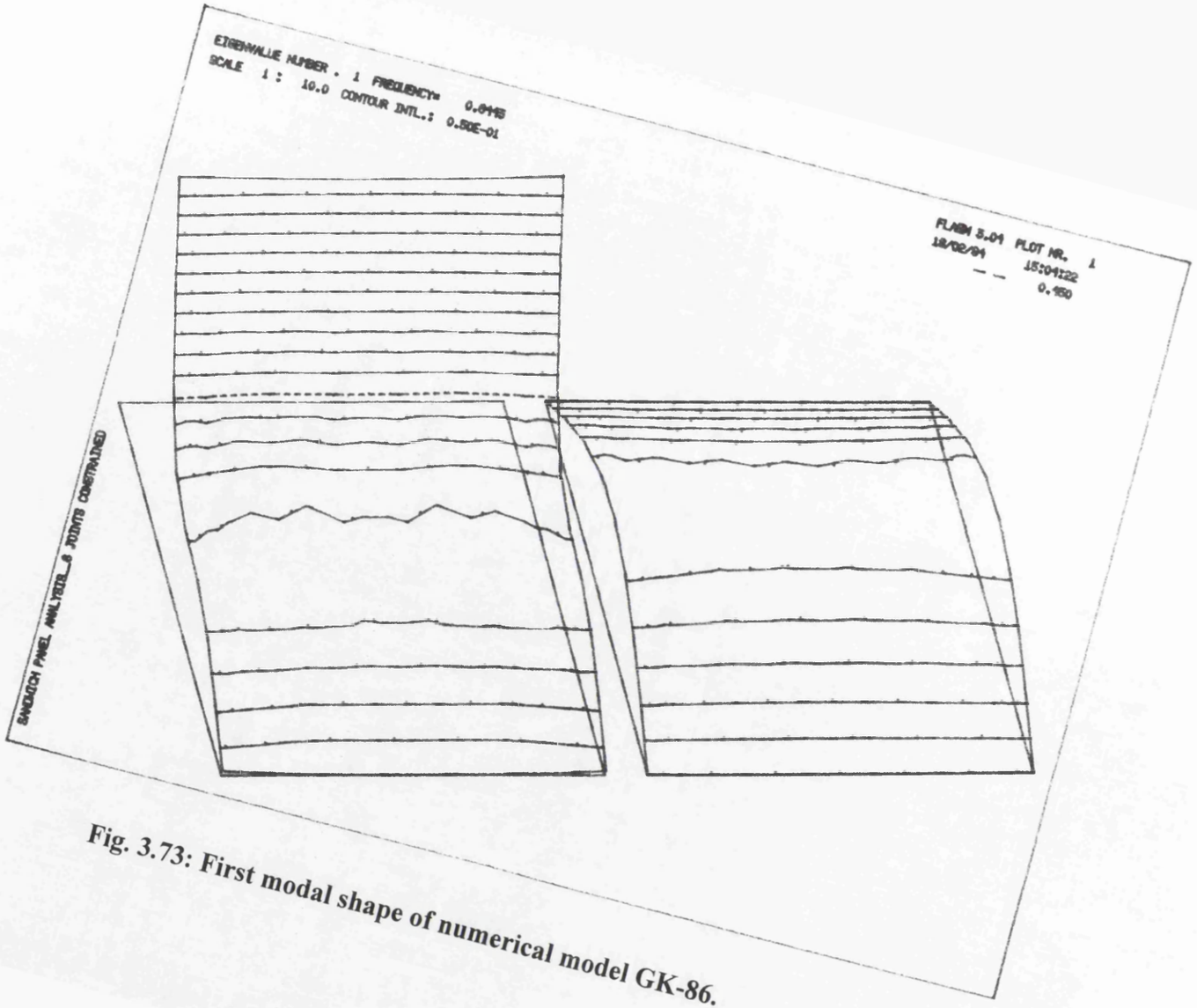

Fig. 3.73: First modal shape of numerical model GK-86.

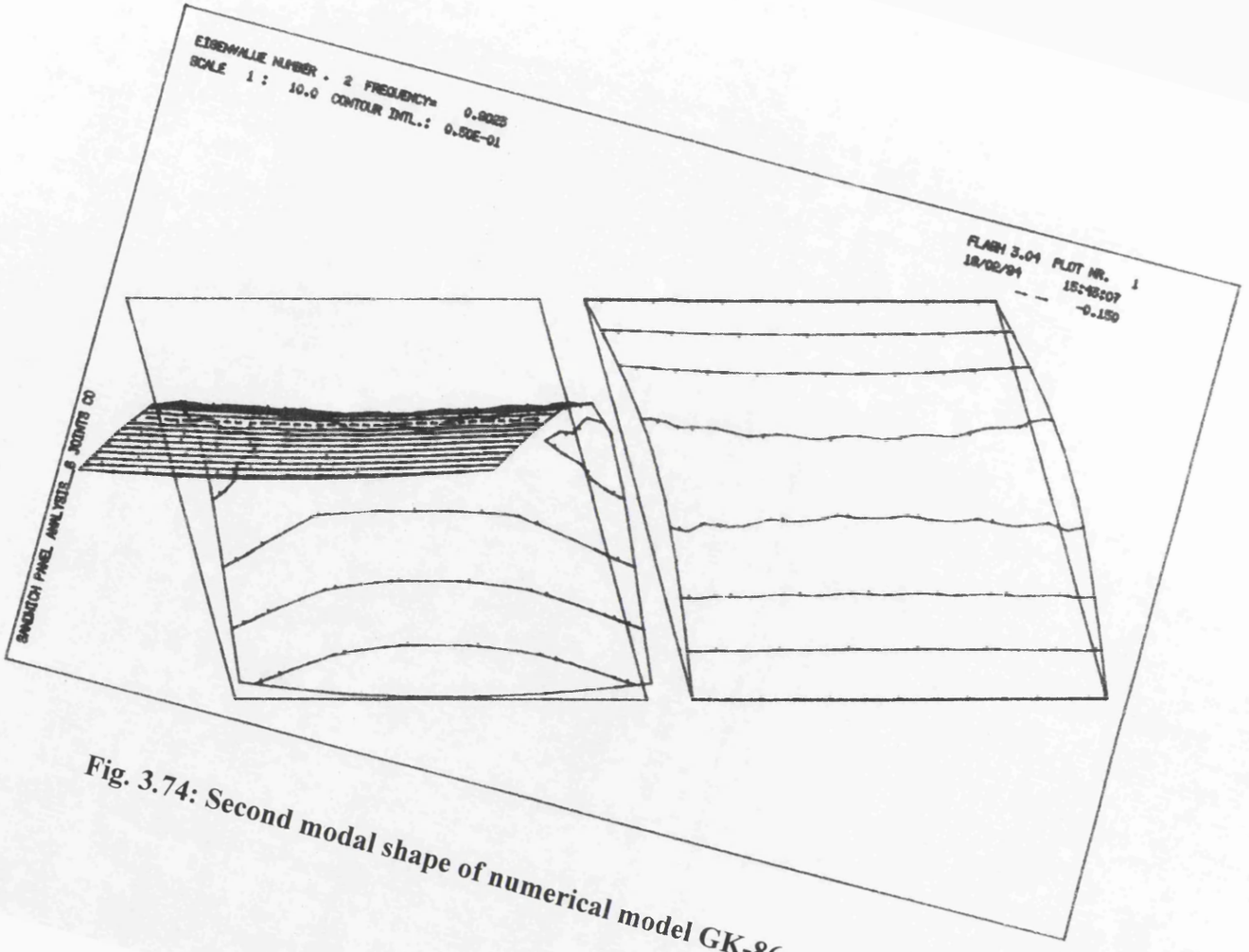

Fig. 3.74: Second modal shape of numerical model GK-86.

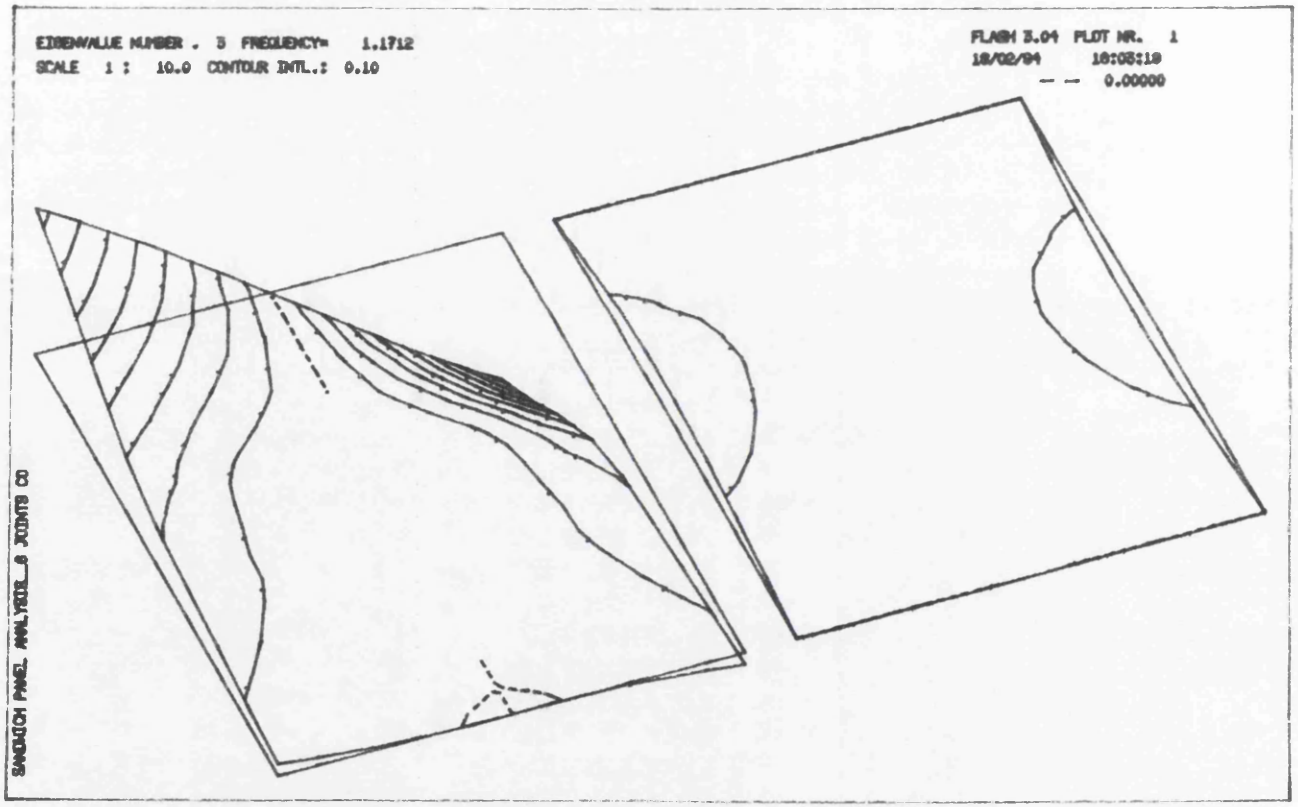

Fig. 3.75: Third modal shape of numerical model GK-86.

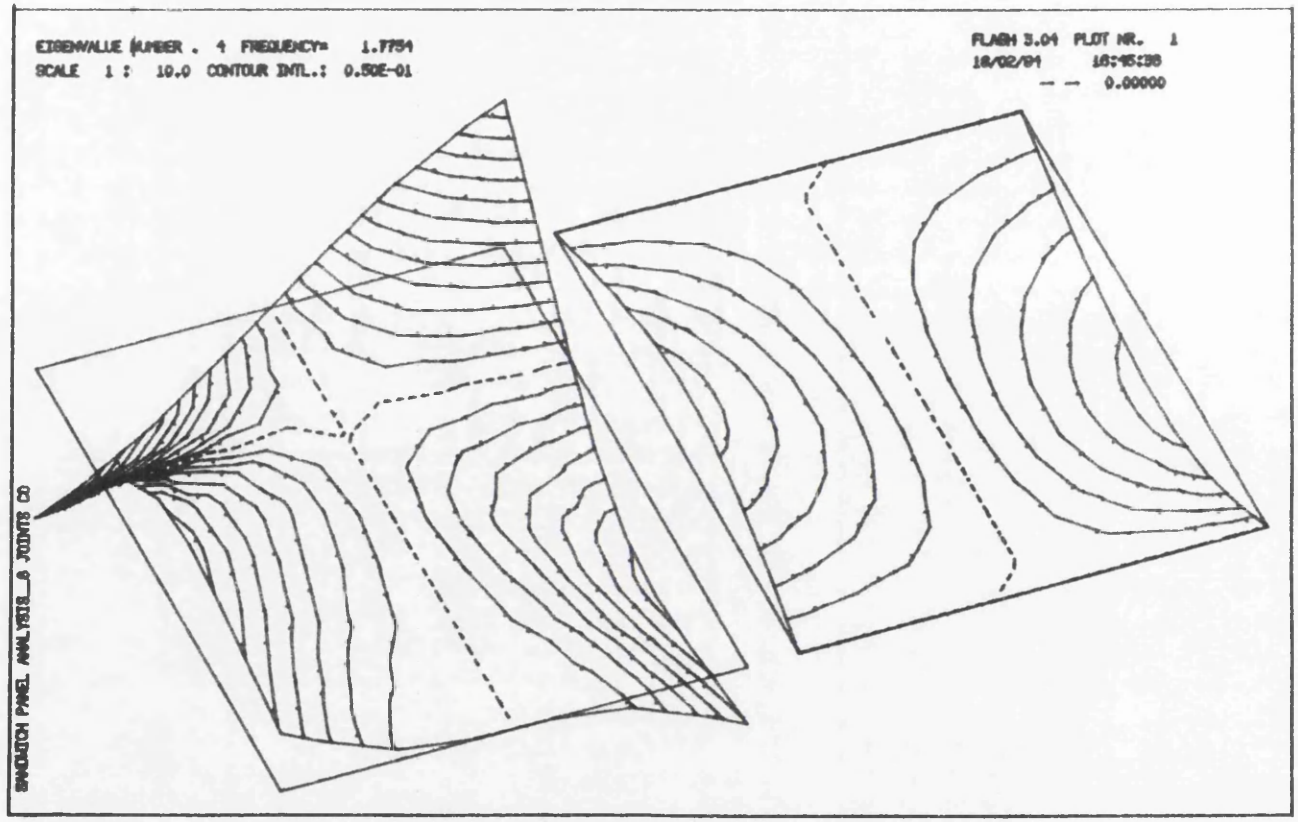

Fig. 3.76: Fourth modal shape of numerical model GK-86.

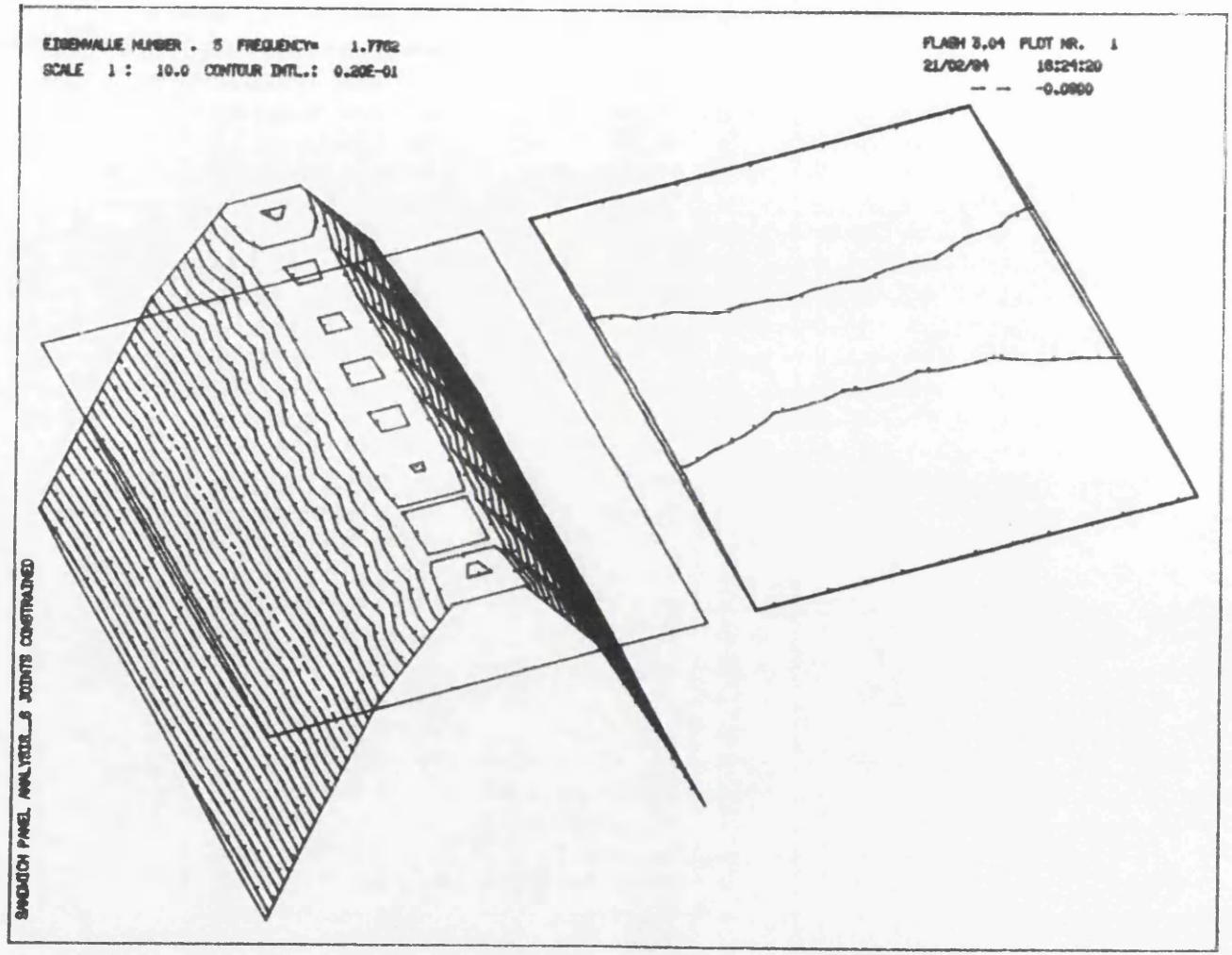

Fig. 3.77: Fifth modal shape of numerical model GK-86.

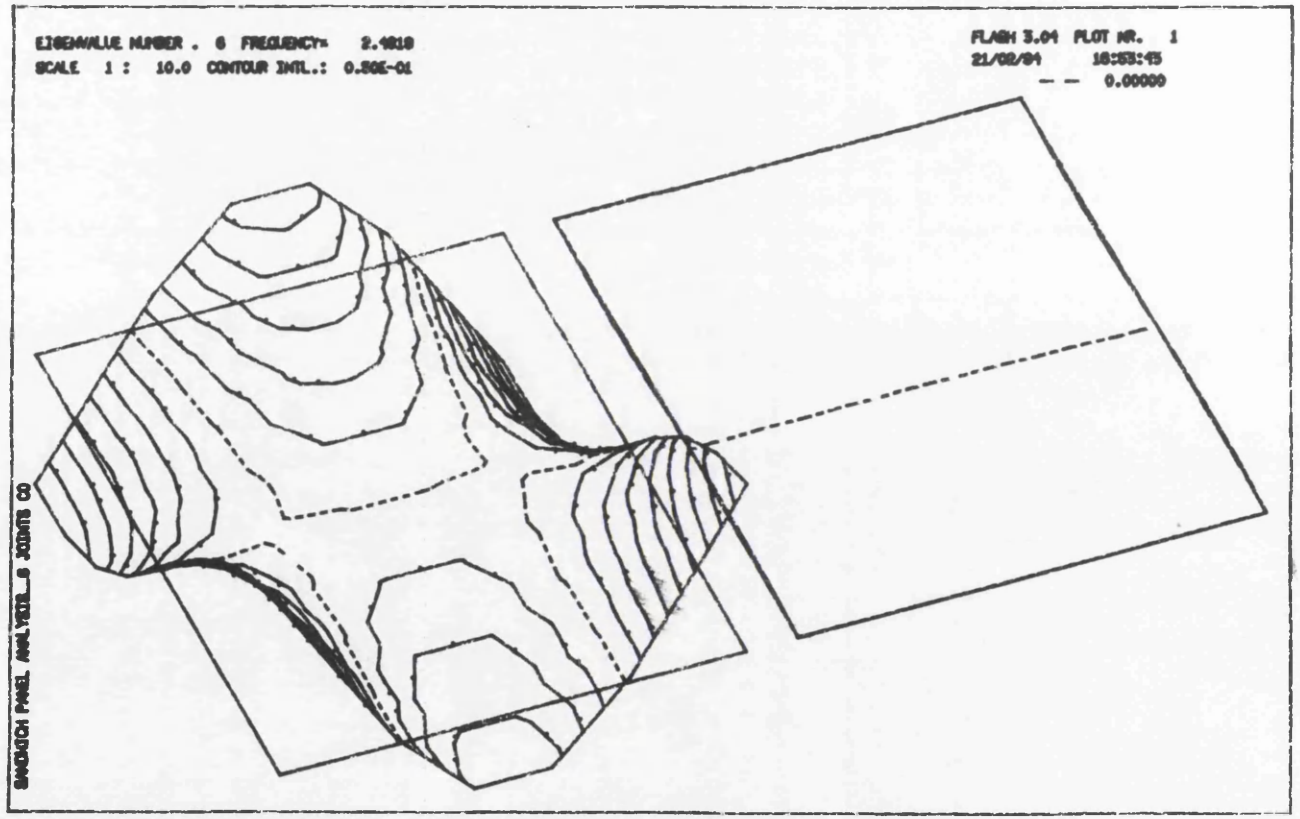

Fig. 3.78: Sixth modal shape of numerical model GK-86.

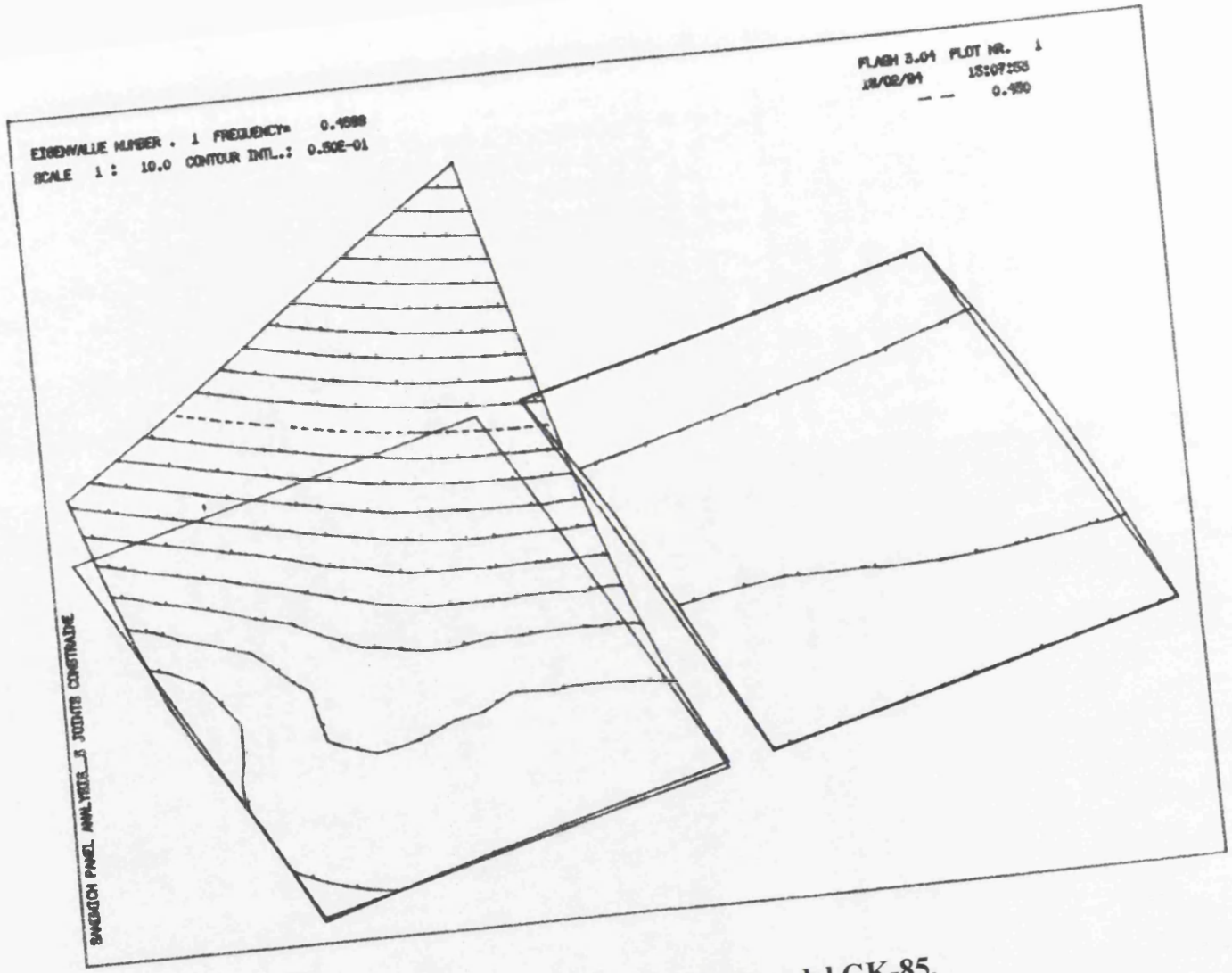

Fig. 3.79: First modal shape of numerical model GK-85.

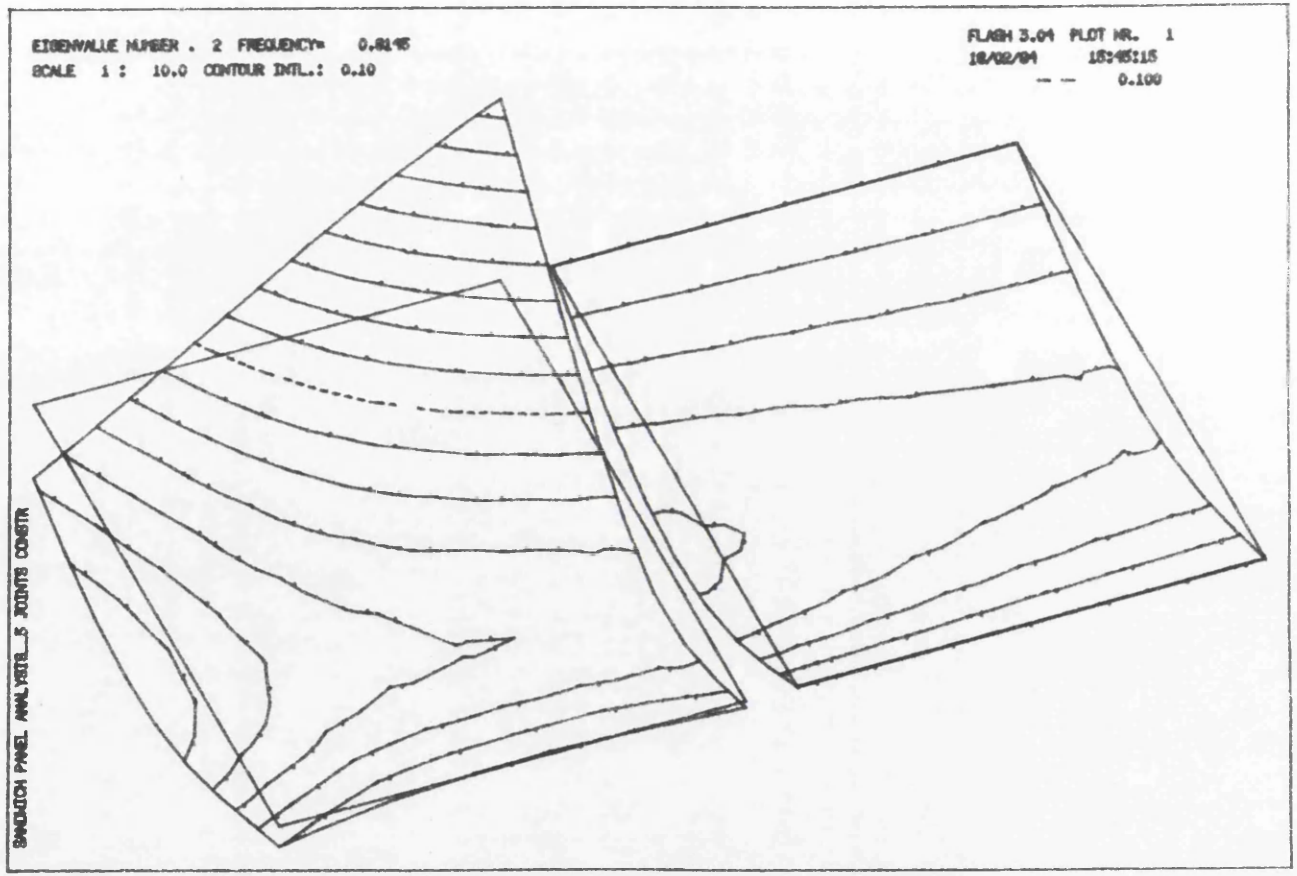

Fig. 3.80: Second modal shape of numerical model GK-85.

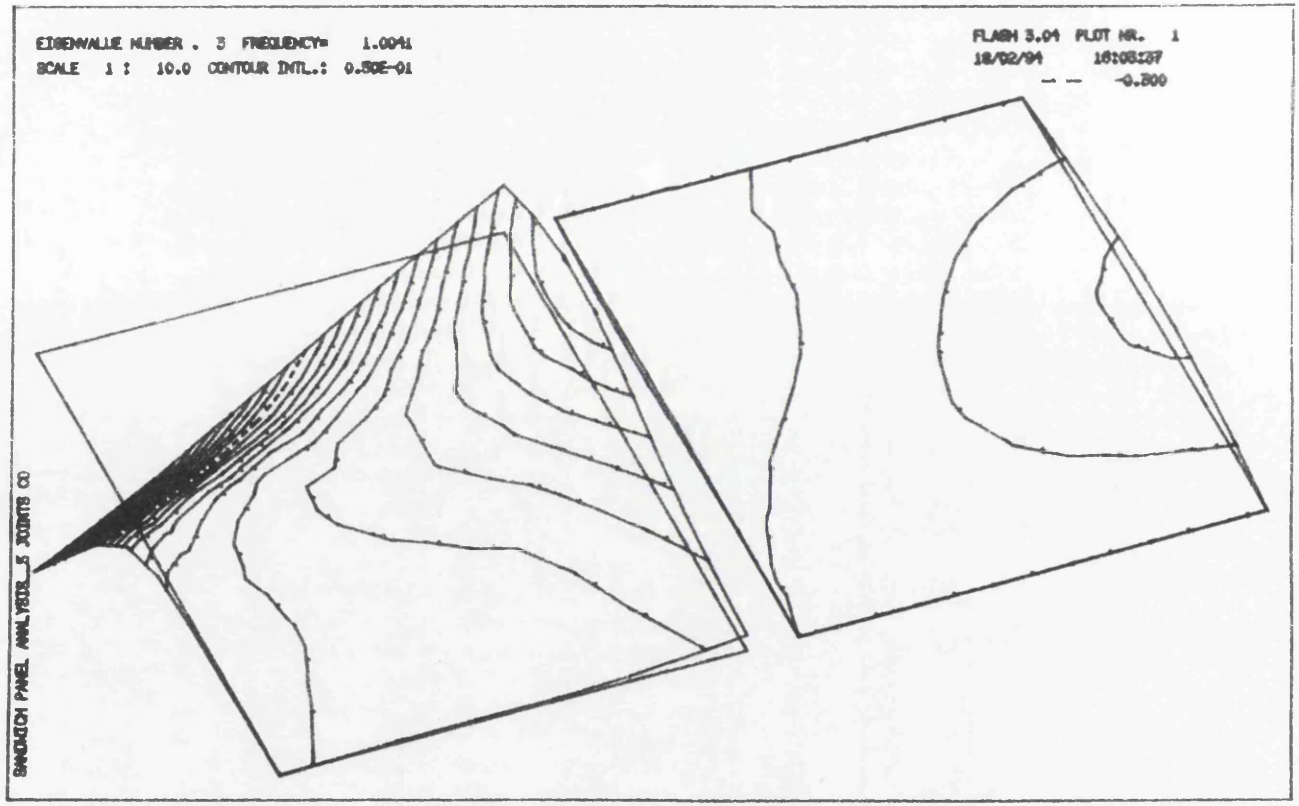

Fig. 3.81: Third modal shape of numerical model GK-85.

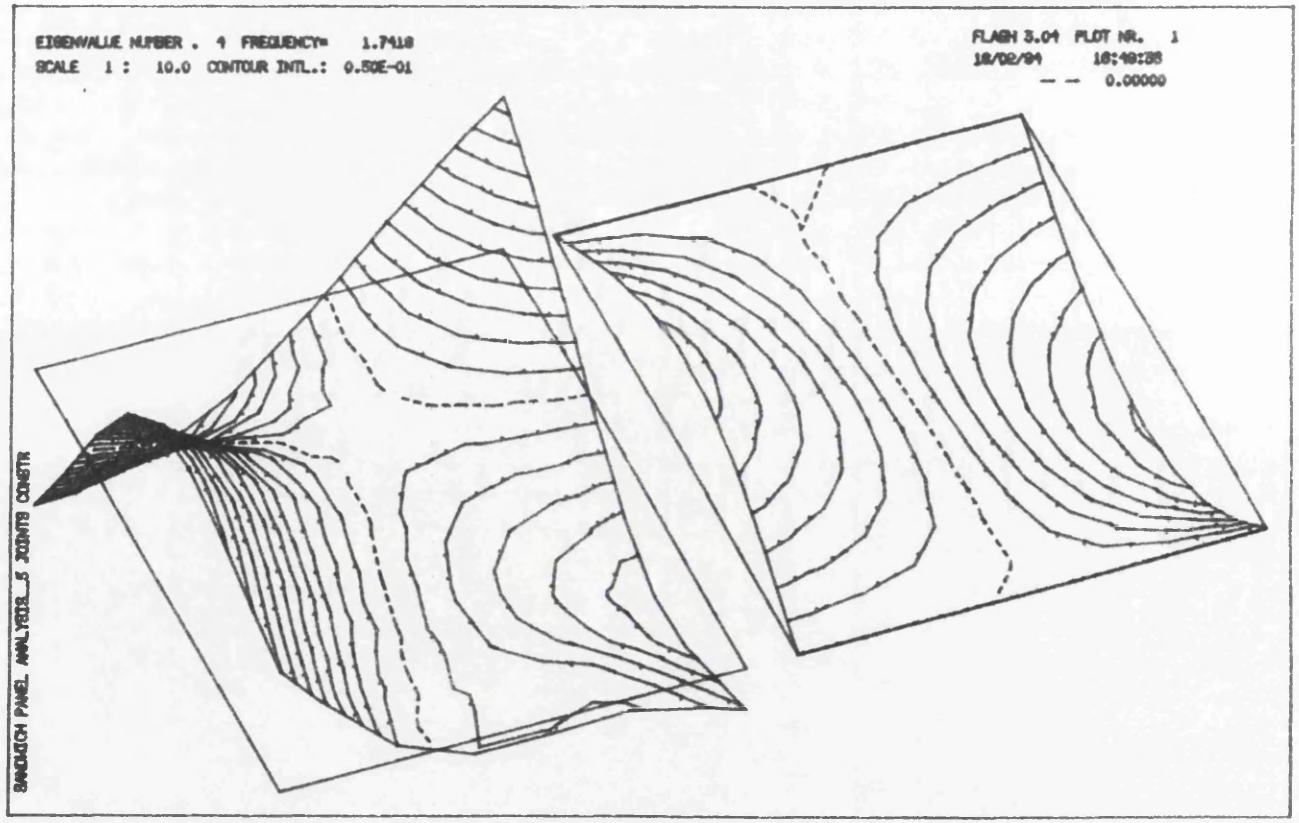

Fig. 3.82: Fourth modal shape of numerical model GK-85.

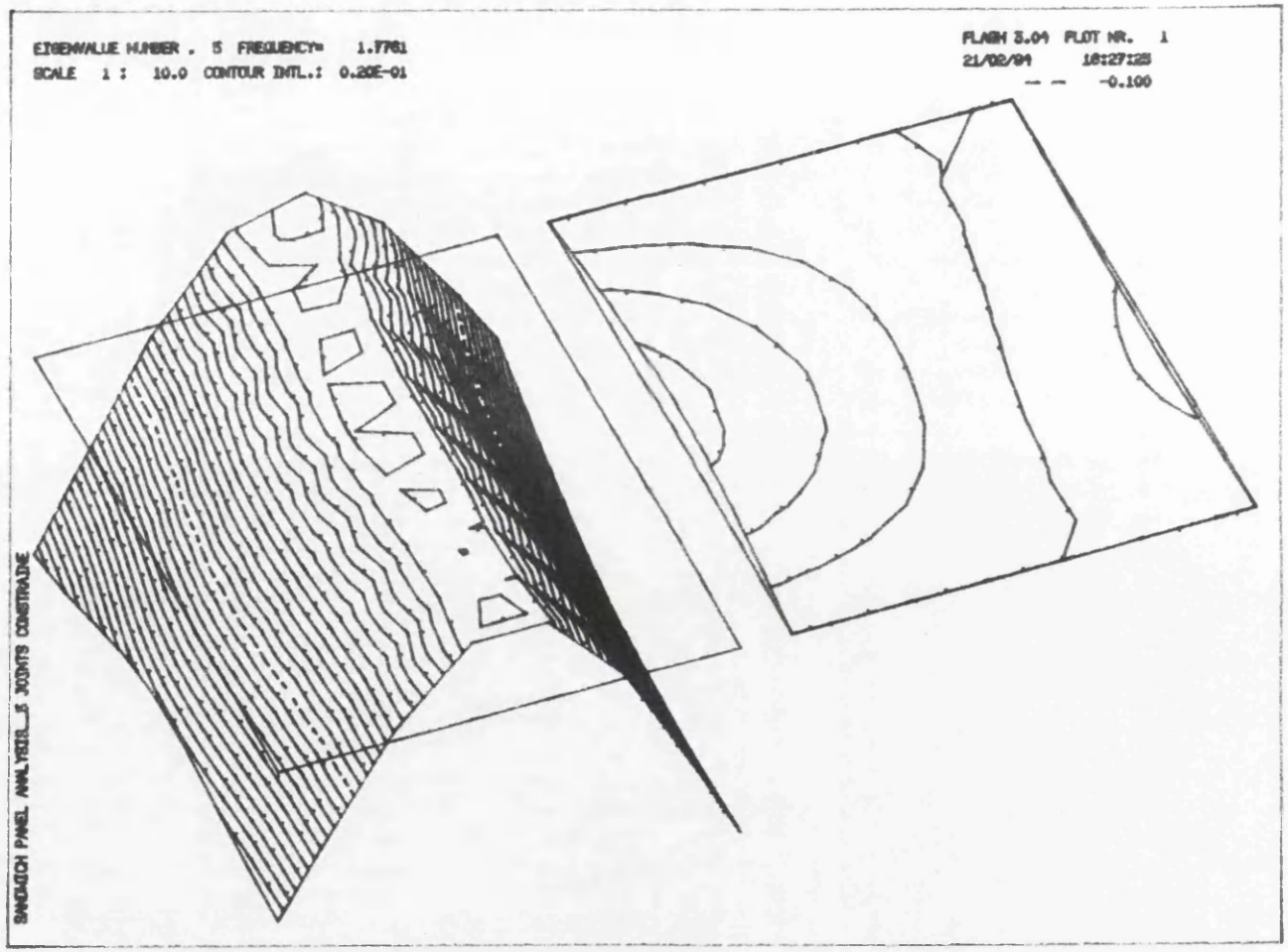

Fig. 3.83: Fifth modal shape of numerical model GK-85.

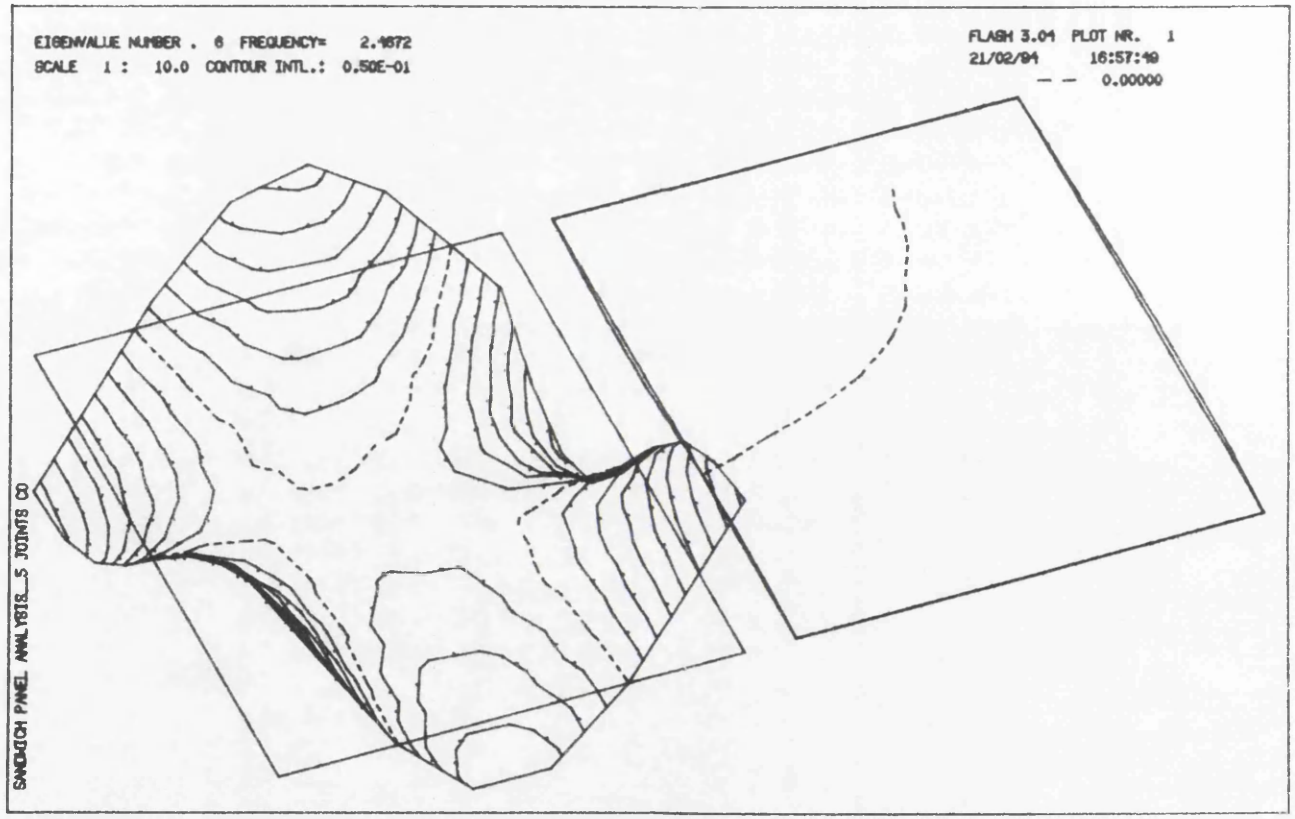

Fig. 3.84: Sixth modal shape of numerical model GK-85.

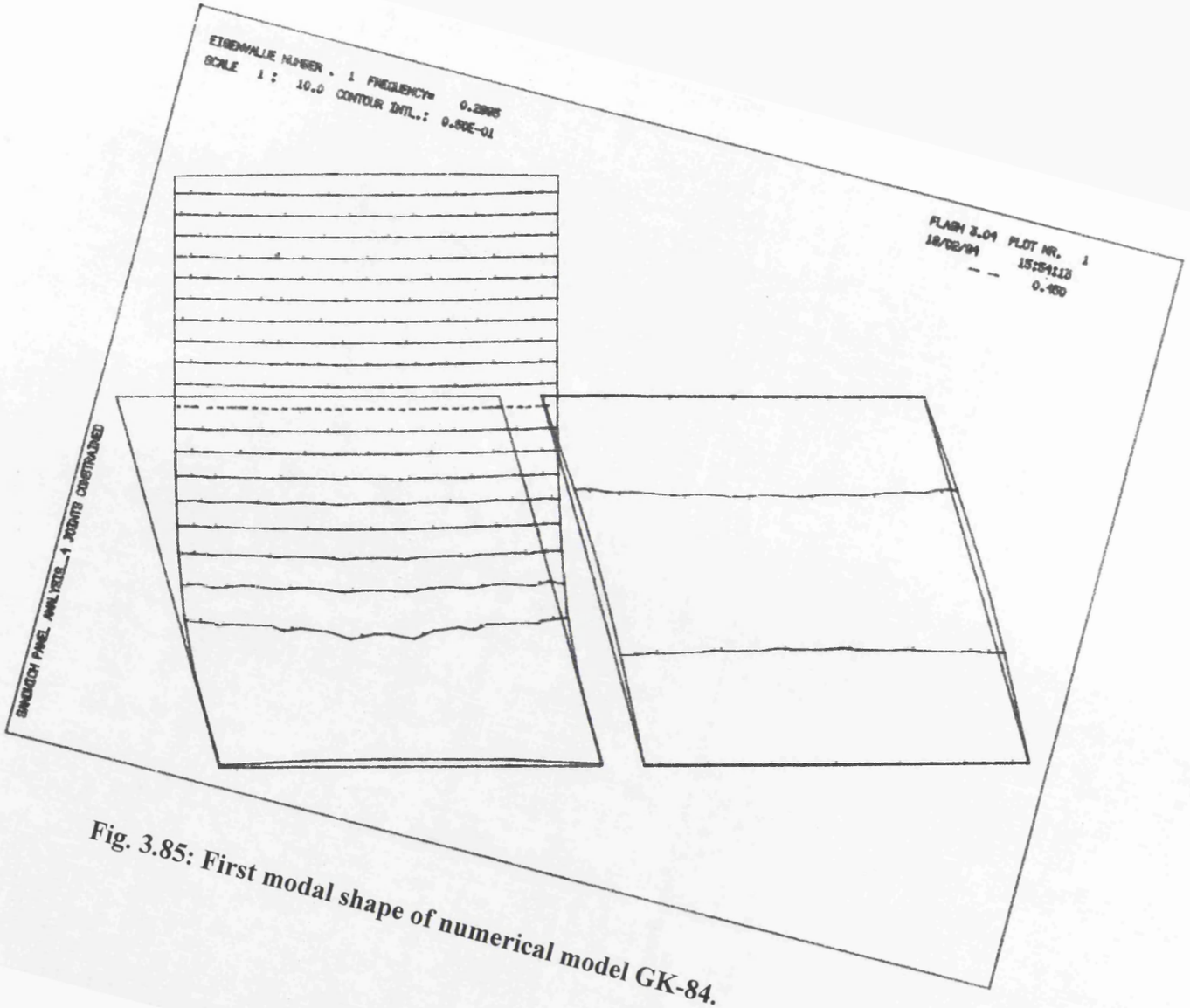

Fig. 3.85: First modal shape of numerical model GK-84.

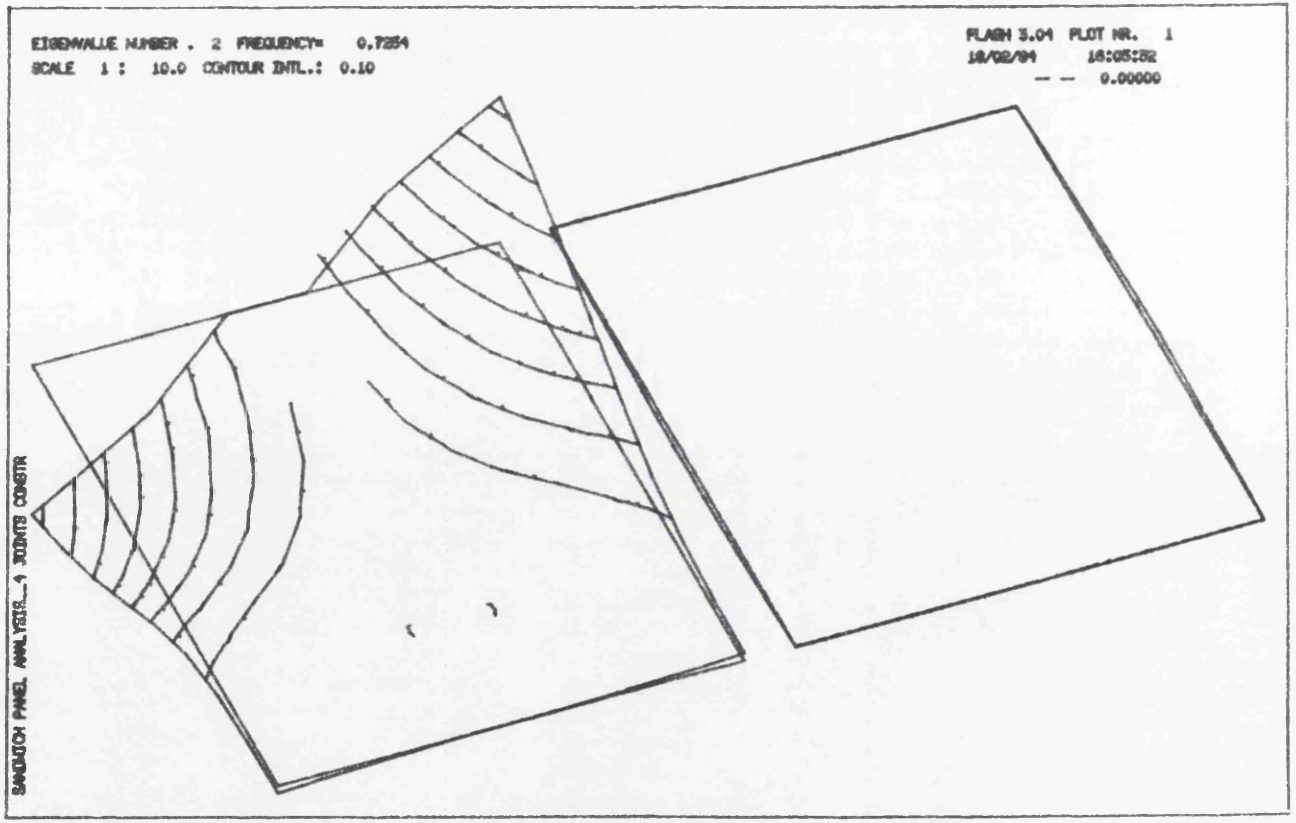

Fig. 3.86: Second modal shape of numerical model GK-84.

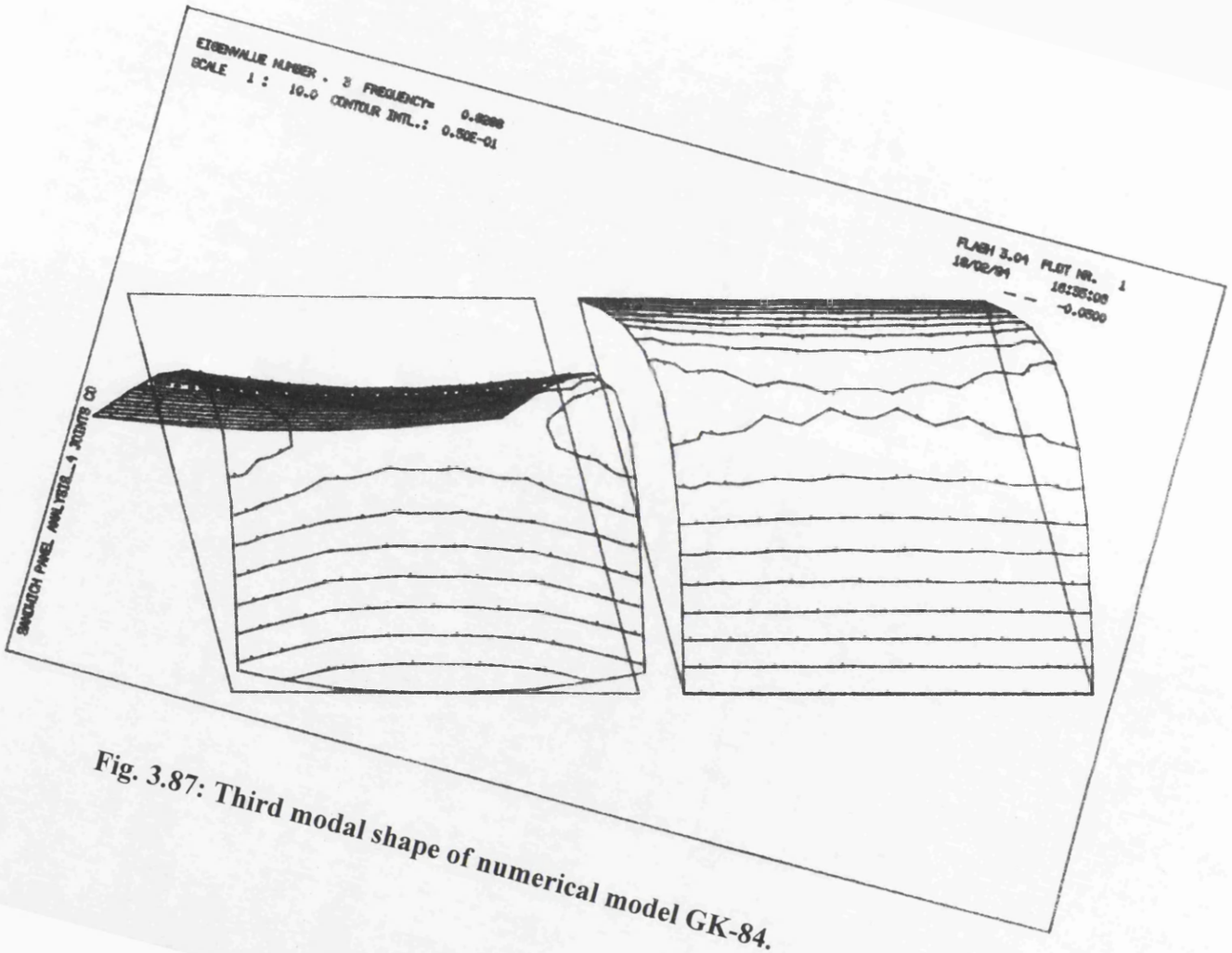

Fig. 3.87: Third modal shape of numerical model GK-84.

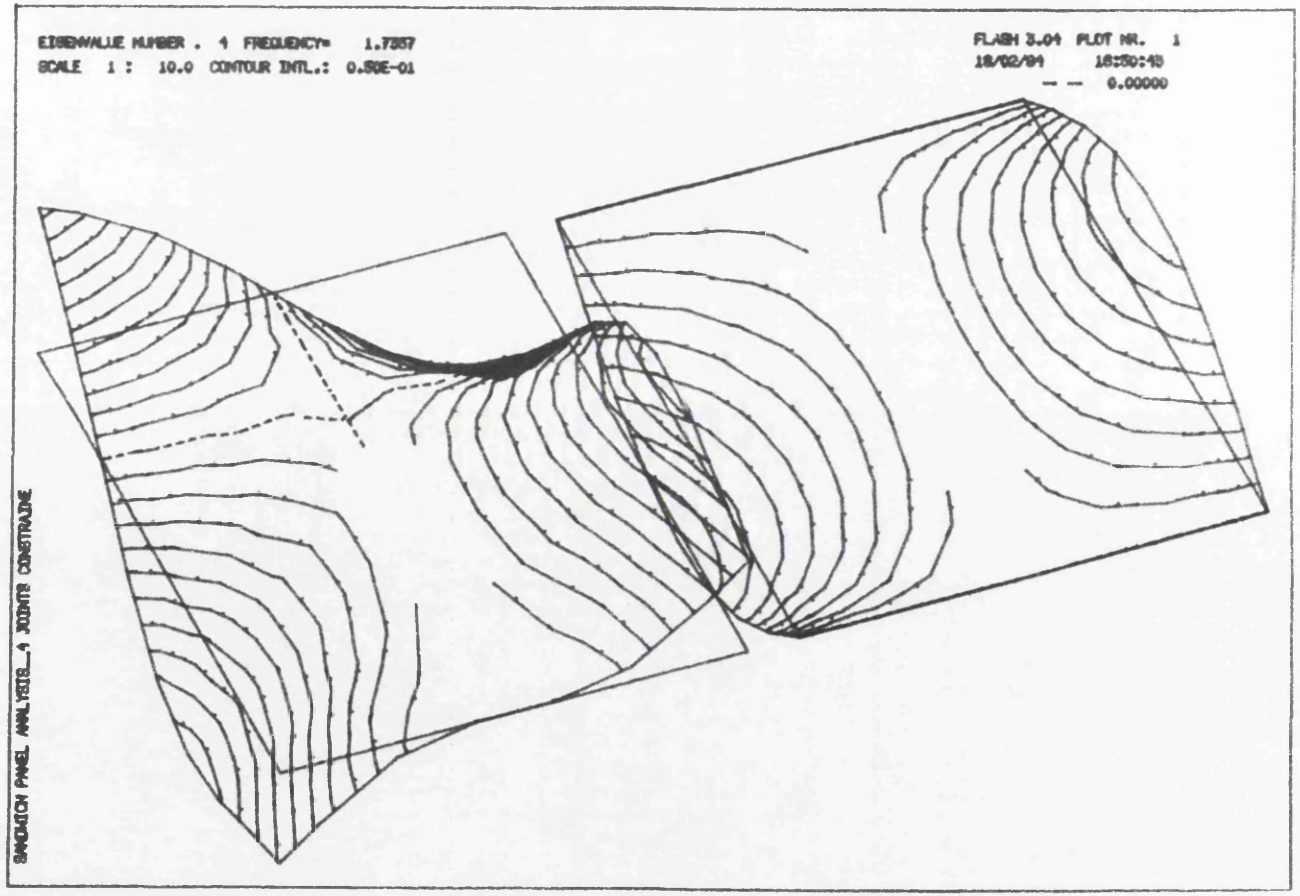

Fig. 3.88: Fourth modal shape of numerical model GK-84.

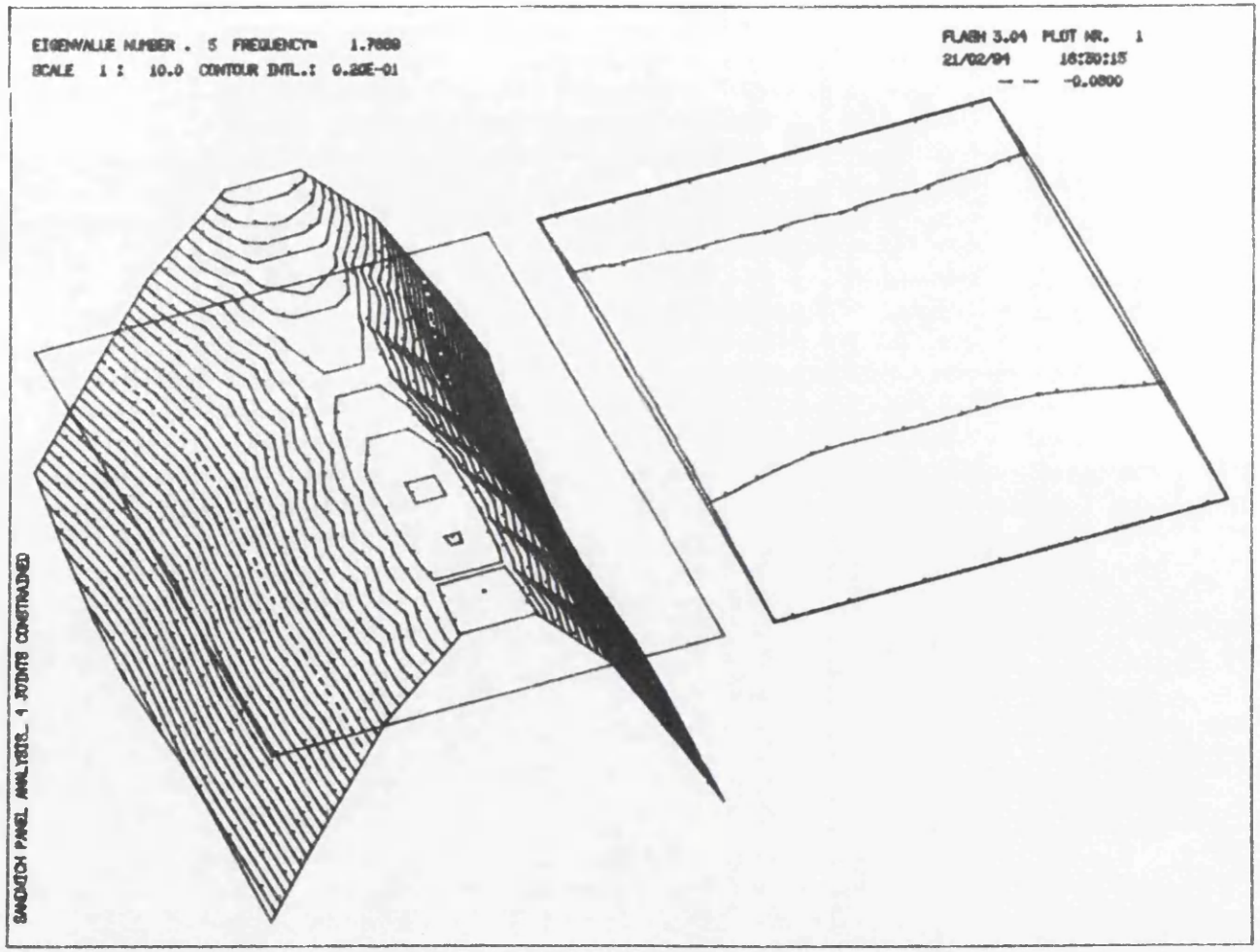

Fig. 3.89: Fifth modal shape of numerical model GK-84.

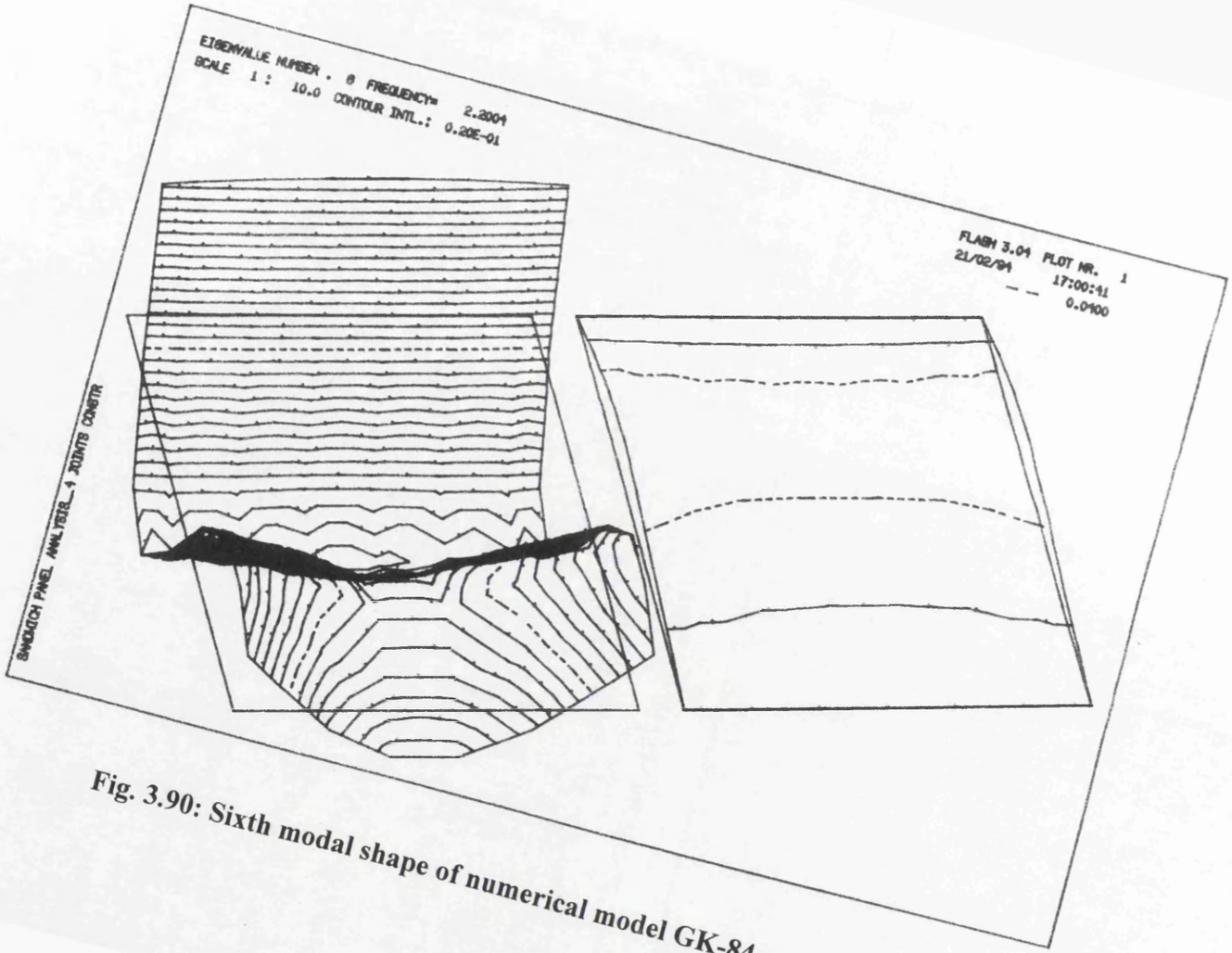

Fig. 3.90: Sixth modal shape of numerical model GK-84.

CHAPTER 4

EXCITATION TECHNIQUES AND EXPERIMENTAL PROGRAMME

This chapter deals with the various excitation techniques that can be employed for modal testing. An introduction is given into the methods of dynamic testing and the associated hardware that is required for performing a dynamic test. Also discussed are the details of the experimental program carried out during this present research. The experimental specimens are discussed and their geometric and material properties are described. Also included is a description of panel casting and a description of the instrumentation used and the details of the test set-up.

4.1 INTRODUCTION

The theoretical analysis of free and forced vibration of undamped and damped multi-degree of freedom systems requires the determination of mass, stiffness and the damping matrices, and from these the response can be obtained in terms of the modal parameters. To provide experimental validation of the theoretical models the inverse of this process has to be performed, that is, to deduce the matrices from the vibration. However, these quantities cannot be directly measured and have to be deduced from measurable quantities, such as the natural frequencies, dampings of the system and the mode shapes. Whenever a continuous structure is to be tested it is important to assume that it is composed of a finite number of degrees-of-

freedom, then each of these can be examined individually, as each degree-of-freedom corresponds to a natural frequency and a mode shape.

As an example, consider a simple free-free beam (Fig. 4.1), and consider it has only the first three degrees-of-freedom. In order to determine the total vibration of the beam, it must be excited at some point and the resulting vibration measured at several points on the beam. If this time domain information is transferred to the frequency domain, the frequency response curves obtained at the three points would be as shown in Fig. 4.1. As can be observed, the sharp peaks (resonances) occur at the same frequency, independent of where they are measured on the beam. The only difference, as we move from point to point, is the relative height of the resonances. From such a response curve the magnitude of the frequency gives the magnitude of the mode shape, whilst the phase information (not indicated) gives the direction of the deflection.

Fig. 4.2 shows the frequency response curves obtained from several accelerometer locations on the beam. By connecting the peaks of the resonances of a given mode, and taking the phase into account, the mode shape at each resonance frequency can be traced out. Along the distance axis a combined frequency response curve is obtained, while the view along the frequency axis shows the three mode shapes, and is generally referred to as the modal domain view. Similar to any wave form that can be expressed as a sum of simple sine waves, a vibration can be represented as a sum of principal modes, and the total vibration envelope as a sum of the three modes can be seen in Fig. 4.2.

To determine the mode shapes, one can either excite the structures at the resonance frequencies and measure the structural deformation in each vibration mode, or they

can be deduced from the frequency responses measured at various points on the structure. While normally sinusoidal excitation is used for the former method, wide band excitation can be used for the latter. These two methods can be further sub-divided into two categories:

i) single shaker techniques, and
ii) multiple shaker techniques, generally required for the excitation of larger structures.

The simplest and most commonly used technique is the "peak amplitude" method, in which the structure is excited by a sinusoidal force from a single shaker and the "response curves" of total amplitude, obtained at several points on the structure, are recorded as a function of frequency. The required information can then be extracted from these curves. This method has certain deficiencies, in that not enough is measured, and what is measured is displayed unsatisfactorily. An alternative method is to use the vector response plot (Kennedy and Pancu [43]) for estimation of damping and the natural frequencies. The mode shapes obtained with this method, using a single shaker, will generally, be better than those obtained with the peak amplitude method.

With the advent of the two channel real time FFT-analysers, measurement of response to wide band excitation signals (in contrast to the traditional sinusoidal excitation) has been made possible. In this particular method/technique, the frequency response function of a structure is measured at a single point, due to impulse excitation at various points on the structure, or the structure can be excited at a single point using various forms of wide band random signals, and the frequency response function measured at several points. The modal parameters can

then be extracted from the measured data in both the time and the frequency domain.

Since the accuracy of the modal parameters depends on how precisely the frequency response function matrix can be measured, a great deal of consideration should be give to exciting the structure adequately, in order to maintain the vibration amplitudes as close as possible to the operating levels in all areas of interest. This is relatively easy in simple structures and individual components which can be excited evenly. However, in the case of larger structures and other large assemblies with numerous joints, vibration energy is quickly dissipated within the structure, producing widely different vibration amplitudes at various locations. Additionally, non-proportional damping, non-linear effects and closely spaced modes are often encountered in large structures, which not only impede the process of locating the frequencies at which to identify the modes, but also the mode shapes based on one exciter position may not agree with those based on another exciter position. Some of these difficulties can be eliminated through the use of multi-point excitation, by which a larger amount of energy can be fed more uniformly into the structure than with the single point excitation.

The testing of large structures is generally carried out in two steps: In the first step the number of modes and their resonant frequencies are roughly established using single shaker sweeps. The presence of modes are indicated by resonant phenomena and phase shifts in the response, and can sometimes be difficult to detect when modes have similar shapes and natural frequencies. Once the existence of a mode has been established, the second step involves isolation of the mode. This is achieved by distributing the available number of shakers around the structure, and adjusting the amplitudes of the mono-phase forces on the shakers, such that only

the mode of interest is dominantly excited in that particular frequency range. The structure thus responds predominantly in the principal mode as a single degree of freedom system, and the modal parameters can than be easily calculated. The accuracy of the results is governed by the number of shakers and their location.

4.2 SINGLE EXCITER TECHNIQUES

A dynamic test mainly involves quantitative measure of the effect of a vibratory force on a structure. If the structure is linear and elastic and excited by a sinusoidal force, the resulting vibratory motion (response) is directly proportional to the exciting force and at the same frequency. Measurement of the exciting force and the resulting motion at a number of points over a range of frequencies would be sufficient to describe the vibratory behaviour of the structure.

Fig. 4.3 shows an instrumentation set-up used for obtaining a response curve in which the vibration exciter is fed with a certain amount of power at a slowly changing frequency. Due to resonances in the test specimen and the vibration exciter, the power necessary to subject the test specimen to a constant force level will not, however, remain constant during the test, but will be a function of frequency. To keep the force level constant a servo-loop could be used, in which the output from the force transducer, mounted between the shaker and the specimen, is fed back to the exciter control via a preamplifier. The output from the accelerometer mounted on the specimen could be fed to an X-Y recorder which traces out a response curve as the frequency is scanned. The response should be measured at enough points on the structure to ensure that all modes will display

their resonant characteristics in the response curve of at least one of the points (this is the most commonly used method of carrying out a resonance test).

Fig. 4.4 shows a typical point inertance curve plotted on linear scales of a free-free beam excited at a constant force, as shown. The first piece of information that can be extracted from an amplitude response curve is the natural frequencies of the specimen, which are usually identified as the frequencies where peaks are attained. It has been shown, however, (Bishop and Gladwell [44]) that theoretically the peaks do not occur exactly at the natural frequencies but at a frequency displaced slightly on one or the other side of them. This is partly due to the damping which couples the modes and partly due to the contribution from the other off-resonant modes at that frequency. The latter contribution will still be there, even if the damping does not couple the motion in the principal modes. However, if the system is lightly damped and the natural frequencies are widely spaced, these errors would be relatively small compared to the experimental errors involved in locating the peaks.

The second piece of information that can be extracted from a response curve is the amount of damping in a particular mode. Damping is determined from the sharpness of the peak (Fig. 4.4b), and is normally measured in terms of the loss factor η, given by

$$\eta = \frac{\omega_2 - \omega_1}{\omega_0}$$

where ω_0 is the natural frequency and ω_1 and ω_2 are frequencies on either side of the natural frequency where the peak amplitude is reduced by a factor of $\sqrt{2}$.

4.3 MULTIPLE EXCITER TECHNIQUES

Since a structure, when excited, vibrates in several modes simultaneously, and thus causes difficulties in the analysis of the results, the unwanted modes have to be somehow eliminated. This can be achieved for simple structures by placing the exciters or pick-ups at nodal points of the unwanted modes, or by making use of the symmetrical and anti-symmetrical properties of the mode shapes. In a complex structure, however, this is not always possible, and systematic methods have to be used for exciting the structure with multiple shakers and forcing them to vibrate in their principal modes. However, this requires rather sophisticated equipment both on the excitation side, as well as on the data acquisition side, on account of the large number of pick-ups, necessary for determining the mode shapes.

Fig. 4.5 shows an instrumentation set-up for testing of large structures using multiple shakers. The system is such, that it can be readily expanded to incorporate any number of shakers and accelerometer channels. All the equipment below the structure constitutes the excitation part of the system, while the instrumentation above the structure is used for data acquisition and further processing and analysis of the results.

For sinusoidal excitation of the structure, the principle of operation of this set-up is basically the same as that of Fig. 4.1. However, on account of the multiplicity of shakers and accelerometers, automatic control of the system is imperative, although manual operation is possible. The fundamental requirement on the excitation side is the accurate control of the amplitude and the phase of the force, applied by each shaker to the test structure at a single frequency. On the data

acquisition side, the acceleration signals have to be measured at several points on the structure.

EXPERIMENTAL PROCEDURE

As mentioned earlier, the testing of large structures is carried out in two stages. In the first step the number of modes and their natural frequencies are roughly established using single shaker sweeps. The response should be monitored at several points to ensure that none of the modes is missed out in the frequency range of interest. Once the existence of a mode has been established, the second step involves isolation (tuning) of the mode using multiple shakers. The test is started using a single shaker (placed preferably at an anti-node of the mode to be excited) with an arbitrary force, and the response from an accelerometer placed at the same shaker (or an anti-node) is fed back to the generator. The natural frequency of the mode to be examined is now found by adjusting the frequency of the generator. Force levels on all the shakers are adjusted in a similar way. It will be found that as more and more forces are applied and adjusted, the more uniform in phase are the various points on the structure. Furthermore, the frequency at which the generator was initially set when the force to the first shaker was applied, would have drifted and approached the true natural frequency of the mode being excited. These trends give definite indications that a principal mode is being approached.

Once the correct phase distribution has been obtained, the rest of the structure should be examined for mono-phase response. If the phase scatter around the structure is unacceptably large, repositioning of the shakers and/or monitoring

points of responses should be considered. With the correct force distribution established, a sinusoidal frequency sweep around the natural frequency is very useful in revealing the characteristics of the modes, such as damping.

4.4 VIBRATION INSTRUMENTS

This section deals with the various devices used in a dynamic test for studying the dynamic characteristics of a specimen. The three main devices required are the transducers (accelerometers), the frequency analysers and the tape recorder. the details and the function of each of these is explained below.

4.4.1 ACCELEROMETERS

The first vibration pickups producing an electrical output were rather bulky velocity sensitive devices. During the last decade or so there has been a marked move towards the use of acceleration sensitive transducers, called accelerometers. Reasons for this transfer of preference mainly being that accelerometers are generally much smaller physically than velocity pickups and that their frequency and dynamic ranges are significantly wider, even after integration to velocity. A wider dynamic and frequency range is a prime requirement of the modern vibration pickup. An additional factor which underlines the benefits of accelerometers is the fact that an acceleration signal can be easily and validly integrated electronically to obtain velocity and displacement, whereas electronic

differentiation used with velocity and displacement transducers is a more complex and dubious affair.

An accelerometer is an electromechanical transducer which produces at its output terminals, a voltage or charge that is proportional to the acceleration to which it is subjected. Piezoelectric accelerometers exhibit better all-round characteristics than any other type of vibration transducer and are more or less universally preferred for measurements covering a wide frequency range.

The heart of the accelerometer is its piezoelectric elements which are usually made from an artificially polarised ferroelectric ceramic. These piezoelectric elements have the property of producing an electrical charge which is directly proportional to strain and thus the applied force when loaded either in tension, compression or shear. In practical accelerometer designs the piezoelectric elements are arranged so that they are loaded by a mass or masses and a preloading ring or spring. When subjected to vibration the masses exert a varying force on the piezoelectric elements which is directly proportional to the vibratory acceleration. For frequencies lying well under the resonant frequency of the assembly, the acceleration of the masses will be the same as the acceleration of the base, and the output signal level will be proportional to the acceleration to which the accelerometer is subjected. The two most commonly used accelerometer configurations are the compression and the shear type which are shown in Fig. 4.6.

4.4.2 TAPE RECORDERS

It is often more convenient to record vibration signals on magnetic tape for later analysis in the laboratory rather than making on-the-spot frequency analysis in the

field. This is especially the case when analysing transient vibrations, shocks and continuous signals. By playing the tape at higher speed, very low frequency signals can be brought into the frequency range of ordinary frequency analysers and analysis time can also be reduced. Since the tape recorder is likely to be the most limiting factor in determining the dynamic range of the system, it is important to choose the parameter of recording (acceleration or velocity) which has the flattest spectrum, regardless of which is to be used for final evaluation. Conversion between the parameters is straight forward once a narrow band spectral analysis has been carried out. It is necessary and convenient to precede each input channel of the tape recorder with a signal amplification device. A wide choice of high and low pass filters can be selected so that unwanted signals, noise, etc. can be prevented from influencing the measurements.

4.4.3 FREQUENCY ANALYZERS

Mainly two types of frequency analysers are used for frequency analysis of vibration signals. The two types most commonly used are the serial analysers and real-time analysers. The serial analysers may be synchronised with, and read out to, level or X-Y recorders. Real-time analysers provide analysis on all frequency bands simultaneously giving a virtually instantaneous graphical display of frequency spectra on a built-in screen or read out to a graphic recorder. As only the real time analysers were used in the frequency analysis, so we shall be limiting our discussion to them.

The most outstanding feature of a real-time frequency analyser is that it provides analysis in all frequency bands over their entire analysis range simultaneously.

The most outstanding feature of a real-time frequency analyser is that it provides analysis in all frequency bands over their entire analysis range simultaneously. Furthermore, as they give a virtually instantaneous graphical display of analysed spectra, which is continuously updated, dynamic and spectral changes which occur when increasing vibration test levels can thus be seen as they actually happen. Similarly, the time saved in not having to wait for a level or X-Y recorder readout is considerable.

Real-time analysers are also particularly well suited for analysis of short duration signals, such as transient vibration shock. Readout and display of analysed transient and shock spectra takes place practically at the very instant of capture. In addition, real-time analysers can store analysed spectra for alternate display with later incoming data.

4.5 EXPERIMENTAL PROGRAMME

The experimental programme consisted of the testing of eleven reinforced concrete, precast, sandwich wall panels. All panels had similar nominal dimensions, and were 1800mm wide by 2400mm high. The variations in the different specimens mainly concerned the type of structural connection and the constraints present between the inner load bearing skin and the outer cladding skin.

The test specimens were tested for their dynamic characteristics, principally their natural frequencies and associated modal shapes. The specimens were tested in an upright position, with the inner load bearing skin being subjected to an in-plane compressive load and being simply supported along the top and bottom edge. The

was measured by means of piezo-electric transducers (accelerometers), which was stored on tape for permanent records. This was then passed through an FFT spectrum analyser to determine the frequency content. From this frequency content the natural frequencies related to the different modal shapes were detected. The details of the instrumentation and the experimental procedure are presented in articles 4.7 and 4.8.

4.6 TEST SPECIMENS

The basic specimen under investigation was a sandwich panel consisting of two skins of reinforced concrete. The inner load bearing concrete skin being 100mm thick and reinforced with 8mm diameter bars @ 200mm c/c both directions, while the outer cladding concrete skin was 50mm thick, and had a reinforcement mesh similar to the inner load bearing skin. The two concrete skins were separated from each other through a 25mm thick layer of polystyrene. The details of this basic specimen are provided in Fig. 4.7.

The eleven experimental specimens tested for their dynamic characteristics were divided into three basic categories based upon the structural connection present between the inner load bearing skin and outer cladding skin. The structural and the constructional details of these specimens are explained herein.

4.6.1 TEST SPECIMENS GK-1, 2, 3

The first batch considered for testing consisted of three specimens, the details of which can be seen in Figs. 4.8-4.10. The basic specimen in this category consisted

of the basic sandwich panel as described above. Test specimen GK-1 had a structural connection between the two concrete skins all around the perimeter over a width of 200mm. The connection was such that in addition to the concrete providing continuity around the perimeter, the reinforcement mesh from both skins was extended through into each other (Figs. 4.8-4.10). This was the only structural connection present between the two concrete skins. For the test specimen GK-2, in addition to this connection , an additional constraint between the two concrete skins was provided at the central point. The test specimen GK-3 was again similar to the first two specimens in terms of the concrete perimeter connection but additionally, the specimen had four more points, located symmetrically within the specimen, which structurally connected the two concrete skins, and thus provided a stiffer constraint. The details of these specimens can be found in Table 4.1. As the same basic specimen GK-1 was used for the remaining two in this batch, the additional structural constraints were provided through two bolts for each constraint, which were locked into the two faces, thus providing restraint against compressive as well as tensile forces. A similar approach was used for the second batch of experimental specimens.

4.6.1.1 CASTING OPERATION

Details of the form work used can be seen in Fig 4.11. The casting operation initially consisted of casting the 100mm thick inner skin, with it's mesh of reinforcement placed mid depth. A pre-mix concrete of 35MPa strength was used for all casting operations. Once the inner skin had been cast and vibrated using immersion vibrators, then on the still wet concrete, a 25mm thick sheet of polystyrene was placed, and then the 50mm thick cladding skin with it's mesh of

reinforcement was cast on top of it. Finally, the face of the top skin was floated to give it a smooth surface. The specimen was eventually covered with wet hessian and a plastic sheet. It was cured in the mould for fourteen days before being lifted out and air cured until the time of testing. The details of the casting operation are presented in Figs. 4.12 and 4.13.

4.6.2 TEST SPECIMENS GK-4, 5, 6

Like the initial batch, the second one also consisted of three specimens. The geometric and reinforcement details of the three specimens is shown in Figs. 4.14-4.16. The basic specimen, being similar to GK-1, 2, 3, consisted of the same skins, reinforcement and polystyrene separation layer but had a concrete connection around three edges of the perimeter over a width of 50mm only, with one 2400mm edge remaining free. Test specimen GK-4, like GK-1, only had this connection between the two concrete "skins", as the structural connection. Similarly, as for specimens GK-2, 3, the test specimens GK-5, 6 in addition to the concrete being continuous over a width of 50mm around three edges of the perimeter, were further connected at one and four points respectively, through the use of steel bolts. The location of these was the same as for test specimens GK-2, 3. The details of these specimens can be found in Table 4.1 as well.

4.6.2.1 CASTING OPERATION

The details of the casting for these three specimens were identical to those for the test specimens GK-1, 2 ,3. Compared to the first three test specimens, in which case, the polystyrene sheet stopped 200mm short of the edge around all four edges,

to enable continuity of concrete around the perimeter, in this case the polystyrene was extended up to 50mm of the edges on three sides and right up to the edge on one 2400mm side. Then the concrete cladding skin was cast on top of it, thus completing the casting operation of the sandwich panel having a concrete continuity over a width of 50mm around three edges of the perimeter. The specimens were cured in a manner similar to the first three and had similar material properties. Details of the casting operation can be seen from Figs. 4.17 and 4.18.

4.6.3 TEST SPECIMENS GK-88, 87, 86, 85, 84

The third and final batch of sandwich wall panels, consisted of five specimens. The sandwich wall panel again had overall dimensions of 1800mm wide and 2400mm high. The two skins of the sandwich panel were, as previously, 100mm and 50mm thick respectively. This batch of test specimens differed from the two previous batches, in that the two skins, did not have a separating layer of polystyrene between them. Also there was no continuity between the two skins, around the perimeter for this batch. The structural connection between the two skins was provided through a number of reinforcement "ties", varying from eight for GK-88 through to four for GK-84. The details for the placement of these ties as well as the cross-sectional and reinforcement details of these specimens are shown in Figs. 4.19 through 4.23.

4.6.3.1 CASTING OPERATION

The basic casting operation of these five test specimens was fairly similar to that of the previous two batches. The specimen was cast face-up, with the inner load

bearing skin, 100mm thick, with it's mesh of reinforcement being cast first. Unlike the first two batches, there was no concrete continuation around the perimeter between the two skins. For specimen GK-88, the inner load bearing concrete skin was cast with the eight reinforcement ties placed at pre-determined locations as indicated in Fig. 4.19. These ties were to provide the only structural connection between the two skins. Once the inner load bearing skin had been cast it was allowed to harden and cure for some time. The concrete surface was then covered with a 100mm thick layer of sand, covered with a polythene sheet, and then the outer cladding skin with it's mesh of reinforcement was cast. The eight connecting ties from the bottom concrete layer were embedded 30mm into the concrete of the top layer. Both concrete layers were cast using a premix concrete of 35MPa strength. The specimen was further cured for seven days after which it was lifted out of the form work and the sand allowed to flow out from between the two concrete layers. The same specimen was used for the remaining four specimens of this particular batch, with the connecting "ties" being cut off successively. The details of the casting operation can be seen in Figs. 4.24 and 4.25.

4.7 SPECIMEN PREPARATION, INSTRUMENTATION AND EXPERIMENTAL SET-UP

All eleven test specimens were tested in an upright position and were simply supported along the top and bottom 1800mm edge. The 100mm thick load bearing concrete skin was supported over a 100mm square, steel hollow box-section, to ensure that the applied in-plane loads were transferred through it alone (Fig. 4.20).This was done to duplicate the actual site conditions, where only the inner

panels would be subjected to any structural loads, except for the wind loads which acted upon the outer cladding. The surface instrumentation on the specimen consisted of Demec points placed along the width of the specimen on both faces, to measure the magnitude of the in-plane load. Piezoelectric accelerometers were also located on the surface at pre-determined locations, to measure the dynamic response of the test specimen. The details of the locations of these accelerometers as well as the Demec points are shown in Figs. 4.27-4.29, for all eleven test specimens.

Besides the instrumentation on the specimen surface, the test set-up involved the use of excitation devices, recording instruments and an R.T.A. (real time analyser), the details of which have already been discussed.

The test set-up comprised of the sandwich panel being placed in a 10,000kN Universal Testing Machine as shown in Fig. 4.30. The panel was supported along one of its 1800mm edges on a 100mm square, hollow box-section. A similar 100mm square, hollow box-section was placed along the top 1800mm edge of the specimen as well (Fig. 4.30). The in-plane compressive loads were applied through the lowering down of the top platen of the Universal Testing Machine, to which a steel I-section was attached, to ensure the uniform application of the loads along the entire width of the test specimen.

The dynamic characteristics of the specimens were determined, when under the influenece of these in-plane compressive loads. The dynamic input was provided by two means. The first of these involved the use of an electro-magnetic sinusoidal vibrator, while the second approach was to excite the specimen was through the impact of a hammer blow.

Fig. 4.30 also shows the assembly used for holding the vibrator alongside the wall panel, in such a position, so that the vibrations could be imparted to the wall panel at it's central point. This assembly, basically consisted of a steel section, on to which the vibrator and its supporting assembly were bolted. the steel section itself, was made to rest on the base plate of the testing rig, and was clamped rigidly on to the threaded columns of the testing machine at three locations. This was done to ensure that the natural frequencies of the steel section were much higher than the applied vibration frequencies, to eliminate resonance occurring between the vibrator and it's supporting assembly.

Two variations of the hammer were used initially. The first method consisted of using a hand held hammer and striking the specimen at pre-determined locations. The hammer had a plastic head and a contact area of $50mm^2$ The second approach was to attach the hammer onto the specimen and let it free fall as a pendulum through an arc of ninety degrees. The hammer was fabricated, insuring that the hammer head was similar to the one used initially. The hammer shank had a length of 1.2 meters and was used with variable mass. The advantage of such an assembly was the controlled input of force used to excite the specimen. The details of the arrangement are described in Fig. 4.31.

4.8 TESTING PROCEDURE

The experimentation itself, consisted of applying a 500kN in-plane compressive load to the specimen in conjunction with a vibratory load, through either the electro-magnetic sinusoidal vibrator or the impact of a hammer blow. When using

the sinusoidal vibrator, the specimen was vibrated at different frequencies, while maintaining the location of the vibrator. In comparison the force of impact of the hammer blow was varied and different locations were chosen, the details of which can be found in Fig. 4.32. The response of the two concrete skins, obtained from the accelerometers located on both faces was permanently stored, for future analysis on a tape recorder. The accelerometers were attached to the surface of the panel through the use of threaded bolts. The location of the accelerometers can be seen from Figs. 4.28 and 4.29. The signals from these accelerometers were passed through a high impedance micro dot cable which was reduced to a low impedance cable by using a voltage amplifier, before being fed into the tape recorder. The reason for the impedance transfer was the longer length of cables required, and the necessity to reduce the loss of signal power.

As only a limited number of accelerometers were available to measure the response of the specimen, therefore they were moved around successively through their different locations until the response for every point was obtained and recorded for one impact location. This was achieved by first having the accelerometers at the five designated locations, such as A1-A5, and impacting at point I1. Once the output from these five points was obtained, the accelerometers were then moved to positions B1-B5, while the point of impact was kept at location I1 and the resulting response was observed. This process was repeated and the response from all accelerometer locations was obtained for the one impact location. A similar procedure was adopted for each of the pre-determined points of impact. Finally, these recordings of the accelerometer output signals were then passed through an attenuator and an amplifier and displayed on the real time analyser for their frequency content.

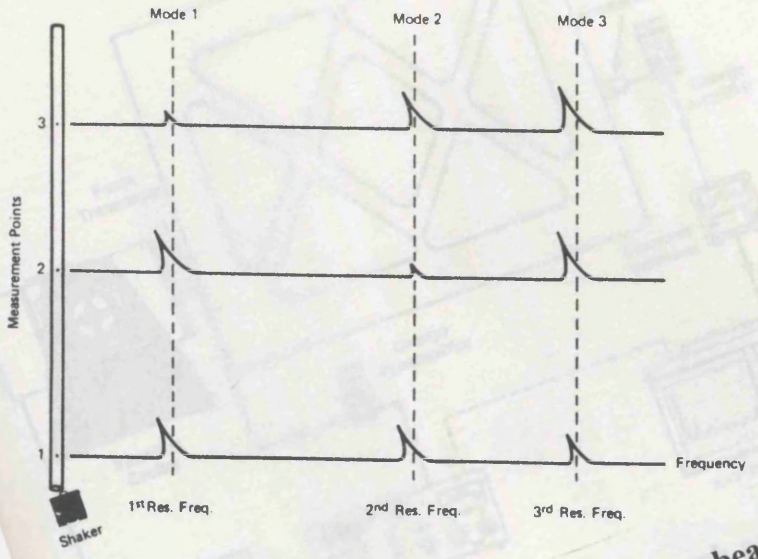

Fig. 4.1: Frequency response of a free-free-beam.

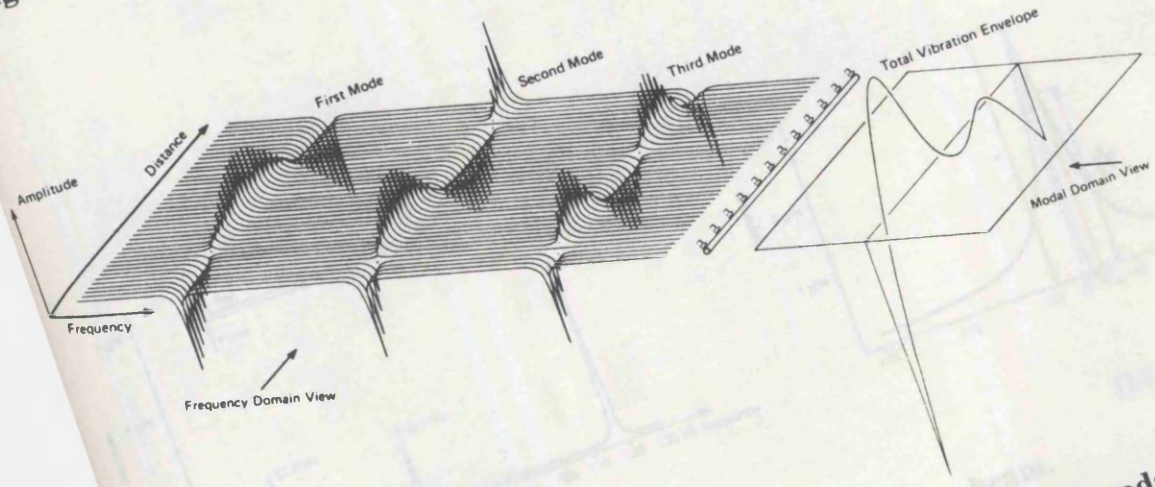

Fig. 4.2: Three dimensional view showing the frequency and modal domain.

(source: "Modal Analysis of Large Structures", by K. Zaveri, Bruel & Kjaer, 1984)

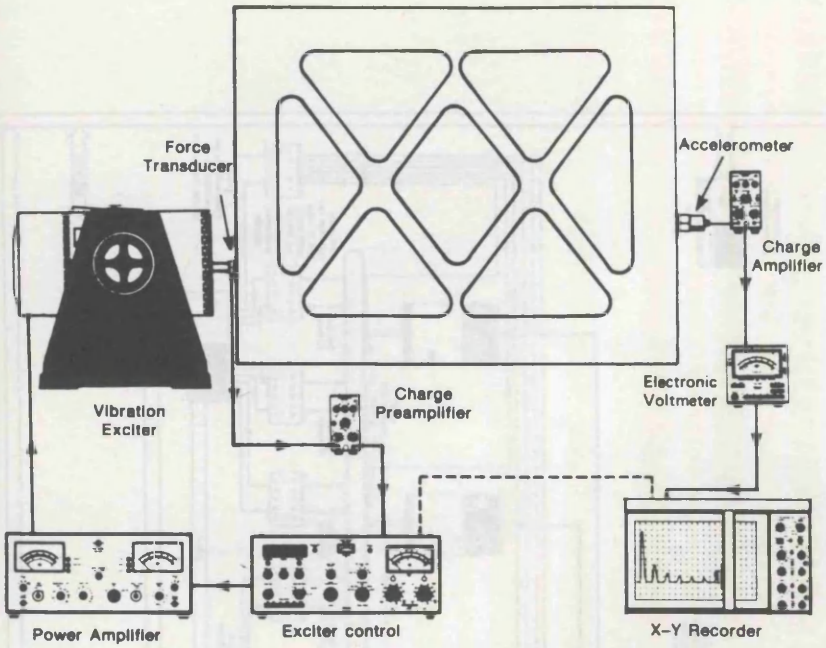

Fig. 4.3: Instrumentation set-up for the peak amplitude method.

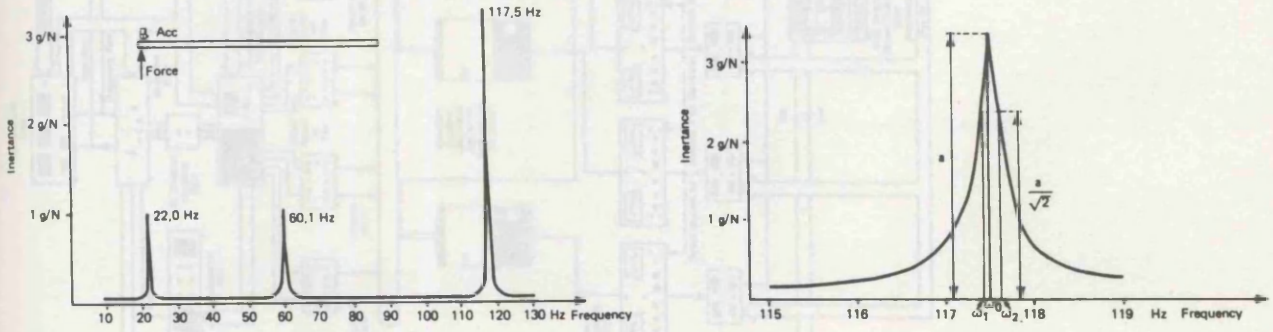

(a) **(b)**

Fig. 4.4: (a) Point inertance curve for a free-free-beam.
(b) Third resonance plotted on an enlarged scale.

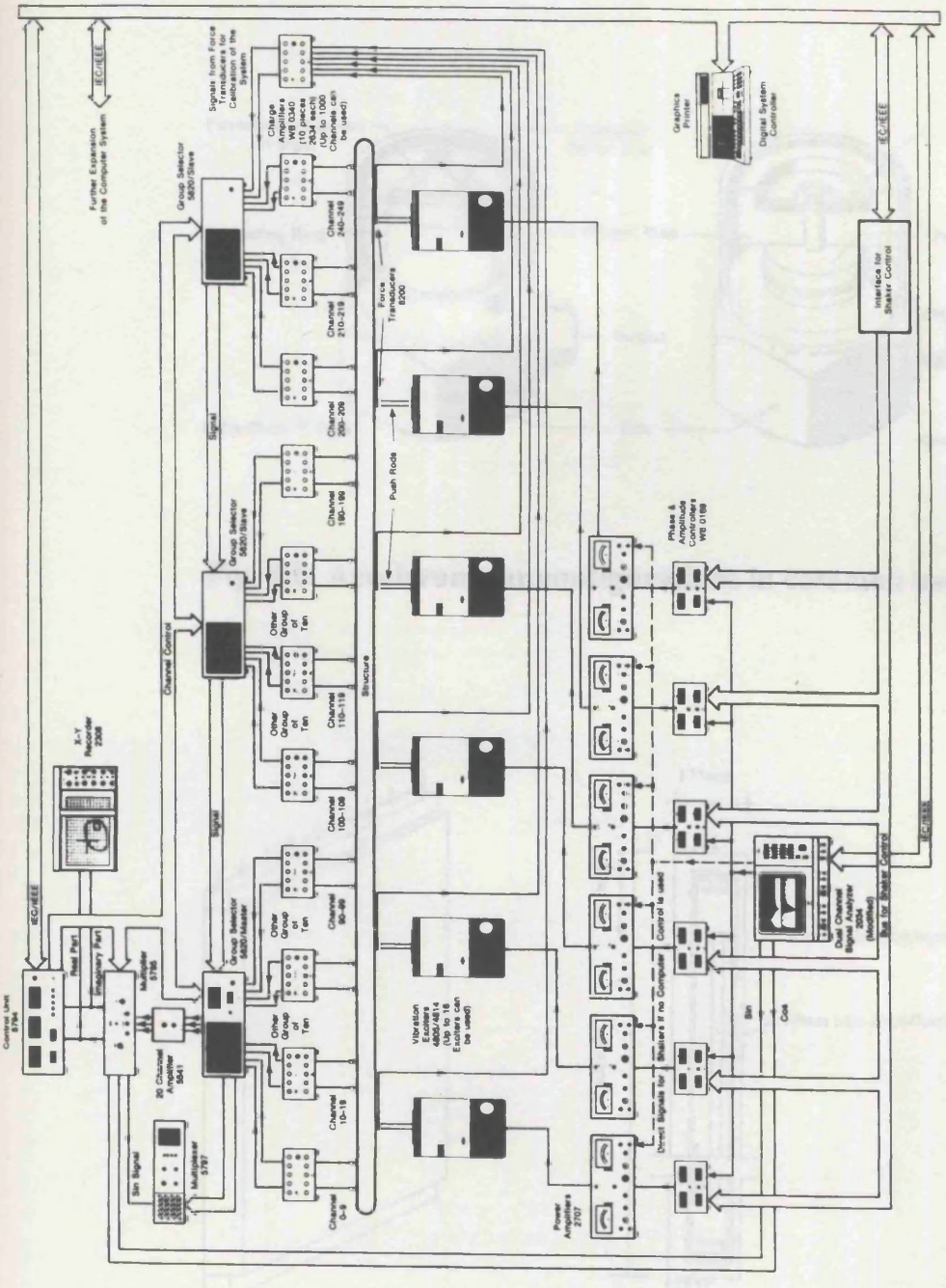

Fig. 4.5: Instrumentation set-up for testing of large structures.

(source: "Modal Analysis of Large Structures", by K. Zaveri, Bruel & Kjaer, 1984)

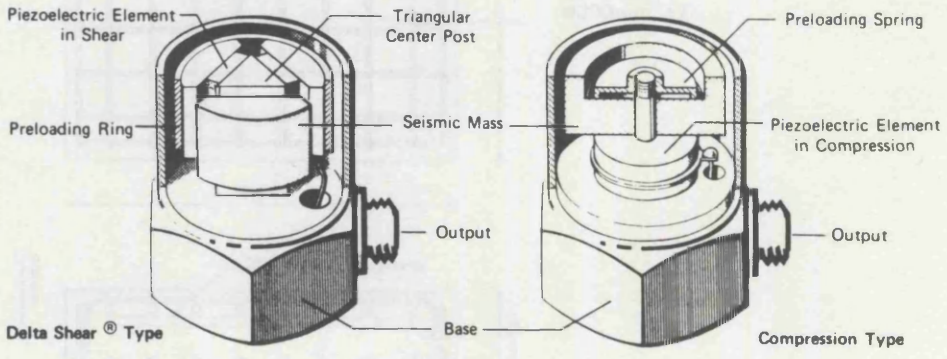

Fig. 4.6: Accelerometer configurations in common use.

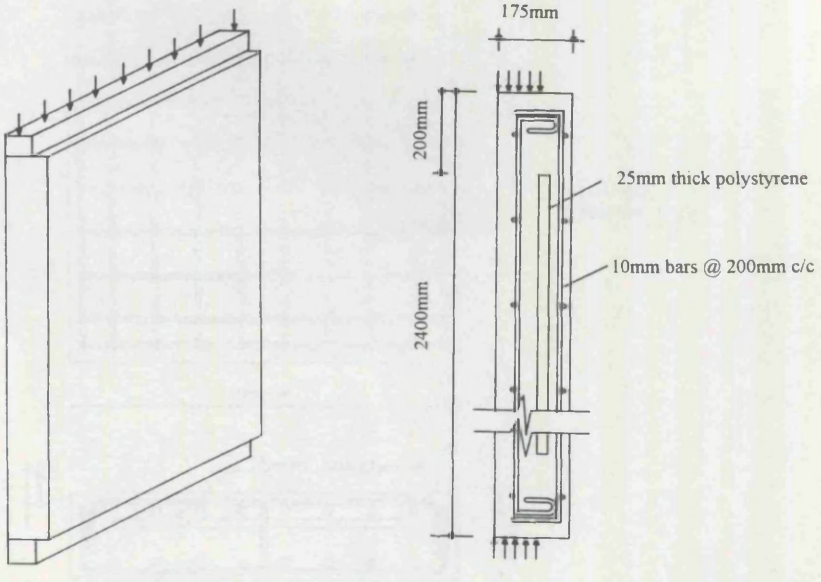

Fig. 4.7: Details of the basic test specimen.

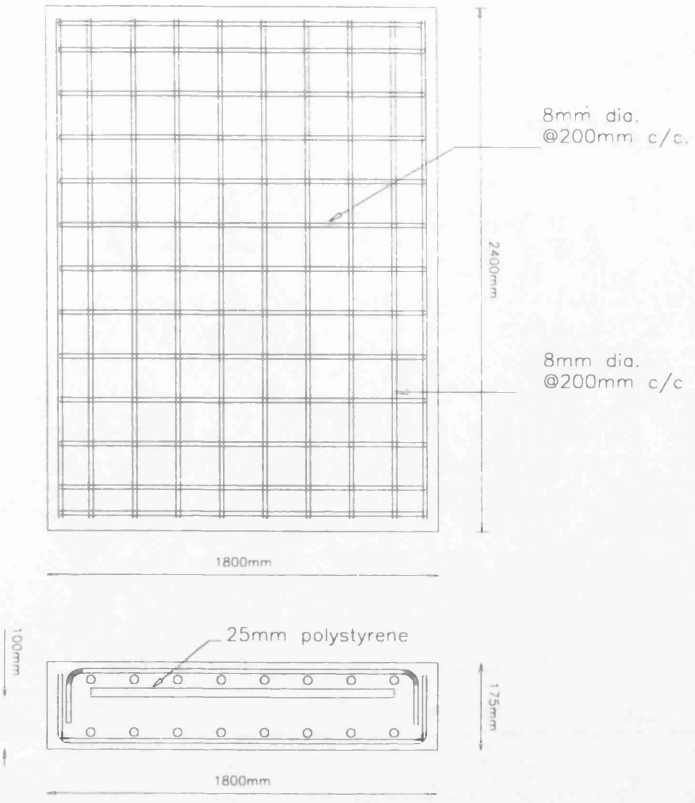

Fig. 4.8: Details of test specimen GK-1.

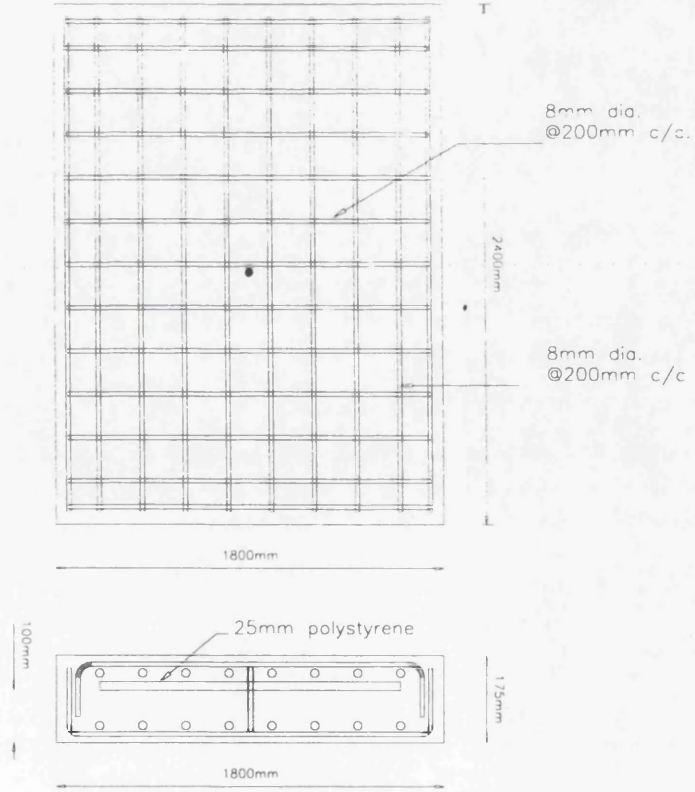

Fig. 4.9: Details of test specimen GK-2.

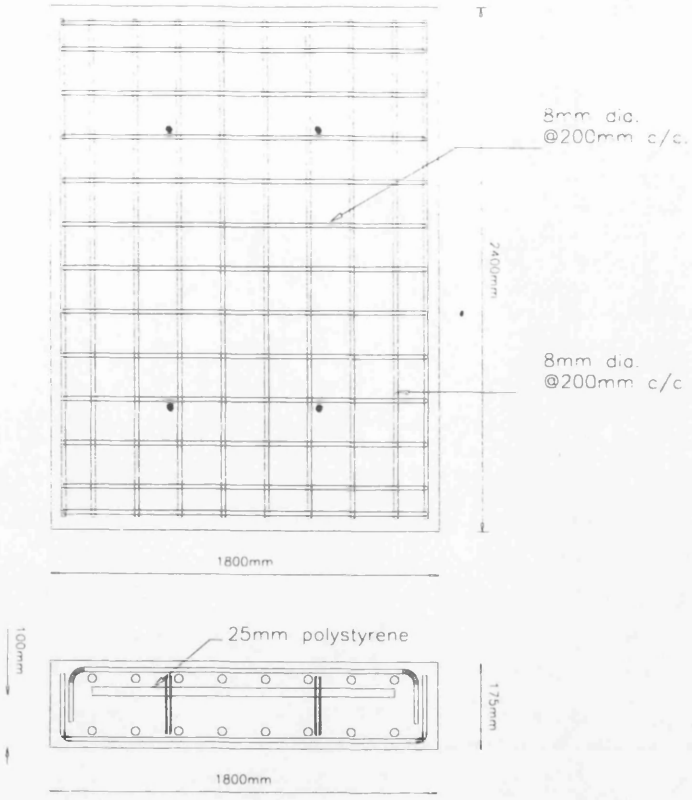

Fig. 4.10: Details of test specimen GK-3.

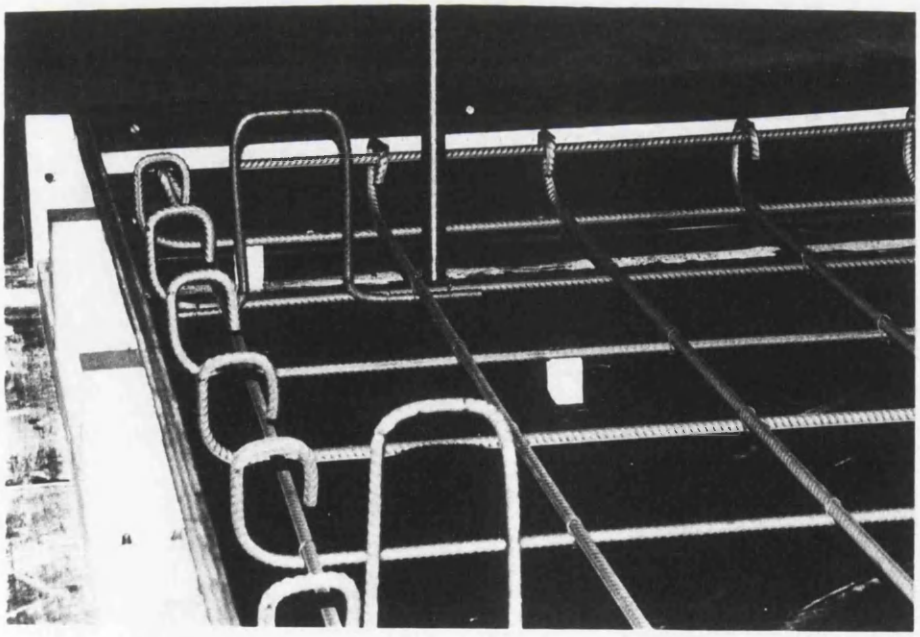

Fig. 4.11: Details of the form work and reinforcement of test specimens.

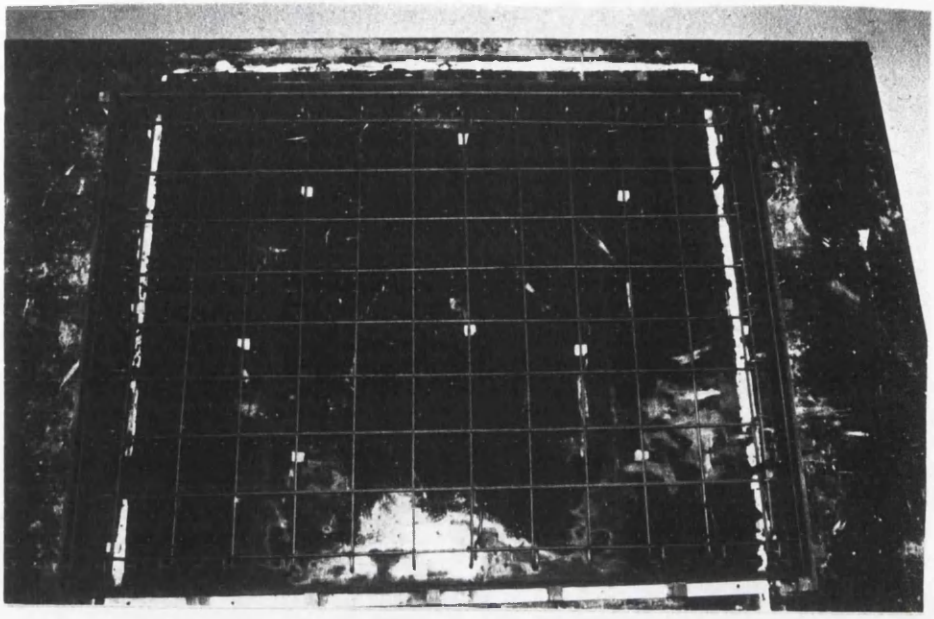

Fig. 4.12: Details of casting operation for GK-1, 2, 3.

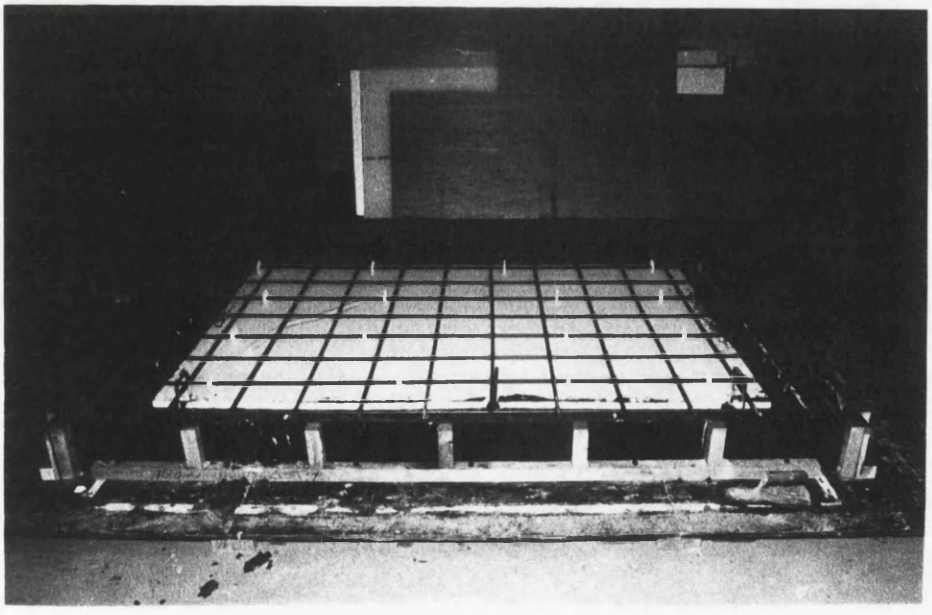

Fig. 4.13: Details of casting operation for GK-1, 2, 3.

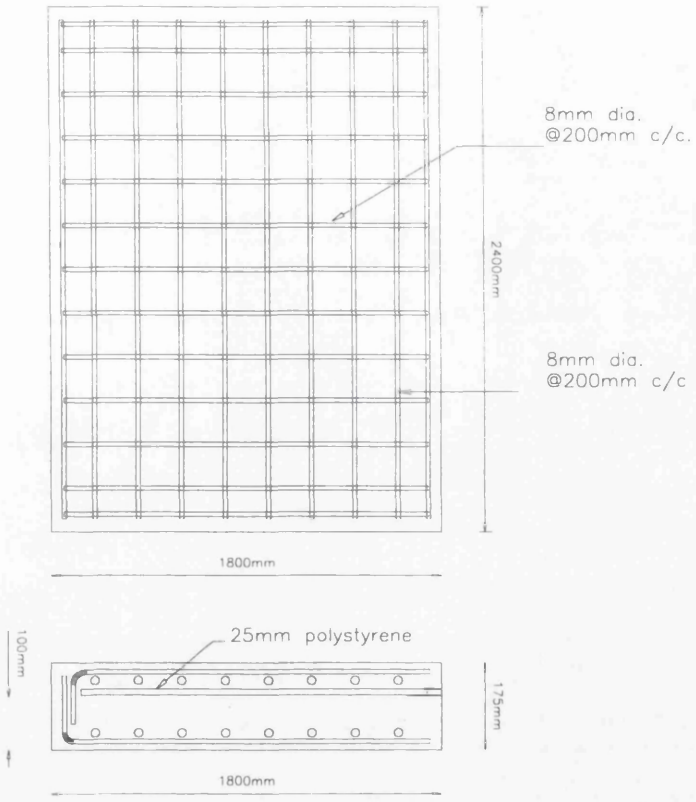

Fig. 4.14: Details of test specimen GK-4.

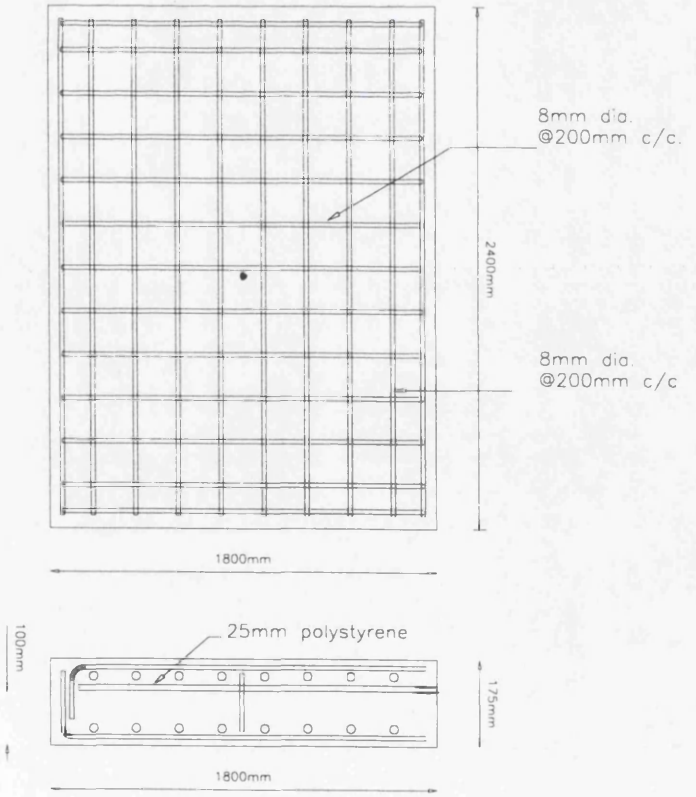

Fig. 4.15: Details of test specimen GK-5.

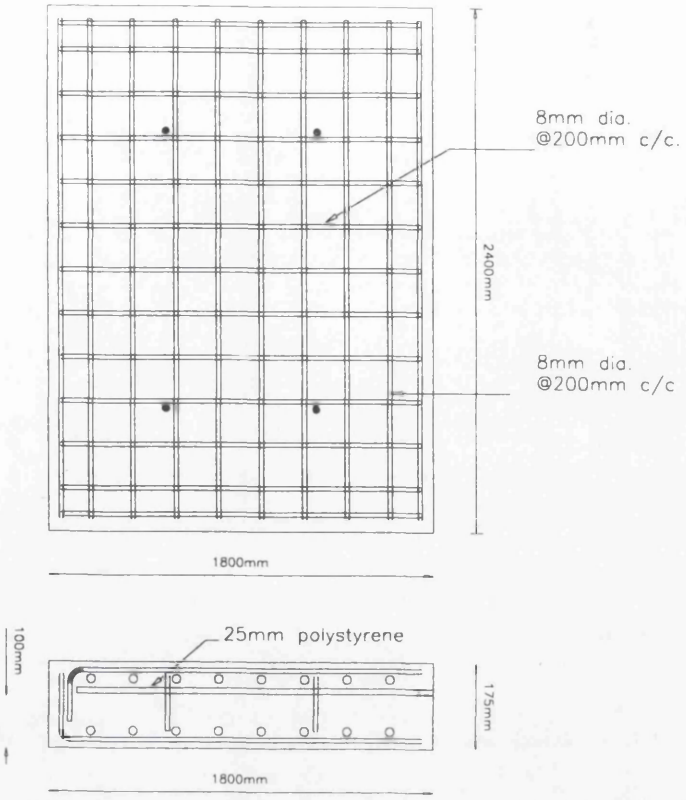

Fig. 4.16: Details of test specimen GK-6.

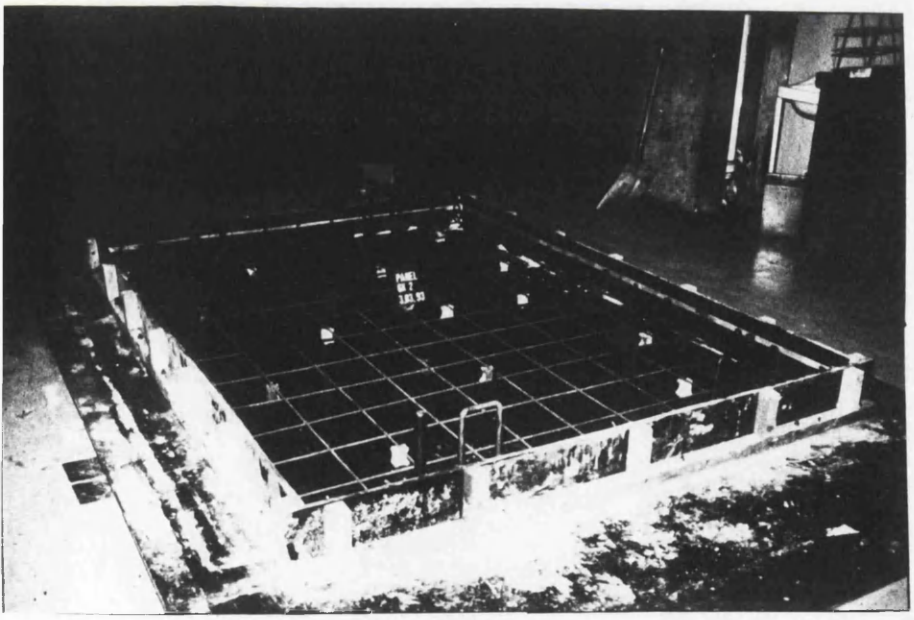

Fig. 4.17: Details of the casting operation for GK-4, 5, 6.

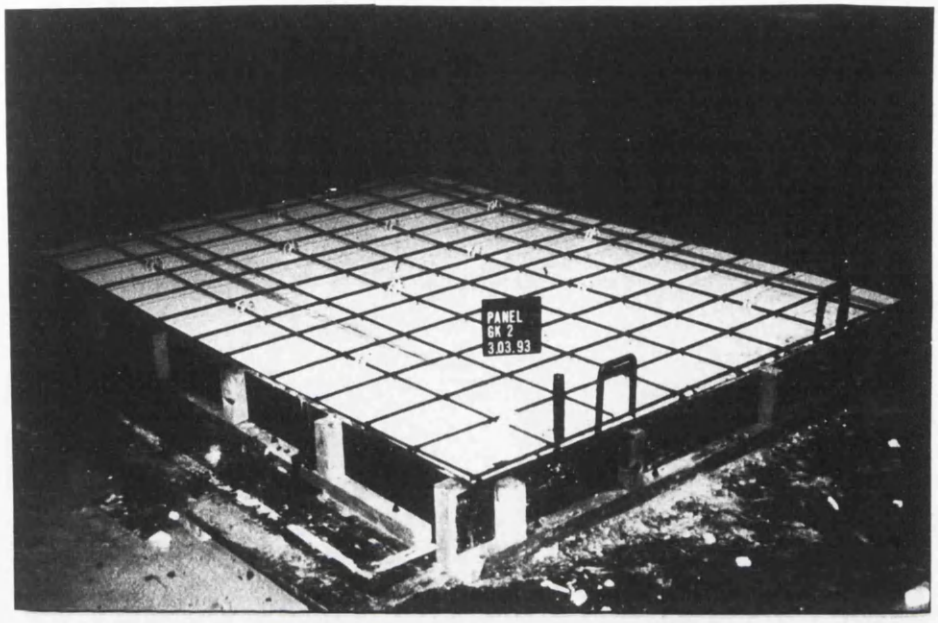

Fig. 4.18: Details of the casting operation for GK-4, 5, 6.

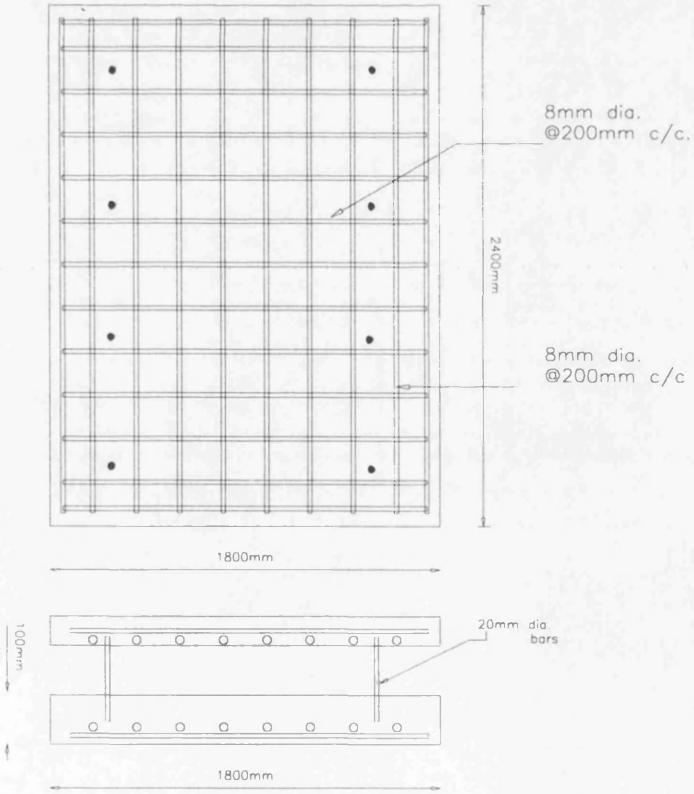

Fig. 4.19: Details of test specimen GK-88.

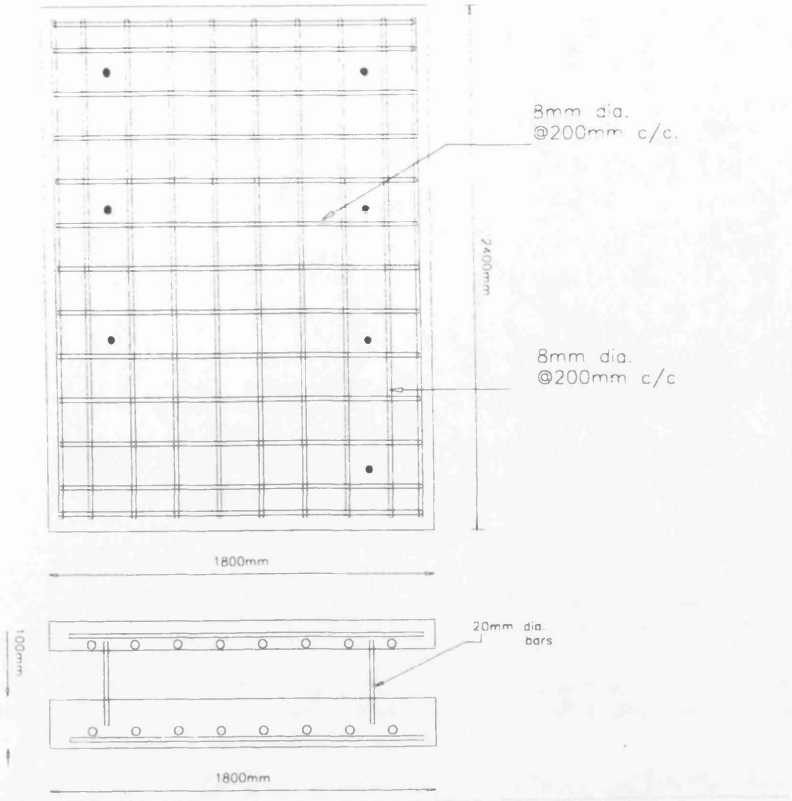

Fig. 4.20: Details of test specimen GK-87.

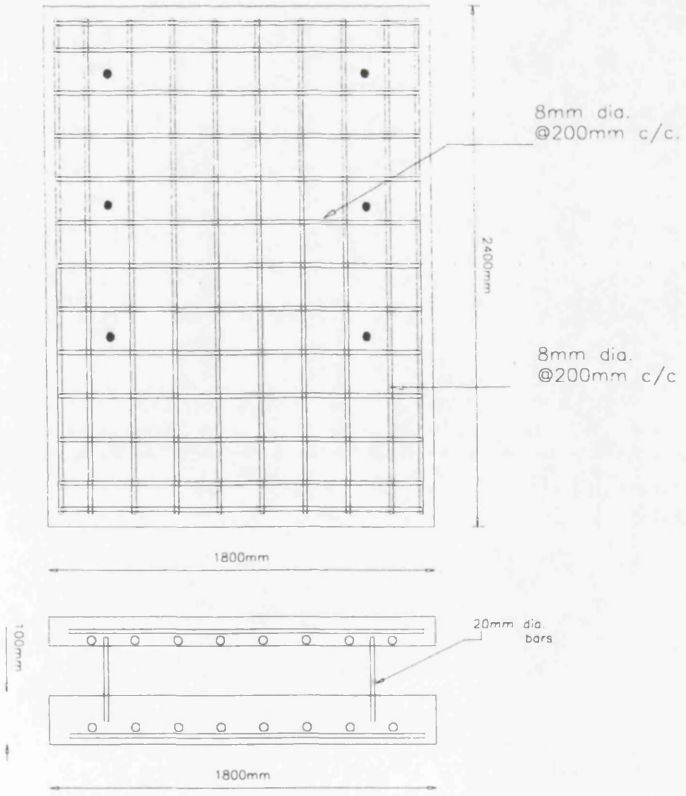

Fig. 4.21: Details of test specimen GK-86.

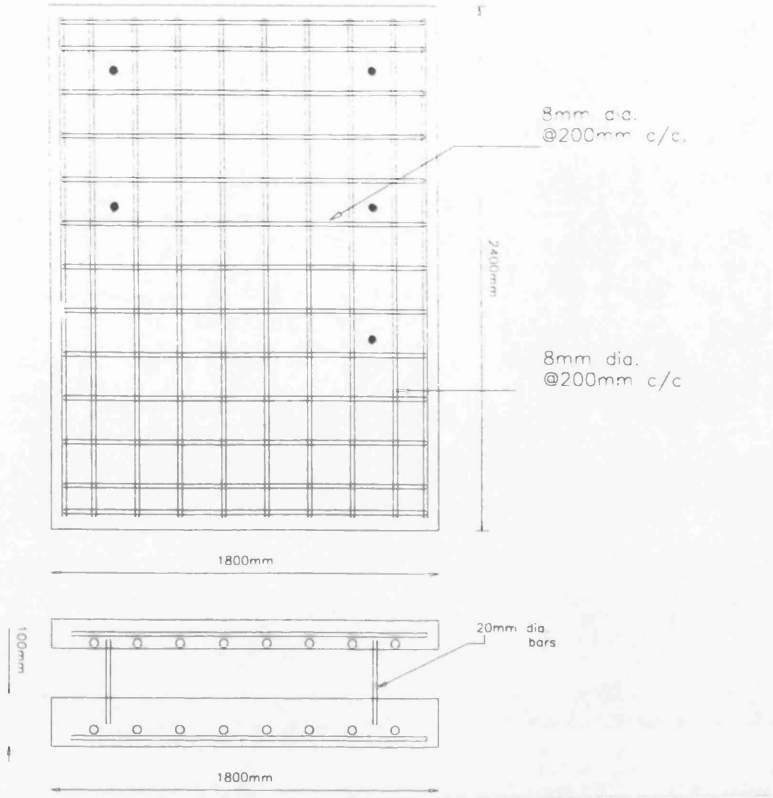

Fig. 4.22: Details of test specimen GK-85.

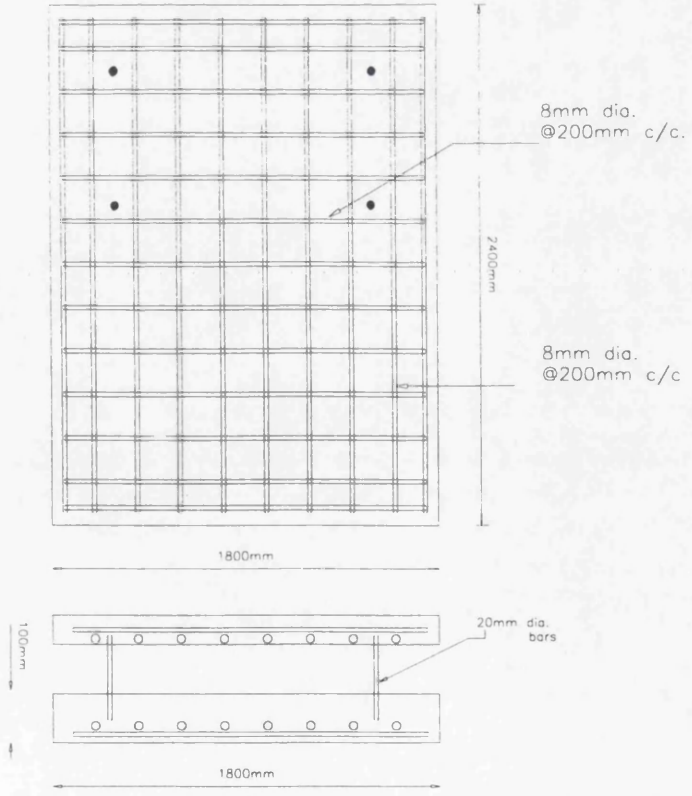

Fig. 4.23: Details of test specimen GK-84.

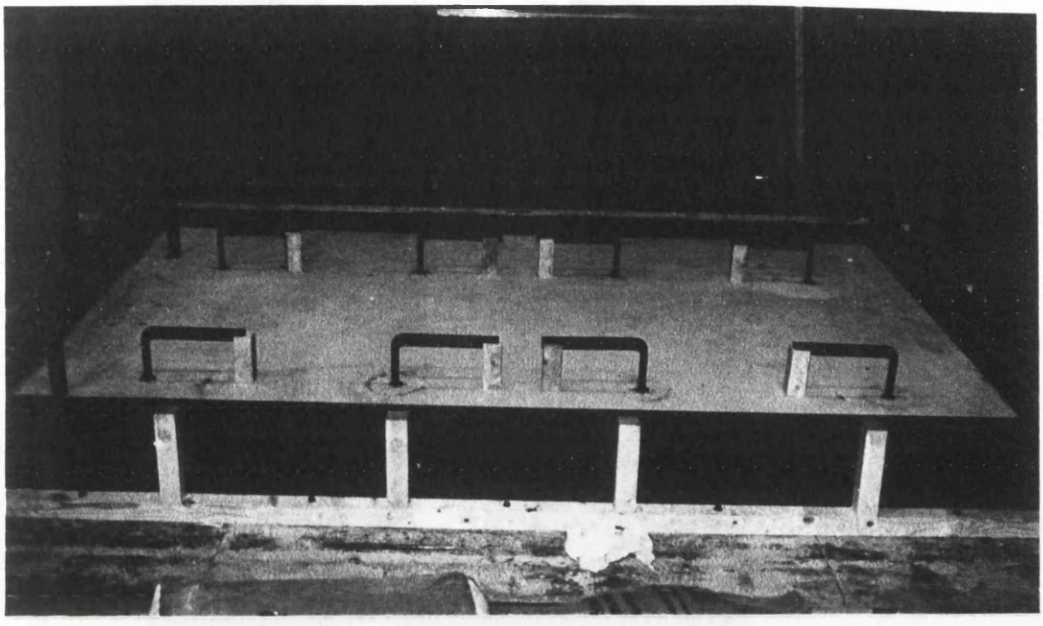

Fig. 4.24: Details of the casting operation for GK-88.

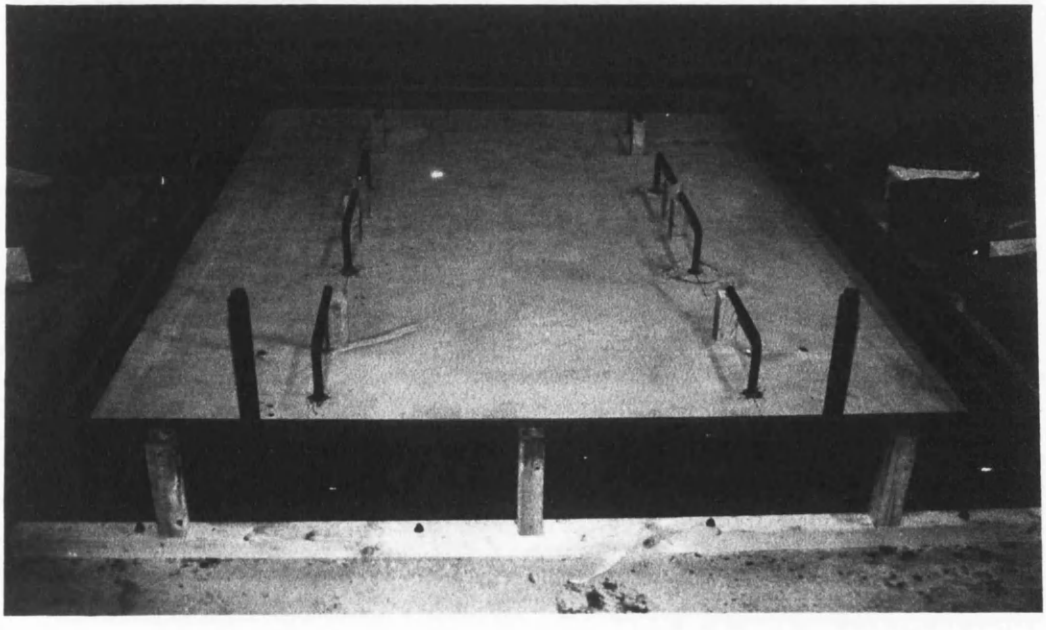

Fig. 4.25: Details of the casting operation for GK-88.

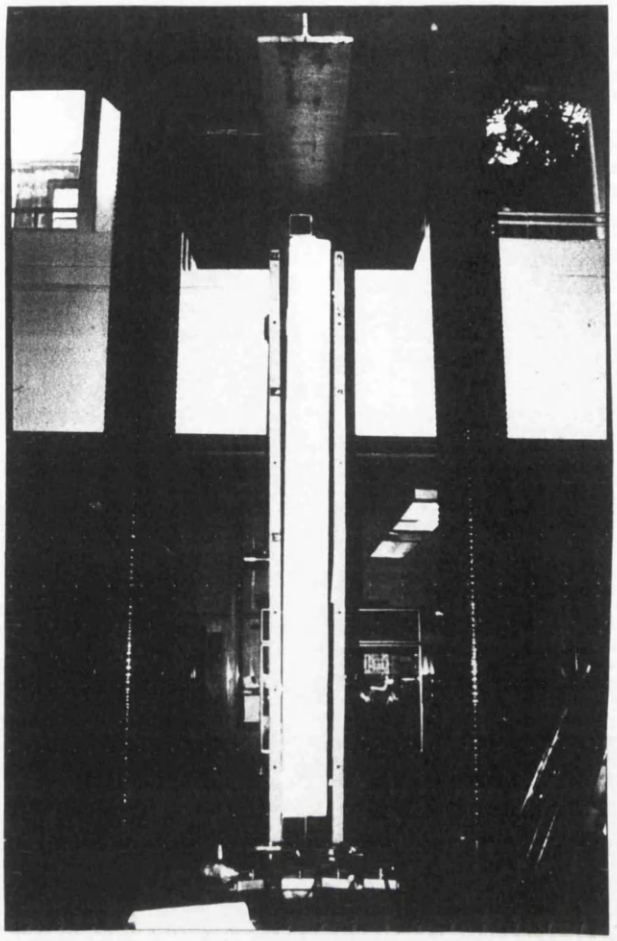

Fig. 4.26: Loading arrangement for the test set-up.

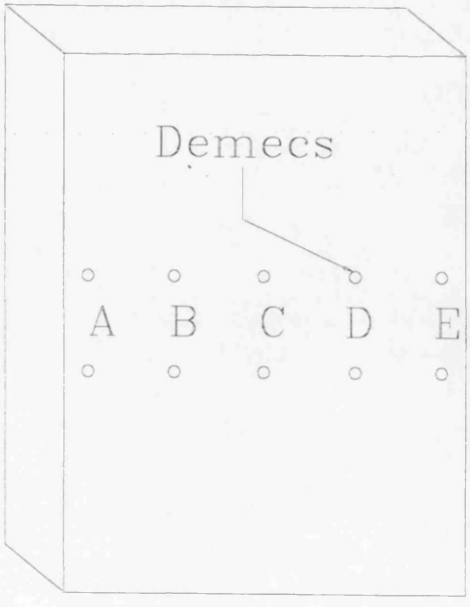

Fig. 4.27: Location of demec points for all eleven test specimens.

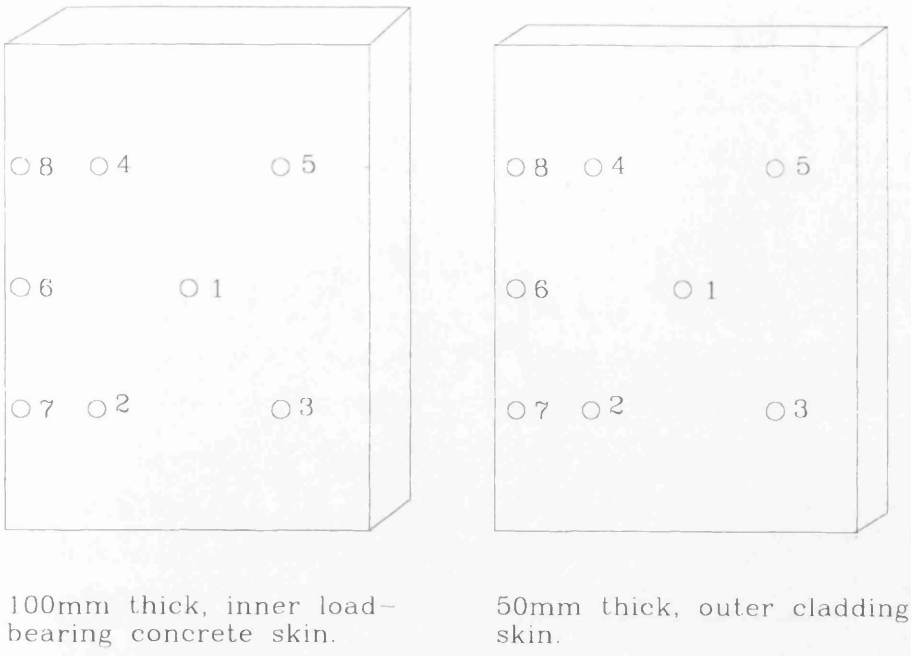

100mm thick, inner load-bearing concrete skin.

50mm thick, outer cladding skin.

Fig. 4.28: Accelerometer locations for test specimen GK-1, 2, 3, 4, 5, 6.

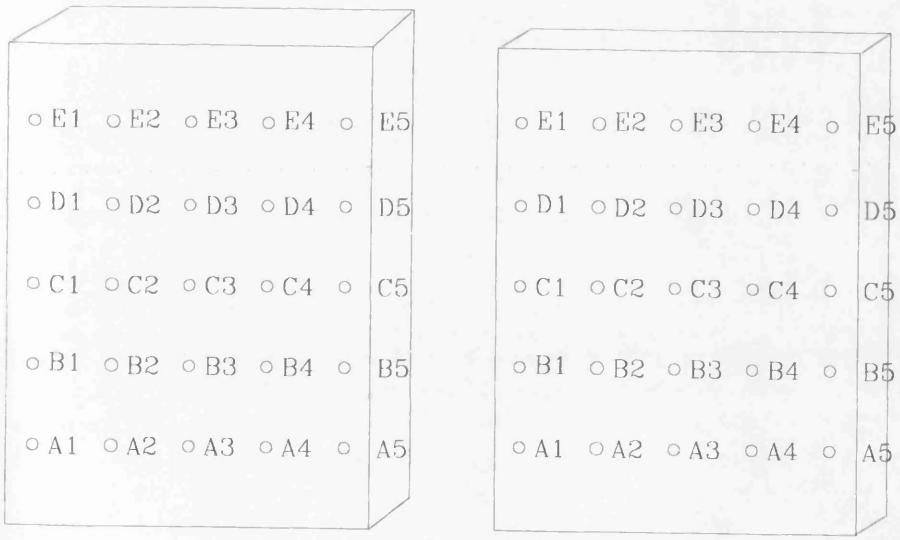

100mm thick, inner load-bearing concrete skin.

50mm thick, outer cladding skin.

Fig. 4.29: Accelerometer locations for test specimens GK-88, 87, 86, 85, 84.

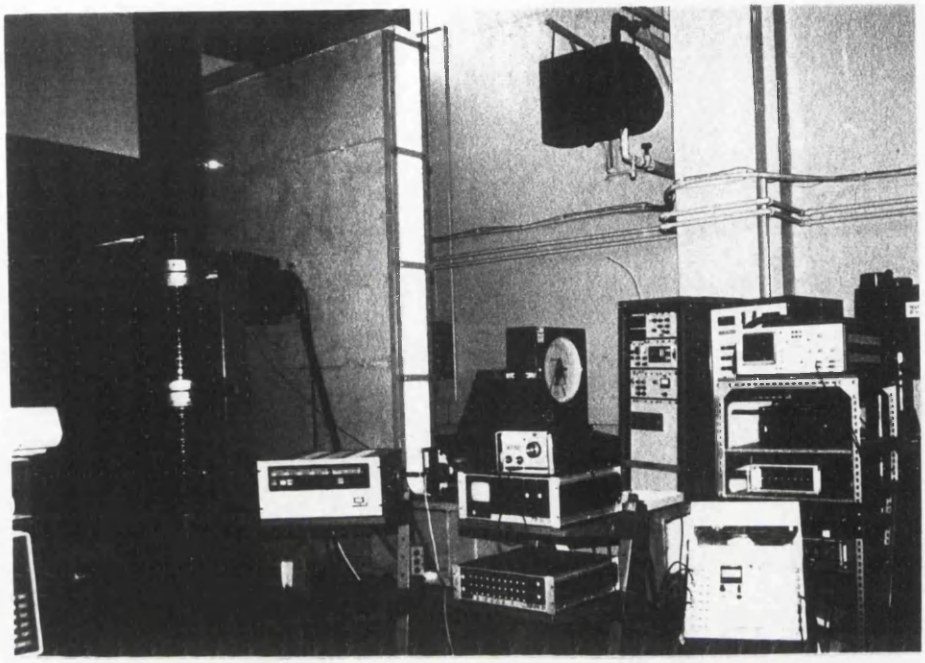

Fig. 4.30: Details of the test rig with the vibrator assembly.

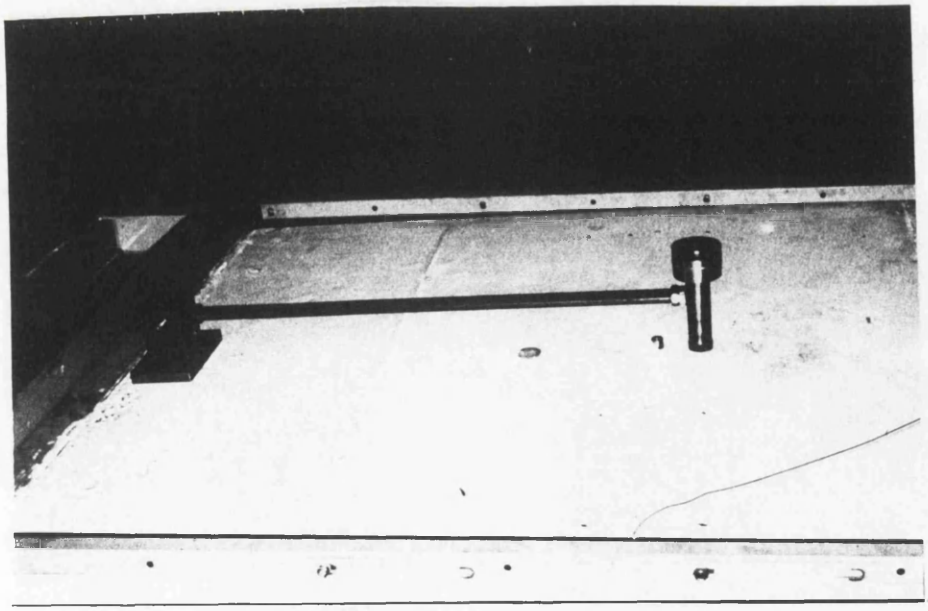

Fig. 4.31: Details of the hammer used.

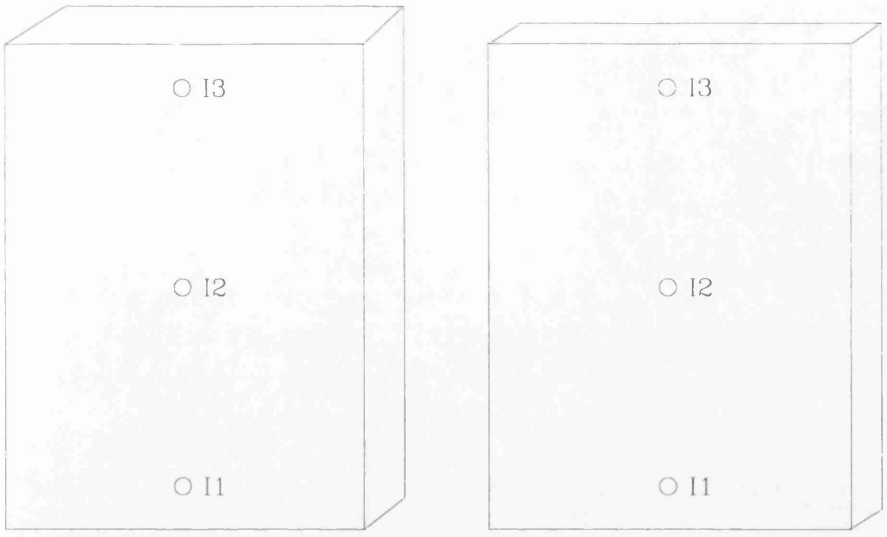

100mm thick, inner load-bearing concrete skin.

50mm thick, outer cladding skin.

Fig. 4.32: Blow locations for hammer and vibrator impacts.

CHAPTER 5

EXPERIMENTAL RESULTS

5.1 INTRODUCTION

In the previous chapter the details of the test specimens and the experimental set-up were given. Also described were the various methods used for the dynamic testing of structures and the procedures used for testing of the various experimental models in the investigation. This chapter mainly deals with the results obtained for the eleven experimental models. A discussion is presented on the various dynamic characteristics of the specimens as inferred from the experimental observations and an attempt is made to distinguish the structural differences present between them.

Before moving on to the experimental observations, it is worth while to briefly discuss the experimental procedure, especially the method of vibrating the specimens. As was explained in the previous chapter, two methods were employed to excite the specimens, (i) the mechanical sinusoidal vibrator and (ii) the hammer blow, with two variations of the hammer being used. The need to experiment with these two forms of exciting devices, was made necessary because of the large and extremely stiff nature of the sandwich wall panels. Complete excitation of the specimens was envisaged to be a fairly complicated problem at the begining of the experimental program and it was concluded that, to achieve the best results, a pilot series of tests using these various possibilities of excitation would be performed. Then, based upon the information obtained from these results, further investigations could be carried out. The following articles describe the advantages and disadvantages of the two approaches adopted for imparting vibrations to the test specimens.

5.1.1 MECHANICAL VIBRATOR

The likelihood of analysing the experimental dynamic response, being a relatively simpler task, if one can impart controlled sinusoidal vibrations at a particular frequency, is quite strong. With this understanding, this was the first form of exciter that was used for obtaining the dynamic characteristics of the specimens. This approach had a certain number of limitations, such as the limited amount of energy imparted to the specimen and the point of impact. While using the electro-magnetic vibrator it was observed that the energy induced to the specimens through the use of only one vibrator was not sufficient to get the specimen vibrating in any one particular mode. This might only have been possible through the application of a multi-vibrator system, but due to the problems associated with this approach (highlighted in the previous chapter) and the limited resources available, this method was ruled out. Secondly, because of the way the vibrator was supported alongside the specimen, it was quite difficult and cumbersome to alter the location of the point of impact, which once again produced a severe limitation on the experimental set-up. Considering these two draw backs when using the electro-magnetic sinusoidal vibrator, after a series of trial runs it was decided to shelve this approach as the results being obtained were clearly not exhibiting much and it was decided to solely concentrate on impacts to the specimen through the use of hammer blows.

5.1.2 HAMMER BLOWS

Producing vibrations in structures by the use of hammer blows has been quite extensively used and the results obtained have indicated towards the success of this approach. It has been shown by various authors (as indicated in chapter 1) that

the transient input from hammer impacts is quite capable of vibrating the specimen in its different modal shapes. Investigations have also been carried out on the effects that different hammer heads might have on the observed response, and although they do not produce vastly different results, they certainly tend to have some effect on the natural frequencies. For determining the dynamic characteristics in the present study, plastic headed hammers were used. The main advantage of using a hammer is in the simplicity of use. One can have absolute flexibility as to the location of impact points as well as having control over the force of impact and consequently knowing the energy imparted to the specimen, which can be later on used for determining the relative magnitudes of deformations for all transducer locations. This is generally achieved by locating an impedance head in the tip of the hammer, which measures the force imparted through the hammer head. As the main purpose of the present study was to determine the possibility of detecting the natural frequencies of the sandwich panels for the various modal shapes, as well as to be able to determine through the changes in these natural frequencies the structural changes in the panel thus, the relative magnitudes of the various transducer responses were not considered that important and the hammers used were not fitted with impedance heads in the tips. This approach had its drawbacks though, in that it made it impossible to use the response obtained from the transducers to plot out the modal shapes of the specimen as the relative displacements were not measured.

As has already been mentioned through the preceding chapters, two types of hammer blows were used, and the response of the specimens from the transducers was obtained from the various accelerometer locations. For the first series of experiments the hammer was attached to the specimen. The hammer was allowed to free-fall under its own weight through an arc of ninety degrees. The fall was

kept constant, but the weight of the hammer head was a variable and could be increased by the addition of weights. The hammer arm was supported on an almost friction less pin and held in place through the use of a locking assembly as shown in Fig. 4.31 of the previous chapter. The entire assembly was bolted on to the specimen and held in place by four bolts. Once the hammer had struck the specimen, falling through the pre-set arc, as it bounced off the specimen surface it was held back so as to eliminate any subsequent impacts.

While performing tests in this manner, a number of complications were encountered. The first one was that as the hammer struck the specimen surface, additional impacts were passed on to the specimen at the location of the supporting assembly of the hammer, and despite the fact that efforts were made to dampen this effect by using spring bolts, the effectiveness of this approach was not one hundred percent, and as a consequence the response of the specimen showed extremely complex wave forms, and made for extremely difficult analysis of the observations. Secondly, the same problem as encountered with the mechanical vibrator of conveniently changing the points of impact was also present, thus it was once again limited to basically one impact point.

It was found out through trial experimentation that these difficulties and discrepancies could be eliminated, simply by using a hand held hammer. Because the hammer was not controlled in the force of impact and once again as impedance heads were not used, there was no sure way of controlling the amount of energy being imparted to the specimen, but through trial and error, it was fairly simple to determine the approximate force of impact required to impart enough energy to the specimen, to excite the various dynamic modes.

Keeping all of the above mentioned discrepancies, regarding the different possible forms of excitation and after going through preliminary rounds of investigation, it was decided to just use the mode of excitation through the use of a hand held hammer for the controlled testing of all specimens. The results of these tests with the conclusions drawn are presented in the proceeding articles.

5.2 EXPERIMENTAL MODELS GK-1 & GK-4

Tests were performed on these two specimens for the determination of their structural characteristics through the identification of the dynamic properties. The dynamic properties that we were mainly concerned with, were the natural frequencies of the different mode shapes and the differences that would show up in the response frequencies for detecting the distinctions between various specimens. Before carrying out a discussion of the experimental results obtained, let us just remind ourselves once more about the main structural differences present between experimental models GK-1 and GK-4. Both specimens, if we recall, were of the same geometric properties as well as the reinforcement details for both leaves of the sandwich panels. The major differences in these sandwich wall panels related to the structural constraints present between the two leaves. Where as, panel GK-1 was modelled to have a complete connection between the two leaves around the perimeter, extending over a width of 200mm, panel GK-4 had a connection only around three edges and over a width of 50mm only. The one remaining edge of the panel was left without any structural connection, this was done to simulate the situation of a crack between the two leaves. Also, the width over which the concrete was structurally connected was reduced. This was done to reduce the stiffness of this panel compared to GK-1. The main reasoning behind introducing

these changes between the two specimens was to reduce the structural connection and as a consequence reduce the stiffness, which would lead to a change in the natural frequencies, hence enabling us to determine the structural differences in the panels through them.

Fig. 5.1 gives the natural frequencies for the various modal shapes of the two panels, GK-1 and GK-4, as observed from the experimental response obtained from the different transducer locations. As was described earlier, the transducers (accelerometers) which were used for measuring the response of the two leaves of the sandwich panel were located at various points. The observed natural frequencies for the two specimens were seen to be fairly similar for these different accelerometers, with obviously different magnitudes, as would be expected, depending upon the location of the transducer and the dominant mode of excitation. As the excitation of the specimens was through the use of a hammer blow, producing a transient force, there was no way in which to ensure the excitation of one particular mode. As a result, the frequency response showed peaks corresponding to a number of natural frequencies. The difficulties encountered in such a mode of testing, were obviously, in separating the various modes of excitation and in trying to realise from the observed spectrum the actual modes of the specimen and the different reflected waves which would be induced in the specimen.

As can be seen from Fig. 5.1, the observed natural frequencies of specimens GK-1 and GK-4 are fairly close together for the first couple of modes, as is to be expected because of the type of deformations occurring in the panels for these particular modes. But as we move on towards the higher modes, they show a reasonably large difference. This result once again is what one would expect, as

the greater stiffness of specimen GK-1, would result in larger natural frequencies in comparison to the less stiffer specimen GK-4. These results are also confirmed by the numerical models.

The results from these two specimens suggested that from the frequency response spectrum, it is possible to differentiate between the two specimens and be said with a fair degree of certainty as to which is the stiffer of the two specimens. This can lead to the conclusion that, because of the fact that its behaviour indicates a stiffer response, it should contain relatively more structural constraints between the two leaves of the panel. The trends observed from the experimental response of these two specimens definitely indicated, that from the dynamic response of sandwich panels one can comment with a fair degree of certainty as to which of the panels is structurally more sound than the other.

Once it had been established, through the experimental results of test specimens GK-1 and GK-4, that it was possible to distinguish between the stiffness of the connection around the perimeter between the two leaves, it was decided to go one step further and test specimens GK-2,3,5,6 and to try and differentiate between the reinforcement constraints present between the two leaves. The dynamic response of specimens GK-2 and GK-3 was very similar to the one obtained for GK-1. The results for these two specimens indicated that it was not possible from the obtained response for the various accelerometer locations, to distinguish between the natural frequencies of the two specimens which was visibly identical to each other as well as to that of GK-1. Similar observations were made from the tests carried out on specimens GK-5, 6, which produced a response similar to GK-4. Such a result was obtained in spite of the fact that these two specimens had one and four additional constraints present, respectively. Considering, that changes in the natural

frequencies were observed, when the constraint conditions around the perimeter between the two leaves were altered, it is safe to conclude that the concrete constraint around the edges is the one dominant structural change (from the different parameters considered in the present study) which greatly effects the dynamic response of the sandwich panel. Thus, if any structural variations concerned with altering the concrete connection around the perimeter, such as additional cracks are introduced into such a panel, they would be more readily distinguishable from the frequency response spectrum, in terms of changes in natural frequencies. On the other hand the minor variations in the natural frequencies which would be taking place through increasing or reducing the number of reinforcement ties, which are structurally connecting the two leaves of the sandwich panel, would be extremely difficult to detect.

Such a result is somewhat to be expected as the introduction of a stiffer constraint around the perimeter would tend to have a greater effect on the overall mass of the specimen and, as a consequence, the natural frequencies would show relatively greater change. On the other hand the introduction of additional reinforcement ties would not have that great an effect on the structures mass and, following on the same principle as before, would tend to show a much lower variation in the natural frequencies. One must remember, that although the natural frequencies of the various modal shapes may not vary that much with the introduction of additional reinforcement ties, it would invariably have a much significant influence on the modal shapes corresponding to these natural frequencies. These changes in the modal shapes can possibly be detected through the response spectrums, if a fairly detailed set-up is used, and the magnitudes of deformations at a reasonable number of transducer locations are measured. Then on plotting these out, one can obtain a fairly close match of the modal shape of the specimen for one particular natural

frequency. This would of course require, that the specimen is basically vibrated in one particular modal shape, which in itself can be a fairly complicated problem for such a stiff structure. Unfortunately, in the present research, the main interest was the development of a fairly simple approach to determine the structural integrity, or in other words, damage location, through the detection of changes in natural frequencies. Therefore the magnitudes of the response from the different transducer locations were not measured.

5.3 EXPERIMENTAL MODELS GK-88, 87, 86, 85, 84

Although similar to test specimens GK-1 and GK-4 in their geometric and reinforcement properties, these specimen were principally different in the type of constraint present between the two leaves of the sandwich panels. Where as the specimens GK-1 and GK-4 had some form of concrete connection around the perimeter, the specimens in this batch were singularly connected through a certain fixed number of reinforcement ties varying from eight in GK-88 to four in GK-84. Once it was shown, through the analysis of specimens GK-1, 2, 3, 4, 5, 6 that the connection around the perimeter tended to over shadow any effect the reinforcement ties could possibly have on the experimentally observed natural frequencies, it was logical to try and study, solely the effect that the reduction of ties might have on the dynamic response of the test panels. Based upon this, the specimens in this batch were modelled with only the reinforcement ties, structurally connecting the two leaves of the sandwich panel. The test set-up was the same as before, with the boundary support conditions and the in-plane loading on the load bearing leaf being kept as before. The input of the dynamic force was

as for the previous batches, a transient force and imparted to the specimen through the use of a hand held hammer.

The experimentally observed response of the five specimens in this batch, plotted out in terms of the natural frequencies for the various mode shapes are presented in Fig. 5.2. As can be seen from this figure the observed natural frequencies of experimental models GK-84 and GK-85 (containing four and five reinforcement ties, respectively) are very close together and from this response it is exceedingly difficult to detect any structural change within the two sandwich panels. As the number of constraining ties is increased to six, seven and eight for specimens GK-86, 87 and 88 respectively, the observed natural frequencies do tend to show a slightly greater change. The models tend to exhibit a stiffer response and the magnitude of the natural frequencies increased with increase in the number of constraints. This trend is again very similar to what one would expect, as the increasing number of ties would by and large increase the stiffness of the specimen and thus increase the natural frequency for a particular modal shape. It can also be observed from Fig. 5.2, that the differences in natural frequencies for the lower modal shapes are more difficult to detect, for example, for the first modal shape, the natural frequencies vary from 0.4 hertz for the least stiff specimen GK-84 to 0.5 hertz, for the most stiff specimen GK-88. This is synonymous with the trends observed for the previous batches. Additionally, the problems encountered in analysing the results and trying to differentiate between the various specimens, to determine their structural differences were very similar to the one's faced for the previous two batches. Figs. 5.3-5.6 give typical response spectrums of the various test specimen, as obtained from the spectrum analyser.

In conclusion one can say from the experimentally observed response for this batch, that with the approach adopted for determining the structural damage through their dynamic response, it is possible to distinguish between the various panels, and state with a fair amount of certainty, as to which of the panels is structurally more sound. But at the same time the results do not give any indication as to the overall structural integrity of the panel, neither is it possible to detect the actual structural damage that might have occurred in the panel.

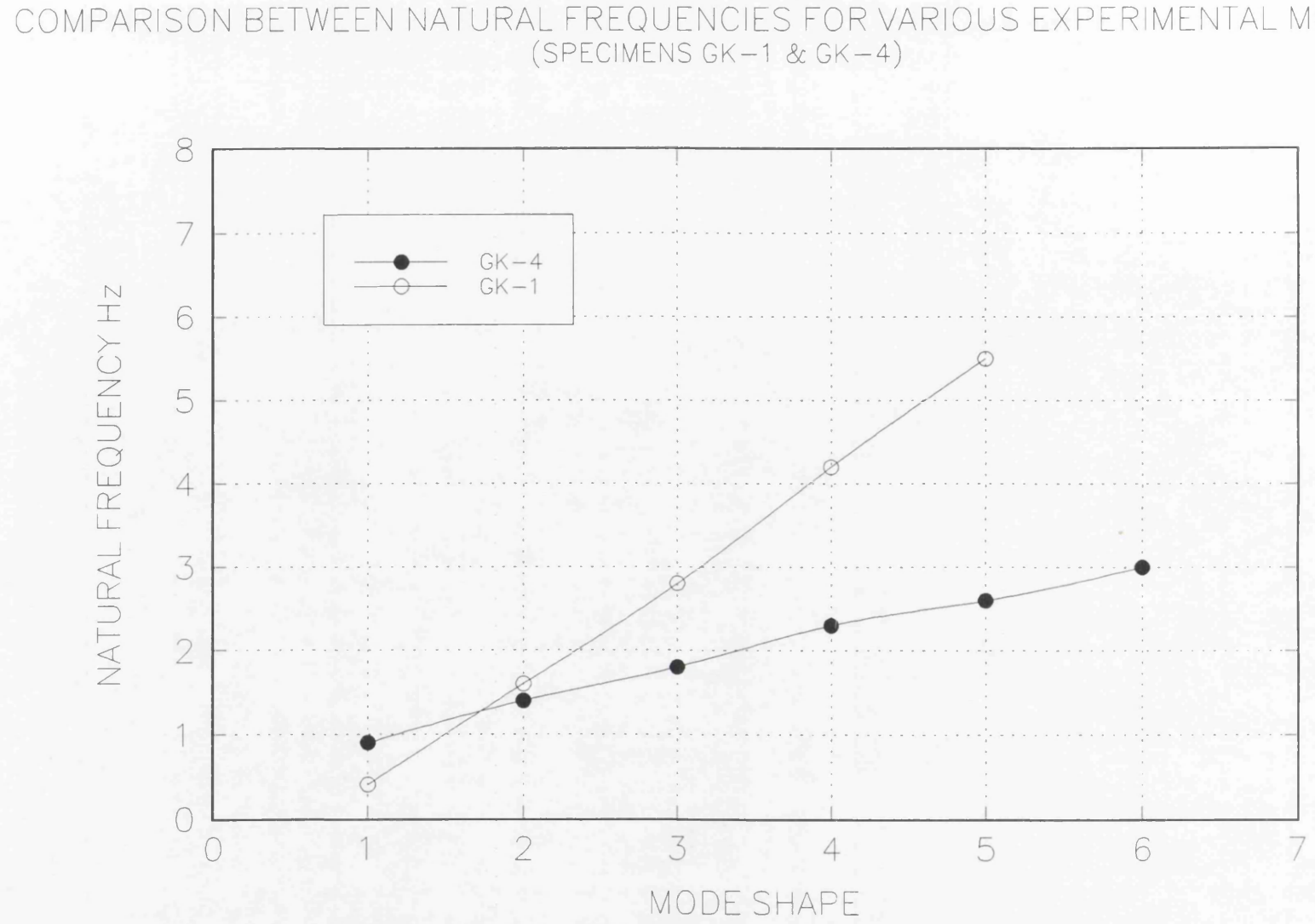

Fig. 5.1 : Natural frequencies for experimental models GK–1 and GK–4.

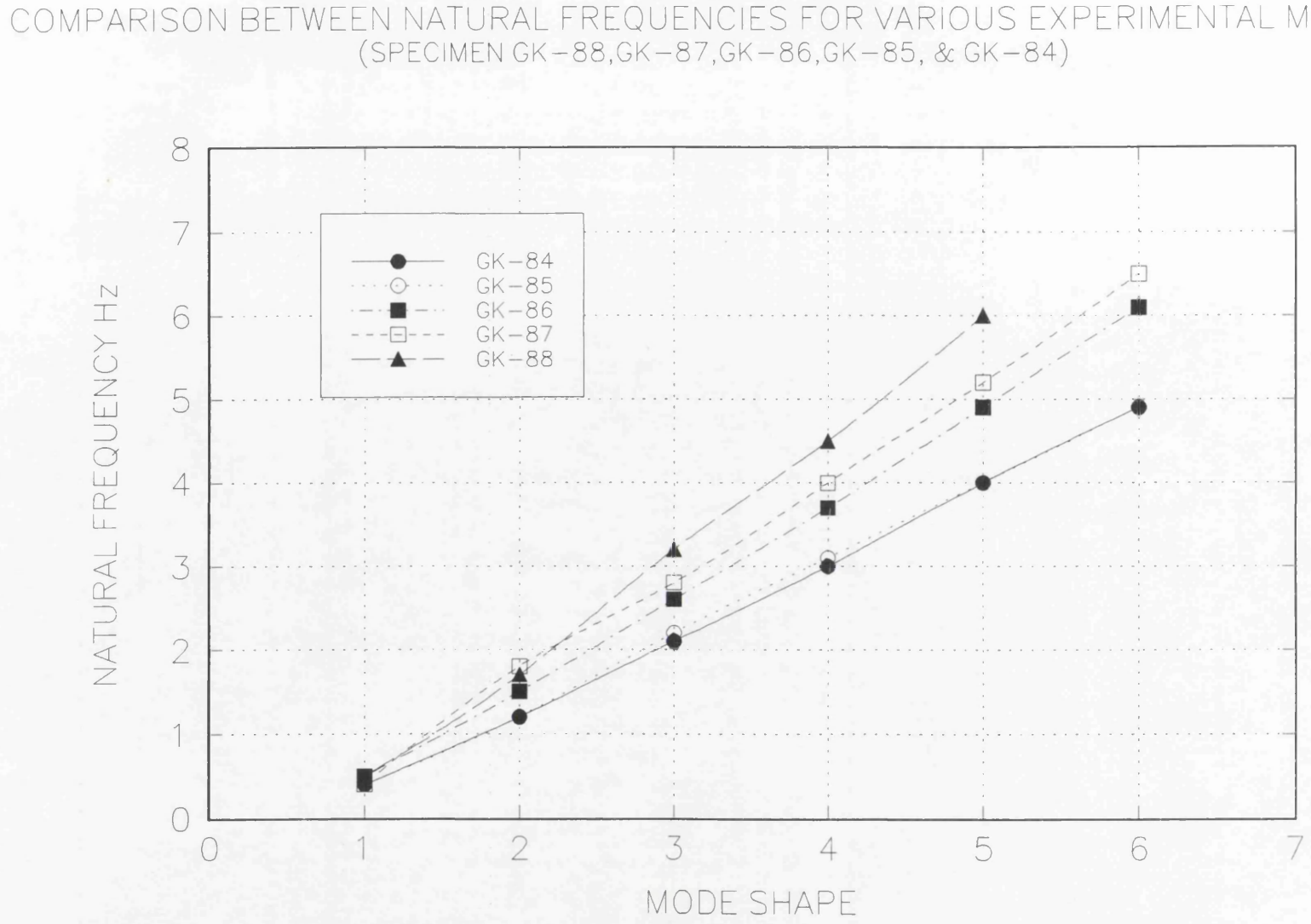

Fig. 5.2:Natural frequencies for experimental models GK-88,87,86,85,84.

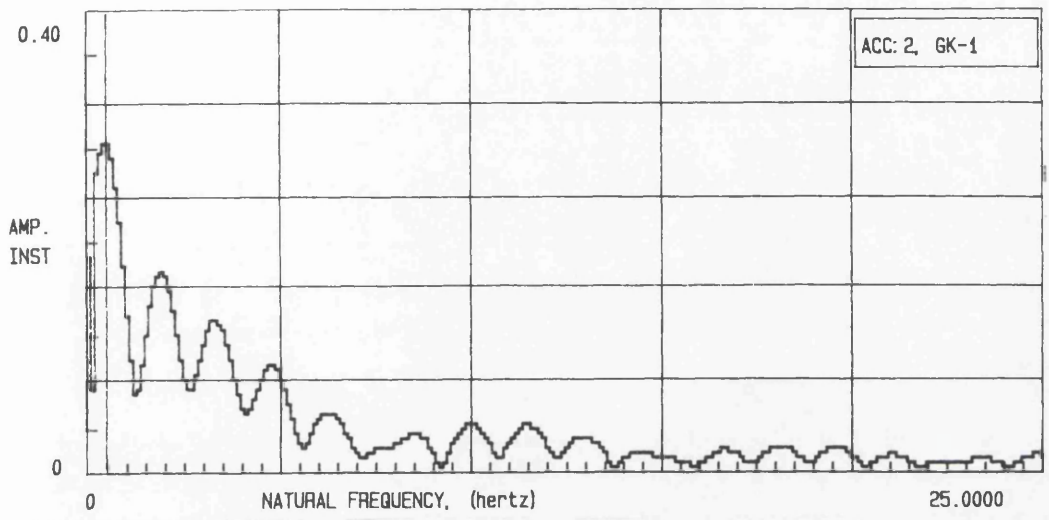

Fig. 5.3: Frequency reponse spectrum for specimen GK-1.

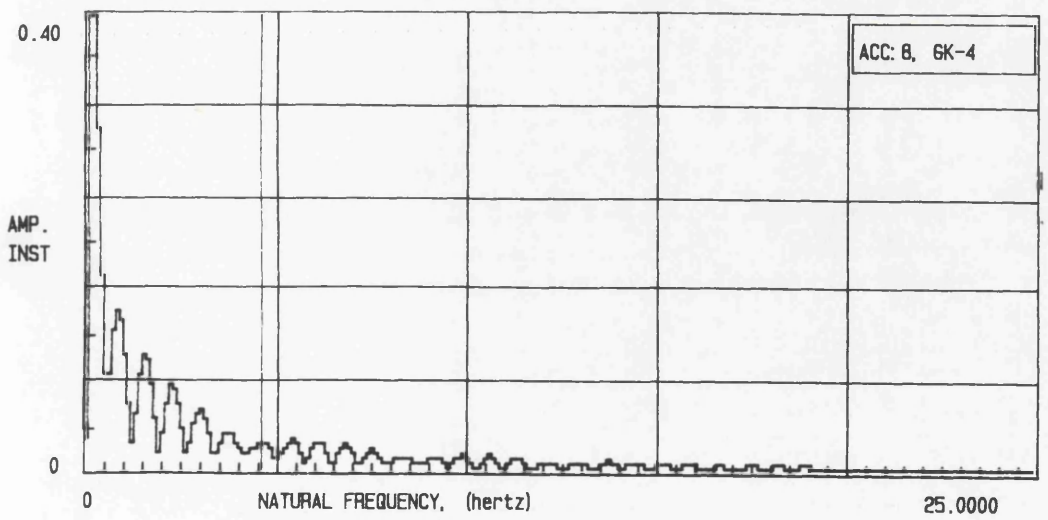

Fig. 5.4: Frequency reponse spectrum for specimen GK-4.

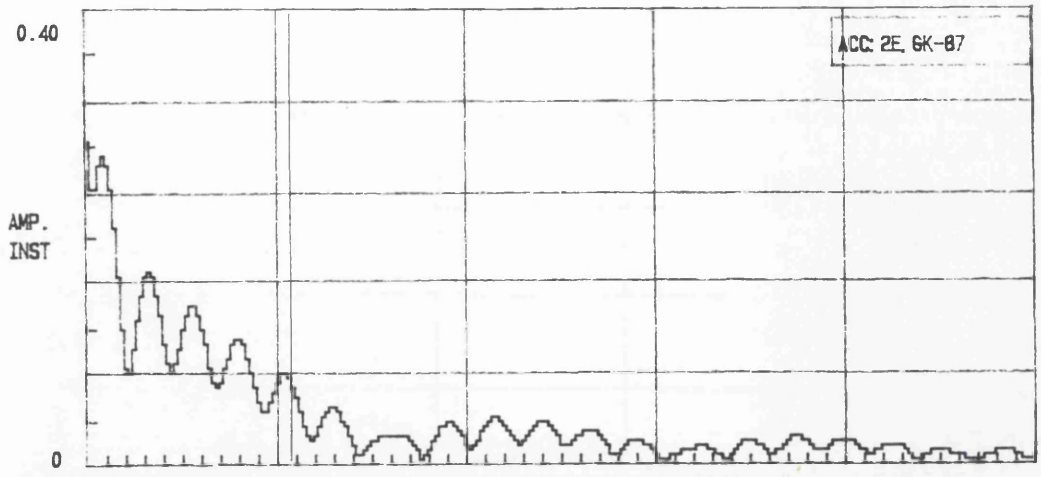

Fig. 5.5: Frequency reponse spectrum for specimen GK-87.

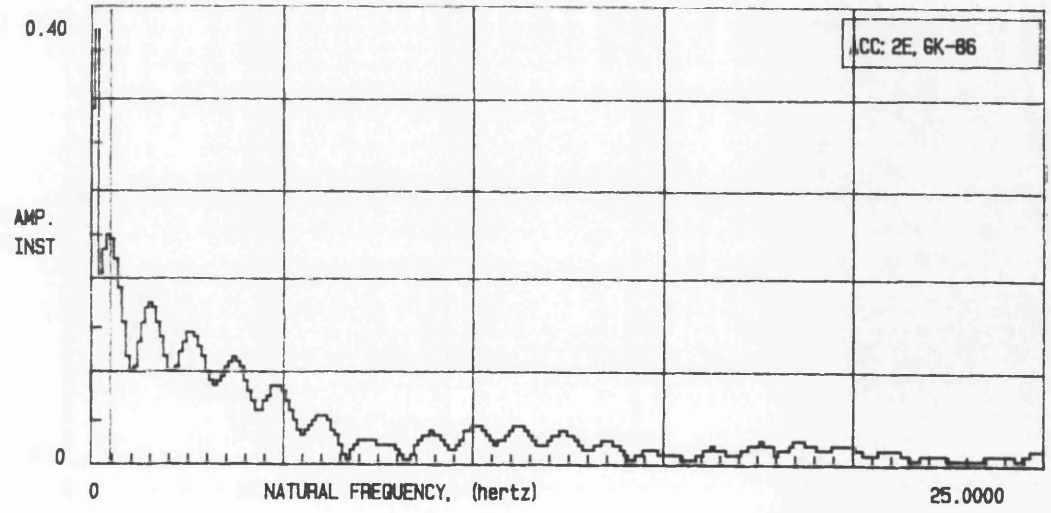

Fig. 5.6: Frequency reponse spectrum for specimen GK-86.

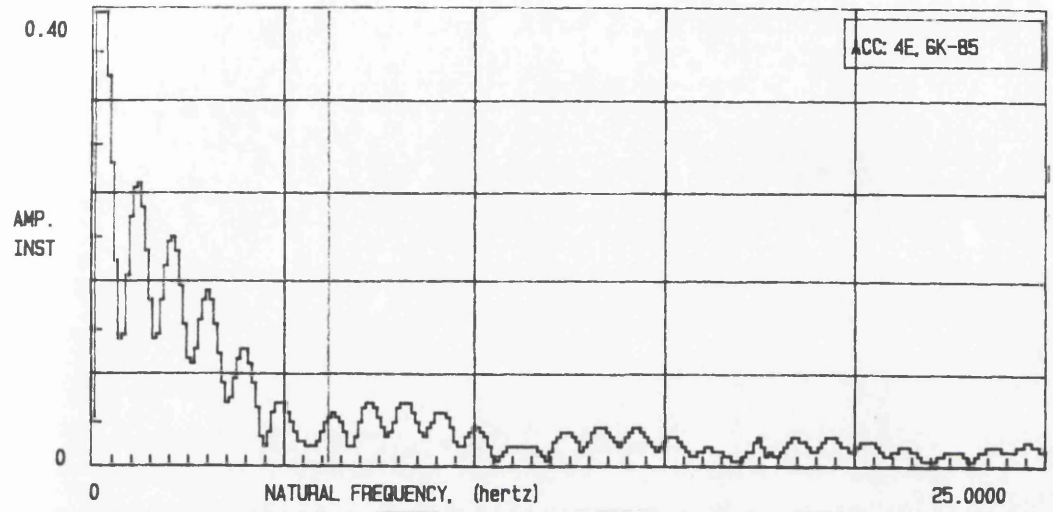

Fig. 5.7: Frequency reponse spectrum for specimen GK-85.

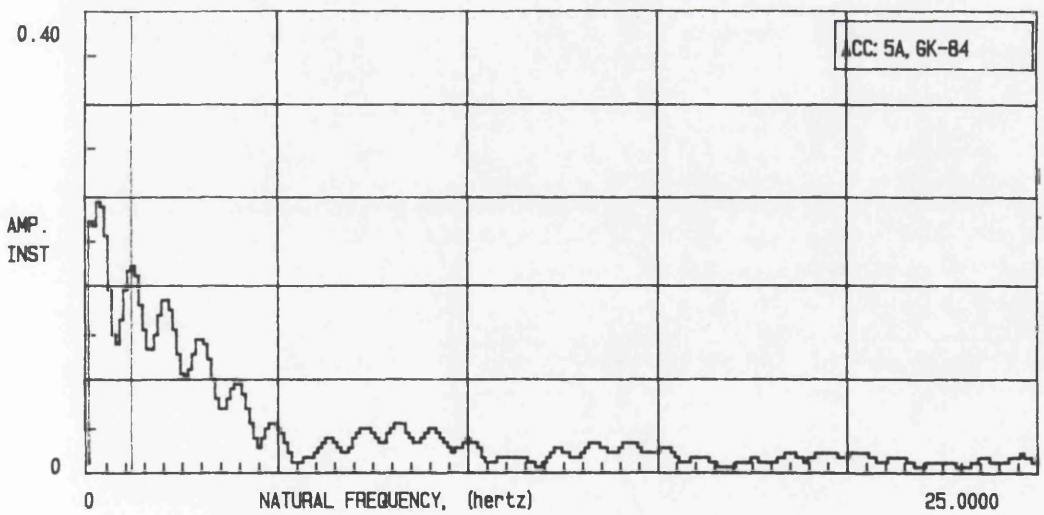

Fig. 5.8: Frequency reponse spectrum for specimen GK-84.

CHAPTER 6

COMPARISON BETWEEN NUMERICAL AND EXPERIMENTAL RESULTS

6.1 INTRODUCTION

Chapters 2 to 4 described the details of the numerical and experimental models, as well as discussing in detail the results of the analysis and the observed dynamic response, whereas the previous chapter discussed the results obtained from the dynamic testing of the test specimens. This chapter deals with the comparison between the numerical and experimental models. The results obtained for the various experimental models are compared to the results obtained from the twin numerical models. Comparisons are made between the observed and the calculated/predicted natural frequencies, as this was the main characteristic being experimentally detected. Each model is dealt with individually and based upon the results conclusions are drawn.

6.2 SPECIMEN GK-1

Fig. 6.1 displays the natural frequencies of GK-1 for the first six modal shapes as obtained from the results of the numerical analysis and observed from the experimental response. As can be seen from the figure, the observed natural frequencies for the first three modal shapes compare well with the numerical model. For the higher modes though, it can be seen that the experimental model exhibits a much stiffer response than the numerical model. This being a trend which was observed for nearly all specimens. The tendency of the observed

response to be stiffer for the higher modes could possibly be due to the way the experimental model was supported and restrained at the edges. The numerical model was analysed as a plate bending element and being simply supported along the top and bottom edges, with the in-plane loading on the inner 100mm thick concrete leaf not having any effect on the natural frequencies of the various modal shapes. In contrast to this, the experimental model was clamped along the top and bottom edge, by the application of a compressive load through a 100mm square hollow steel box-section, which might have introduced a boundary support condition, somewhat different to that of the numerical model. Obviously, it is quite difficult to predict with any degree of confidence the magnitude of error that this might induce, but it is safe to assume that it will have contributed to an extent. The second possible source of discrepancy, could solely lie in the observed responses. Taking a look at the frequencies obtained from the numerical models, it can be observed that some of them (e. g. modes 3 and 4) lie very close together. Now, because of the fact that during the experimental phase the specimens were excited through a transient input, rather than at one controlled frequency, there is a very strong likelihood that the natural frequencies which are in close proximity of each other, overlap and through the experimental response they are only observed as one. This could lead to inaccurate conclusions and comparisons which are often misleading. This is possibly the one single source of error which has the greatest contribution towards the discrepancy between the observed responses and the calculated values.

The fact that the layer of polystyrene was not modelled while performing the numerical analysis, is another possible source of error, as is the observation that, the observed response could have the two leaves of the panels vibrating independently and in their own modes in addition to a combined mode. This would

again complicate the observed response and make it quite difficult to isolate them, leading to somewhat different results from the numerical model.

6.3 SPECIMEN GK-4

In contrast to specimen GK-1, this model exhibited an observed response, almost identical to the results obtained from the numerical analysis. Fig. 6.2 presents the results of the observed and calculated natural frequencies for the various modal shapes. Unlike, all other specimens tested, which showed a much stiffer observed response than the calculated one, specimen GK-4 was the complete opposite. For this case the numerical model exhibited a slightly stiffer response. As the test conditions for the experimental model were identical to those for GK-1 as well as all other models, it would be fair to assume, that the possible sources of discrepancies and errors would be similar and have the same effect on the results, as described for specimen GK-1. Quite surprisingly, contrary to this, they show no such effect in this particular case, and the observed response matches extremely well with the numerical model. The numerical model showing such good comparisons in this case could be due to the relatively low stiff structural connection between the two leaves. The constraints used between the two leavesof the panel for the numerical model possibly, do not duplicate the stiffness of the experimental specimens and, hence generally calculate frequencies which are lower than the observed one s. With the repeatability of the observed response being assured, it is fair to conclude that for panel GK-4 which is structurally damaged quite extensively, it is possible to predict as well as observe the natural frequencies for the various modal shapes. Thus, it is fair to suggest that it might be possible to extend this conclusion to other similar panels.

6.4 SPECIMENS GK-88, 87, 86, 85, 84

Figs. 6.3-6.7 show the comparisons between the experimentally observed response and the numerically calculated results for the natural frequencies of the first six modal shapes for specimens GK-88 to GK-84. The one obvious observation that can be drawn from the presented results is the similarity between these five specimens in this batch and specimen GK-1. The experimentally observed response showing the specimens to be behaving a lot stiffer then the predictions obtained from the numerical models. The disparity between the two results being a lot more pronounced than for specimen GK-1. As we move from GK-88, that is the specimen with eight constraints present between the two leaves, to specimen GK-84, one with only four constraints, it can be observed that the relative difference between the two responses decreases (Figs. 6.3-6.7). The differences still being large enough though, to make any absolutely valid comparisons impossible.

Most of the discussion made for specimen GK-1, would apply to these specimens, and even at the risk of repetition it is appropriate and pertinent to make some of the observations again. A fairly significant observation was that the experimental response of the five specimens in this group, especially GK-88, 87 and 86, was closer to specimen GK-1 than GK-4, while the numerical results, by all accounts indicate a response which should be more like that of GK-4, at least in terms of the natural frequencies. Taking a look at the numerically obtained values of the natural frequencies, for these five specimens, it can be seen that they are very close to each other, making it extremely difficult to observe the changes through them, as they would again have a tendency of overlapping and being exhibited as one. This

complicates the problem and the one probable way around it is to try and vibrate the specimen at one of its natural frequencies only, and observe the corresponding response. Understandably, the problem with such an approach is that, if the structural details of the specimen are unknown, then, how does one determine the exciting frequency? As mentioned earlier, predictably the problems associated with trying to vibrate a reinforced concrete panel of this size and the correspondingly high stiffness are quite a few. The parameteric study carried out on the numerical models, once again did not show a good comparison with the observed response.

Quite a few questions were left unanswered by the experimentally observed response of these five specimens. These five test specimens were modelled, once the results of the previous six test specimens had shown that it was quite difficult to detect, the influence of a few additional constraints on the dynamic characteristics, mainly the natural frequencies, for specimens which had some form of concrete connection, around the perimeter between the two leaves. The results of this batch quite clearly indicated the possibility of distinguishing between the different specimens with varying number of constraints but, at the sme time the observed response showed the specimens to be a lot stiffer then what the numerical model predicted.

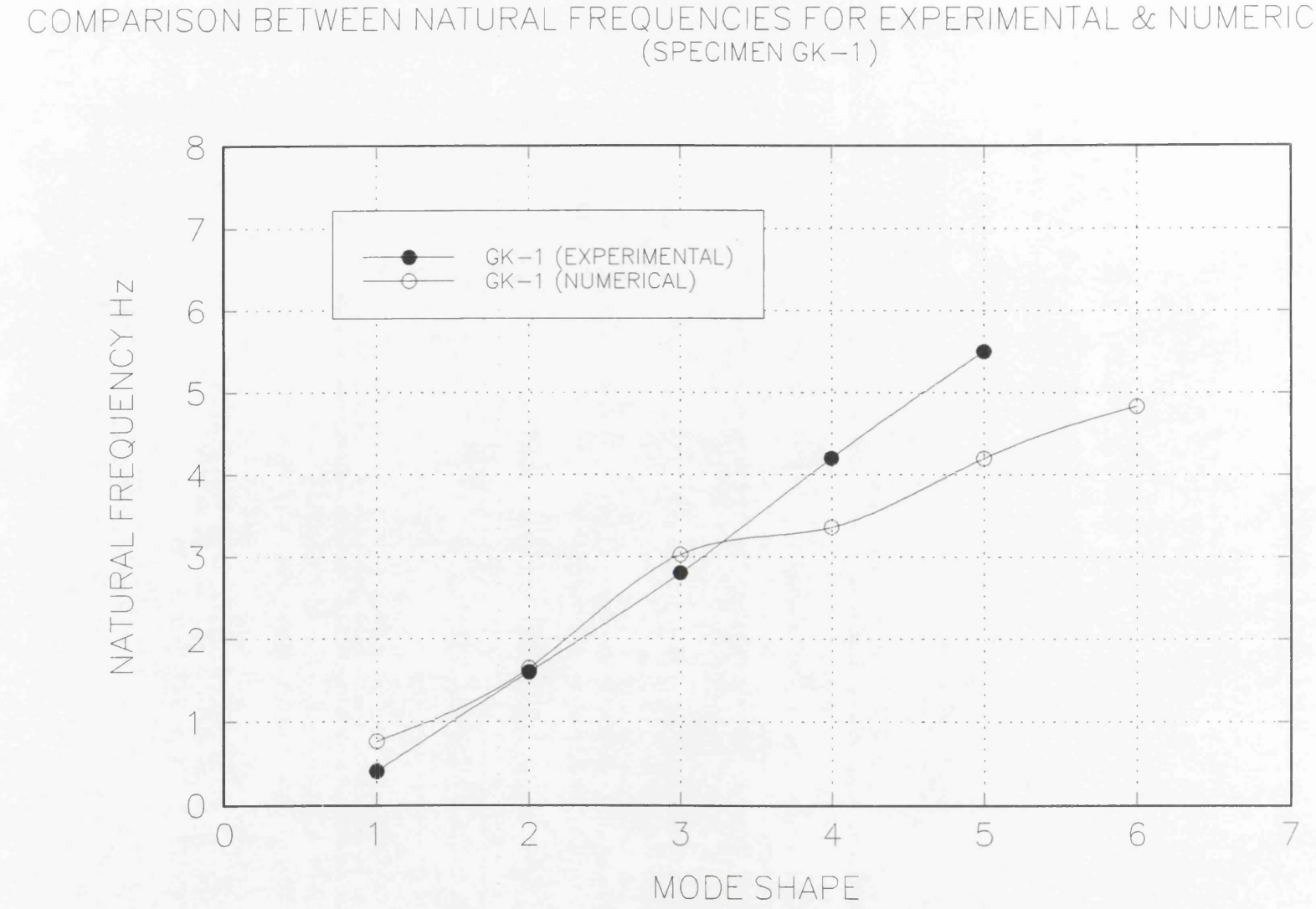

Fig. 6.1 : Natural frequencies for experimental and numerical model GK–1.

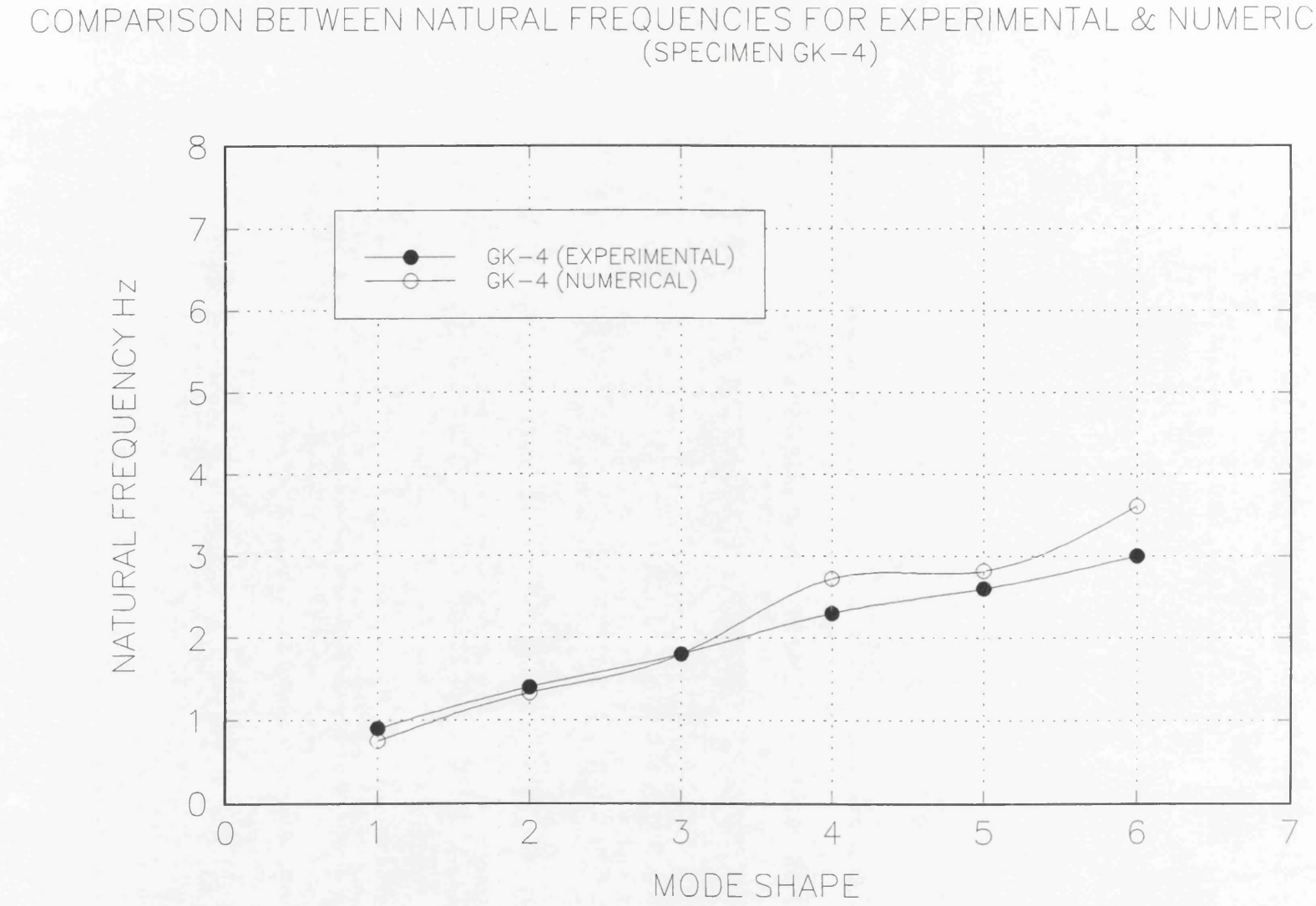

Fig. 6.2:Natural frequencies for experimental and numerical model GK-4.

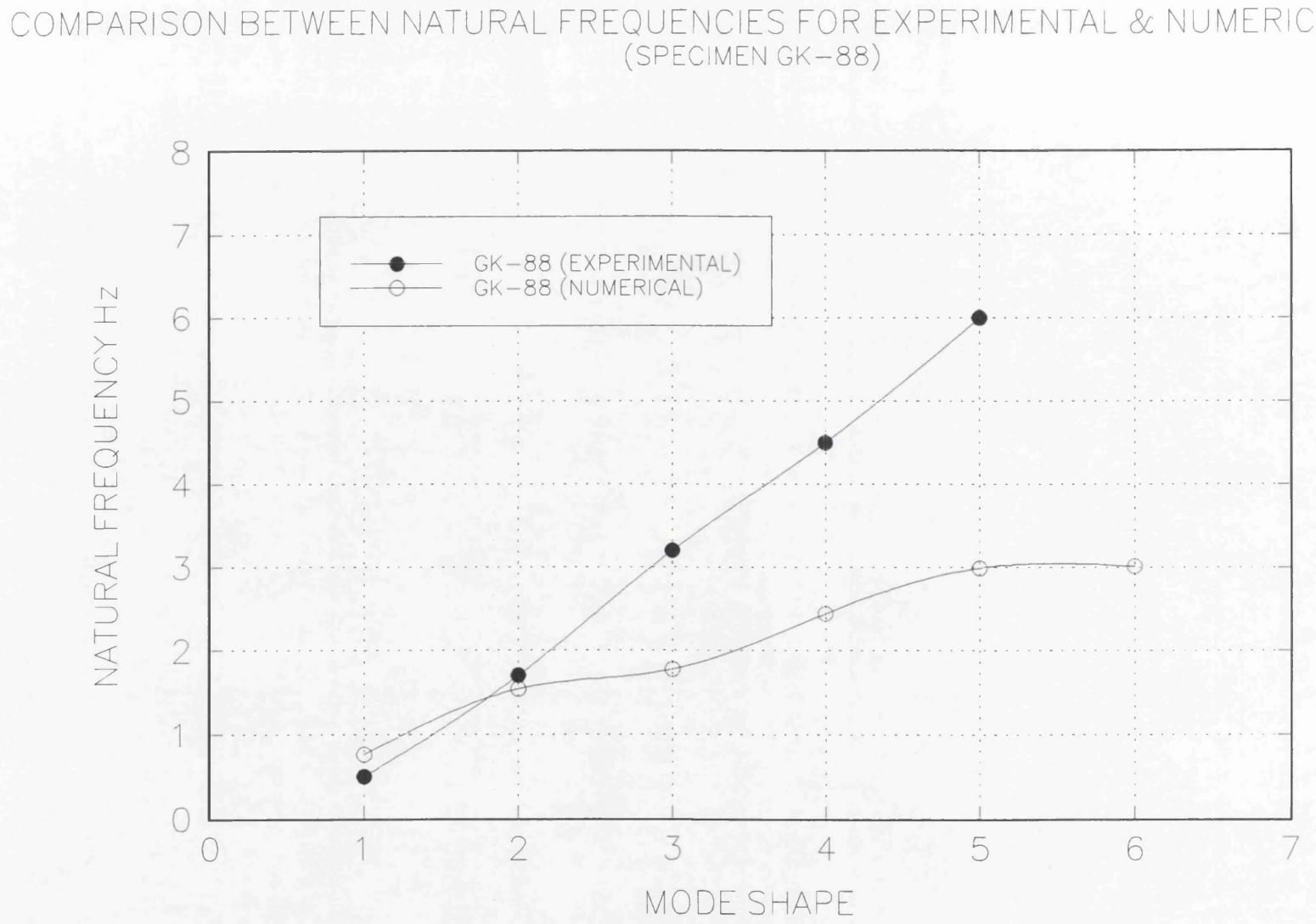

Fig. 6.3:Natural frequencies for experimental and numerical model GK–88.

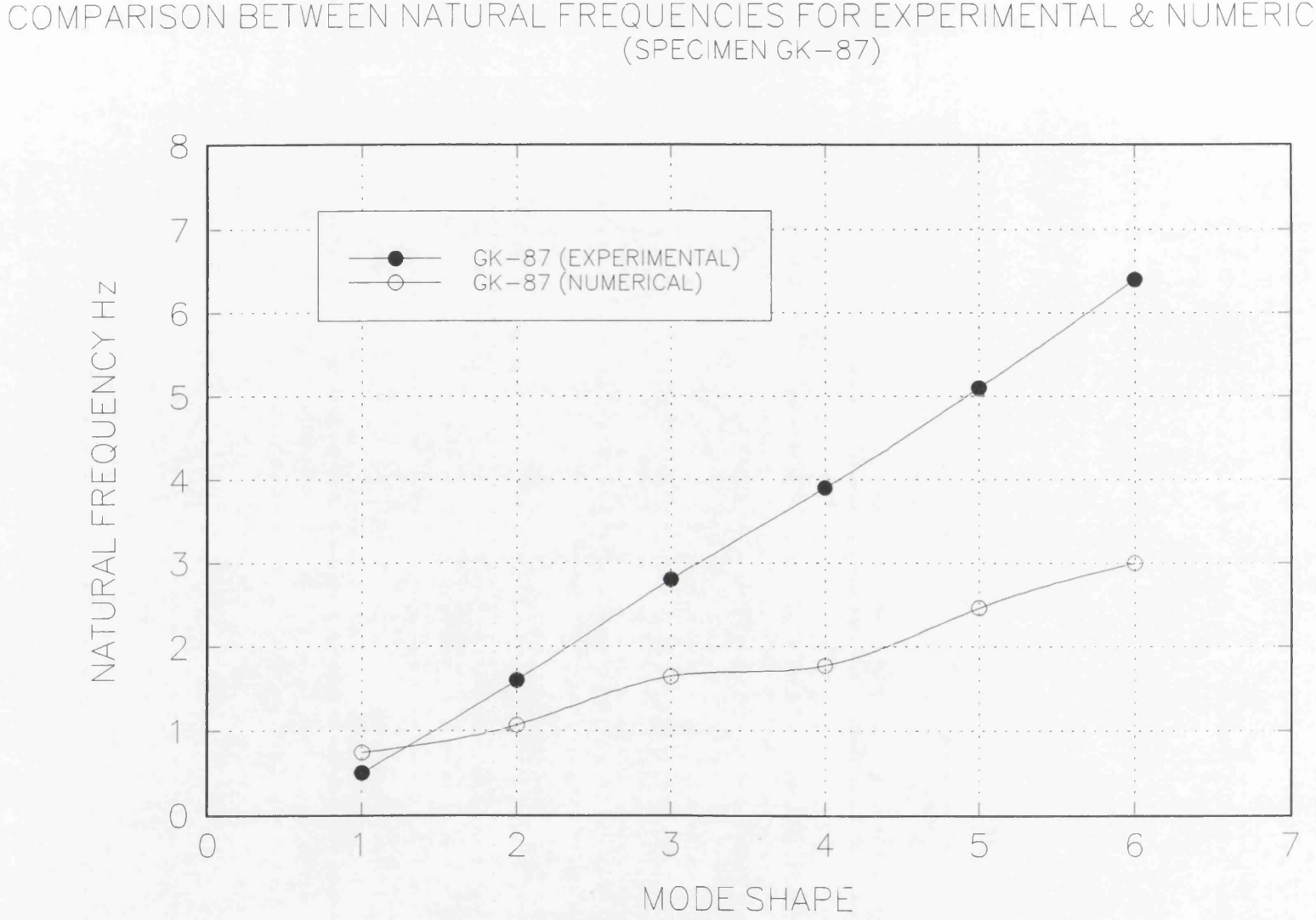

Fig. 6.4:Natural frequencies for experimental and numerical model GK–87.

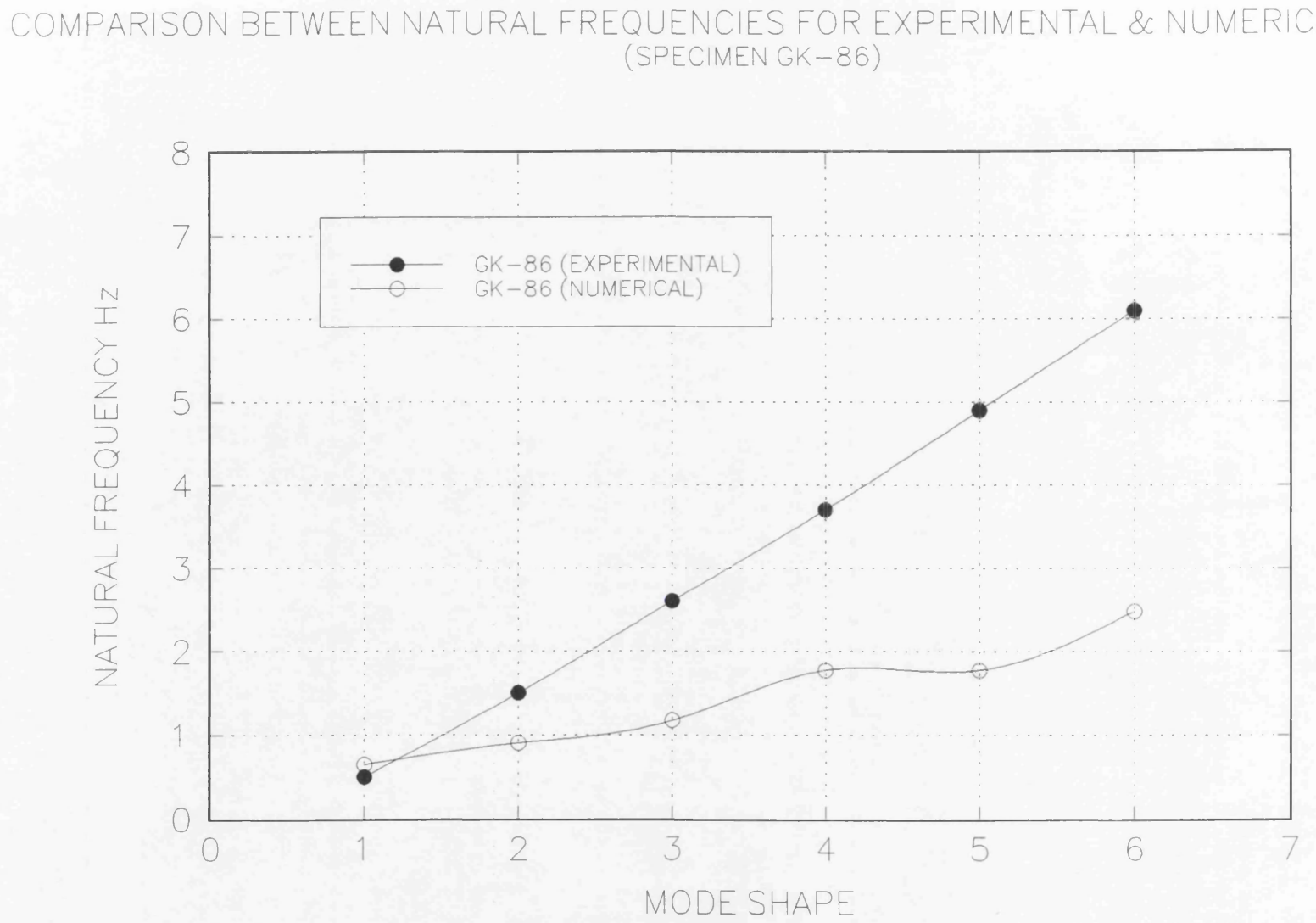

Fig. 6.5:Natural frequencies for experimental and numerical model GK-86.

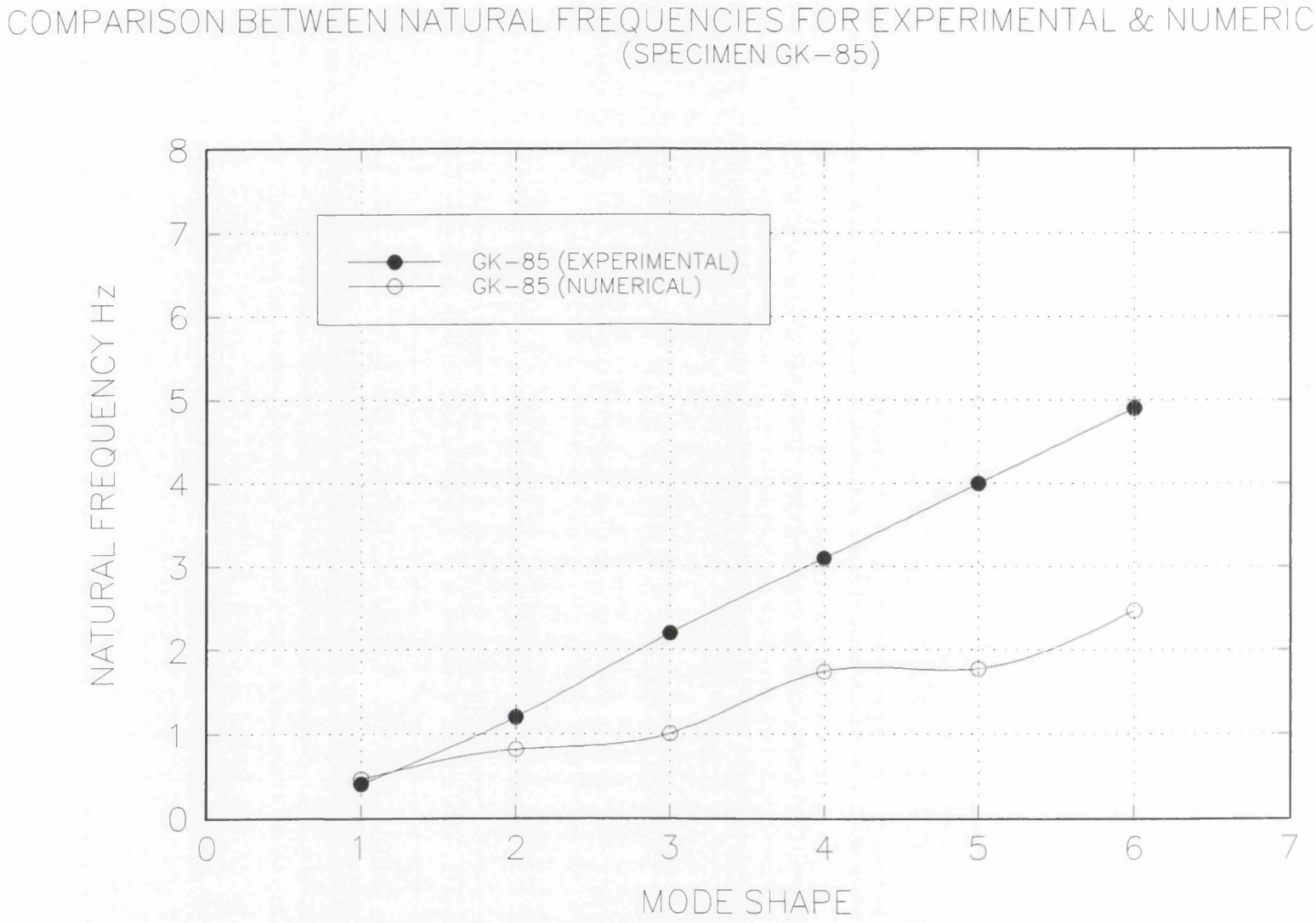

Fig. 6.6:Natural frequencies for experimental and numerical model GK–85.

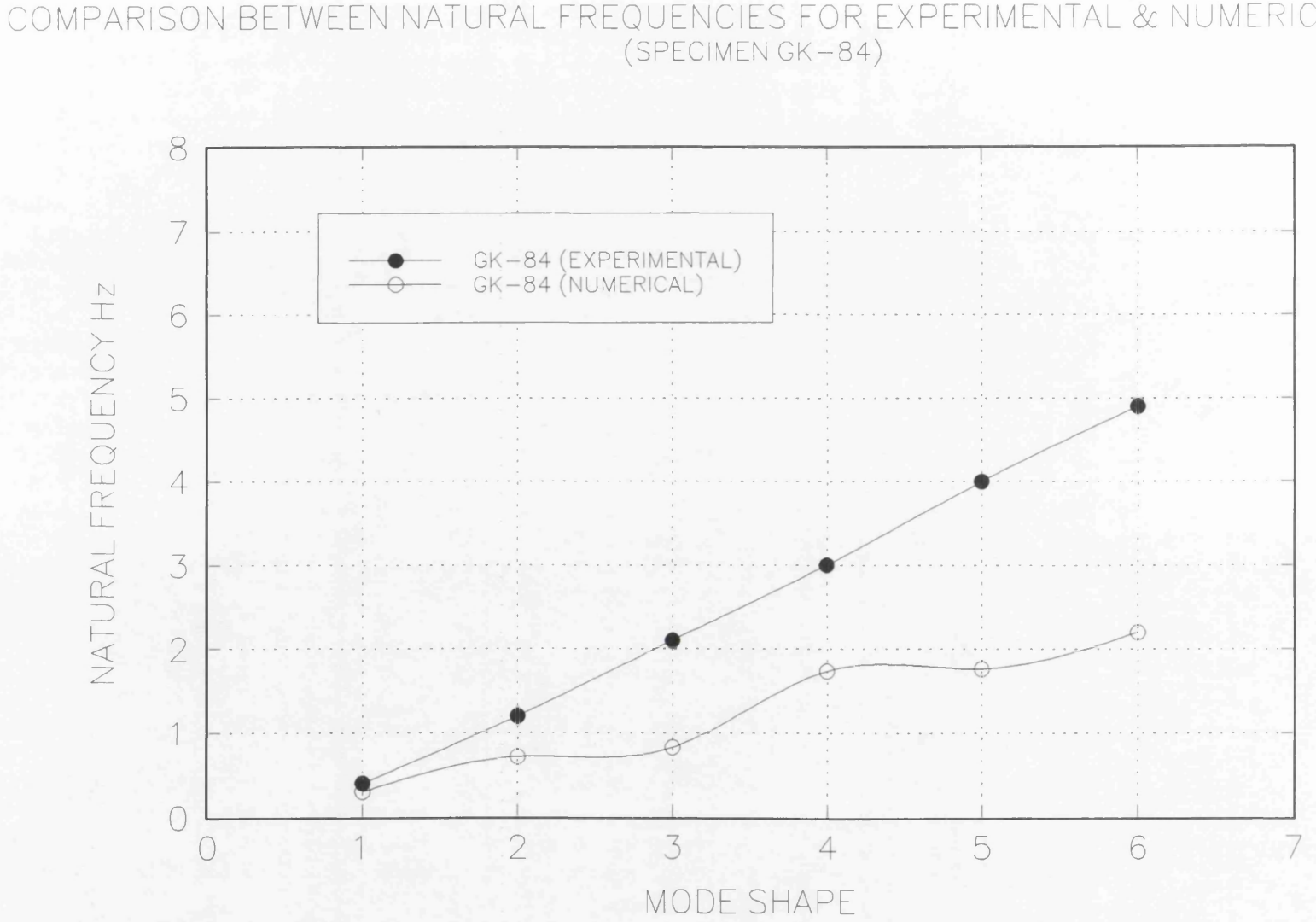

Fig. 6.7:Natural frequencies for experimental and numerical model GK-84.

CHAPTER 7

CONCLUSIONS

Tests were carried out on eleven full-scale, reinforced concrete, sandwich wall cladding panels. The panels had nominal geometric dimensions of 2400mm x 1800mm, and the two leaves of the panels, that is, the inner load bearing leaf and the outer cladding leaf were a 100mm and 50mm thick, respectively. The specimens were reinforced with 8mm diameter bars @ 200mm centre-to-centre in both directions, for both leaves of the panel. For all test specimens a pre-mix concrete of 35MPa strength was used. Three principal variations of the specimens were cast. These were dependant upon the type of structural connection present between the two leaves which varied from a fairly stiff connection all around the perimeter to absolutely no concrete connection between the two leaves, with only a limited and pre-determined number of reinforcement ties providing the structural constraint between them. The presence or absence of the insulation layer of polystyrene was the other main difference between the different specimens. The structural and constructional details of these specimens can be found in chapters 4 and 5.

All eleven specimens, in the present research, were analysed for their dynamic characteristics. The numerical analysis for the dynamic properties was carried out through the use of the finite element program, FLASH. The program allows for a great deal of applications for both static and dynamic loading, as detailed in chapter 2. All models were analysed for their natural frequencies for the first six modal shapes which were also obtained. Plate bending elements were used for the analysis, as savings achieved in terms of computer time far outweighed any

numerical advantage, that could be gained by using shell elements. The results, thus obtained, were used as a basis for the experimental program.

The experimental program consisted of testing the eleven specimens for their dynamic characteristics, mainly their natural frequencies. The specimens were simply supported along the top and bottom edge and subjected to an in-plane compressive loading of 500kN, distributed uniformly along the 100mm thick, inner load bearing concrete leaf, in addition to a dynamic force. The dynamic force was applied to the reinforced concrete sandwich panel through the impact of a hammer blow. The response of the specimen from both leaves, under the influence of the applied loading, was measured at various locations through the use of accelerometers. The response was then analysed through the use of a spectrum analyser and the natural frequencies determined. From these observed natural frequencies, an attempt was made to distinguish between the various test specimens and detect the structural differences present between them. After establishing the distinction between the various experimental specimens, based upon the observed response, comparisons were made with the numerical results. The conclusions drawn are presented below.

1. The results of the numerical analysis showed that it was possible to detect the differences in the natural frequencies, between the two specimens GK-1 and GK-4, which had different degrees of constraint between the two leaves around the perimeter. The natural frequencies for these specimens, showed enough difference between them for the various modal shapes, to make experimental detection possible. In contrast to this, specimens similar to these in terms of the edge constraints (GK-2, 3 and GK-5, 6, respectively), but having additional structural constraints, through the use of reinforcement ties, did not exhibit enough

difference in the natural frequencies, between the different modal shapes, thus making it somewhat difficult for experimental observation.

2. Numerical models GK-88, 87, 86, 85, 84, had only reinforcement ties present between the two leaves, as the structural constraints, and ranging from eight in GK-88 to four in GK-84. The natural frequencies obtained from the analysis did not show a great deal of difference between the successive modal shapes, but were enough to allow distinction between the different models. Additionally, the modal shapes of all models were distinct from each other, making the experimental detection of the structural differences between them a distinct possibility which might be worth investigating.

3. The experimental observations of specimen GK-1 showed a fair comparison with results achieved from the numerical analysis, for at least the first three modal shapes. For the higher mode shapes, the experimental model exhibited a much stiffer response compared to the predicted one. Similar trends were observed for specimens GK-2, 3 and, compounding the problem even more, was the fact that from the observed response it was not possible to distinguish between them and specimen GK-1. Consequently, it was not possible to determine the structural differences between them, through the observance of the natural frequencies.

4. The dynamic response of test specimen GK-4 compared extremely favourably with the natural frequencies obtained from the numerical analysis. This being the only specimen, in the present research, which did not exhibit an experimental response that indicated the specimen was a lot stiffer than that of the numerical analysis. As was the case with test specimens GK-2, 3, the results of specimens GK-5, 6 being very similar to GK-4. The results again demonstrated the

limitations of using only the observed natural frequencies for determining the structural differences present between the individual specimens and at the same time detecting the damage locations.

5. The experimentally observed response of the natural frequencies for the various modal shapes, for specimens GK-88, 87, 86, 85, 84 compared favourably with each other. The specimens with the greater number of reinforcement ties (used for the structural constraint) between the two leaves, showing a stiffer response, compared to those with a lesser number of these reinforcement ties. In spite of this observation, the results did not compare too well with the numerical predictions , with the observed response indicating much stiffer elements.

6. From the results obtained by analysing the experimentally observed dynamic characteristics of the eleven test specimens, it can be ascertained with a fair degree of confidence, that although it is possible to differentiate between the various specimens (different from each other in terms of the type of the structural connection and the degree of stiffness) through the natural frequencies, it is not easy to assess the type or location of damage. In other words, it is not possible to determine the structural differences present between the different specimens from only measuring and detecting their natural frequencies. Another fairly important observation made during the experimental program was the fact, that the test specimens which had any form of concrete connection present between the two leaves, did not show any substantial difference between the natural frequencies even when additional structural constraints, in the form of reinforcement ties were introduced. This suggests that the connection around the perimeter tends to dominate and overshadow the effect that these other constraints may have on the response of the specimen.

Based upon the above mentioned conclusions, it is fair to say that although it is quite possible to determine the relative difference in stiffness, between the various reinforced concrete sandwich cladding panels-tested during the present research, through observing their natural frequencies, it is quite difficult to make any valid comparisons between the experimentally observed response and the predicted numerical values.

FUTURE WORK

The aim of the present research was to develop a fairly simple, non-destructive experimental procedure, based upon the dynamic characteristics of the specimen, which would give an indication to the structural integrity of the panel in question. For this reason, it was a requirement to make the testing program as uncomplicated as possible. The results of the tests indicated a relative success, in that, it was shown that through a relatively simple approach it was possible to determine the dynamic characteristics of the panels and make a distinction between the various structural panels. At the same time it exposed quite a few limitations of the adopted approach. The main flaw being, the difficulty in detecting the actual structural differences in the sandwich panels. This being, to a certain extent, a pilot series in this sort of research at the University of Glasgow, the author feels that the lessons learnt could be put to good use in avoiding future pitfalls in furthering the research work and coming up with a more workable experimental approach. A few points worth mentioning to this effect are:

1. It might be feasible, to initially work with a scaled down specimen, rather then a full-scale model. This would reduce the stiffness of the specimen, thus

making it relatively simple to vibrate it in one particular mode, through the use of a sinusoidal vibrator. This could lead to the elimination of the experimental error induced in observing the natural frequencies which are quite close to each other and have a tendency of overlapping, when transient forces are used. Furthermore, the use of scaled down models would allow for better control over the boundary support conditions, which would certainly reduce experimental error and make for better comparisons with the numerically analysed characteristics.

2. For better understanding of the dynamic characteristics of the reinforced concrete sandwich wall cladding panels and their behaviour, when subjected to a dynamic force, it is probably quite important to be able to plot out the experimentally observed modal shapes. This can only be achieved through having a controlled input force and having a fairly large number of transducer locations. These experimentally observed modal shapes would give a fairly good indication of the type of structural constraint present between the two leaves. Once this deeper understanding of the dynamic behaviour of the panels has been established it might be possible to comment with a greater degree of confidence on the possible structural damage in a panel.

3. As a last word, because of the problems allied to the dynamic testing of reinforced concrete and the inherent problems of trying to get the specimens vibrating in a particular mode, it is probably quite difficult to say with any great amount of conviction as to how successful such an approach would eventually prove to be. But with sufficient experimental knowledge and enough data to determine the possible dynamic characteristics, there is no reason not to believe in the applicability of such an approach.

REFERENCES

REFERENCES

1. Green, D. R. "The security of cladding in large panel structures", CONCRETE, Journal of the concrete society, June 1986, Vol. 20, Number 6, pp. 33-35.

2. Currie, R. J., Armer, G. S. T. and Moore, J. F. A., "The structural adequacy and durability of large panel system dwellings, part 1: Investigations of construction", BRE report, 1987.

3. Currie, R. J., Armer, G. S. T. and Moore, J. F. A., "The structural adequacy and durability of large panel system dwellings, part 2: Guidance on appraisal", BRE report, 1987.

4. Hotchkiss, A. R. and Edwards, Marilyn J., "Reema large panel system dwellings: constructional details", BRE report, 1987.

5. Hotchkiss, A. R. and Edwards, Marilyn J., "Bison large panel system dwellings: constructional details", BRE report, 1988.

6. Macleod, I. A. et. al., "Guidance note on the security of cladding on large panel concrete construction", The Institution of Structural Engineers, Scottish branch, September, 1984.

7. Kenley, R. M. and Dodds, C. J., "West Sole W. E. platform: Detection of damage by structural response measurements", Offshore Technology Conference, Houston, 1980.

8. Loland, O., "A vibration method for integrity monitoring of fixed offshore steel platforms", Ph.D. thesis , University of Glasgow, Glasgow, 1978.

9. Cawley, P., "A high frequency coin-tap method of non-destructive testing", Mechanical systems and signal processing, No. 6, November, 1991, pp. 1-11.

10. Cawley, P., "The sensitivity of an NDT instrument based on the membrane resonance method", NDT International, No. 22, 1989, pp. 209-210.

11. Cawley, P. and Adams, R. D., "The sensitivity of the coin-tap method of non-destructive testing", Materials evaluation, No. 47, 1989, pp. 558-563.

12. Cawley, P., "The sensitivity of the mechanical impedance method of non-destructive testing", NDT International, No. 20, 1987, pp. 209-215.

13. Craig, J. I. and Goodno, J. B., "Response measurements for glass cladding panels", Journal of the structural division, ASCE, Vol. 107, No. ST11, 1981, pp. 2199-2214.

14. Maguire, J. R. and Severn, R. T., "Assessing the dynamic properties of prototype structures by hammer testing", Proc. Instn. Civil Engineers, Part 2, 1987, pp. 769-784.

15. Pavic, A., Williams, M. S. and Waldron, D., "Dynamic FE model for post-tensioned concrete floors calibrated against field test results", Second International Conference on Engineering Integrity Assessment, Glasgow, 10-12 May, 1994.

16. Brownjohn, J. M. W., Dumanoglu, A. A. and Taylor, C. A., "Dynamic investigation of a suspension footbridge". Personal contact.

17. Hearn, G. and Testa, R. B., "Modal anlysis for damage detection in structures", Journal of the structural engineering, ASCE, Vol. 117, No.10, 1991, pp. 3042-3063.

18. Cawley, P. and Adams, R. D., "The location of defects in structures from measurements of natural frequencies", Journal of strain analysis, Number 14, 1979, pp. 49-57.

19. Sammam, M. M., Biswas, M. and Pandey, A. K. "Employing pattern recognition for detecting cracks in a bridge model", Journal of analytical and experimental modal analysis, Number 6, 1991, pp. 35-44.

20. Worden, K., Ball, A. D. and Tomlinson, G. R., "Fault location in a framework structure using neural networks", Smart mater. structures, Number 2, 1993, pp. 189-200.

21. Kudva, J., Munir, N. and Tan, P. W., "Damage detection in smart structures using neural methods and finite element analysis", Smart materials and structures, 1992, pp. 108-112.

22. Tomlinson, G. R. and Worden, K., "Damage location and quantification using neural networks". Personal contact.

23. Tourk, O. M. S., "The effect of cracking of the concrete on the dynamic characteristics of reinforced concrete beams", M. Sc. thesis, University of Strathclyde, Glasgow, 1979.

24. Sim, K. L., "Vibration of concrete beams", M. Sc. thesis, University of Strathclyde, Glasgow, 1980.

25. Hashim, E. M., "Vibration of concrete structure", M. Sc. thesis, University of Strathclyde, Glasgow, 1981.

26. Tan, C. L., "The vibration characteristics of reinforced concrete beams under load", M. Sc. thesis, University of Strathclyde, Glasgow, 1985.

27. Priyosulistyo, H., "Detection of defects in concrete structures using vibration technique", Ph. D. thesis, University of Strathclyde, Glasgow, 1992.

28. Brigham, E. D., "The fast fourier transform", Prentice Hall, Inc.

29. Ramirez, R. W., "The FFT fundamentals and concepts", Prentice Hall, Inc., New Jersey, U.S.A.., 1985.

30. Hanning, R. W., "Digital filters", Prentice Hall, Inc., 2nd edition, 1983.

31. Gold, B. and Rabiner, L. R., "Theory and application of digital signal processing", Prentice Hall, Inc., New Jersey, U.S.A., 1975.

32. Mcgonnagle, W. J., "Non-destructive testing", 2nd. edition, Gorden and Breach, London.

33. Sharpe, R. S., "Research techniques in non-destructive testing".

34. "FLASH, finite-element-analysis-program, user's manual", by Dr Walder and partners, 8th edition, May, 1985.

35. "Modal analysis of large structures", by K Zaveri, Bruel & Kjaer, 1984.

36. "Modal testing principles", by George F Lang, technicalreport number 023/87, Solartron instruments, 1987.

37. "Mechanical vibration and shock measurement", by Jens Trampe Broch, Bruel & Kjaer, 1990.

38. "Modal testing: theory and practice", by D J Ewins, Research Studies Press Ltd., 1984.

39. Reema system copyright drawing, NBA, 1966.

40. Conclad construction details published by Reema, 1967-70.

41. Conclad construction details published by Reema, 1966.

42. Contrad housing: metric house shells, Reema publication, October, 1969.

43. Warburton, G. B., "Dynamical behaviour of structures", 2nd edition, Pergamon press, Oxford, 1976.

44. Fertis, G. D., "Dynamics and vibrations of structures", John Wiley & sons, London, 1973.

45. Kennedy, C. C. and Pancu, C. D. P., "Use of vectors in vibration measurement and analysis", Journal of Aeronautical Sciences, Vol. 14, No. 11, 1947, pp. 603-625.

46. Bishop, R. E. D. and Gladwell, G. M. L., "An investigation into the theory of resonance testing", Phil. Trans. of the Royal Society of London, Series A, Vol. 255, Mathematical and Physical Sciences, 1963, pp. 241-280.

APPENDIX A

TYPICAL FLASH INPUT FILE

```
BEGIN
GK-3, SIMPLY SUPPORTED
PLATE 260 216 2 E D 6
MATRIX 13 10 JOINT 1 1 13 COORD 0. PLUS 0. 0.2 AND 0.2 /
FACTORS 1. 1. 1. 1. 1. 1. 1. 1. 1. 1. 1. 1. AND 1. 1. 1. /
1. 1. 1. 1. 1. 1.
MATRIX 13 10 JOINT 131 1 13 COORD 2. PLUS 0. 0.2 AND 0.2 /
FACTORS 1. 1. 1. 1. 1. 1. 1. 1. 1. 1. 1. 1. AND 1. 1. 1. /
1. 1. 1. 1. 1. 1.
*
*
ISOTROPIC 3.0E7 0.17 0.1 TYPE 1
ISOTROPIC 3.0E7 0.17 0.05 TYPE 2
MASS 2.4E3 TYPE 1 2
*
MATRIX 12 9 ELEMENT 1 JOINTS 14 15 2 1 TYPE 1 I 1 12
MATRIX 12 9 ELEMENT 109 JOINTS 144 145 132 131 TYPE 2 I 1 12
*
*
N F F 1 T 118 S 13
N F F 13 T 130 S 13
C S C TO JT. 1 O P 1 O J 131
C S C TO JT. 2 O P 1 O J 132
C S C TO JT. 3 O P 1 O J 133
C S C TO JT. 4 O P 1 O J 134
C S C TO JT. 5 O P 1 O J 135
C S C TO JT. 6 O P 1 O J 136
C S C TO JT. 7 O P 1 O J 137
C S C TO JT. 8 O P 1 O J 138
C S C TO JT. 9 O P 1 O J 139
C S C TO JT. 10 O P 1 O J 140
C S C TO JT. 11 O P 1 O J 141
C S C TO JT. 12 O P 1 O J 142
C S C TO JT. 13 O P 1 O J 143
C S C TO JT. 14 O P 1 O J 144
C S C TO JT. 15 O P 1 O J 145
C S C TO JT. 16 O P 1 O J 146
C S C TO JT. 17 O P 1 O J 147
C S C TO JT. 18 O P 1 O J 148
C S C TO JT. 19 O P 1 O J 149
C S C TO JT. 20 O P 1 O J 150
C S C TO JT. 21 O P 1 O J 151
C S C TO JT. 22 O P 1 O J 152
C S C TO JT. 23 O P 1 O J 153
C S C TO JT. 24 O P 1 O J 154
C S C TO JT. 25 O P 1 O J 155
C S C TO JT. 26 O P 1 O J 156
```

C S C TO JT. 27 O P 1 O J 157
C S C TO JT. 28 O P 1 O J 158
C S C TO JT. 38 O P 1 O J 168
C S C TO JT. 39 O P 1 O J 169
C S C TO JT. 40 O P 1 O J 170
C S C TO JT. 41 O P 1 O J 171
C S C TO JT. 51 O P 1 O J 181
C S C TO JT. 52 O P 1 O J 182
C S C TO JT. 53 O P 1 O J 183
C S C TO JT. 54 O P 1 O J 184
C S C TO JT. 64 O P 1 O J 194
C S C TO JT. 65 O P 1 O J 195
C S C TO JT. 66 O P 1 O J 196
C S C TO JT. 67 O P 1 O J 197
C S C TO JT. 77 O P 1 O J 207
C S C TO JT. 78 O P 1 O J 208
C S C TO JT. 79 O P 1 O J 209
C S C TO JT. 80 O P 1 O J 210
C S C TO JT. 90 O P 1 O J 220
C S C TO JT. 91 O P 1 O J 221
C S C TO JT. 92 O P 1 O J 222
C S C TO JT. 93 O P 1 O J 223
C S C TO JT. 103 O P 1 O J 233
C S C TO JT. 104 O P 1 O J 234
C S C TO JT. 105 O P 1 O J 235
C S C TO JT. 106 O P 1 O J 236
C S C TO JT. 107 O P 1 O J 237
C S C TO JT. 108 O P 1 O J 238
C S C TO JT. 109 O P 1 O J 239
C S C TO JT. 110 O P 1 O J 240
C S C TO JT. 111 O P 1 O J 241
C S C TO JT. 112 O P 1 O J 242
C S C TO JT. 113 O P 1 O J 243
C S C TO JT. 114 O P 1 O J 244
C S C TO JT. 115 O P 1 O J 245
C S C TO JT. 116 O P 1 O J 246
C S C TO JT. 117 O P 1 O J 247
C S C TO JT. 118 O P 1 O J 248
C S C TO JT. 119 O P 1 O J 249
C S C TO JT. 120 O P 1 O J 250
C S C TO JT. 121 O P 1 O J 251
C S C TO JT. 122 O P 1 O J 252
C S C TO JT. 123 O P 1 O J 253
C S C TO JT. 124 O P 1 O J 254
C S C TO JT. 125 O P 1 O J 255
C S C TO JT. 126 O P 1 O J 256
C S C TO JT. 127 O P 1 O J 257
C S C TO JT. 128 O P 1 O J 258
C S C TO JT. 129 O P 1 O J 259
C S C TO JT. 130 O P 1 O J 260
C S C TO JT. 44 O P 1 O J 174
C S C TO JT. 48 O P 1 O J 178
C S C TO JT. 83 O P 1 O J 213
C S C TO JT. 87 O P 1 O J 217

```
*
*
OPTIMIZATION
*
LOADCASE DYNAMIC LOADING
D E N E 6 P 6
*
LOADCASE 1 D P 6
*
D E 1 Z V 1.5 3.8 3.8 E
D E 2 Z V 1.5 3.8 3.8 E
D E 3 Z V 1.5 3.8 3.8 E
D E 4 Z V 1.5 3.8 3.8 E
D E 5 Z V 1.5 3.8 3.8 E
D E 6 Z V 1.5 3.8 3.8 E
*
```

FLASH INPUT SCHEME

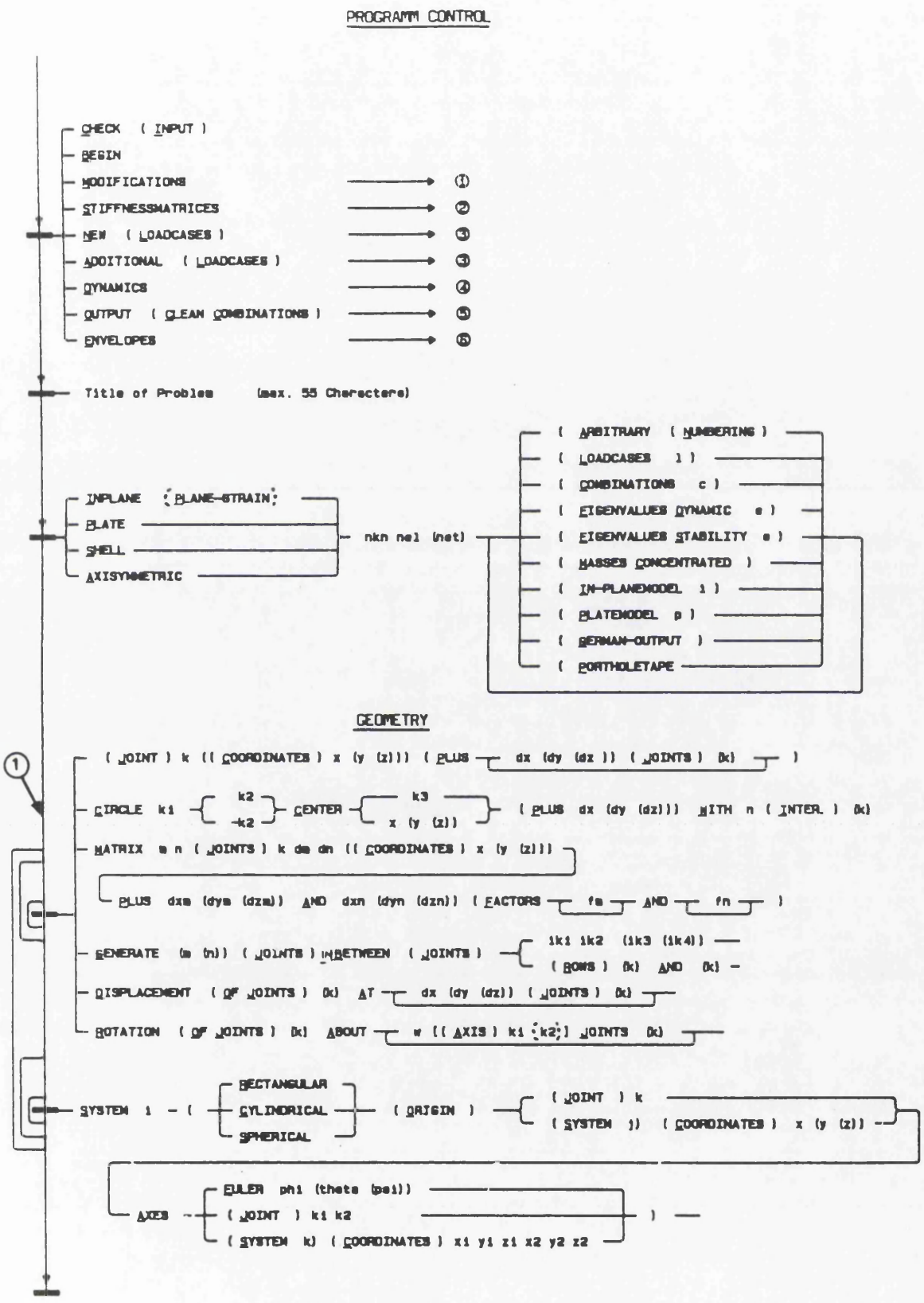

BEAM CROSS SECTION PROPERTIES

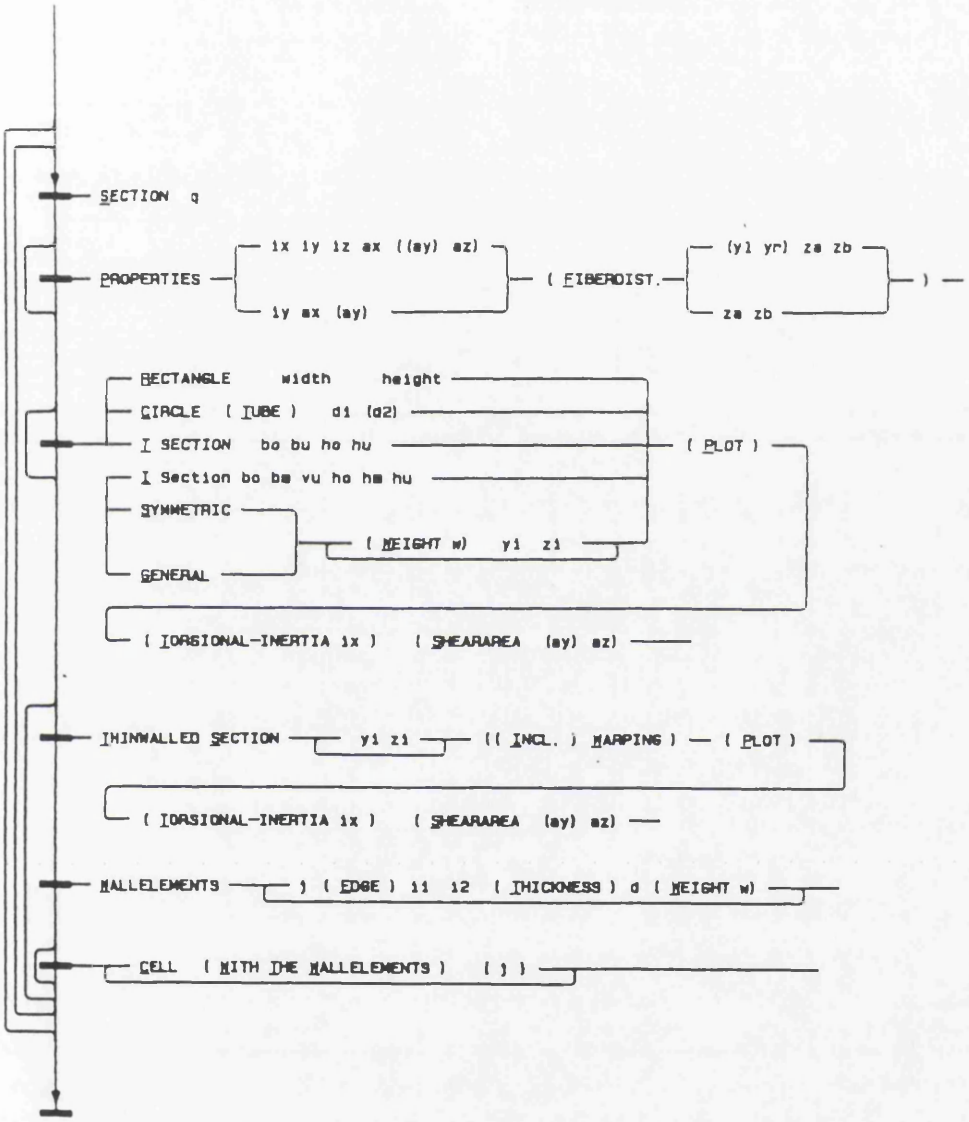

PROFILE LIBRARY, MATERIAL PROPERTIES

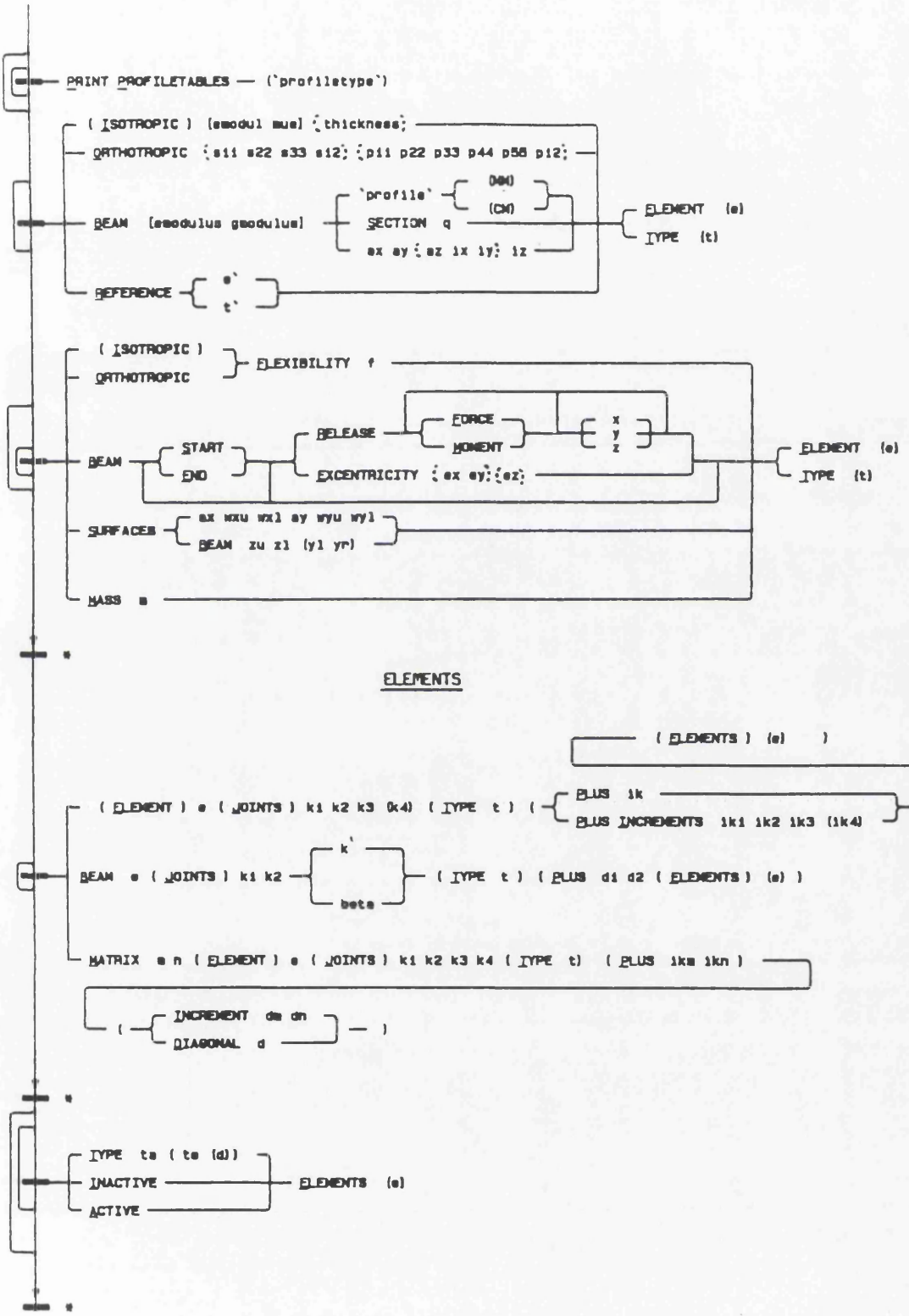

BOUNDARY CONDITIONS, MASS MATRIX, CONSTRAINTS

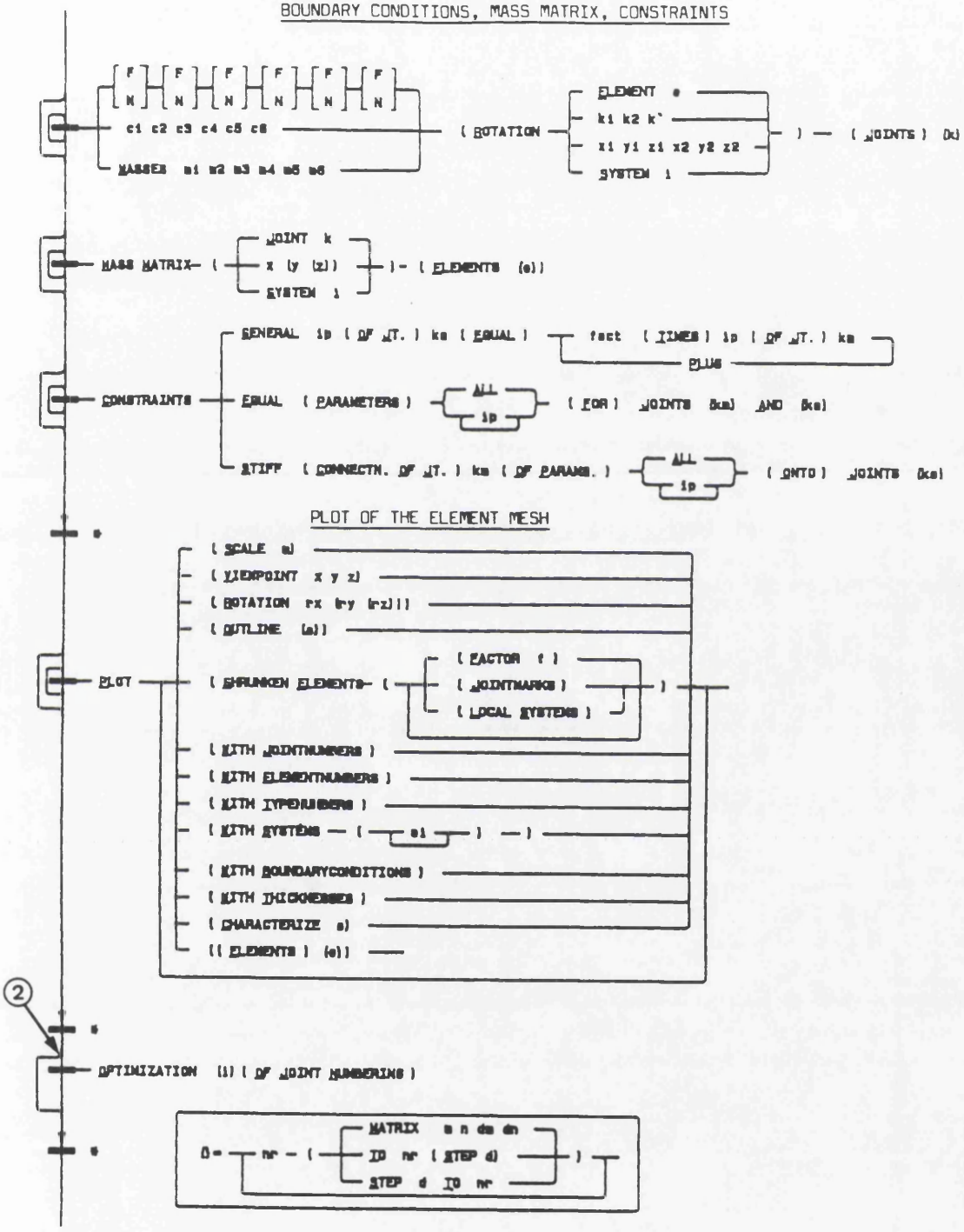

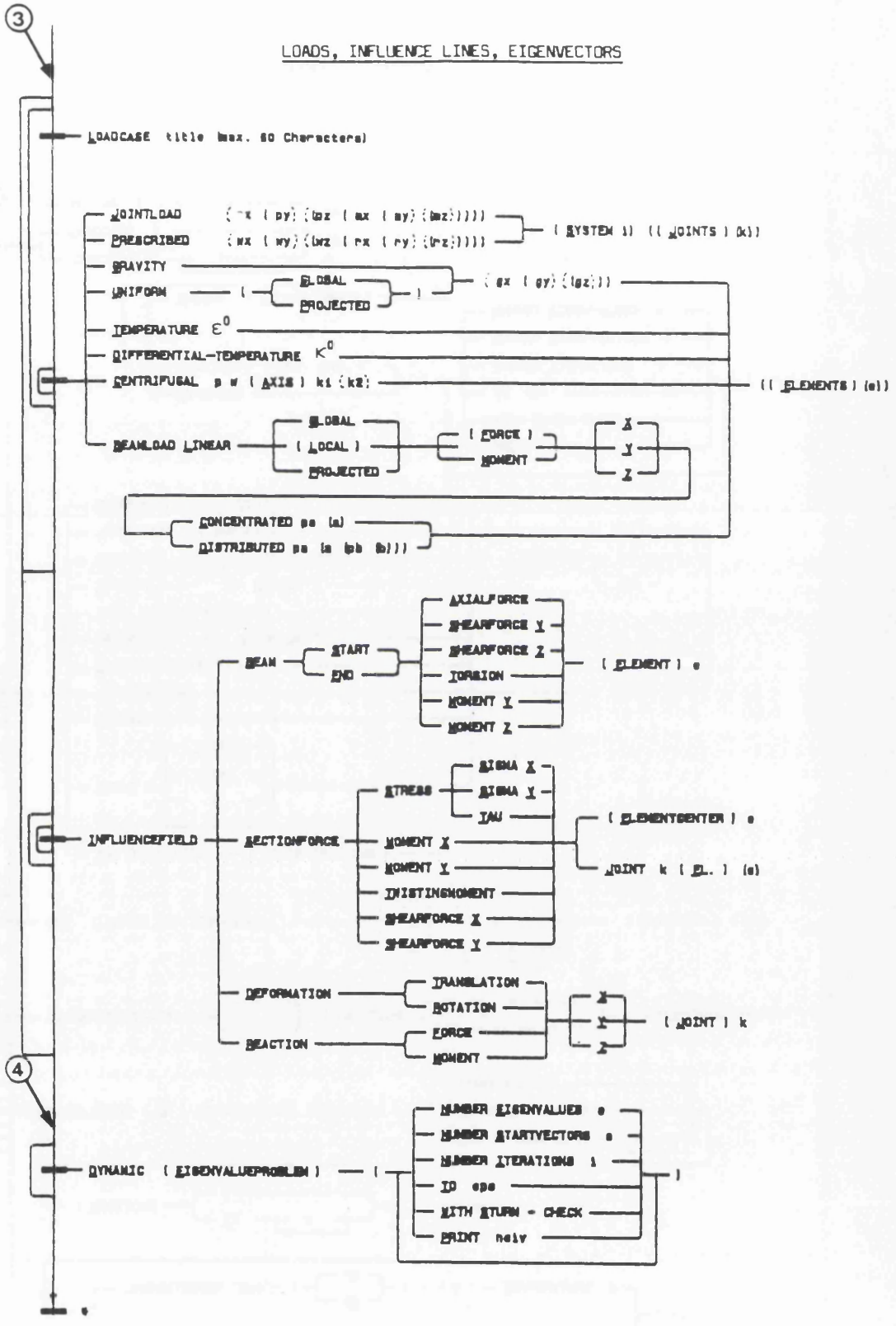
3
LOADS, INFLUENCE LINES, EIGENVECTORS
LOADCASE title (max. 80 Characters)
JOINTLOAD
PRESCRIBED
GRAVITY
UNIFORM
GLOBAL
PROJECTED
TEMPERATURE
DIFFERENTIAL-TEMPERATURE
CENTRIFUGAL
BEAMLOAD LINEAR
GLOBAL
LOCAL
PROJECTED
FORCE
MOMENT
CONCENTRATED
DISTRIBUTED
SYSTEM
JOINTS
ELEMENTS
INFLUENCEFIELD
BEAM
START
END
AXIALFORCE
SHEARFORCE Y
SHEARFORCE Z
TORSION
MOMENT Y
MOMENT Z
ELEMENT
SECTIONFORCE
STRESS
SIGMA X
SIGMA Y
TAU
MOMENT X
MOMENT Y
INISTINSMOMENT
SHEARFORCE X
SHEARFORCE Y
ELEMENTSENTER
JOINT
DEFORMATION
REACTION
TRANSLATION
ROTATION
FORCE
MOMENT
4
DYNAMIC
EIGENVALUEPROBLEM
NUMBER EIGENVALUES
NUMBER STARTVECTORS
NUMBER ITERATIONS
ID eps
WITH RTURN - CHECK
PRINT neiv

NUMERICAL OUTPUT

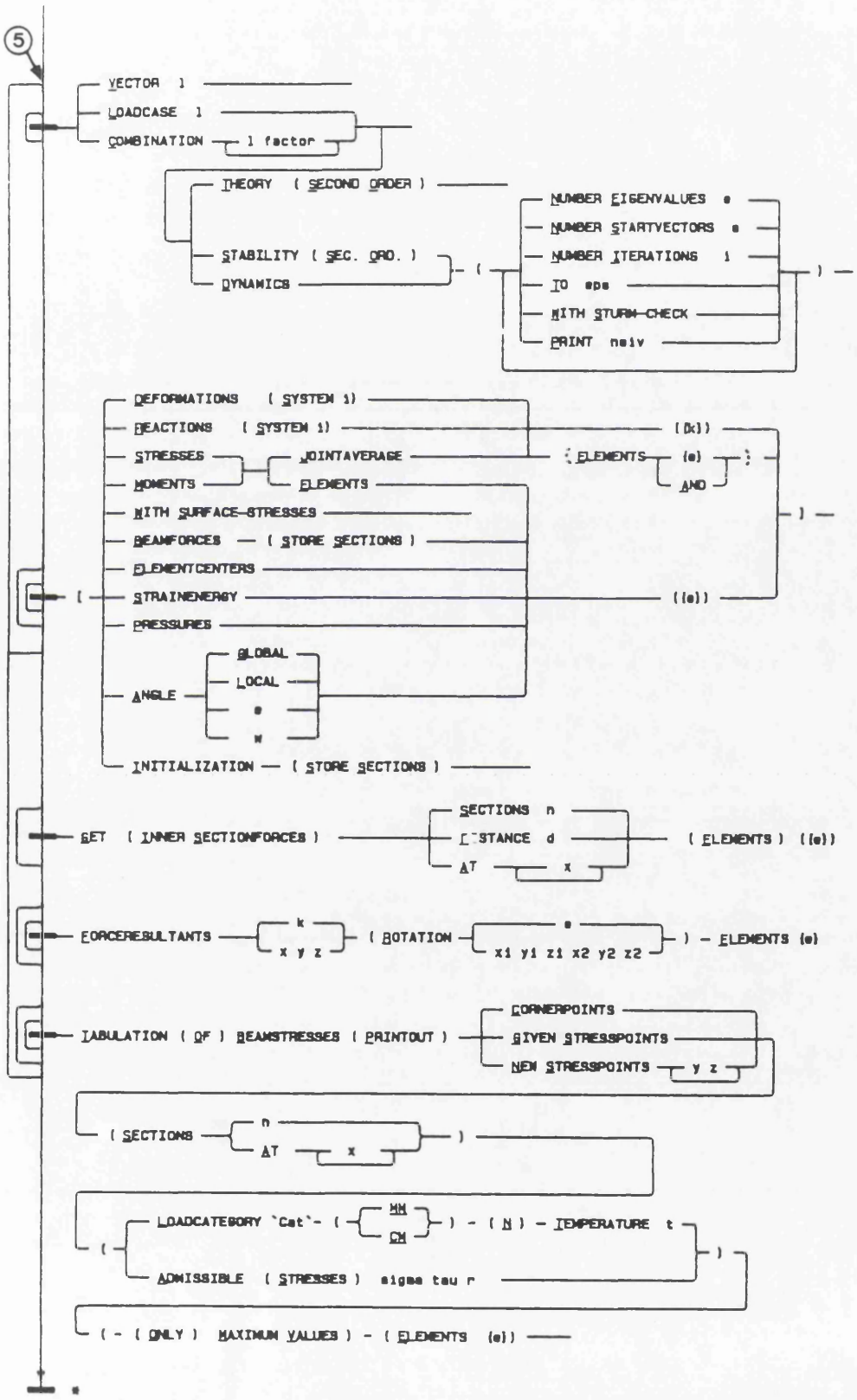

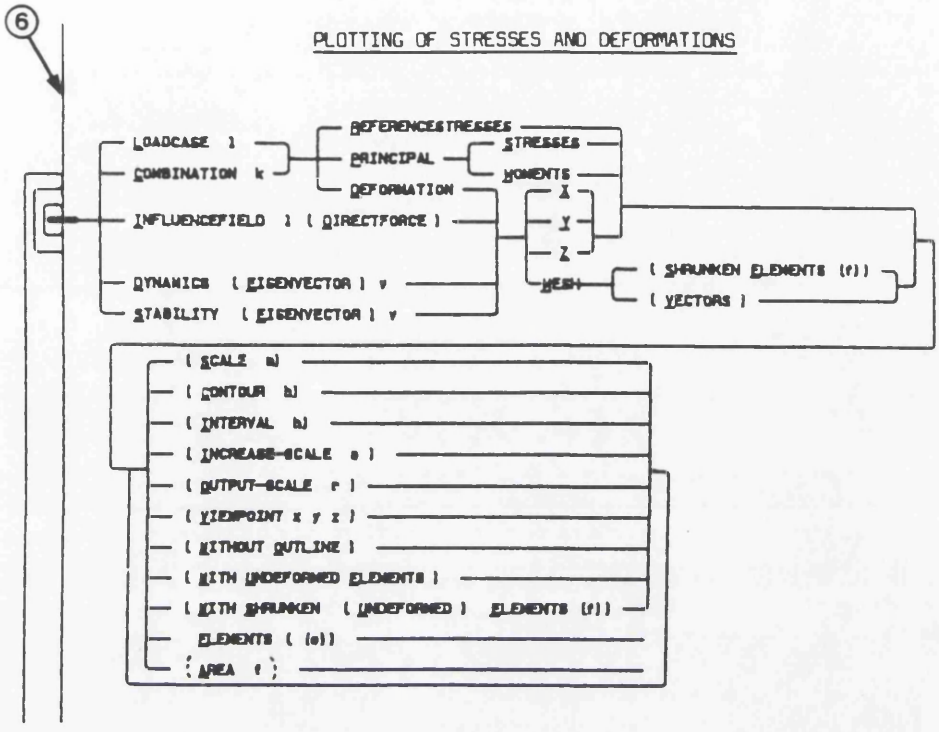
6
PLOTTING OF STRESSES AND DEFORMATIONS
LOADCASE l
COMBINATION k
REFERENCESTRESSES
PRINCIPAL
STRESSES
MOMENTS
DEFORMATION
INFLUENCEFIELD l (DIRECTFORCE)
X
Y
Z
MESH
(SHRUNKEN ELEMENTS (f))
(VECTORS)
DYNAMICS (EIGENVECTOR) v
STABILITY (EIGENVECTOR) v
(SCALE m)
(CONTOUR h)
(INTERVAL h)
(INCREASE-SCALE s)
(OUTPUT-SCALE r)
(VIEWPOINT x y z)
(WITHOUT OUTLINE)
(WITH UNDEFORMED ELEMENTS)
(WITH SHRUNKEN (UNDEFORMED) ELEMENTS (f))
ELEMENTS ((e))
{ AREA f }